VOLTAGE REGULATION

RESEARCH & DEVELOPMENT

QUARTERLY PROGRESS REPORT NO. 6

VOLTAGE REGULATION AND POWER STABILITY
IN UNCONVENTIONAL ELECTRICAL GENERATOR SYSTEMS

PREPARED UNDER NAVY, BUREAU OF NAVAL WEAPONS

CONTRACT NOw 60-0824-C

SEPTEMBER 30, 1961

ASTIA

APR 10 1962

TISIA

AIRCRAFT ACCESSORY TURBINE DEPARTMENT

GENERAL ELECTRIC

VOLTAGE REGULATION AND POWER STABILITY

IN UNCONVENTIONAL ELECTRICAL

GENERATOR SYSTEMS

DECEMBER 31, 1961

PREPARED UNDER NAVY, BUREAU OF NAVAL WEAPONS

CONTRACT NO. 60-0824-C

QUARTERLY PROGRESS REPORT NO. 6

30 SEPTEMBER 1961 THROUGH 31 DECEMBER 1961

GENERAL ELECTRIC COMPANY

AIRCRAFT ACCESSORY TURBINE DEPARTMENT

950 WESTERN AVENUE, WEST LYNN, MASS.

CONTENTS

1.0 Abstract

The technical progress for the sixth quarter of activity (September 30, 1961 through December 31, 1961) on the study of "Voltage Regulation and Power Stability in Unconventional Electrical Generator Systems" for the Bureau of Naval Weapons is presented in this report. Test results are presented which illustrate the control of fuel cell output voltage by varying the velocity of mixtures of inert gas and reactant gas past the appropriate electrode. Information is included showing typical dynamic characteristics of thermo-electric and thermionic power sources. Design data giving weight, volume, and efficiency of series regulating switching circuits and DC-DC and DC-AC power transistor voltage converter circuits are presented. Weight versus efficiency characteristics of various combinations of source voltage control and external voltage converters are included. Weight data on minimum weight complete systems incorporating voltage regulation and conversion are presented. A laboratory model system consisting of a fuel cell and a DC-DC voltage converter-regulator is described. Performance test results for this laboratory model system are presented.

2.0 PURPOSE OF PROJECT

In recent years considerable attention has been given to the development of unconventional energy conversion techniques. In general, the effort has been devoted to development and improvement of the energy conversion devices. Little attention has been given to the system considerations of practical application of these generating devices. Usually the problem of compatibility of the dynamic characteristics of the device with the load with which it is to be used has been ignored. The possibility of internal control of source voltage has not been seriously considered.

During the same period great strides have been made in solid-state device technology. Devices such as the silicon controlled rectifier now make possible the development of static voltage regulation and conversion circuits with much higher efficiency and reliability than previously attainable. To date very little effort has been devoted to the development of such circuits for use with unconventional electrical power sources. Emphasis has been on applications in more conventional fields such as aircraft electrical systems.

The purpose of this study is to investigate the system problems connected with the use of static external voltage converters and regulator and unconventional power sources; to determine the most desirable systems to use; and to establish the performance characteristics of these systems. The overall purpose is satisfied by contributions from three areas of activity.

(a) Methods of internal control of electrical source voltage are being determined and evaluated. In the process, static and dynamic behavior of the sources is being determined.

(b) Optimum external voltage regulator and converter circuits for use with unconventional power sources are being determined and evaluated.

(c) System performance characteristics are being determined by a combination of the external voltage regulator and converter characteristics with the characteristics of the power sources. The resultant system characteristics will allow selection of the optimum system for any given application.

- 3 -

3.0 PROJECT ORGANIZATION AND PERSONNEL

In order to ensure maximum utilization of the General Electric
Company's technical resources, the work effort has been divided
among several departments. The overall responsibility and
technical coordination of the program rests with the Aircraft
Accessory Turbine Department (AATD) in Lynn, Massachusetts.
In addition AATD is directing the effort in the area of internal
voltage control of power sources. In conducting the effort on
internal source voltage control, AATD is obtaining the services
of sister departments such as the Power Tube Department in
Schenectady, New York, and company laboratories such as the
Research Laboratory and General Engineering Laboratory both
in Schenectady, New York.

The external voltage conversion and regulation portion of the
study is being performed primarily at the General Engineering
Laboratory (GEL) in Schenectady, New York, with the assistance
of the Electronics Laboratory in Syracuse, New York, and the
Specialty Control Department (SCD) in Waynesboro, Virginia.

The systems portion of the study involving the determination
of the system characteristics from the characteristics of the
power sources and external voltage regulators and converters
is being performed at AATD with the assistance of SCD and the
General Engineering Laboratory.

This project is under the overall direction of Mr. C. C. Christianson
Project Engineer, Aircraft Accessory Turbine Department at the
Lynn River Works.

The principal contributors to the report are as follows:

Aircraft Accessory Turbine Department

C.C. Christianson
J.H. Russell
J.M. Shinn
M.D. Marvin
J.P. Dankese

General Engineering Laboratory

R.L. Maul
W.R. Oney
S. Battone

Electronics Laboratory

D.R. Paynter

4.0   Technical Progress - Internal Voltage Control of Power Sources

4.1   Resume'

During the past reporting period the effort in the power source area
has been devoted to completing various portions of the study. For
example, the investigation of internal methods of fuel cell voltage
control was finished with completion of the investigation of the
effect of various gas compositions and velocities past either the
hydrogen or oxygen electrode. Also the dynamic analysis of both
thermoelectric and thermionic converters was completed. In addition,
the remaining performance data of the switching-series regulating
circuit was determined.

Section 4.2 presents the results of an experimental investigation
concerned with the control of fuel cell output voltage by means of
varying gas composition (reactant plus inert) and gas velocity past
either the hydrogen or oxygen electrode. The results of the study
indicate that such a means of voltage control is feasible; however,
the reduction in fuel cell efficiency at partial loads as well as
the relatively slow transient response will limit the range of
applicability of this method of voltage control.

The results of a dynamic analysis of a typical thermoelectric
generator are presented in section 4.3. The results indicate that
the effective DC internal resistance of a typical generator is
approximately 1.35 times the ohmic resistance. The apparent in-
crease in DC resistance is the result of junction temperature
variation with load. For electrical load disturbances of
frequencies greater than .01 cps, the output impedance of the
generator becomes equal to the ohmic resistance of the generator.

Section 4.4 presents the results of a dynamic analysis of a typical
vapor thermionic generator. In this case the effective DC internal
resistance is approximately four times that obtained from the
volt-ampere curve assuming constant temperature conditions. In
this case also, the apparent increase in DC resistance is due to
the variation in cathode, anode, and cesium reservoir temperature
with load. However, for electrical disturbance frequencies greater
than .01 cps, the output impedance of the generator approaches that
obtained from the slope of the volt-ampere curve for a constant
cathode, anode, and cesium reservoir temperature.

Section 4.5 presents additional weight versus efficiency data for
technique of voltage control by changing the number of sources in
series. In addition, information on volume and design limitations
is also presented. As indicated in previous reports, this technique
of source voltage control appears very desirable, since it has low
weight and high efficiency.

4.2   Fuel Cells

The theory of operation and steady state electrical characteristics of the General Electric ion-exchange membrane fuel cell were presented in progress reports 1 and 2. Preliminary dynamic electrical characteristics have been measured and were presented in progress reports 3 and 4. In addition, progress report 4 presented the results of an experimental investigation of the feasibility of using a grid between the electrodes of an ion-exchange membrane fuel cell for purposes of controlling the output voltage of the cell. The investigation of control of fuel cell output voltage has continued and this report presents the results of an experimental study of control of fuel cell output voltage by varying gas composition and gas velocity at either the hydrogen or oxygen electrode.

4.2.1   Voltage Control by Changing the Gas Composition and Velocity Past the Electrodes

4.2.1.1   Introduction

In the hope of obtaining possible advantages in low system weight and volume, it was decided to evaluate "internal" fuel cell output voltage control schemes. Internal voltage control schemes could include their main parts in with each cell assembly in a compact manner so as to affect the voltage output of the cell by modifying some cell mechanism. The control grid investigation previously reported is an example of the main control element being in the membrane itself while the variation of gas velocity and composition past the electrodes is an example of affecting the mechanism of the cell directly.

The objective of the experimental work included in this report was to determine the feasibility of controlling the G.E. ion-exchange membrane fuel cell output voltage by varying the reactant velocity and composition on both the hydrogen and oxygen electrode. The concept was first presented in progress report no. 1 as indicated by the following quotation:

> "A second possible method of internal voltage control involves controlling the percent of oxygen in the gas supplied to the oxygen electrode. As the percent of oxygen is reduced, the output voltage of the cell reduces at any given current level. This is the result of the lower partial pressure of oxygen at the electrode and is increased if an inert gas blanket is formed in the vicinity of the electrode. For example, in the case of a fuel cell using air at the oxygen electrode, it is no doubt possible to control output voltage by controlling the air flow rate past the oxygen electrode. The transient response of such a method would probably be slow and the range of feasible control is not known. However, it appears desirable to evaluate the feasibility of this method of voltage control in much more detail. Such an evaluation is planned."

These considerations provided the basis for an experimental evaluation of the inert gas concept.

A summary of the procedures used and the results of this experimental work are presented in this report.

4.2.1.2 Summary and Conclusions

An experimental investigation designed to determine the feasibility of controlling the output voltage of a General Electric ion-exchange membrane fuel cell by varying the velocity and composition of the gas supplied to both the hydrogen and oxygen electrodes has been completed. The results of this investigation indicate that the control of fuel cell output voltage by the variation of gas velocity and composition past the electrodes is feasible. The range of voltage control with air at the oxygen electrode or a 20% hydrogen - 80% nitrogen or carbon dioxide mixture at the hydrogen electrode is from 0 volt to a voltage which is about 4% below the dead-ended hydrogen-oxygen voltage level for a given external load. The transient response rate for the hydrogen electrode is approximately .28 volts/sec. while that for the oxygen electrode is about four times this value. With proper design and increased transient velocity, the response rates may be increased appreciably. Below a certain velocity, the decrease in voltage with decrease in velocity is due to "starving" of the electrode while above it, the decrease in voltage with decreased gas velocity is due to decreased rates of diffusion of the reactive gas through a thin liquid film on the catalyst surface.

There is no significant difference between the performance levels with various inert gases (nitrogen, carbon dioxide, helium, and argon).

The control of fuel cell output voltage by partial vacuum operation of the hydrogen and oxygen sides is also possible. However, it does not appear desirable due to the tendency for the electrodes to drown and the slow response time.

Although the results of this investigation show the feasibility of control of output fuel cell voltage by variation of gas velocity past either electrode, the approach has some significant disadvantages. For example, this method is inherently inefficient particularly at partial loads since it achieves voltage control by increasing the cell losses. Thus, if efficiency is important, the approach would not be satisfactory. An additional disadvantage is the relatively slow transient response compared to usual electronic means. These factors will seriously limit the range of applicability of the gas velocity method of voltage control; however, use of the technique in special applications is quite possible.

4.2.1.3 Experimental Procedure

The experimental results were obtained using a cell having a 4" x 4" membrane of the phenolic type. The test setup was arranged such that various gas compositions and velocities could be readily passed

through the hydrogen and oxygen electrode fuel cell compartments.
A fixed resistance electrical load was maintained on the fuel cell
during the testing. Fuel cell output voltage and current were
measured at each steady-state value of gas composition and gas
velocity. The performance of the fuel cell was stable at all gas
velocity conditions. The test results are presented in the following
paragraphs and curves.

4.2.1.4 Results

Oxygen Electrode

The measured output voltages and currents for various gas compositions
and velocities past the oxygen electrode are shown by Figures 4.2-1
through 4.2-3. Figure 4.2-1 shows the behavior with variable velocity
air; Figure 4.2-2 shows the effect of a 50% oxygen - 50% nitrogen
mixture; Figure 4.2-3 shows the behavior with 20% oxygen - 80% helium
mixture. In all cases, volt ampere lines for two velocities of 100%
oxygen past the oxygen electrode are included for reference. The 100%
oxygen, .0036 ft/sec. condition is that corresponding to normal
dead-ended operation of a hydrogen-oxygen cell. The higher velocity
(.037 ft/sec.) 100% oxygen condition yielded a higher cell performance
than true with dead-ended operation. The reasons and significance
of this result will be discussed later.

Although measurements were made only at a single resistive load
condition, estimated volt-ampere curves have been indicated on Figures
4.2-1 through 4.2-3. As shown, the output voltage decreases as the
gas velocity past the oxygen electrode decreases, with the output
voltage approaching zero at zero gas velocity.

The cell output voltage for a constant resistance external load is
shown as a function of gas velocity for various gas compositions
in Figures 4.2-4 through 4.2-6. The external load was .0342 ohm-ft^2,
thus the corresponding cell current density can be obtained by dividing
the cell voltage by .0342. Figure 4.2-4 shows the cell voltage versus
gas velocity for several different gas compositions; Figure 4.2-5
shows the cell voltage versus gas velocity for several mixtures of
oxygen and nitrogen; and Figure 4.2-6 illustrates the cell voltage
versus gas velocity for several different mixtures of oxygen and
helium.

A quantity "R" has been defined as the ratio of the actual (A) oxygen
supplied to the cell at any given condition to the theoretical (T)
oxygen required by the fuel cell at the control point. The control
point is a fuel cell output of about 0.806 volts and 23.5 amps/ft^2 and
approximately corresponds to the dead-ended 100% oxygen operation for the

fixed resistance load used. A value of R less than 1.0 indicates
the cell was being starved of oxygen, whereas a value greater than
1.0 indicates excess oxygen was available.

Figure 4.2-7 indicates the ratio "R" corresponding to various gas
velocities and compositions for the test conditions involved.
Figure 4.2-7a shows the gas velocity required to maintain an R of
1.0 for various percentages of oxygen in the feed gas for the test
points involved. Figure 4.2-7b shows the average pressure and
percent of oxygen in the oxygen electrode compartment for the test
conditions involved. The average was obtained by averaging
the inlet and outlet gas conditions.

Hydrogen Electrode

Tests similar to those conducted on the oxygen side were performed
for the hydrogen side. Mixtures of hydrogen and the inert gases
of nitrogen, helium, carbon dioxide, and argon were studied. The
resultant estimated volt-ampere curves for various gas compositions
and velocities are shown in Figures 4.2-8 and 4.2-11. In all cases,
volt-ampere lines for two velocities of 100% hydrogen past the
hydrogen electrode are included for reference. The 100% hydrogen,
.0034 ft/sec. condition is that corresponding to the normal dead-
ended operation of a hydrogen-oxygen fuel cell.

The cell output voltage for a constant resistance external load is
shown as a function of gas velocity for various gas compositions
in Figures 4.2-12 through 4.2-15. In this case, the external load
corresponded to .0428 ohm-ft^2, thus the cell current density can be
obtained by dividing the cell voltage by .0428.

As is the case of the oxygen electrode, a quantity "R" has been
defined as the ratio of the actual (A) hydrogen supplied to the
cell at any given condition to the theoretical (T) hydrogen required
by the fuel cell at the control point. In this case, the control
point is a fuel cell output of .722 volts and 16.8 amps/ft^2 and
approximately corresponds to the dead-ended 100% hydrogen-oxygen
operation for the fixed resistance load used. The tests involving
the hydrogen electrode were run at a slightly different temperature
and external resistance load than were the oxygen electrode tests.

Figure 4.2-16 shows the ratio "R" corresponding to various gas
velocities and compositions for the test points involved. Figure
4.2-16a shows the gas velocity required to maintain an R of 1.0 for
various percentages of oxygen in the feed gas for the test points used.
Figure 4.2-16b shows the average pressure and percent of hydrogen in
the hydrogen electrode compartment for the test conditions involved.

Transient Response Time

The fuel cell fixture used in the experiments was not designed
primarily for obtaining fast transient response; however, an indication
of the transient response capability could be obtained. The transient
response time was obtained by reducing the velocity of a particular

feed gas composition so that the cell performance decreased to
about 0.40 volt and 10 amps/ft^2 from an initial value of .728
volt and 16.8 amps/ft^2 for a constant resistance external load.
The gas velocity was then increased to the original value (.06 ft/
sec.) and voltage rise with time recorded. In the case of the
hydrogen electrode, the resultant rate of change of voltage was
about 0.28 volts/sec. up to a value of 90% of the final voltage.
For the oxygen electrode the rate of change of voltage was
approximately 0.07 volts/sec. Approximately five additional
seconds were required for the voltage to go from 90% to the final
voltage.

Vacuum Operation

The possibility of control of the output voltage by operating
the cell hydrogen and oxygen pressures at partial vacuums was
also investigated. Operation at two different load conditions
was studied. In both cases, a reduction in output voltage of 15 to
20% was accomplished in changing the gas pressures from atmospheric
to vacuum of approximately 5 inches of mercury. The amount of
voltage reduction was a function of time spent at a point as well
as the magnitude of the vacuum. However, a further increase in
vacuum beyond 5 inches of mercury resulted in a severe and rapid
decrease in cell performance to a low level. When the hydrogen
and oxygen pressures were returned back to zero vacuum, the cell
voltages and currents returned back to those corresponding to the
original dead-ended condition. There was a small overshoot and a
settling time of approximately four minutes.

4.2.1.5 Discussion of Results

Effect of Gas Velocity Upon Output Voltage

The results show the output voltage of the fuel cell can be controlled
by varying the gas velocity of a reactant-inert gas mixture past
either electrode. For gas velocities such that the value of "R" is
less than 1.0, the decrease in cell performance was mainly by starving
the electrode of reactant. At gas velocities where the value of "R"
is greater than 1.0, the change in cell performance is due primarily
to the change in rates of diffusion of reactant to the catalyst
surface due to a change in the thickness of the thin liquid film on
the catalyst surface. Calculations indicate that the thin liquid
film on the catalyst surface is the primary reactant diffusion
barrier. Increasing the gas velocity past the electrode surface
tends to decrease the thickness of this liquid film, thus allowing
greater diffusion of reactant to the catalyst which results in
greater cell output. This is also the explanation for improved
performance in those cases where the undiluted reactant is passed by
the electrode at a finite velocity.

The results also show that a performance nearly equal to that of a
dead-ended hydrogen-oxygen cell could be obtained even with mixtures
of reactant and inert gas providing the velocity past the electrode
is sufficiently high.

Effect of Gas Composition upon Output Voltage

At any given gas velocity, decreasing the percentage of reactant (hydrogen or oxygen) in the gas mixture decreases the output voltage of the cell. Thus, in order to maintain the same output performance the gas velocity past the electrodes would have to be increased. This, of course, is as expected since the total quantity of reactant per unit time supplied to the electrode is the important item, and not the total quantity of gas.

Effect of Type of Inert upon Output Voltage

The type of inert in the gas mixture had little effect upon the output of the cell. This is to be expected since the rate of diffusion of the reactant is primarily dependent upon the partial pressure of reactant, the catalyst liquid film thickness, and the diffusion coefficient of the reactant in the liquid film.

Transient Response Time

The response rate of approximately 0.28 volts/sec. for the hydrogen electrode and .07 volts/sec. for the oxygen electrode is slow, but would be acceptable in some applications where electrical load changes are slow and voltage response is not critical. With proper electrode gas compartment design and greater transient gas velocities, a faster voltage response should be possible; however, the ultimate response capability is not presently known.

Effect of Vacuum Operation Upon Output Voltage

As indicated in the results, experimental control of the output voltage by means of vacuum operation was not very satisfactory. Response rates were slow and beyond vacuums of approximately 5" Hg output deteriorated to a low value. A reasonable explanation for the cell behavior is that the electrodes progressively drowned in the vacuum range. The action of the vacuum was to draw membrane water up the capillaries of the catalyst so that a progressively thicker layer of water formed on the surface of the catalyst. When the pressure was returned to atmospheric the water was forced back into the capillaries and returned the membrane to the original equilibrium conditions as is indicated by the return to the original performance levels.
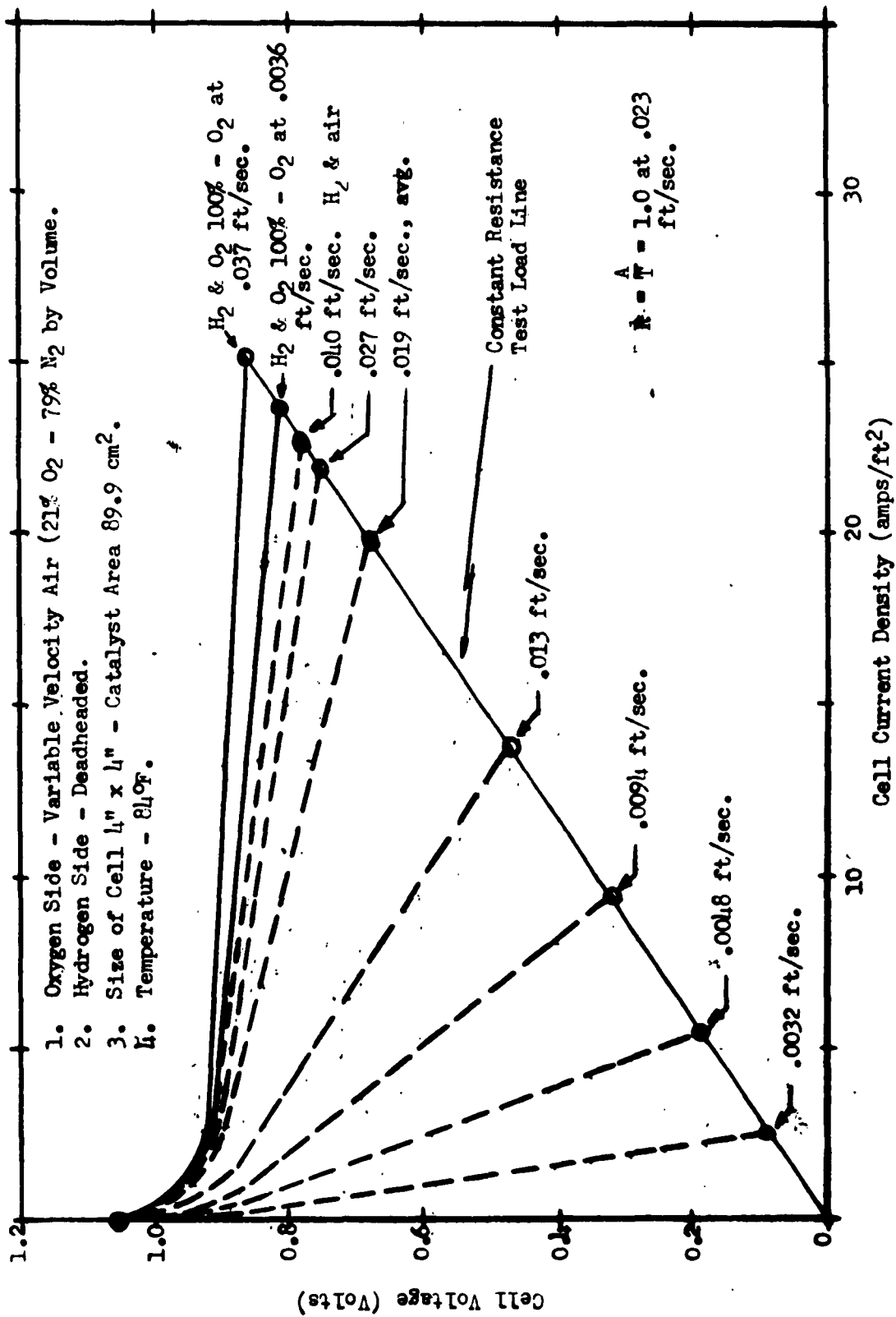
Figure 4.2-1

G.E. Ion Exchange Membrane Fuel Cell

The Effect of Gas Velocity on the Performance of the Fuel Cell
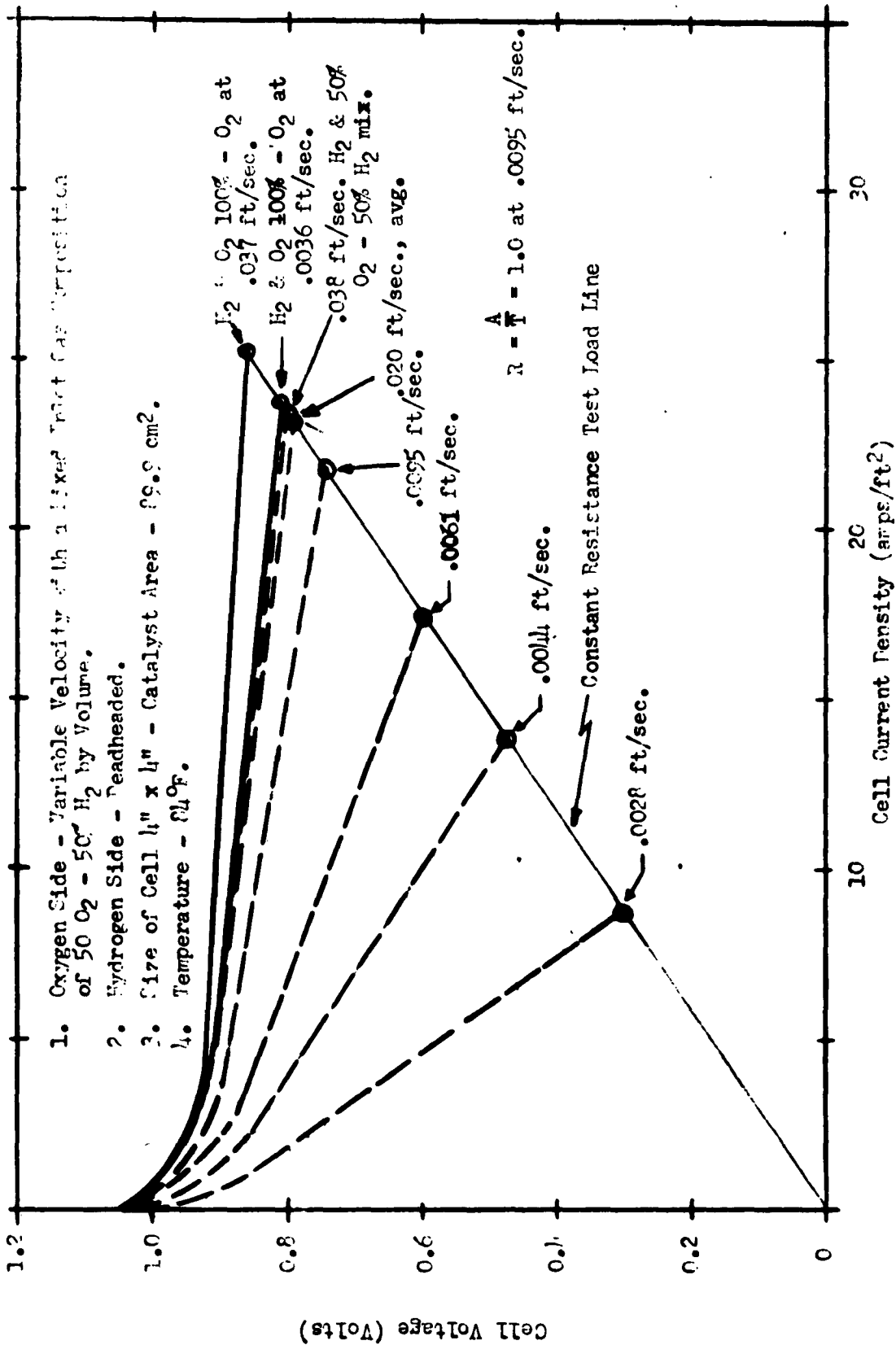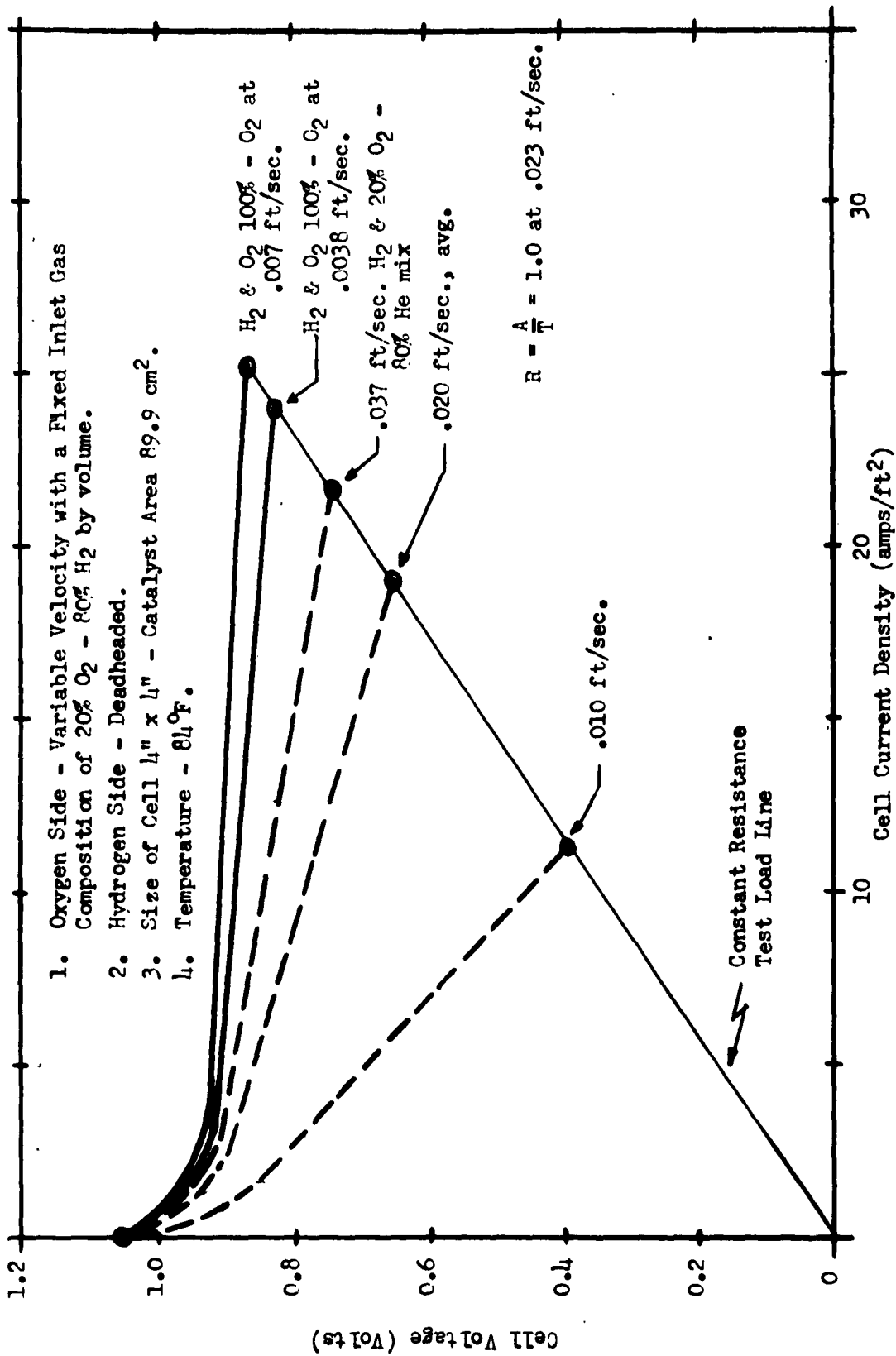with a Constant Resistance External Load

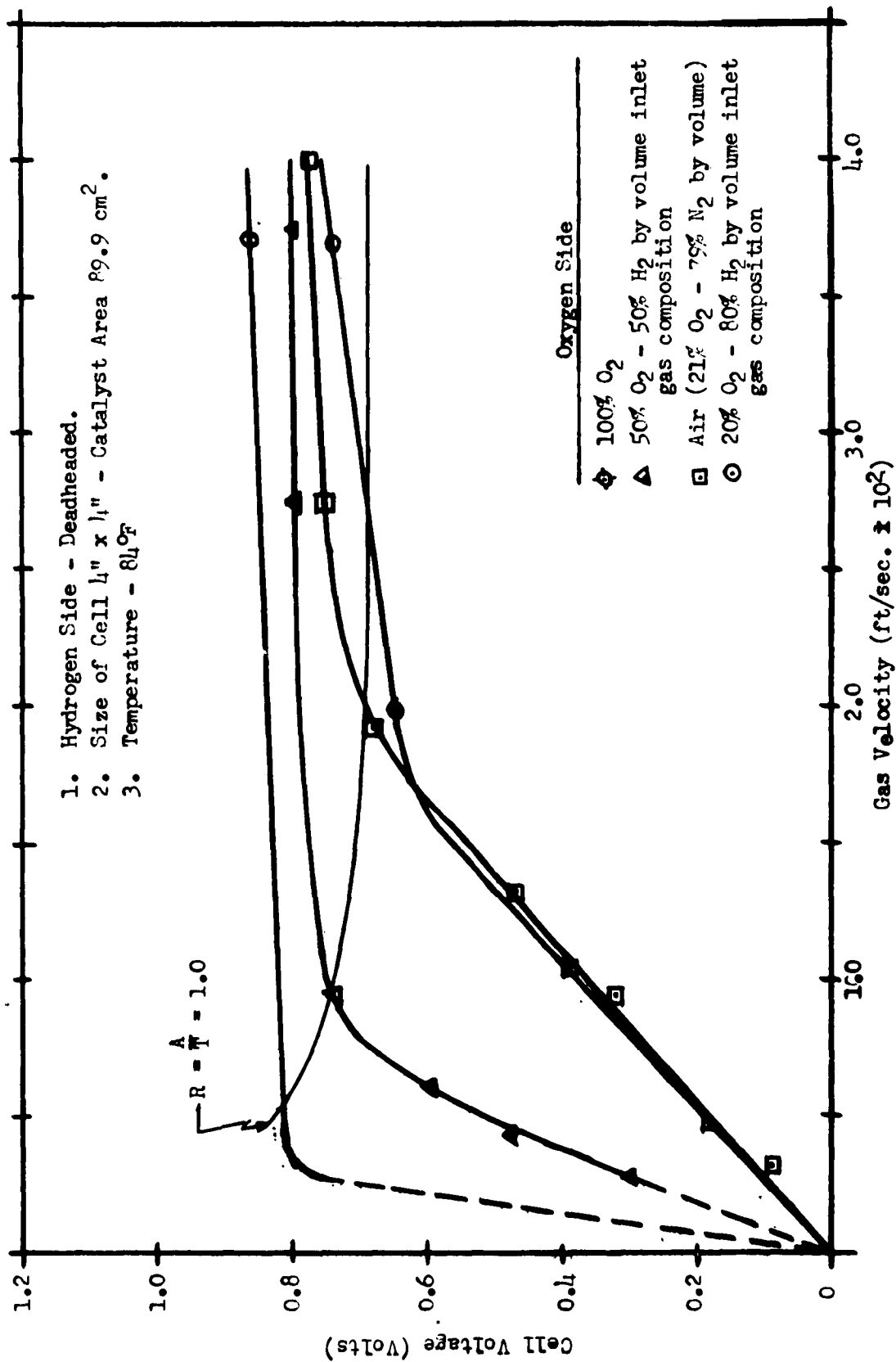1. Oxygen Side - Variable Velocity with a Fixed Inlet Gas Composition of 50 O₂ - 50% H₂ by Volume.
2. Hydrogen Side - Deadheaded.
3. Size of Cell 4" x 4" - Catalyst Area - 89.9 cm².
4. Temperature - 84°F.

H_2 & O_2 100% - O_2 at .037 ft/sec.

H_2 & O_2 100% - O_2 at .0036 ft/sec.

.038 ft/sec. H_2 & 50%
O_2 - 50% H_2 mix.

.020 ft/sec., avg.

.0095 ft/sec.

.0061 ft/sec.

.0044 ft/sec.

$R = \dfrac{A}{E} = 1.0$ at .0095 ft/sec.

Constant Resistance Test Load Line

.0028 ft/sec.

Cell Current Density (amps/ft²)

Figure 4.2-2

G.E. Ion Exchange Membrane Fuel Cell

The Effect of Gas Velocity on the Performance of the Fuel Cell
with a Constant Resistance External Load

Cell Voltage (Volts)

1.2   1.0   0.8   0.6   0.4   0.2   0

10   20   30

1. Oxygen Side – Variable Velocity with a Fixed Inlet Gas Composition of 20% O_2 – 80% H_2 by volume.
2. Hydrogen Side – Deadheaded.
3. Size of Cell 4" x 4" – Catalyst Area 89.9 cm².
4. Temperature – 84°F.

H_2 & O_2 100% – O_2 at .007 ft/sec.

H_2 & O_2 100% – C_2 at .0038 ft/sec.

.037 ft/sec. H_2 & 20% O_2 – 80% He mix

.020 ft/sec., avg.

$R = \frac{A}{I} = 1.0$ at .023 ft/sec.

.010 ft/sec.

Constant Resistance Test Load Line

Cell Current Density (amps/ft²)
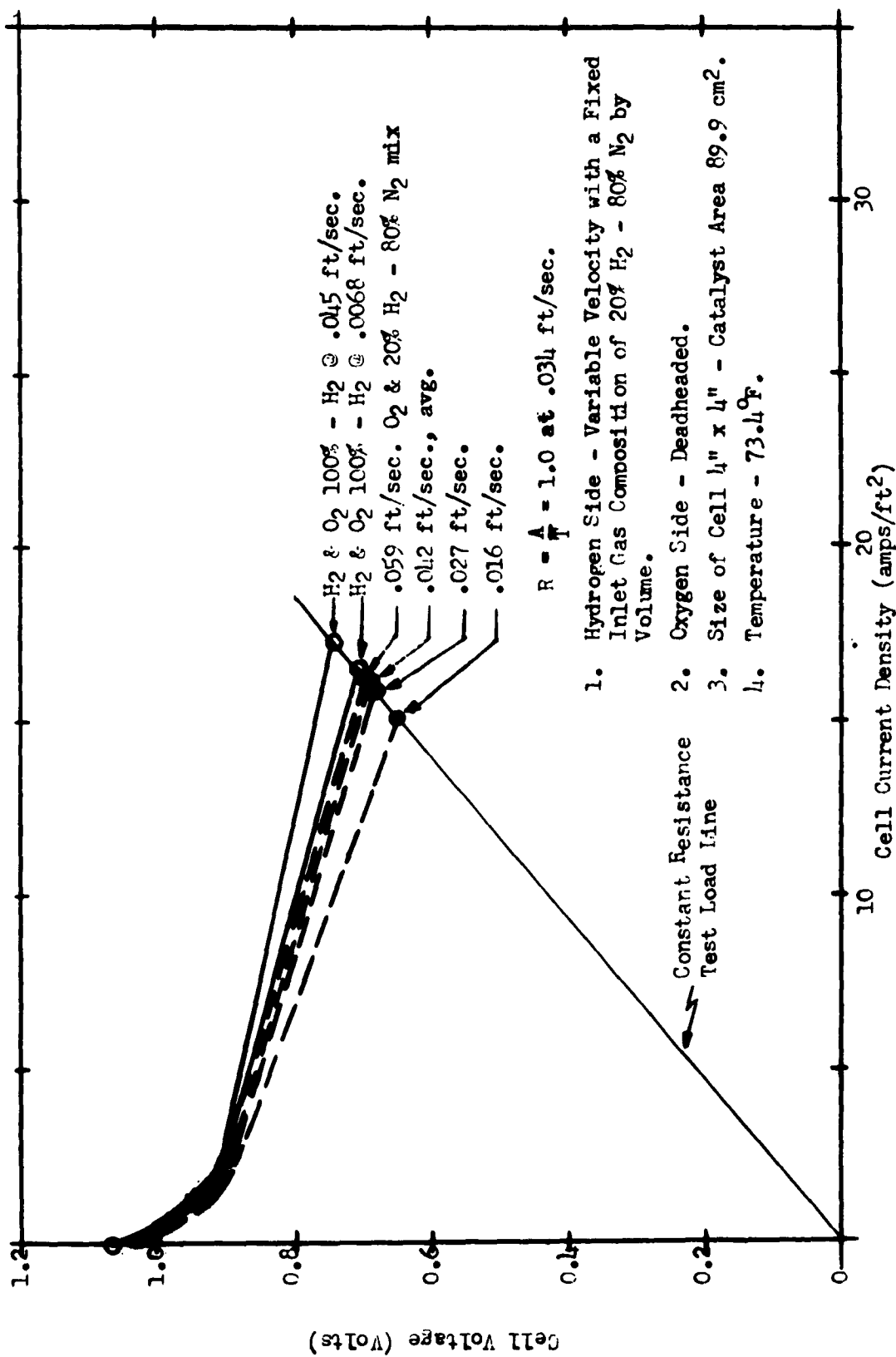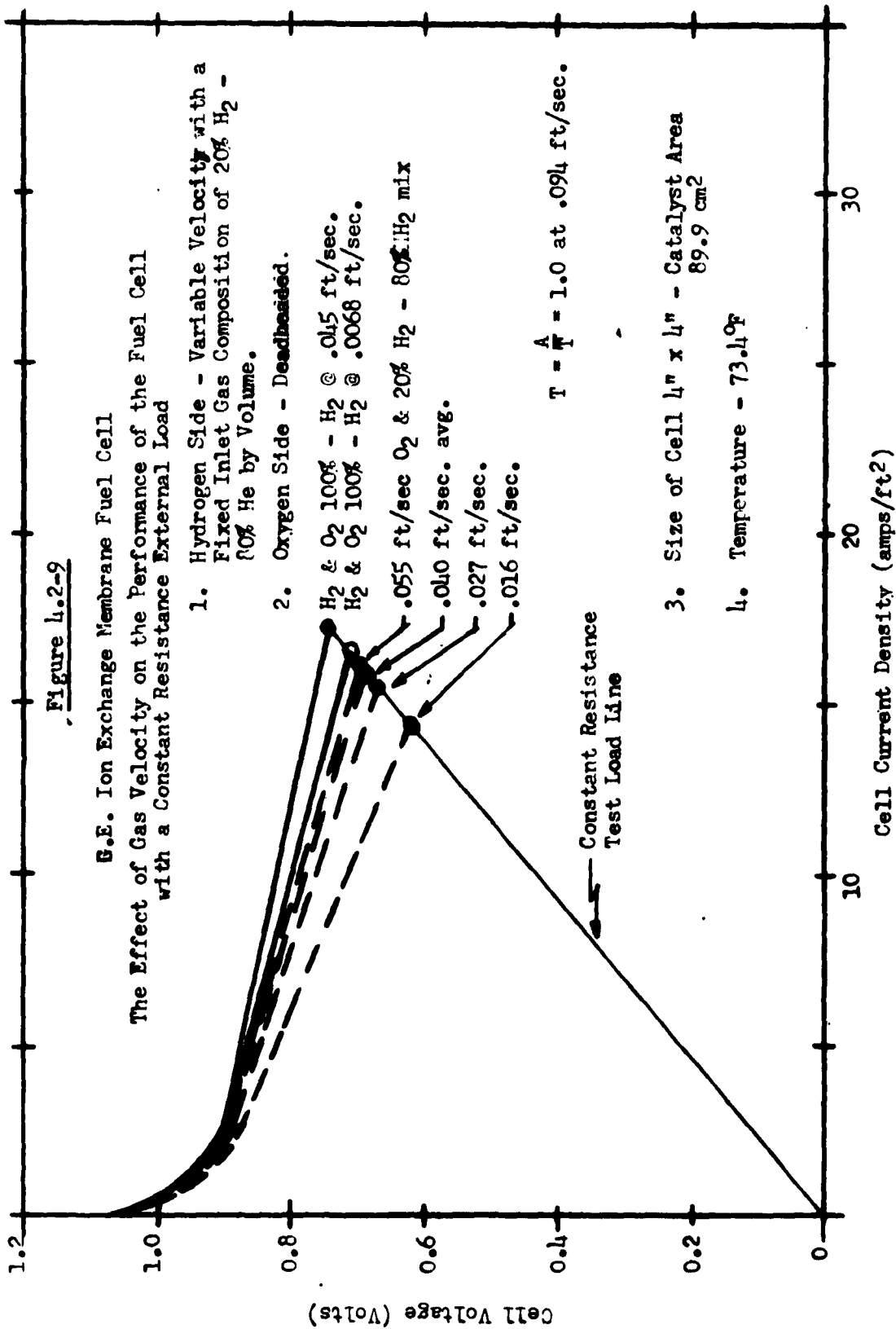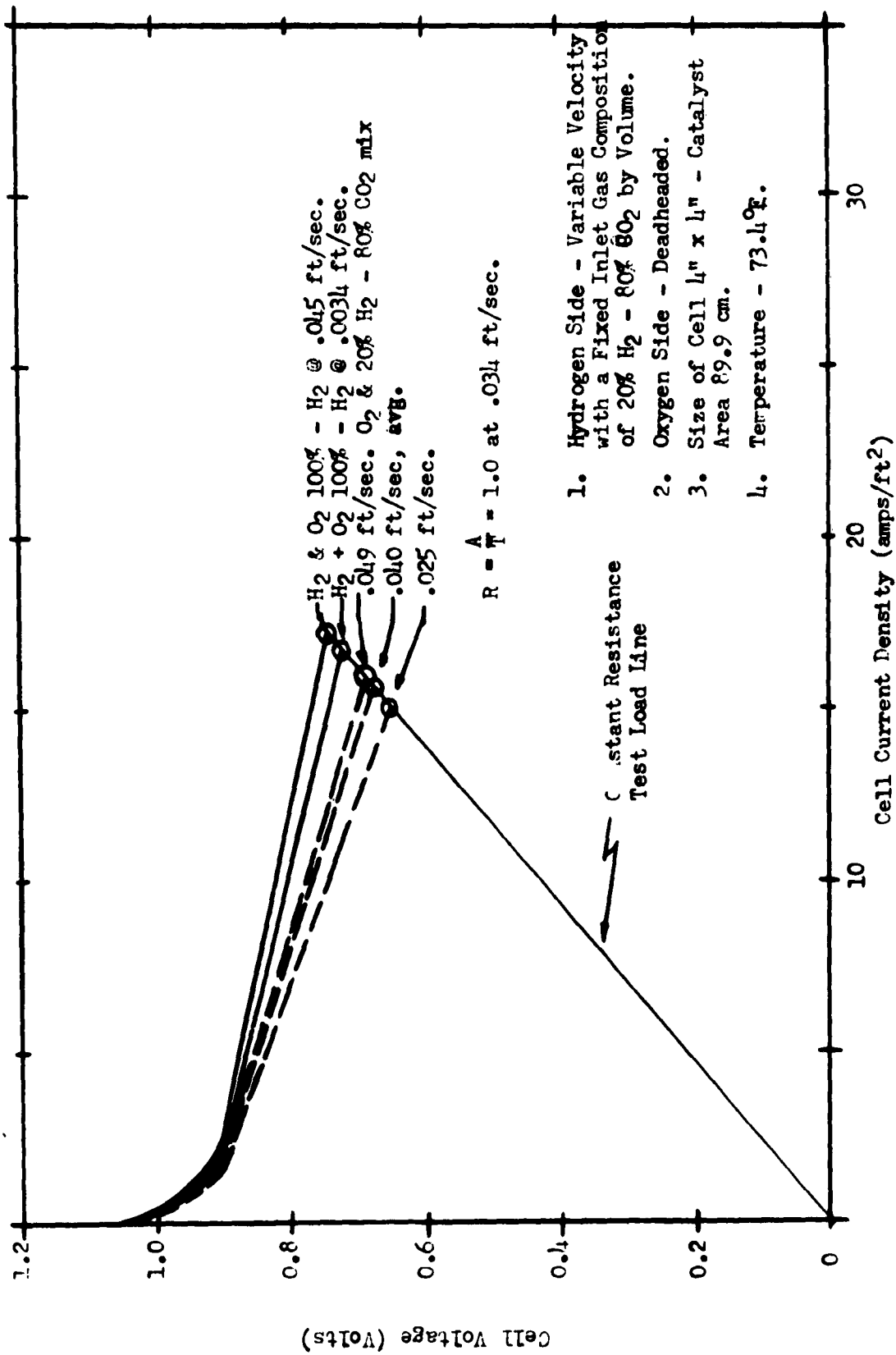
Cell Voltage (Volts)

Figure 4.2-3

The Effect of Gas Velocity on the Performance of the Fuel Cell with a Constant Resistance External Load

G.E. Ion Exchange Membrane Fuel Cell

1. Hydrogen Side - Deadheaded.
2. Size of Cell 4" x 4" - Catalyst Area 89.9 cm^2.
3. Temperature - 84°F

Oxygen Side

◇ 100% O$_2$

◬ 50% O$_2$ - 50% H$_2$ by volume inlet
   gas composition

▣ Air (21% O$_2$ - 79% N$_2$ by volume)

⊙ 20% O$_2$ - 80% H$_2$ by volume inlet
   gas composition

$R = \dfrac{A}{T} = 1.0$

Gas Velocity (ft/sec. x 10^2)

Cell Voltage (Volts)

1.2   1.0   0.8   0.6   0.4   0.2   0

1.0   2.0   3.0   4.0

Figure 4.2-4

G.E. Ion Exchange Membrane Fuel Cell

The Effect of Gas Velocity, Gas Composition and Type of Inert
on the Voltage at a Constant Resistance External Load

- 15 -

Figure 4.2-5

G.E. Ion Exchange Membrane Fuel Cell
The Effect of Gas Composition and Velocity on the Voltage
at a Constant Resistance External Load

1) Hydrogen Side - Deadheaded
2) Size of Cell 4"x4" - Catalyst Area 89.9cm^2
3) Inert Gas is Nitrogen
4) Temperature -80°F

Oxygen Side
% of O_2 in inlet Gas
◇ 100%   ⊙ 21%(Air)
⊡ 75%   ⊘ 19%
▲ 50%   ⊕ 15%
✳ 30%   ▲ 12%
          ✳ 9%

GAS VELOCITY (FT./SEC.x10^2)

CELL VOLTAGE - (VOLTS)
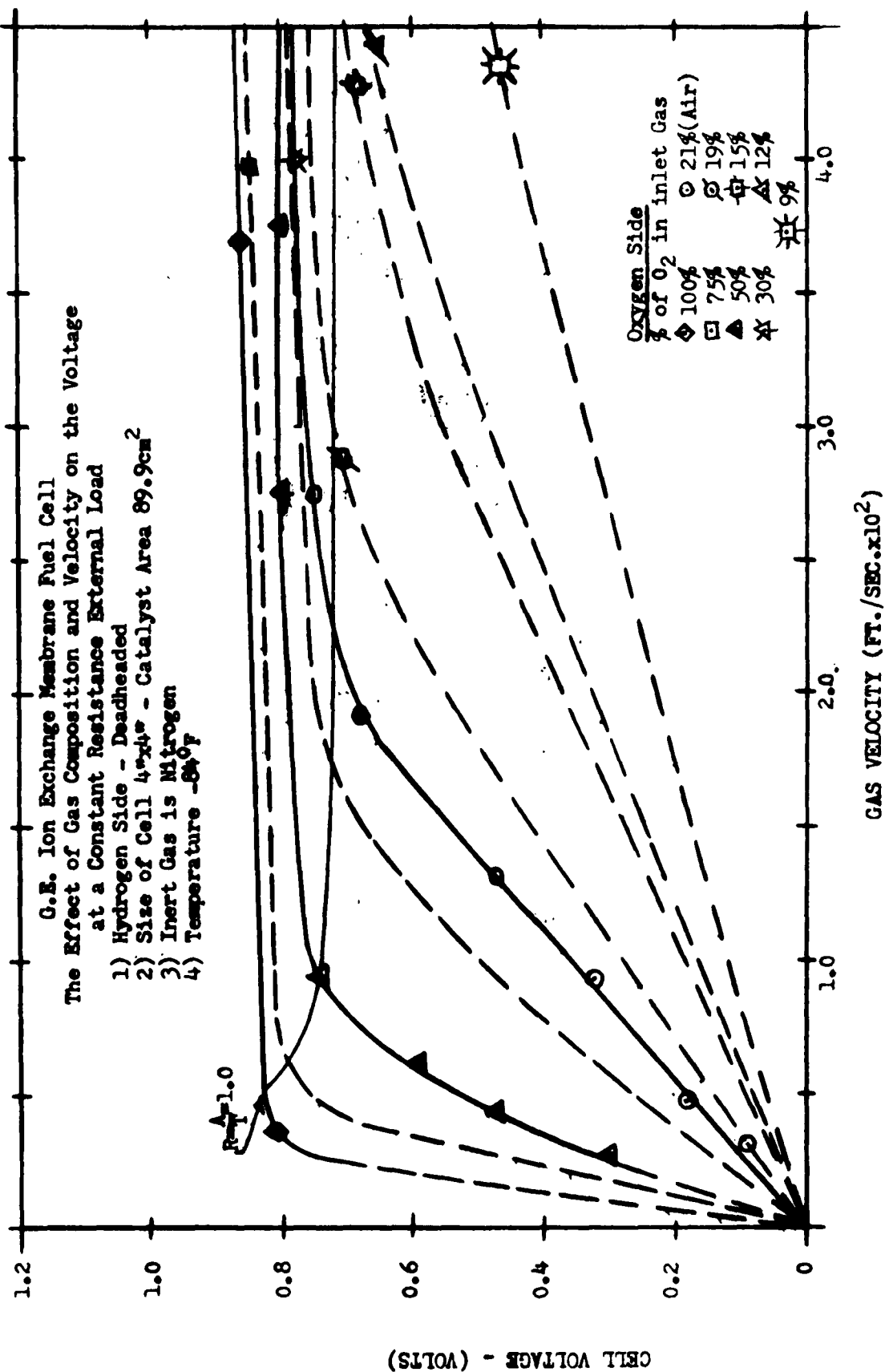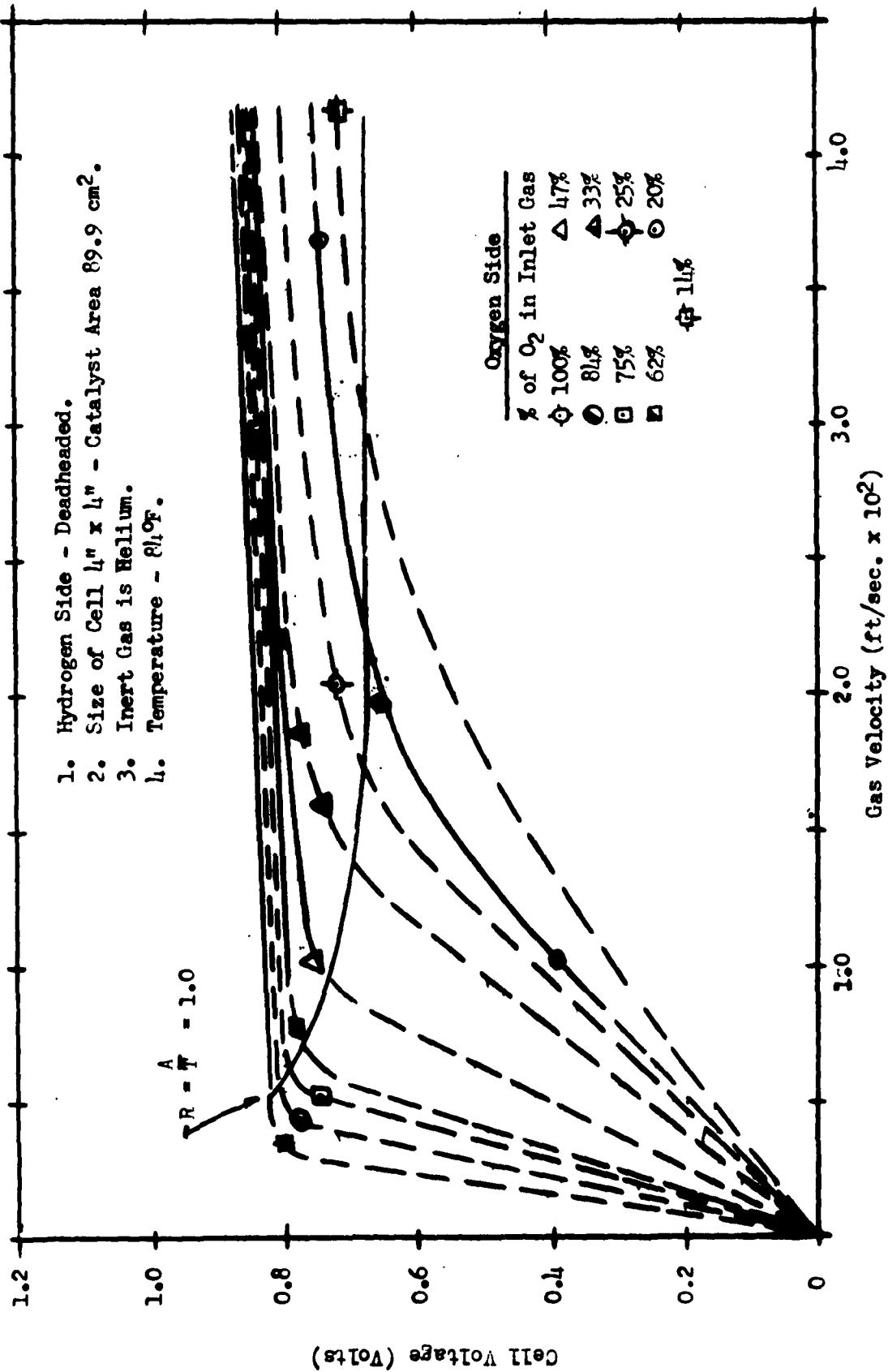
Figure 4.2-6

G.E. Ion Exchange Membrane Fuel Cell

The Effect of Gas Composition and Velocity on the
Voltage at a Constant Resistance External Load

Gas Velocity (ft/sec. x 10^2)
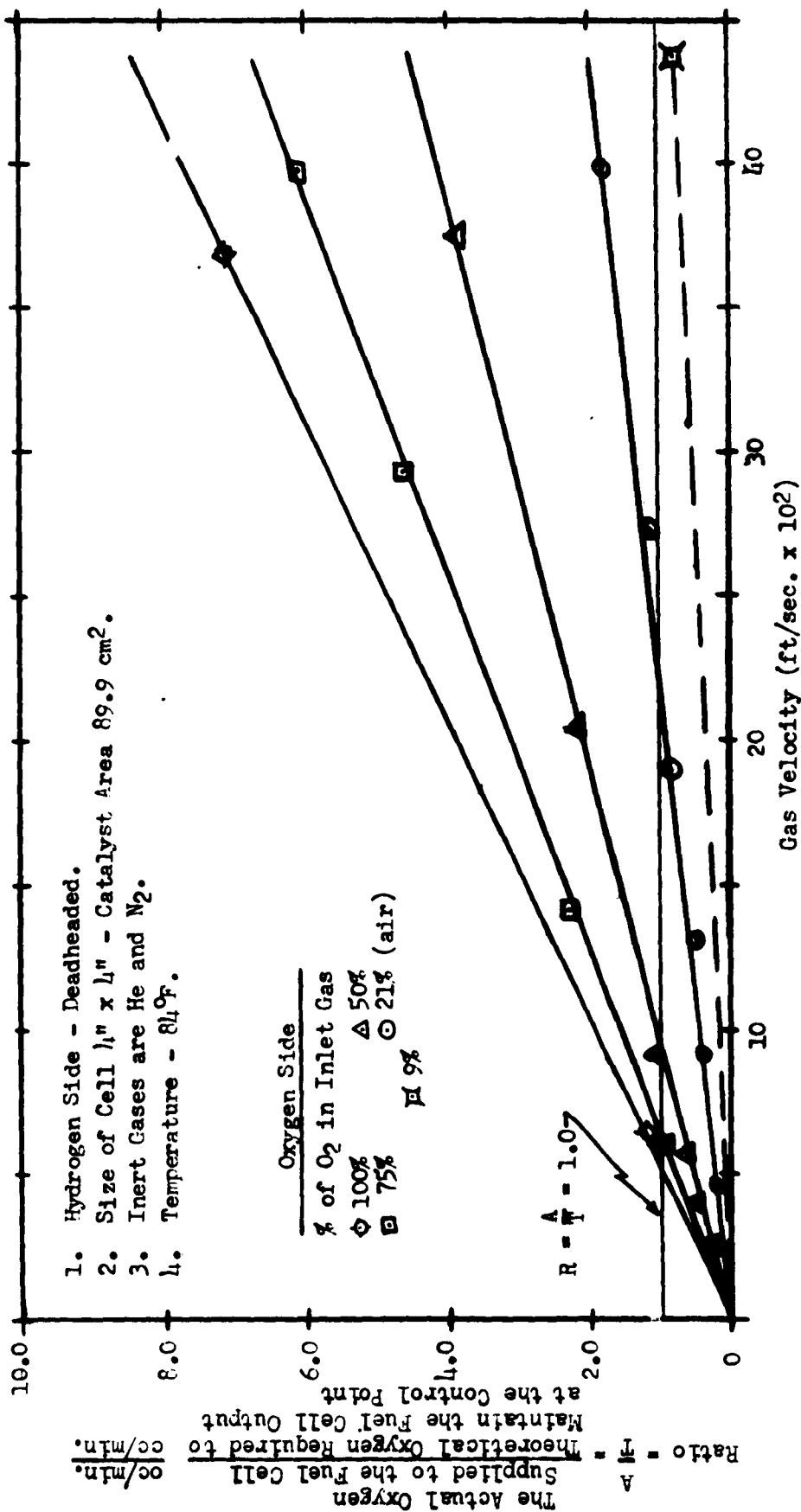
Figure 4.2-7

G.E. Ion Exchange Membrane Fuel Cell

The Effect of Gas Velocity and Composition on the
Excess Oxygen Supplied to the Fuel Cell

1. Hydrogen Side - Deadheaded.
2. Size of Cell 4" x 4" - Catalyst Area 89.9 cm².
3. Inert Gases are He and N_2.
4. Temperature - 84°F.

Oxygen Side
% of O_2 in Inlet Gas
◇ 100%   △ 50%
⊡ 75%   ◻ 9%   ⊙ 21% (air)

$R = \frac{A}{T} = 1.07$

$Ratio = \frac{A}{T} = \frac{The\ Actual\ Oxygen\ Supplied\ to\ the\ Fuel\ Cell\ \ cc/min.}{Theoretical\ Oxygen\ Required\ to\ Maintain\ the\ Fuel\ Cell\ Output\ \ cc/min.}$ at the Control Point

1. Hydrogen Side - Deadheaded.
2. Size of Cell 4" x 4" - Catalyst Area 89.9 cm^2.
3. Inert Gases are He and N$_2$.
4. Temperature - 84°F.

$$V = 0.546 \, (\% \, O_2)^{-1.043}$$

% Oxygen in the Feed Gas Mixture

Gas Velocity (ft/sec. x 10^2)

Figure 4.2-7a

G.E. Ion Exchange Membrane Fuel Cell

The Effect of Feed Gas Composition on the Velocity
Required to Maintain R = A/T = 1.0 for the Control Point
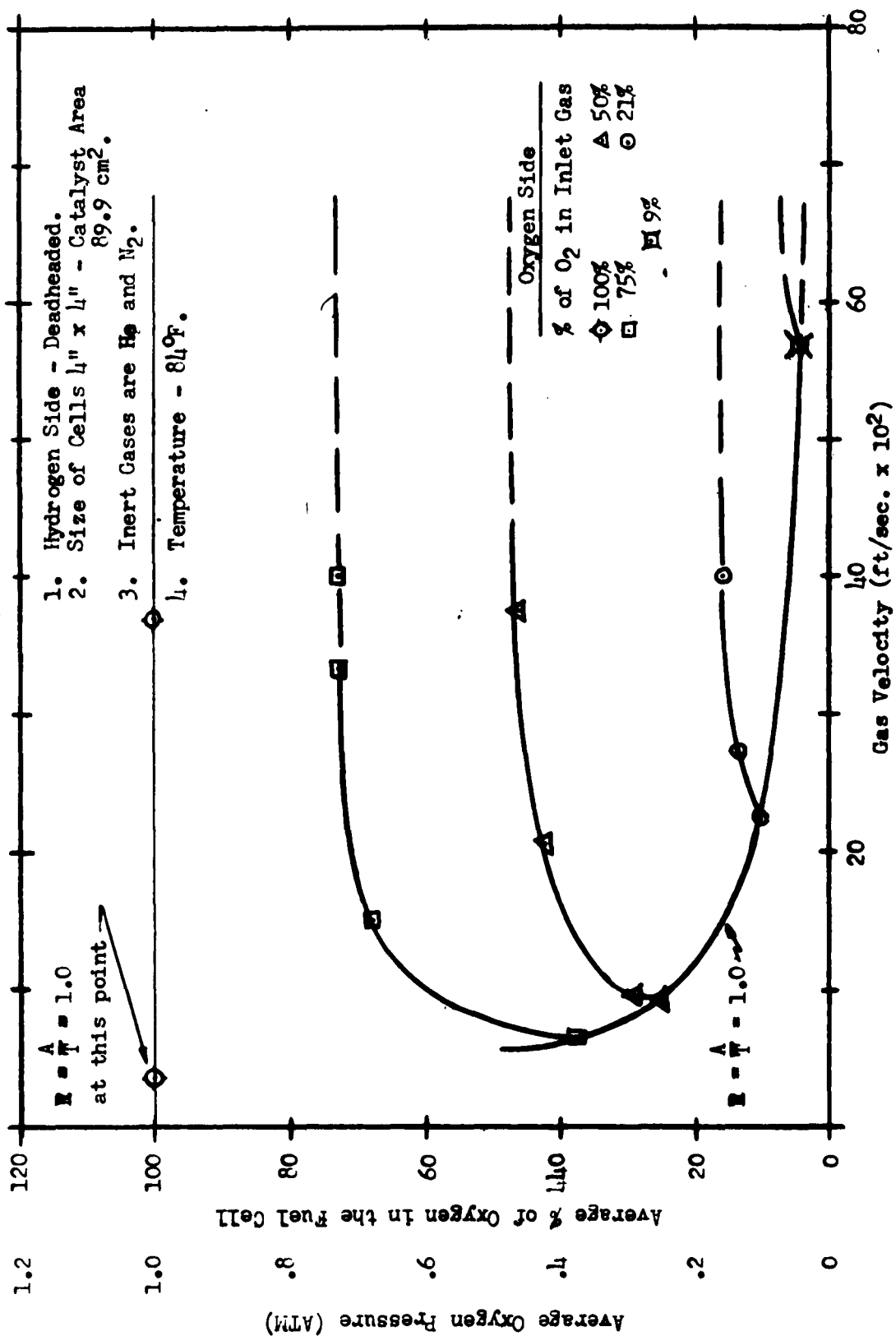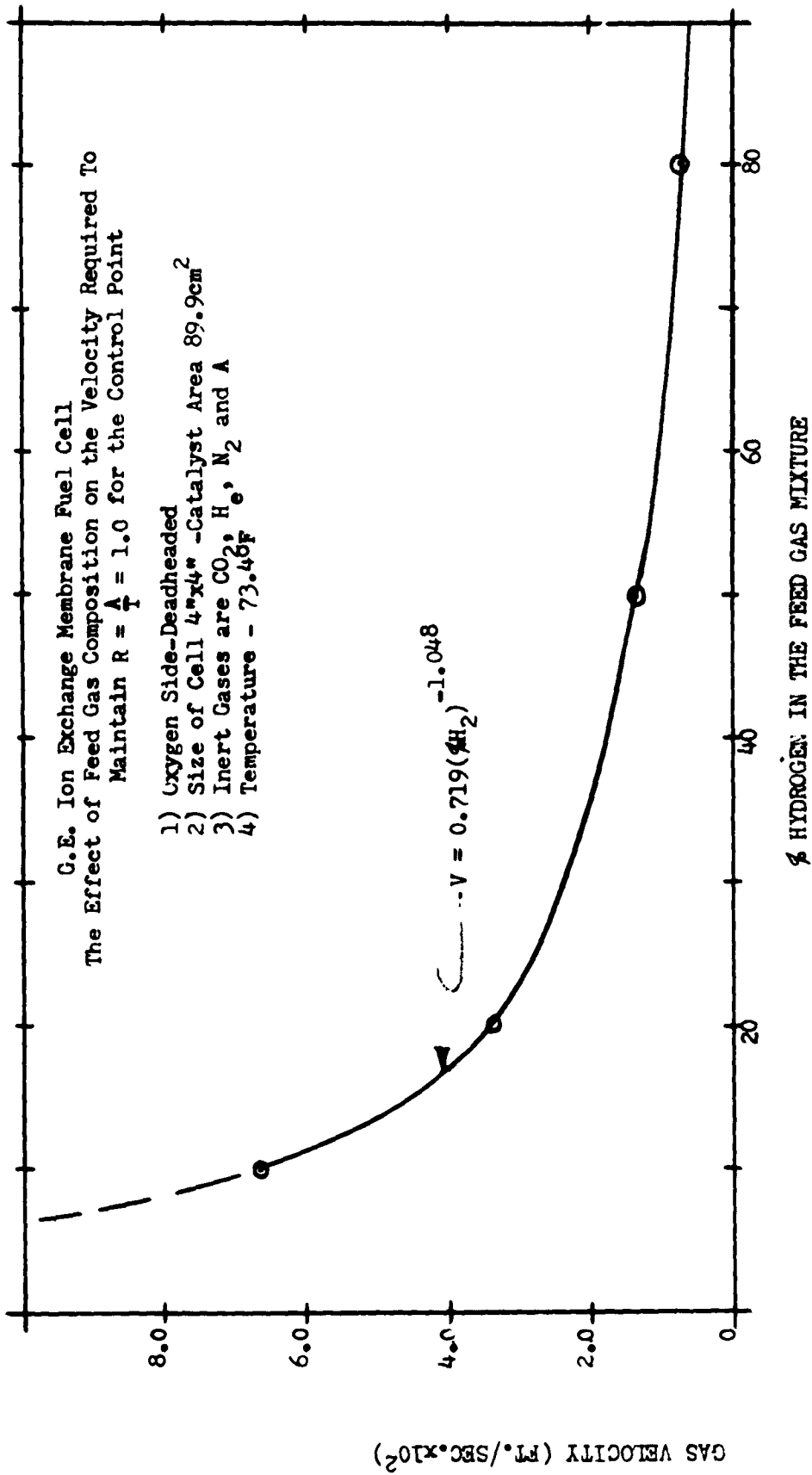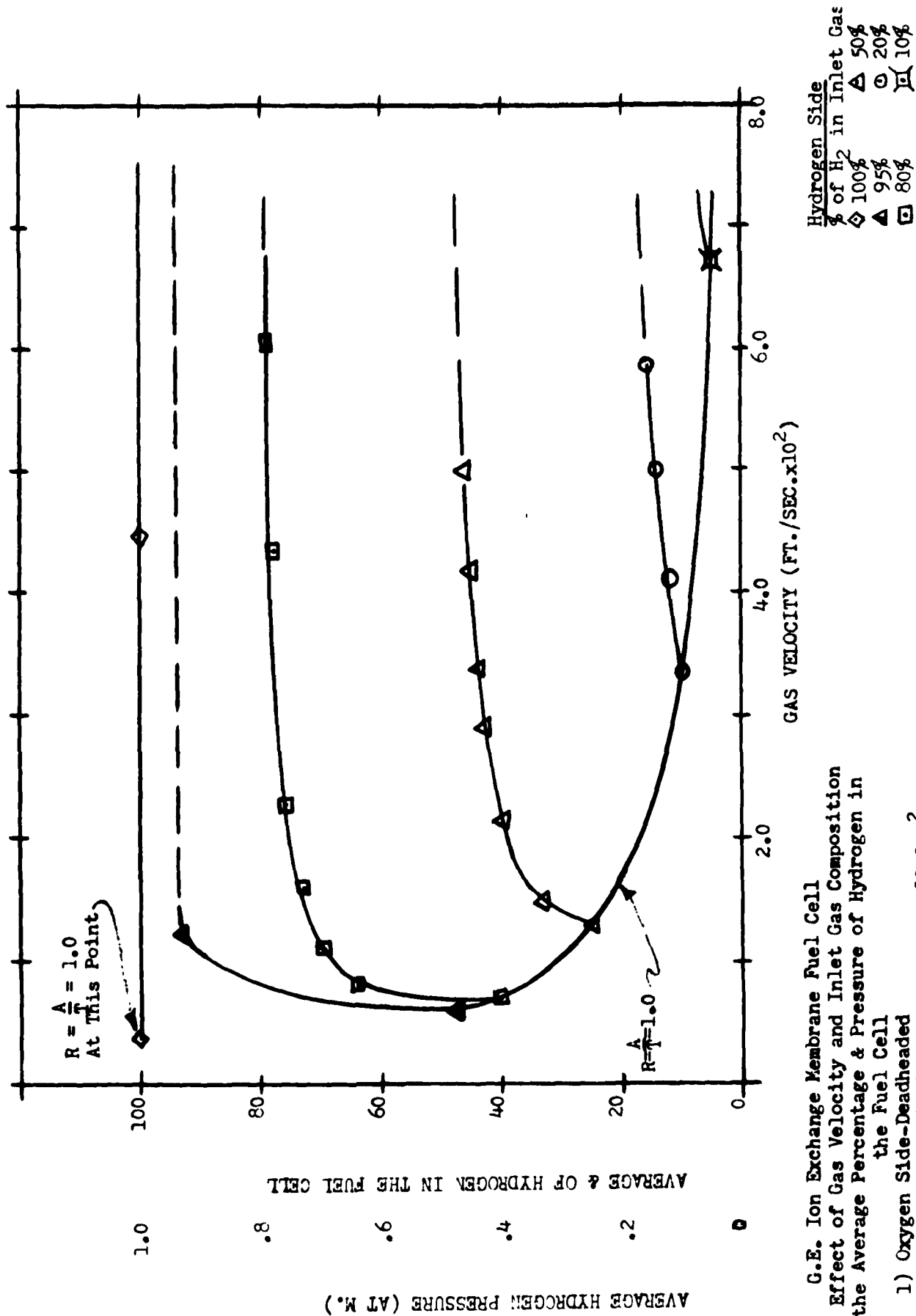
G.E. Ion Exchange Membrane Fuel Cell

Figure 4.2-7b

The Effect of Gas Velocity and Inlet Gas Composition on the
Average Percentage and Pressure of Oxygen in the Fuel Cell

Figure 4.2-8

The Effect of Gas Velocity on the Performance of the Fuel Cell
with a Constant Resistance External Load

G.E. Ion Exchange Membrane Fuel Cell

Figure 4.2-9

G.E. Ion Exchange Membrane Fuel Cell

The Effect of Gas Velocity on the Performance of the Fuel Cell
with a Constant Resistance External Load

1. Hydrogen Side - Variable Velocity with a
   Fixed Inlet Gas Composition of 20% H$_2$ -
   80% He by Volume.

2. Oxygen Side - Deadheaded.

   H$_2$ & O$_2$ 100% - H$_2$ @ .045 ft/sec.
   H$_2$ & O$_2$ 100% - H$_2$ @ .0068 ft/sec.

   .055 ft/sec O$_2$ & 20% H$_2$ - 80% H$_2$ mix
   .040 ft/sec. avg.
   .027 ft/sec.
   .016 ft/sec.

   Constant Resistance
   Test Load line

   $T = \dfrac{A}{T} = 1.0$ at .094 ft/sec.

3. Size of Cell 4" x 4" - Catalyst Area
   89.9 cm^2

4. Temperature - 73.4°F

Cell Current Density (amps/ft^2)

Cell Voltage (Volts)

- 22 -

Figure 4.2-10

The Effect of Gas Velocity on the Performance of the Fuel Cell
with a Constant Resistance External Load

G.E. Ion Exchange Membrane Fuel Cell

Figure 4.2-11

G.E. Ion Exchange Membrane Fuel Cell
The Effect of Gas Velocity on the Performance of the Fuel Cell
With a Constant Resistance External Load

1) Hydrogen Side - Variable Velocity with a Fixed Inlet Gas
   Composition of 50% H_2 - 50% A By Volume
2) Oxygen Side - Deadheaded
3) Size of Cell 4"x4" - Catalyst Area 89.9cm^2
4) Temperature - 73.4°F

$H_2 \& O_2$ 100% -H_2 @ .045 ft./sec.
$H_2 \& O_2$ 100% - H_2 @ .0034 ft./sec.
.042ft./sec. O_2 @ 50% H_2 A Min
.022 ft./sec. avg
.012 ft./sec.

$R = \frac{A}{T} = 1.0$ at .013 ft./sec.

Constant Resistance
Test Load Line

.0058 ft./sec.

CELL CURRENT DENSITY (AMPS./FT.^{2})

CELL VOLTAGE (VOLTS)

Figure 4.2-12

G.E. Ion Exchange Membrane Fuel Cell
The Effect of Gas Velocity Gas Composition and Type of Inert
On the Voltage at a Constant Resistance External Load

1) Oxygen Side-Deadheaded
2) Size of Cell 4"x4" - Catalyst Area 89.9cm^2
3) Temperature - 73.4°F

Hydrogen Side
◇ 100% H$_2$
△ 50% H$_2$ - 50% N$_2$ by volume inlet
   gas composition
▽ 50% H$_2$ - 50% A by volume inlet
   gas composition
⊙ 20% H$_2$ - 80% N$_2$ by volume inlet
   gas composition
⊡ 20% H$_2$ - 80% N$_2$ by volume inlet
   gas composition
⊘ 20% H$_2$ - 80% CO$_2$ by volume inlet
   gas composition

Figure 4.2-13

G.E. Ion Exchange Membrane Fuel Cell
The Effect of Gas Composition and Velocity on the Voltage
At a Constant Resistance External Load

1) Oxygen Side—Deadheaded
2) Size of Cell 4"x4"—Catalyst Area 89.9cm^2
3) Inert Gas is Nitrogen
4) Temperature -73.4°F

Hydrogen Side
◇ 100% H$_2$
▽ 95% H$_2$ - 5% N$_2$ by volume inlet gas composition
□ 80% H$_2$ -20% N$_2$ by volume inlet gas composition
△ 50% H$_2$ - 50% N$_2$ by volume inlet composition
○ 20% H$_2$ - 80% N$_2$ by volume inlet gas composition
⬡ 10% H$_2$ - 90% N$_2$ by volume inlet gas composition

GAS VELOCITY (FT./SEC. x 10^2)

CELL VOLTAGE (VOLTS)

Figure 4.2-14

G.E. Ion Exchange Membrane Fuel Cell
The Effect of Gas Composition and Velocity on the Voltage
At a Constant Resistance External Load

1) Oxygen Side—Deadheaded
2) Size of Cell 4"x4"—Catalyst Area 89.9cm^2
3) Temperature—73.4°F
4) Inert Gas is Helium

Hydrogen Side
◇ 100% H$_2$
□ 80% H$_2$–20% H$_e$ by volume inlet
   gas composition
△ 50% H$_2$–50% H$_e$ by volume inlet
   gas composition
⊙ 20% H$_2$–80% H$_e$ by volume inlet
   gas composition
⊘ 10% H$_2$–90% H$_e$ by volume inlet
   gas composition

$R = \frac{A}{T} = 1.0$

GAS VELOCITY (FT./SEC/x10^2)

CELL VOLTAGE (VOLTS)

Figure 4.2-15

G.E. Ion Exchange Membrane Fuel Cell
The Effect of Gas Composition and Velocity on the Voltage
At a Constant Resistance External Load

1) Oxygen Side - Deadheaded
2) Size of Cell 4"x4"-Catalyst Area 89.9 cm^2
3) Inert Gas is Carbon Dioxide & Argon
4) Temperature - 73.4°F

Hydrogen Side
◇ 100% H_2
▣ 80% H_2-20% CO_2 by volume inlet
   gas composition
▲ 50% H_2-50% CO_2 by volume inlet
   gas composition
▽ 50% H_2-50% A by volume inlet
   gas composition
◉ 20% H_2-80% CO_2 by volume inlet
   gas composition

$R = \frac{A}{T} = 1.0$

CELL VOLTAGE (VOLTS)

1.2   1.0   0.8   0.6   0.4   0.2   0

GAS VELOCITY (Ft./Sec.x10^2)

0   2.0   4.0   6.0   8.0

Figure 4.2-16

G.E. Ion Exchange Membrane Fuel Cell
The Effect of Gas Velocity and Composition on the Excess Hydrogen
Supplied to the Fuel Cell

1.) Oxygen Side-Deadheaded
2.) Size of Cell 4"x4"-Catalyst Area
   89.9 cm^2
3.) Inert Gases are CO_2,Xe,N_2,
   and A.
4.) Temperature -73.4°F

Hydrogen Side
% of H$_2$ in Inlet Gas
◇ 100%   ▲ 50%
⊟ 80%   ⊙ 20%
⋈ 10%

$R= \frac{A}{T} 1.0$

Gas Velocity (Ft./Sec.x10^2)

8.0   6.0   4.0   2.0   0

Output at the control point

$$RATIO= \frac{A}{T} = \frac{\text{The actual hydrogen supplied to the Fuel Cell}}{\text{Theoretical hydrogen req'd to maintain the Fuel Cell}} \quad \frac{cc/min}{cc/min}$$

- 29 -

Figure 4.2-16a

G.E. Ion Exchange Membrane Fuel Cell
The Effect of Feed Gas Composition on the Velocity Required To
Maintain $R = \frac{A}{P} = 1.0$ for the Control Point

1) Oxygen Side—Deadheaded
2) Size of Cell 4"x4" —Catalyst Area 89.9cm^2
3) Inert Gases are CO_2, H_e, N_2 and A
4) Temperature – 73.4°F

$V = 0.719(\%H_2)^{-1.048}$

GAS VELOCITY (FT./SEC.x10^2)

% HYDROGEN IN THE FEED GAS MIXTURE

Figure 4.2-16 b

G.E. Ion Exchange Membrane Fuel Cell
The Effect of Gas Velocity and Inlet Gas Composition
on the Average Percentage & Pressure of Hydrogen in
the Fuel Cell

1) Oxygen Side-Deadheaded
2) Size of Cell 4"x4"-Catalyst Area 89.9cm^2
3) Inert Gases are CO_2, H_e, N_2, and A.
4) Temperature - 73.46°F

Hydrogen Side
% of H_2 in Inlet Gas
◇ 100%   ▲ 50%
▲ 95%   ⊖ 20%
☐ 80%   ⊟ 10%

GAS VELOCITY (FT./SEC.x10^2)

AVERAGE % OF HYDROGEN IN THE FUEL CELL

AVERAGE HYDROGEN PRESSURE (AT M.)

$R = \frac{A}{n} = 1.0$
At This Point

$R = \frac{A}{n} = 1.0$

4.3   Thermoelectrics

The thermoelectric generator studies for this program have centered
around the investigation of static and dynamic characteristics and
means of internal voltage regulation. In Progress Report No. 3
thermoelectric theory was briefly summarized and relations were
presented for efficiency, terminal voltage, and junction temperatures
as a function of current density in the thermoelectric arms. The
analysis included the practical effects of heat source-hot junction
and cold junction-heat sink thermal resistances. In Progress Report
No. 5 possible means of internal voltage regulation were discussed
and the steady state characteristics for such regulation were pre-
sented.

During the present reporting period the dynamic analysis of a thermo-
electric generator was completed. The investigation has been carried
out in two steps. First the high frequency (10 to 10,000 CPS) character-
istics of a couple were measured on a test couple. The results reported
in Progress Report No. 5 indicate insignificant dynamic effects in this
frequency range. Next the low frequency (up to 10 CPS) characteristics
were determined analytically. The method of analysis and typical
numerical results are presented in this report.

4.3.1   Dynamic Characteristics

The dynamic characteristics of the thermoelectric generator are needed
in voltage regulation studies in order to 1) design a generator-external
regulator with minimum coupling problems, and 2) evaluate internal
voltage regulation means. The characteristic of primary interest is
the dynamic impedance of the generator. In a practical generator,
dynamic effects will occur because the thermal impedance of the couples
varies as the electrical load is varied. With finite source and sink
thermal resistances, the variation in couple thermal impedance will
cause a change in the junction temperatures producing a corresponding
change in the open circuit voltage. Increasing the load current lowers
the couple thermal impedance causing the open circuit voltage to drop.
Hence the generator appears to have a higher DC internal resistance
than that of the couples themselves because of the effects of the
source and sink thermal resistances. This effect is shown in Progress
Report No. 3 where the steady state characteristics of a generator
with finite source and sink thermal resistances are shown. When the
electrical load is varied in an oscillatory manner, the junction
temperatures will tend to vary correspondingly. As the frequency
is increased, the amplitude of the junction temperature variations
will diminish because of the thermal inertia of the thermoelectric
elements and the electrical and thermal conductors. At high fre-
quencies the generator resistance will approach the DC resistance
of the couples. The expected dynamic impedance of the generator
thus is a lag-lead characteristic with time constants of the order
of several seconds caused by thermal effects.

- 32 -

4.3.1.1 Analysis

Analytical Approach

A lumped parameter, linearized analysis was used in studying the dynamic characteristics. By careful selection of the analytical model, this means of analysis can provide results with the desired accuracy and with relatively simple expressions for ease of later manipulations. The analytical model used is shown in Figure 4.3-1B and a schematic of the typical generator which it represents is shown in Figure 4.3-1A. Only a single couple is shown; with similar thermoelectric properties the n and p elements behave identically except that current flow and polarities are opposite. For the thermal circuit then the elements are considered to be in parallel. In the analytical model the thermo-electric element mass is assumed to be concentrated midway between the junctions, and the conductors and additional hardware masses are assumed to be concentrated at the respective junctions with the thermoelectric element. Considering the thermoelectric mass is concentrated midway between the junctions was believed to be the most severe assumption in this model so an analysis was also made using a distributed parameter model, Figure 4.3-1C, of the thermoelectric element to check the adequacy of the lumped parameter analysis. These results and the comparison of distributed parameter analysis with the lumped parameter analysis are also presented herein.

In both the distributed and lumped parameter analyses, the analytical results are presented in a partially reduced block diagram form. The final reduction is made in numerical form; the method is illustrated with the numerical example.

Lumped Parameter Analysis

The analysis was made considering the performance of a single couple; the dynamic characteristics of the generator would differ from those of a couple only because of edge effects.

Nomenclature used in the analysis is as follows:

C_c - specific heat, cold conductors and radiator

C_e - specific heat, thermoelectric element

C_h - specific heat, hot conductors and container

I - electrical current

K_e - thermal conductance, junctions to element centers

K_0 - thermal conductance, cold junction to sink

K_s - thermal conductance, hot junction to heat source

M_c - mass, cold conductors and radiator for couple

M_e - mass, thermoelectric elements (n & p)

M_h - mass, hot conductors and container for couple

Q_c - Peltier heat flow at cold junction

Q_h - Peltier heat flow at hot junction

Q_j - Joule heat in element

Q_o - heat flow, cold junction to sink

Q_s - heat flow, source to hot junction

Q_1 - heat conducted into element at hot junction

Q_2 - heat conducted from element at cold junction

R - couple electrical resistance

S - Seebeck coefficient

s - Laplace operator

T_c - cold junction temperature

T_e - element temperatures, lumped mass

T_h - hot junction temerature

T_o - sink temperature

T_s - source temperature

V - terminal voltage

The properties of all materials are assumed constant and the thermo-
electric properties of the n and p elements are assumed the same
except for the polarity of the Seebeck coefficient.

From consideration of Figure 4.3-2 the required relations for the
analysis can be written. These relations and the corresponding
relations in incremental linearized form are as follows:

Basic Equations	Incremental, Linearized Form
$Q_s = K_s(T_s - T_h)$	$\Delta Q_s = K_s(\Delta T_s - \Delta T_h)$
$Q_s = Q_1 + ST_h I + C_h M_h s T_h$	$\Delta Q_s = \Delta Q_1 + ST_h \Delta I + SI\Delta T_h + C_h M_h s \Delta T_h$
$Q_1 = K_e(T_h - T_e)$	$\Delta Q_1 = K_e(\Delta T_h - \Delta T_e)$
$Q_1 + I^2 R = Q_2 + C_e M_e s T_e$	$\Delta Q_1 + 2IR\Delta I = \Delta Q_2 + C_e M_e s \Delta T_e$
$Q_2 = K_e(T_e - T_c)$	$\Delta Q_2 = K_e(\Delta T_e - \Delta T_c)$
$Q_2 + ST_c I = Q_0 + C_c M_c s T_c$	$\Delta Q_2 + ST_c\Delta I + SI\Delta T_c = \Delta Q_0 + C_c M_c s \Delta T_c$
$Q_0 = K_0(T_c - T_0)$	$\Delta Q_0 = K_0(\Delta T_c - \Delta T_0)$
$V = S(T_h - T_c) - RI$	$\Delta V = S(\Delta T_h - \Delta T_c) - R\Delta I$

The final relation shows the terminal voltage to be equal to the open circuit voltage minus the generator IR drop. These equations when combined to give the transfer function from ΔI to ΔV yield the desired result, the dynamic impedance.

The above equations were solved by a combination of block diagram and algebraic manipulations. Figure 4.3-3 shows the initial block diagram of the equations. After partial reduction the block diagram, which will be useful later in the distributed parameter analysis, appears as shown in Figure 4.3-4 where:

$$G_1 = \frac{1}{1 + \tau_e s} \qquad\qquad G_4 = \frac{1}{1 + \tau_e s}$$

$$G_2 = \frac{K_e \tau_e s}{1 + \tau_e s} \qquad\qquad G_5 = \frac{2}{K_e}\frac{\left(1 + \frac{\tau_e}{2} s\right)}{(1 + \tau_e s)}$$

$$G_3 = \frac{2IR}{1 + \tau_e s} \qquad\qquad G_6 = \frac{2IR}{K_e}\frac{1}{(1 + \tau_e s)}$$

and

$$\tau_e = \frac{C_e M_e}{K_e}, \qquad \tau_h = \frac{C_h M_h}{K_e}, \qquad \tau_c = \frac{C_c M_c}{K_0}$$

and

$$G_h = \frac{T_h S}{K_s} - \frac{G_6}{G_5 K_s}, \qquad G_c = -\frac{T_c S}{K_0} + \frac{G_6 G_1}{G_5 K_0} - \frac{G_3}{K_0}$$

After considerable manipulation the final form of the block diagram is outlined as shown in Figure 4.3-5 where the following definitions are used for the parameters:

$$G_{11} = \frac{K_s B}{\Sigma} \qquad\qquad G_{13} = \frac{K_o A}{\Sigma}$$

$$G_{12} = \frac{K_o G_4}{\Sigma\, G_5} \qquad\qquad G_{14} = \frac{K_s G_1}{\Sigma\, G_5}$$

$$\Sigma = AB - \frac{G_1 G_4}{(G_5)^2} \qquad\qquad G_{20} = G_{11}G_{13} - G_{12}G_{14}$$

Here $A = K_s + SI + \dfrac{1}{G_5}$ and $B = K_o - SI + G_2 + \dfrac{G_1 G_4}{G_5}$

From this point the dynamic impedance is obtained by numerical solution after the values for the parameters of the generator of interest are substituted in the block diagram, Figure 4.3-5.

Numerical Results for a Typical Generator

The generator used for these numerical results was described in Progress Report No. 3. Briefly it utilized combustion gases as the heat source and rejects heat by means of a free convection air radiator. The thermoelectric elements are placed in a hermetically sealed module and arranged as shown schematically in Figure 4.3-1A. The numerical values for the constants needed in this analysis are listed below:

$C_c M_c = 4.42$ watt-sec/$^\circ K$ $\qquad\qquad$ $R = 0.0276$ ohms

$C_e M_e = 0.382$ watt-sec/$^\circ K$ $\qquad\qquad$ $S = 0.489 \times 10^{-3}$ volts/$^\circ K$

$C_h M_h = 0.622$ watt-sec/$^\circ K$ $\qquad\qquad$ $T_c = 440^\circ K$

$I = 3.4$ amps $\qquad\qquad$ $T_h = 866^\circ K$

$K_e = 0.0214$ watts/$^\circ K$ $\qquad\qquad$ $T_o = 346^\circ K$

$K_o = 0.058$ watts/$^\circ K$ $\qquad\qquad$ $T_s = 2200^\circ K$

$K_s = 0.00437$ watts/$^\circ K$

The constants are for a single couple. Values for I, T_h, and T_c are the nominal values about which the increments occur; these represent the design point which is approximated the maximum efficiency point as described in Progress Report No. 3.

These constants were used to calculate the parameters shown in the block diagram, Figure 4.3-5. Figure 4.3-6 shows the block diagram after the numerical substitution. In this substitution H_1 and H_2 are approximations determined from Bode plots of H_1 and H_2 circuits as shown in Figure 4.3-5. The feedback paths $\tau_h s$ and $\tau_c s$ (Figure 4.3-5) virtually eliminate the dynamics of the forward paths and therefore produce transfer functions with a single lag. An exact calculation revealed that the approximations were quite good. These values of H_1 and H_2 were used in calculating the numerical values of H_3, H_4, H_5 and H_6 which are shown in Figure 4.3-6. In order to keep the problem from getting unreasonably complex, additional approximations were made for H_3, H_4, H_5 and H_6. In evaluating H_3, Bode plots showed

$$H_3 = \frac{1}{\dfrac{(1 + 36s)}{0.265} - \dfrac{0.394(1 + 19s)^2}{(1 + 8.9s)^2 (1 + 9.4s)^2 (1 + 64s)}} \approx \frac{1}{3.77(1 + 36s) - \dfrac{0.394}{(1 + 64s}}$$

and

$$H_3 \approx \frac{0.295}{(1 + 40s)}$$

both to be good approximations. Similar approximations were made for H_4 and are as follows:

$$H_4 = \frac{1}{\dfrac{(1 + 64s)}{0.867} - \dfrac{0.118(1 + 19s)^2}{(1 + 8.9s)^2 (1 + 9.4s)^2 (1 + 36s)}} \approx \frac{1}{1.15(1 + 64s) - \dfrac{0.118}{(1 + 36s)}}$$

and

$$H_4 \approx \frac{0.970}{(1 + 72s)}$$

Approximations made for H_5 and H_6 are as follows:

$$H_5 = 1 - \frac{0.160(1 + 19s)}{(1 + 8.9s)(1 + 9.4s)(1 + 64s)} - \frac{0.840(1 + 6.5s)(1 + 11s)(1 + 66s)}{(1 + 8.9s)(1 + 9.4s)(1 + 64s)}$$

$$H_5 \approx 0.839$$

$$H_6 = 1 - \frac{0.649(1 + 19s)}{(1 + 8.9s)(1 + 9.4s)(1 + 36s)} - \frac{0.360(1 + 8.4s)(1 + 10s)(1 + 102s)}{(1 + 8.9s)(1 + 9.4s)(1 + 36s)}$$

$$H_6 \simeq 0.351 \frac{(1 + 102s)}{(1 + 36s)}$$

The lead and lag time constants in both G_b and G_c (Figure 4.3-6) are so close to each other that they contribute little dynamics and thus were assumed as simple gain terms. With these approximations the block diagram is easily reduced to the final form in the following manner:
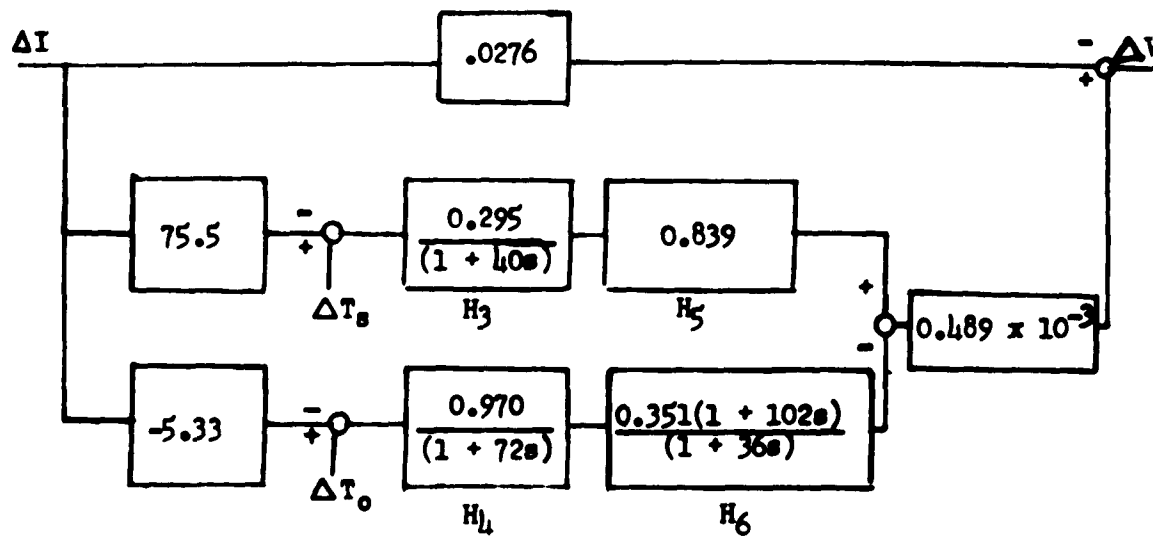
At this point the denominator of H_6 was assumed equal to the denominator of H_3 and after further combination the block diagram becomes:
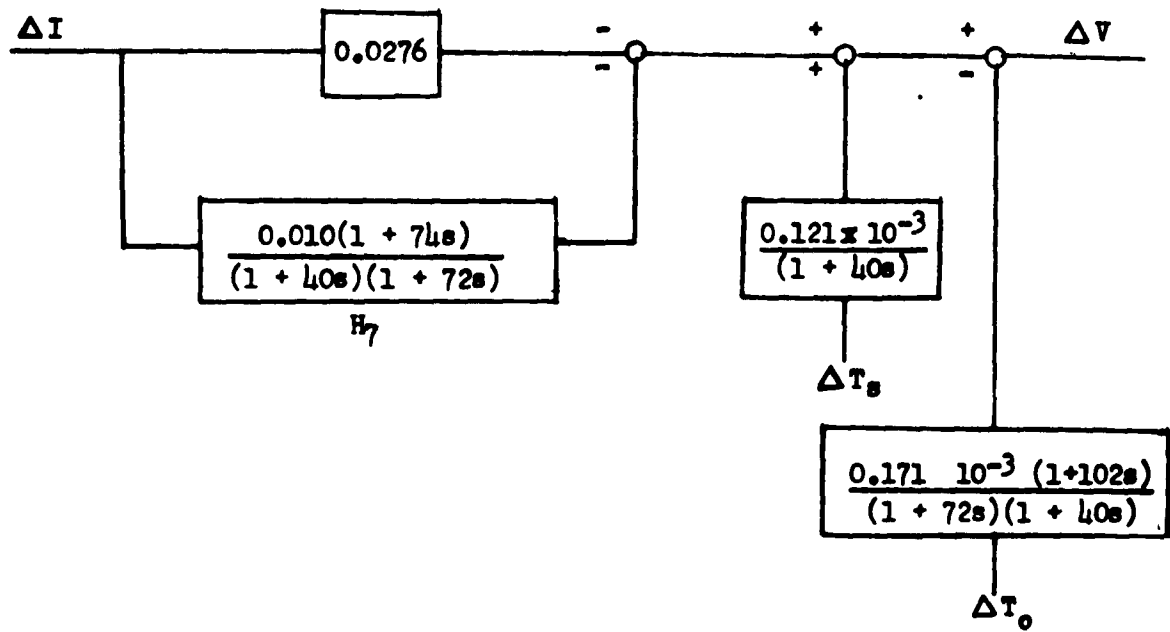
The feed forward term, H_7, was then approximated by:

$$\frac{0.010}{(1 + 40s)}$$

and the resultant block diagram becomes:
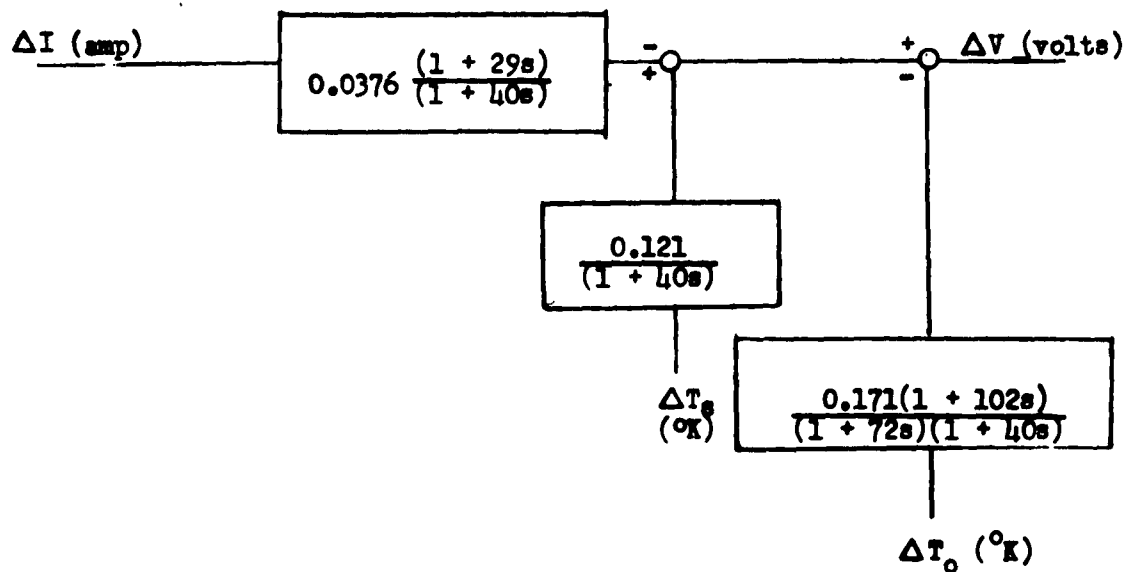
In terms of current density, $J = I/a$, the electrical dynamic impedance is:
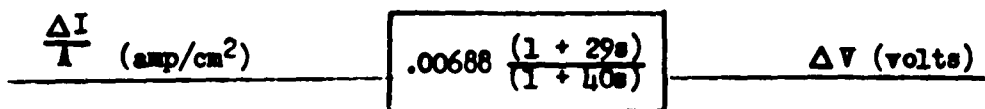
Distributed Parameter Analysis

This analysis considers heat storage and Joule heating to occur continuously along thermoelectric elements. The conductors are assumed to be point storage elements. Differential equations are written for a differential length along the thermoelectric elements as shown in Figure 4.3-7A and the solution of these equations provides distributed parameter analytical expressions for the parameters G_1, G_2, G_4 and G_5 of Figure 4.3-4 and for G_3 and G_6 which appears in G_h and G_c. From this point the analysis proceeds just as described above except that appropriate numerical values are used for the distributed parameter terms. A comparison of the dynamic impedances calculated by the two methods was made to determine the adequacy of the lumped parameter analysis and is presented in the next section.

The thermal circuit for the differential length of the thermoelectric elements is shown in Figure 4.3-7B where $dK_e = k \cdot a/dx$, $d(C_e M_e) = C_e w \cdot a \cdot dx$, and $d(I^2 R) = I^2 \rho dx/a$. In the above expressions k is the material thermal conductivity, w the material density, and ρ the resistivity. Summation of heat flow at the node "a" provides one relation:

$$(1) \qquad -\frac{\partial Q}{\partial x} = C_e w a \frac{\partial T}{\partial t} - \frac{I^2 \rho}{a}$$

and an expression for temperature change along the element provides the second relation:

$$(2) \qquad \frac{\partial T}{\partial x} = -\frac{Q}{ka}$$

Next equation (2) was operated on with $\frac{\partial}{\partial x}$ and substituted in equation (1) to get:

$$(3) \qquad \frac{\partial^2 T}{\partial x^2} = \frac{cw}{k} \frac{\partial T}{\partial t} - \frac{I^2 \rho}{ka^2}$$

Taking $\partial/\partial x$ of equation (1) and $\partial/\partial t$ of equation (2) and combining the resulting equations gives:

$$(4) \qquad \frac{\partial^2 Q}{\partial x^2} = \frac{cw}{k} \frac{\partial Q}{\partial t}$$

Equations (3) and (4) are linearized to give:

$$(5) \qquad \frac{\partial^2 \Delta T}{\partial x^2} = \frac{1}{\alpha} \frac{\partial \Delta T}{\partial t} - \frac{2\rho I}{ka^2} \Delta I$$

and:

(6) $\dfrac{d^2 \Delta Q}{d x^2} = \dfrac{1}{\alpha} \dfrac{d \Delta Q}{t}$

where:

$\alpha = \dfrac{k}{cw}$

Since the response for sinusoidal oscillation is desired, the following definitions are made:

$\Delta T = \Delta T_e^{j \omega t}$, $\Delta Q = \Delta Q_e^{j \omega t}$, and $\Delta I = \Delta I_e^{j \omega t}$

Substitution into equations (5) and (6) yields:

(7) $\left(D^2 - \dfrac{j \omega}{\alpha} \right) \Delta T = - \dfrac{2 \rho I}{ka^2} \Delta I$

(8) $\left(D^2 - \dfrac{j \omega}{\alpha} \right) \Delta Q = 0$ $\qquad D = \dfrac{d}{dx}$

General solutions to equations (7) and (8) are:

(9) $\Delta T = C_1 e^{\beta x} + C_2 e^{-\beta x} + \dfrac{\delta}{\beta^2} \Delta I$

(10) $\Delta Q = C_3 e^{\beta x} + C_4 e^{-\beta x}$

where $\beta = \sqrt{\dfrac{j \omega}{\alpha}}$ $\qquad$ and $\delta = \dfrac{2 \rho I}{ka^2}$

Here C_1, C_2, and C_3 and C_4 are integration constants. Two of these can be eliminated by substituting equations (9) and (10) into one of the original equations, equation (2) for example, to get:

(11) $C_1 = - \dfrac{C_3}{\zeta}$ and $C_2 = \dfrac{C_4}{\zeta}$; $\zeta = \beta ka$

C_3 and C_4 are now evaluated by applying boundary conditions in terms of the independent variables ΔQ, and ΔTc (these can be seen to be input quantities from Figure 4.3-4). Thus:

at $x = 0$, $\Delta Q = \Delta Q_1$ ($x = 0$ at hot junctions)

$x = \ell$, $\Delta T = \Delta T_c$

Substituting these conditions into equations (9) and (10) gives:

$$C_3 = \frac{\Delta Q_1 e^{\beta \ell} - \sigma \Delta T_c + \frac{\sigma \delta}{\beta^2} I}{(e^{\beta \ell} + e^{-\beta \ell})}$$

$$C_4 = \frac{\Delta Q_1 e^{\beta \ell} + \sigma \Delta T_c - \frac{\sigma \delta}{\beta^2} I}{(e^{\beta \ell} + e^{-\beta \ell})}$$

Equations (9) and (10) with the above definitions for the integration constants are the general expressions for ΔQ and ΔT and are now used to determine the dependent variables ΔT_h and ΔQ_2. Applying the conditions that:

$$\Delta T = \Delta T_h \text{ at } x = 0$$

and

$$\Delta Q = \Delta Q_2 \text{ at } x = \ell$$

the results of the distributed parameter analysis are:

(11) $\Delta Q_2 = G_1 \Delta Q_1 + G_2 \Delta T_c + G_3 \angle I$

(12) $\Delta T_h = G_4 \Delta T_c + G_5 \Delta Q_1 + G_6 \angle I$

where:

$G_1 = \dfrac{1}{\cosh \beta L}$ $G_4 = \dfrac{1}{\cosh \beta L}$

$G_2 = \sigma \tanh \beta \ell$ $G_5 = \dfrac{\tanh \beta \ell}{\sigma}$

$G_3 = \dfrac{\sigma \delta \tanh \beta \ell}{\beta^2}$ $G_6 = \dfrac{\delta}{\beta^2}\left(1 - \dfrac{1}{\cosh \beta L}\right)$

- 43 -

These constants are more convenient to use in the numerical reduction which is to follow if the hyperbolic functions are in the following form of factored infinite series:

$$G_1 = G_4 = \frac{1}{(1 + \tau s)\left(1 + \frac{\tau s}{9}\right)\left(1 + \frac{\tau s}{25}\right) \cdots (1 + \tau_n s) \cdots}$$

where: $\quad \tau = \frac{8}{\pi^2} \frac{C_e M_e}{k_e} \qquad \tau_n = \frac{\tau}{(2n + 1)^2}$

$$n = 0, 1, 2, 3 \cdots \infty$$

$$G_2 = \frac{C_e M_e s \left(1 + \frac{\tau s}{4}\right)\left(1 + \frac{\tau s}{16}\right) \cdots (1 + \tau_m s)}{(1 + \tau s)\left(1 + \frac{\tau s}{9}\right)\left(1 + \frac{\tau s}{25}\right) \cdots (1 + \tau_n s)}$$

$$\tau_m = \frac{\tau}{(2m)^2}$$

$$n = 1, 2, 3 \cdots \infty.$$

$$G_3 = \frac{2IR \left(1 + \frac{\tau s}{4}\right)\left(1 + \frac{\tau s}{16}\right) \cdots (1 + \tau_m s)}{(1 + \tau s)\left(1 + \frac{\tau s}{9}\right)\left(1 + \frac{\tau s}{25}\right) \cdots (1 + \tau_n s)}$$

$$G_5 = \frac{2}{k_e} \frac{\left(1 + \frac{\tau s}{4}\right)\left(1 + \frac{\tau s}{16}\right) \cdots (1 + \tau_m s)}{(1 + \tau s)\left(1 + \frac{\tau s}{9}\right)\left(1 + \frac{\tau s}{25}\right) \cdots (1 + \tau_n s)}$$

$$G_6 = \frac{2IR}{k_e} \frac{\left(1 + \frac{\tau s}{16}\right)\left(1 + \frac{\tau s}{64}\right) \cdots (1 + \tau_o s)}{(1 + \tau s)\left(1 + \frac{\tau s}{9}\right)\left(1 + \frac{\tau s}{25}\right) \cdots (1 + \tau_n s)}$$

$$\tau_o = \frac{\tau}{(4n)^2}$$

$$n = 1, 2, 3 \cdots \infty$$

In arriving at this reduction it must be recognized that:

$$R = \frac{\rho \ell}{a} \quad \text{and} \quad k_e = 2\frac{ka}{\ell}$$

Also the Laplace operator, s, has been substituted for $j\omega$.

Further evaluation of constants yields:

$$G_{11} = \frac{Ks\gamma}{D}$$

$$G_{12} = \frac{K_o G_4}{D\, G_5}$$

$$G_{13} = \frac{K_s \delta}{D}$$

$$G_{14} = \frac{Ks\, G_1}{D\, G_5}$$

$$\text{where} \quad D = \gamma\delta - \frac{G_1\, G_4}{(G_5)^2}$$

$$\text{and} \quad \delta = K_s + SI + \frac{1}{G_5}$$

$$\gamma = K_o - SI + G_2 + \frac{G_1 G_4}{G_5}$$

It was found convenient to analytically evaluate the parameters below before numerical substitution is made.

$$\frac{G_{20}}{G_{11}} = \frac{K_o}{\gamma} = \frac{K_o}{K_o - SI + \sigma \coth \beta \ell}$$

$$\frac{G_{20}}{G_{13}} = \frac{K_s}{\delta} = \frac{K_s}{K_s + SI + \sigma \coth \beta \ell}$$

$$\frac{G_{12}}{G_{20}} = \frac{G_4}{K_s G_5}$$

$$\frac{G_{14}}{G_{20}} = \frac{G_1}{K_o G_5}$$

At this point the analytical analysis was ended and the final reduction was done in numerical form.

Numerical Results for Distributed Parameter Analysis

The first step in obtaining a numerical value for the dynamic impedance from the distributed parameter analysis is to evaluate the transfer functions G_h, G_6, H_3, H_4, H_5 and H_6 (Figure 4.3-6). In order to evaluate H_3 and H_4, H_1 and H_2 respectively must be evaluated first (see Figure 4.3-5).

$$H_1 = \quad +\bigcirc- \quad \boxed{\dfrac{G_{20}}{G_{13}}} \qquad \dfrac{G_{20}}{G_{13}} = \dfrac{K_s}{K_s + SI + \coth\beta l}$$

$$\boxed{\tau_h s}$$
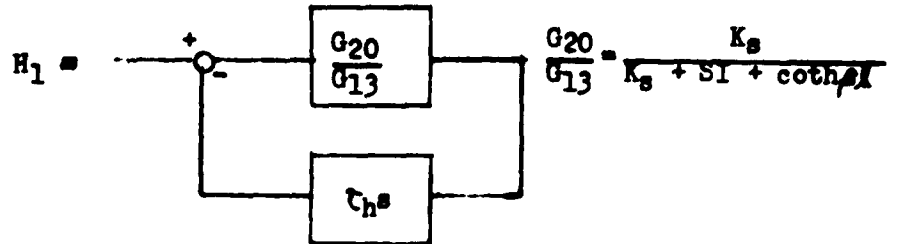
The block diagram is rearranged to:

$$+\bigcirc- \quad \boxed{\dfrac{K_s}{K_s + SI}}$$

$$\boxed{\tau_h s + \dfrac{C}{K_s} \coth\beta l}$$
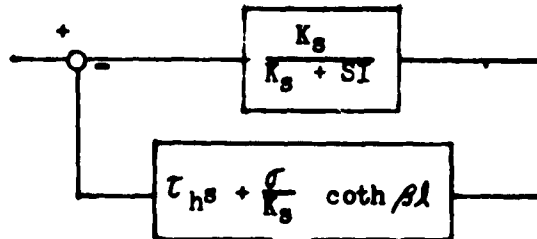
As was shown in the previous section, the hyperbolic term is character-ized by an infinite number of factors or time constants. Both terms in the feedback block are shown in a Bode plot, Figure 4.3-8, which was used to arrive at a simplifying approximation for the feedback block. A criterion was used that is common in control work; i.e., when the spread between two terms on a Bode plot is greater than 20 db (10 to 1), the smaller term can be neglected. From Figure 4.3-8 it can be seen that when this criterion is used only two lead and two lag factors of the hyperbolic term need be considered. With this assumption the combined feedback terms, H, appear as shown below:

$$H_1 = \quad +\bigcirc- \quad \boxed{0.724}\,G$$

$$H$$

$$\boxed{\dfrac{2.45(1 + 69s)(1 + 3.2s)(1 + .85s)}{(1 + 3.6s)(1 + .91s)}}$$
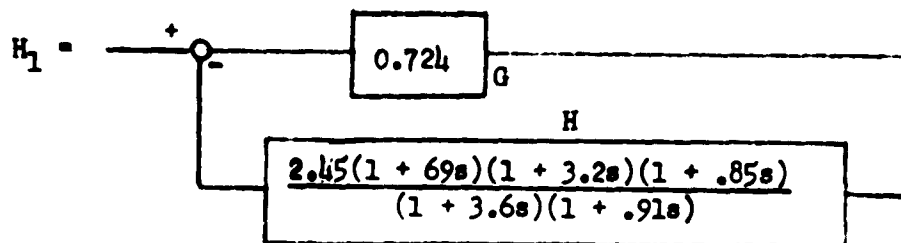
The general solution for this diagram is:

$$\frac{G}{1 + GH}$$

where G is the feed-forward term and H is the feedback term. The above 20 db criterion again was applied to this reduction. This can be accomplished by comparing the magnitude of GH with unity on a Bode plot. Figure 4.3-9 is a sketch of the plot which shows that only the first lead term in the feedback block is of significance. H_3 at this point then appears as:
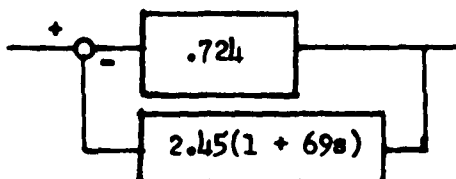
which is readily reduced to:

$$H_1 = \frac{0.265}{(1 + 45s)}$$

From Figure 4.3-6 it can be seen that the H_3 transfer function is:
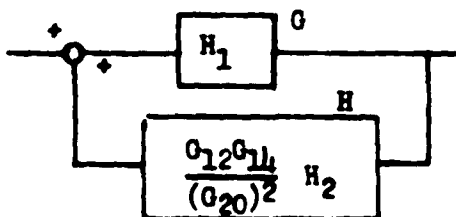
As was described above, a Bode plot of GH was made to determine the significant time constants. Although the plot (Figure 4.3-10) showed two lags to approximately at the 20 db down point, they were retained. After this approximation the block diagram for H_3 in numerical form appears as:
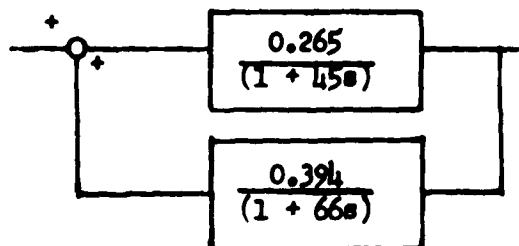
which is readily reduced to:

$$H_3 = \frac{0.295(1 + 66s)}{(1 + 87s)(1 + 38s)}$$

The transfer function H_4 was evaluated in a very similar manner and became:

$$H_4 = \frac{0.97(1 + 45s)}{(1 + 87s)(1 + 38s)}$$

The transfer functions H_5 and H_6 were evaluated using the 20 db spread criterion. Although they have feed-forward paths, the technique for evaluating them is very similar to that above.
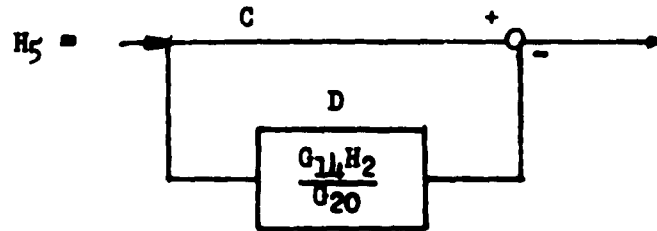
Figure 4.3-11 is a Bode plot of the feed-forward paths C and D from which it can be seen that only a single lag term is of significance. The block diagram form of H_5 is then:
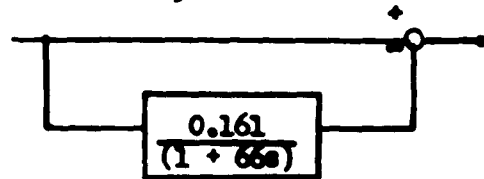
which reduces to:

$$H_5 = \frac{0.839(1 + 79s)}{(1 + 66s)}$$

Similarly H_6 was found to be:

$$H_6 = \frac{0.351(1 + 128s)}{(1 + 45s)}$$

The same technique was used to evaluate G_h.

$$G_h = \frac{T_{hs}}{K_s} - \frac{G_6}{G_5 K_s} \approx 97.0 - \frac{75.5}{(1 + 3.6s)}$$

and thus:

$$G_h = 75.5 \ \frac{(1 + 4.6s)}{(1 + 3.6s)}$$

The lead and lag time constants here are sufficiently close that a good approximation is:

$$G_h \cong 75.5$$

In evaluating G_c at least 5 lead and lag terms would have to be retained from the infinite series representation if the 20 db spread criterion were used. Since these dynamics reduce the value of G_c by only 30% at higher frequencies and since the forward-feed path which contains G_c is only 10% of the parallel path (containing G_h; see block diagram below), neglecting these dynamics causes little error. With this approximation:

$$G_c = -5.30$$

The block diagram in numerical form for the distributed parameter analysis now appears as:
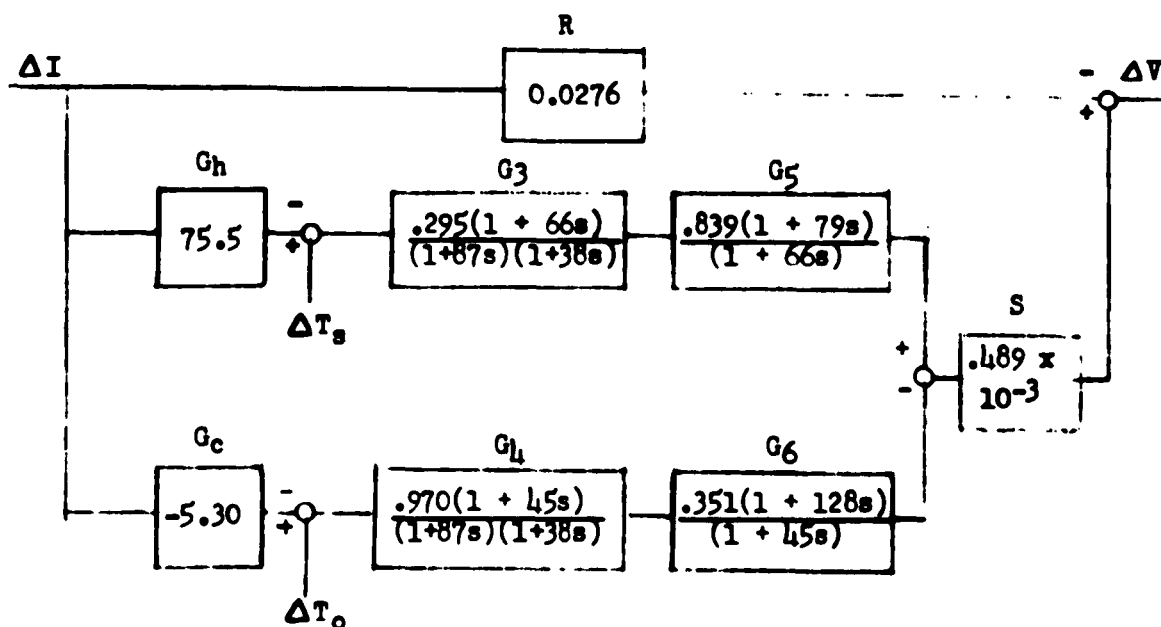
which becomes:
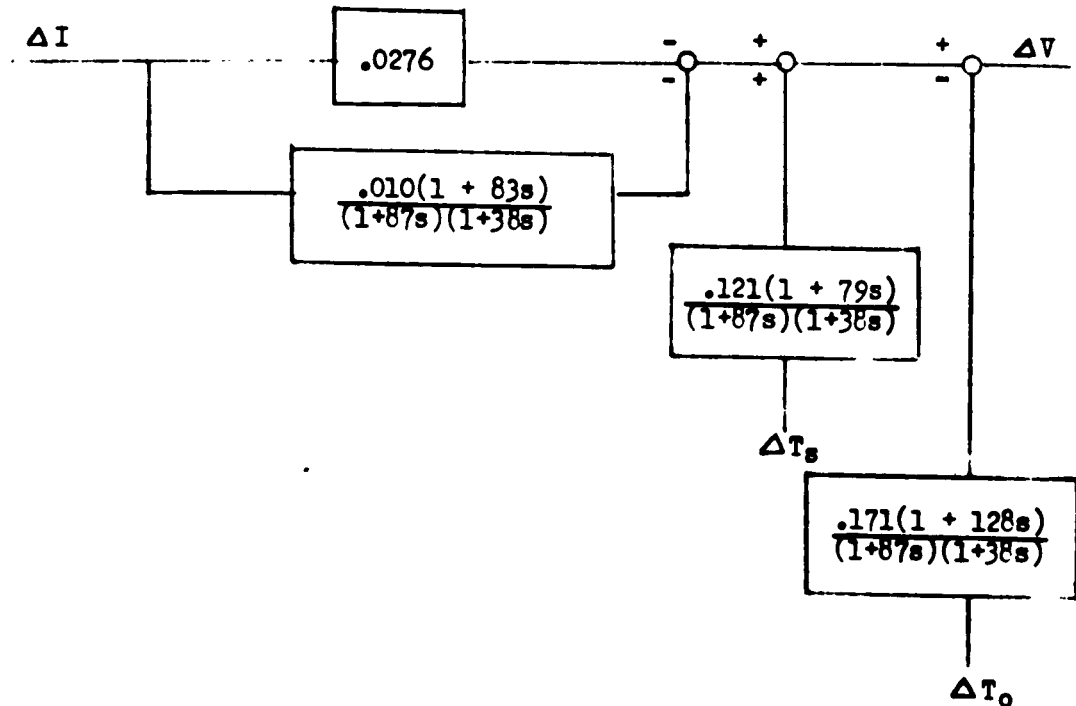
and by simplifying the dynamic feed-forward path to:

$$\frac{.010}{(1 + 38s)}$$

the electrical dynamic impedance is:

$$\Delta I \text{ (amp)} \quad \boxed{.0376 \; \frac{(1 + 28s)}{(1 + 38s)}} \quad \Delta V \text{ (volts)}$$

or in terms of current density, J,

$$\Delta J \text{ (amp/cm}^2\text{)} \quad \boxed{.00688 \; \frac{(1 + 28s)}{(1 + 38s)}} \quad \Delta V \text{ (volts)}$$

4.3.1.2 Results and Conclusions

Block diagrams showing transfer function characteristics of a typical thermoelectric couple are shown in Figure 4.3-12 based on both a lumped parameter and a distributed parameter analysis. From these it can be seen that the lumped parameter results differ very little from the distributed parameter results. Hence, the lumped parameter analysis can be used with good results for determining the dynamic impedance of generators which have the general characteristics of the example generator.

The general block diagram for a thermoelectric couple is given in Figure 4.3-5. Final solution for a particular problem is obtained by numerical reduction of this diagram. Definitions of the parameters are listed in the "Lumped Parameter Analysis" section.

It is often convenient to represent the electrical dynamic impedance by means of an equivalent electrical circuit. Figure 4.3-13 shows an equivalent electrical circuit based on the lumped parameter results of Figure 4.3-12. This circuit represents the characteristics of a single couple. Thermoelectric generators characteristically have all the couples thermally in parallel. The dynamic characteristics of a generator would then differ from those of a single couple only by the DC gain of the transfer function; the gain becomes a multiple (the number of couples) of the gain for a single couple. The thermal time constants are not altered by the number of couples considered.

The results show a lead lag characteristic with a DC resistance equal to that shown in Progress Report No. 3 when the effects of source and sink thermal resistances are included. At high frequencies the impedance approaches the DC resistance of the couple itself. The lag and lead time constants are so large (40 sec. and 30 sec. respectively) that they are expected to contribute negligible interaction problems with an external voltage regulator or inverter. The time constants also indicate the order of magnitude of response that can be expected if voltage regulation is accomplished by control of junction temperatures.

Figure 4.3-1C

Distributed Parameter
Thermal Circuit

Figure 4.3-1B

Lumped Parameter
Thermal Circuit

Figure 4.3-1A

Couple from Typical
Thermoelectric Generator
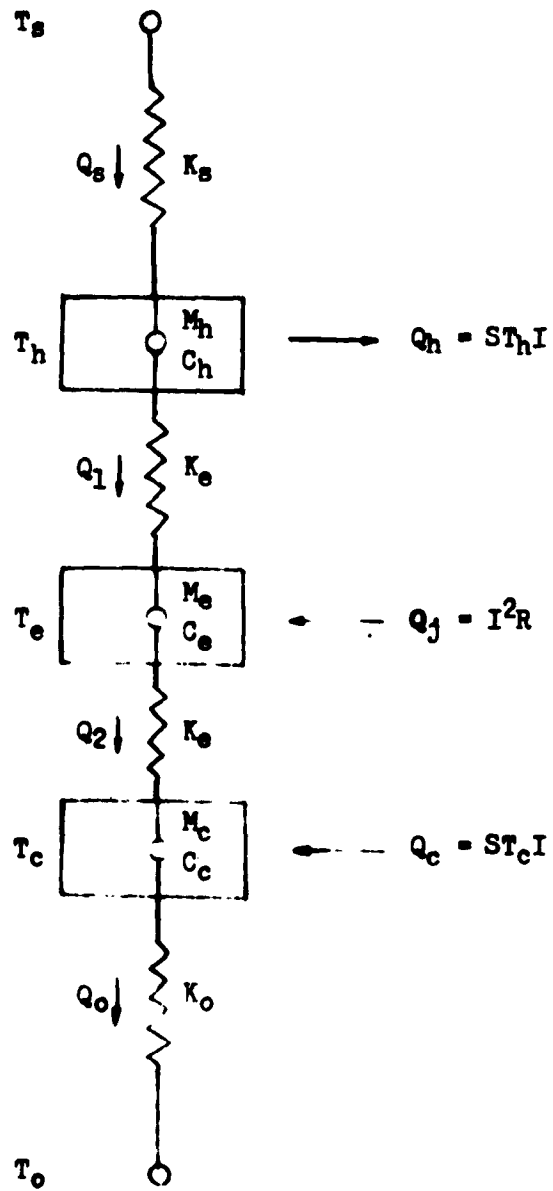
Figure 4.3-2

Lumped Parameter Analytical Model
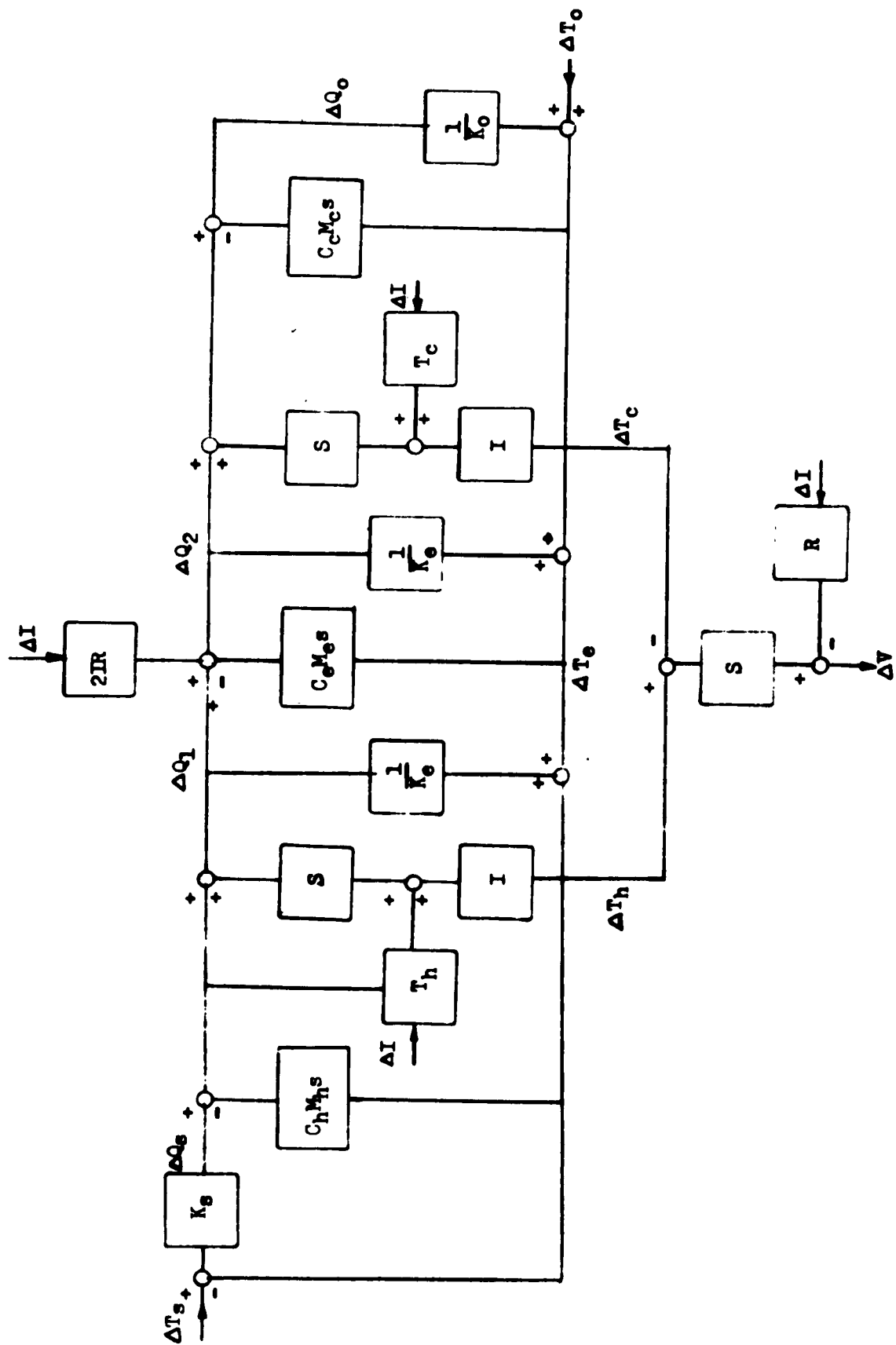
Figure 4.3-3 Block Diagram of Equations
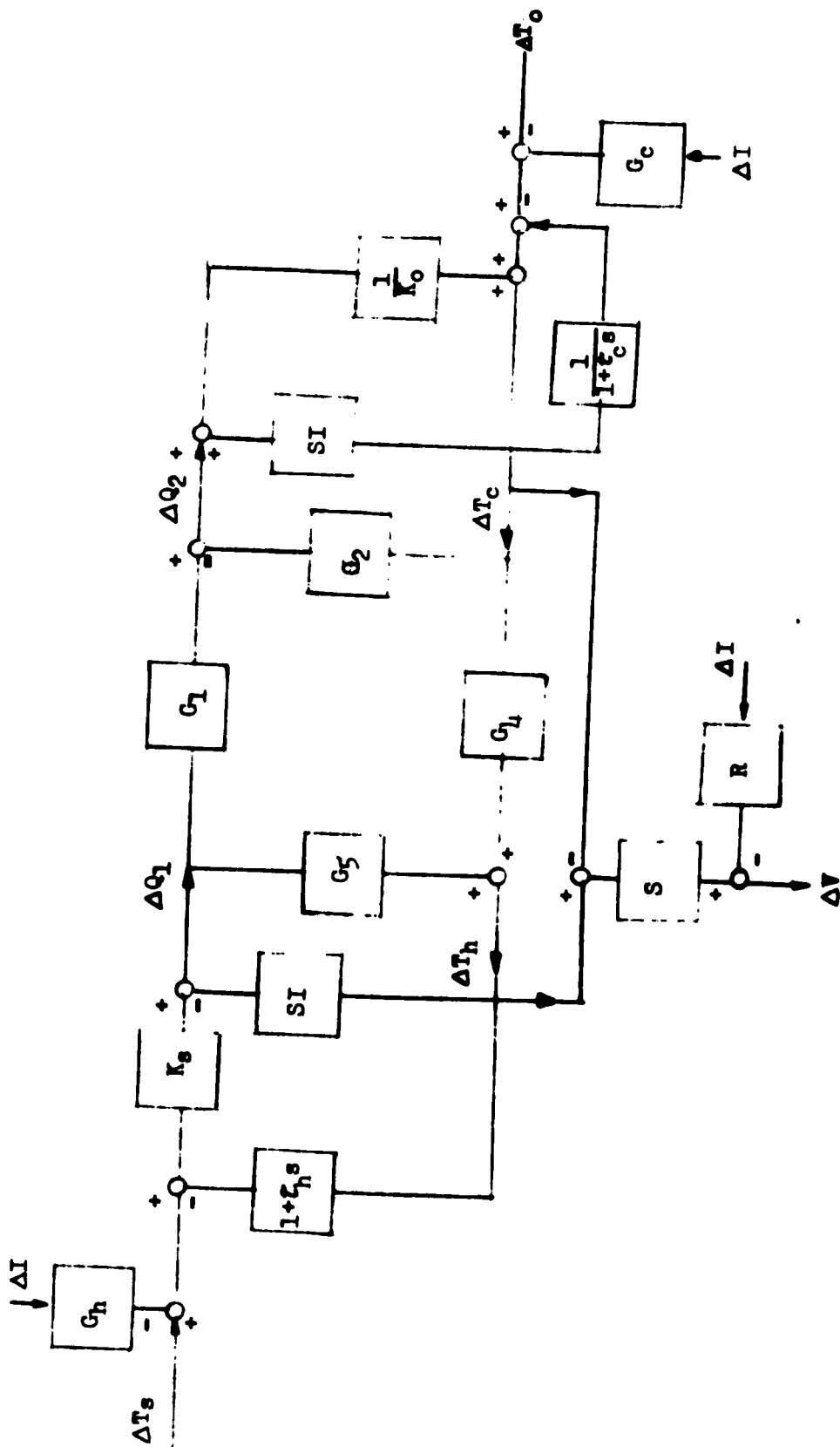
Figure 4.3-4 Partially Reduced Block Diagram
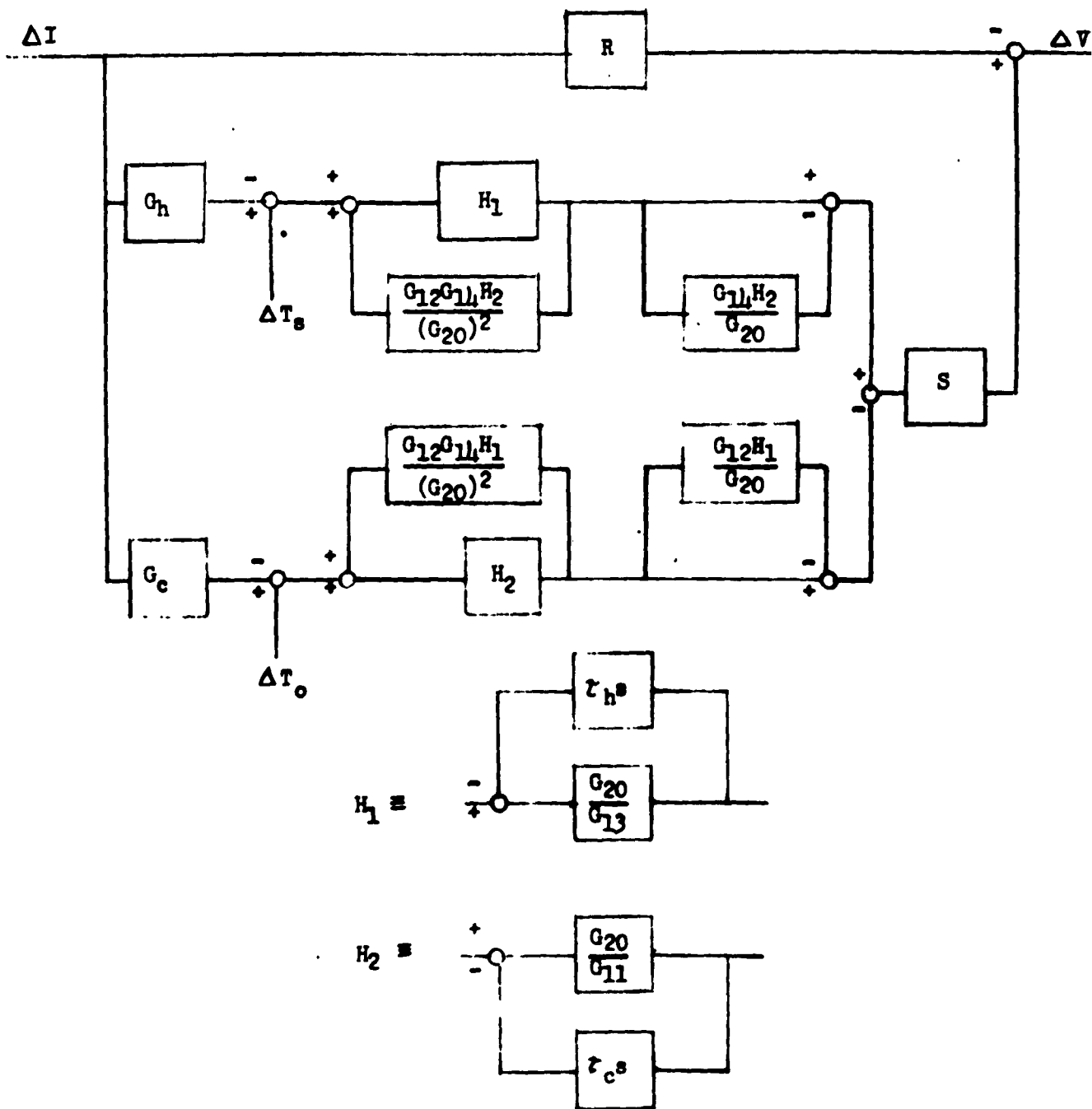
Figure 4.3-5

Block Diagram in Final Form
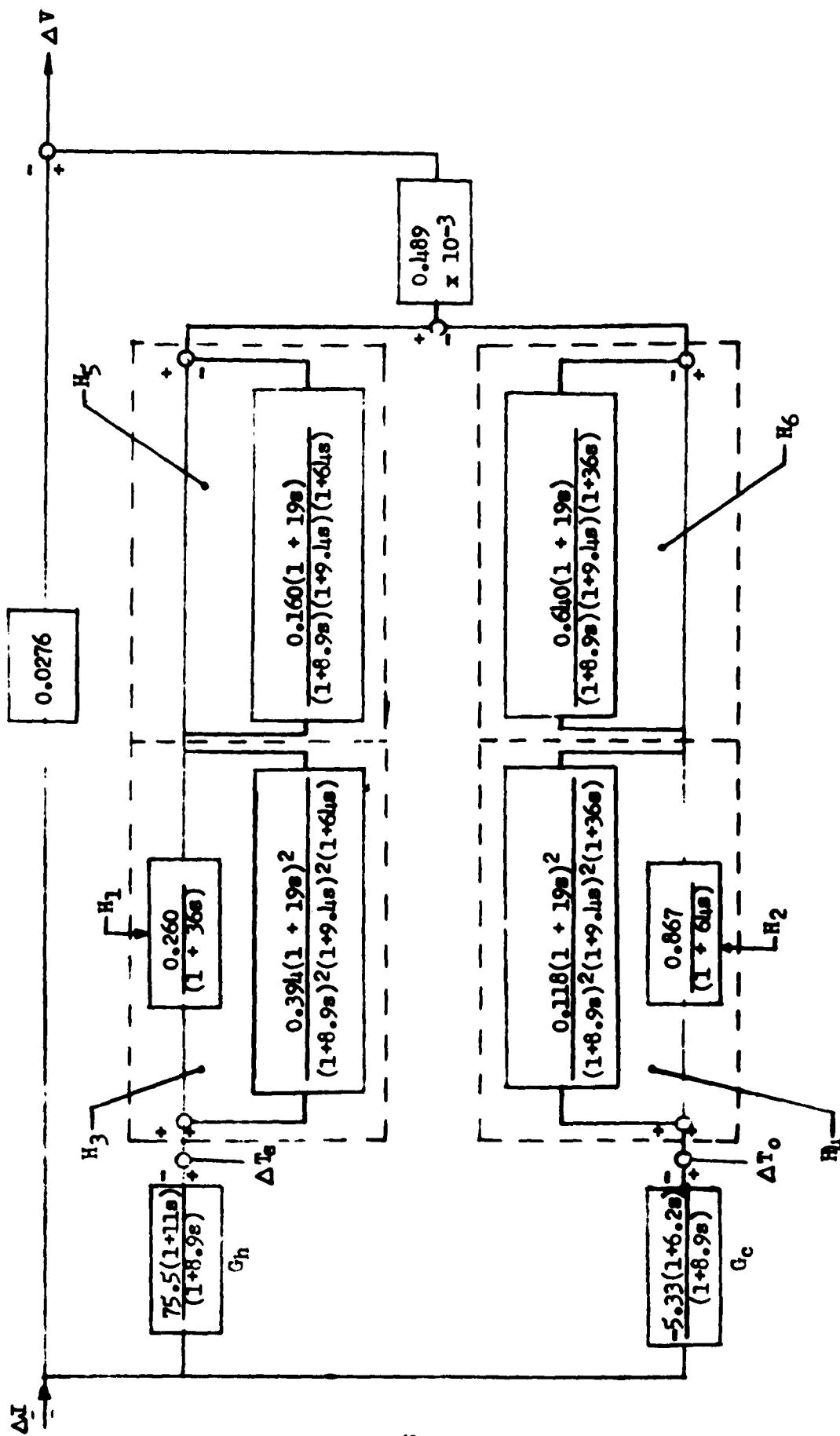
Figure 4.3-6

Block Diagram in Numerical Form

Fig. 4.3-7B Thermal Circuit for Distributed Parameter Analysis

Fig. 4.3-7A Thermocouple Showing Differential Element for Distributed Parameter Analysis
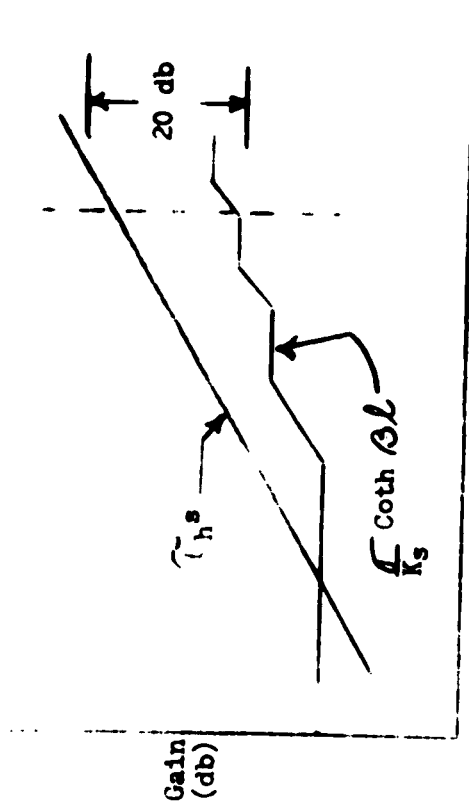
Fig. 4.3-8 Feedback Terms for H_1
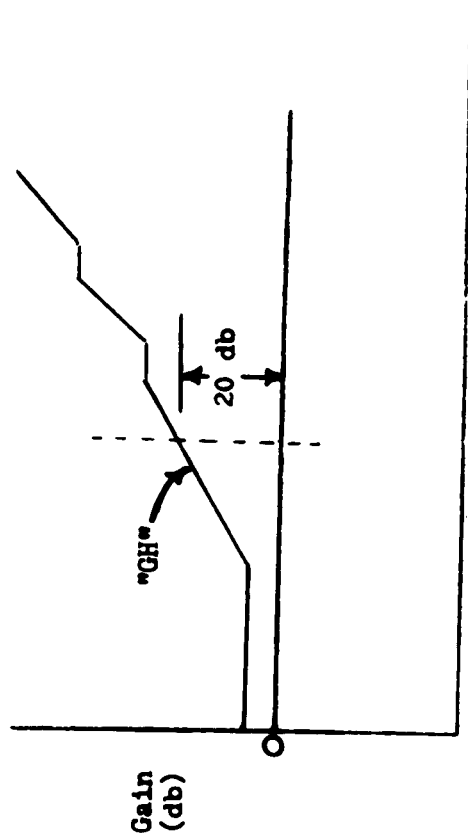
Fig. 4.3-9 Plot of "GH" for H_1
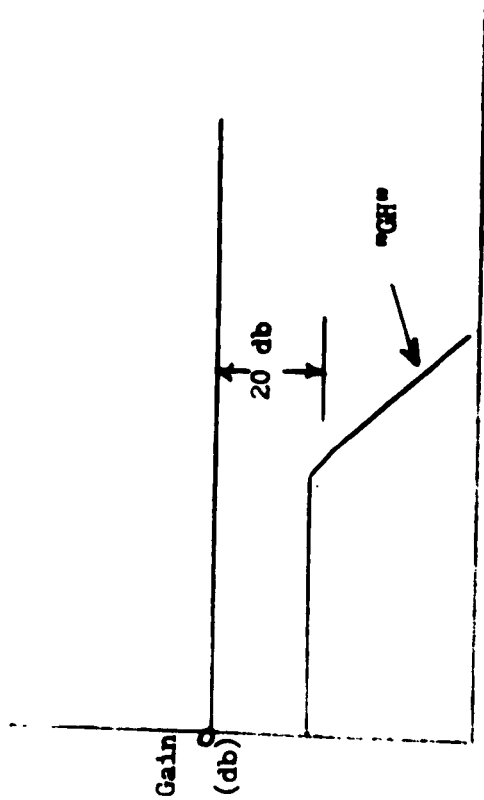
Fig. 4.3-10 Plot of "GH" for H_3
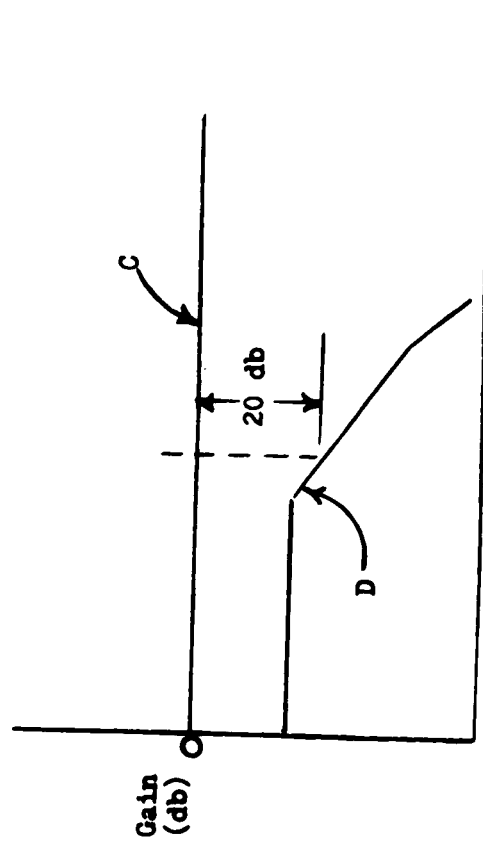
Fig 4.3-11 Bode Plot for H_5
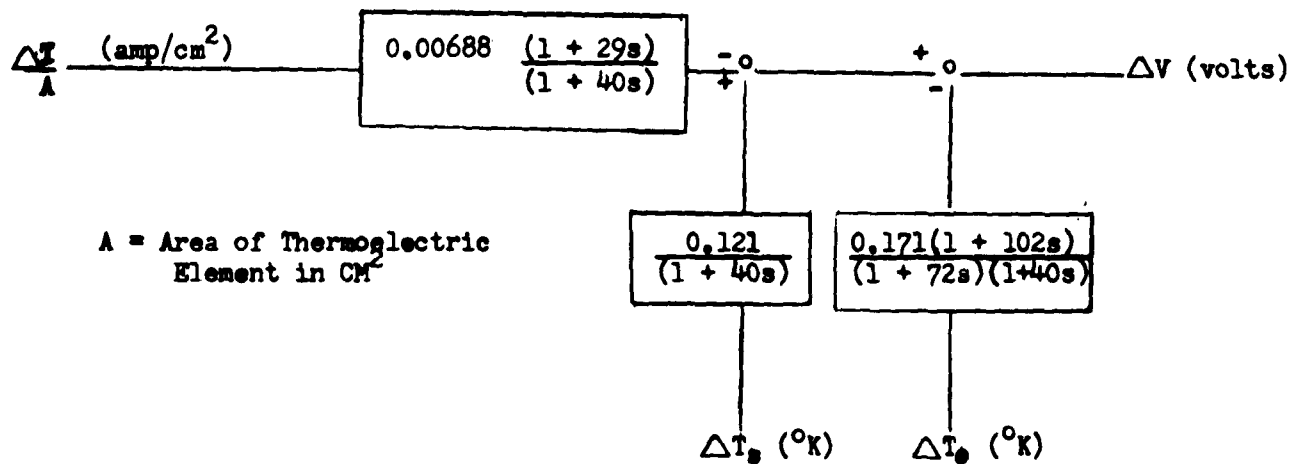
a. Lumped Parameter
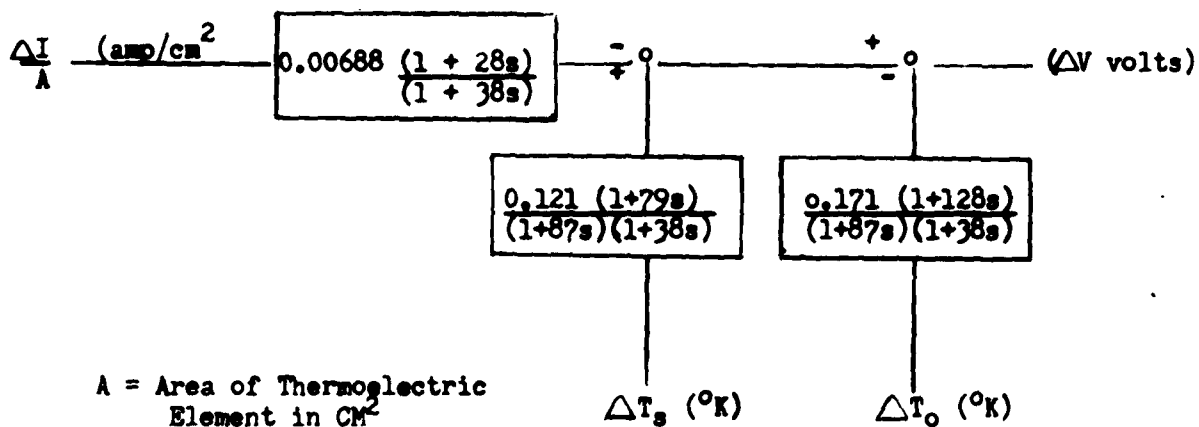
b. Distributed Parameter

Fig. 4.3-12, Block Diagram Results for A Typical Thermoelectric Couple
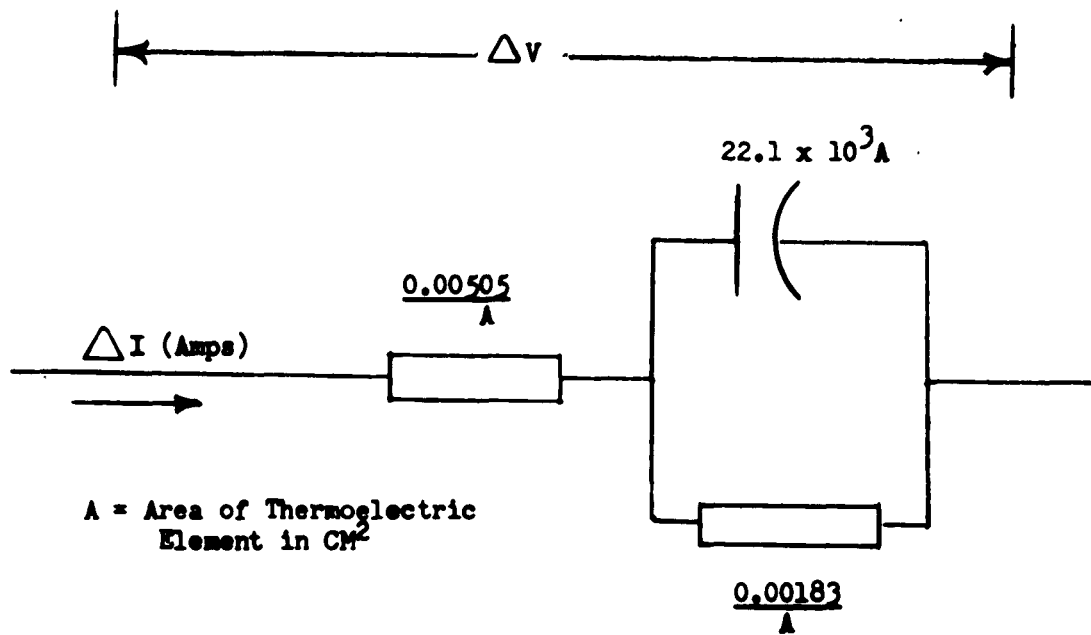
Fig. 4.3-13 Equivalent Circuit for Electrical Dynamic Impedance of
a Thermoelectric Couple

4.4 Thermionics

During the present reporting period an analysis was performed to
determine the dynamic characteristics of the thermionic converter.
In the analysis a vapor type converter was considered in a typical
space application where heat is supplied by means of a solar collector
and is rejected by radiation to space. The analytical results are
summarized below and a numerical example of a typical converter is
presented. Although the analysis considers a space system the re-
sults can be applied to other systems with little modification.

4.4.1 Dynamic Characteristics

The dynamic characteristics of an electrical power source are of
interest to both the power source designer and the electrical system
designer. The AC output impedance of the power source, in this case
the thermionic converter, is of particular interest since it is often
different from the DC resistance. Dynamic effects could be caused by
a) delay or lag phenomena within the converter and b) source to
cathode and anode and cesium reservoir to sink thermal resistances.
In Progress Report No. 5 the dynamics of the converter itself (with
constant temperatures) were discussed and the conclusion was made that
they are negligible in the frequency spectrum of interest. The prin-
cipal cause of dynamics therefore, is expected to be the effects of
the source and sink thermal resistances. If these are significant
they will allow the cathode, anode and cesium reservoir temperatures
to change as the converter thermal impedance is changed by varying
the load current. These three temperatures affect the output voltage
of the converter and thus variations in them produce dynamic effects.
At low current oscillation frequencies these temperatures can vary
but at high frequencies the thermal inertia of the cathode, anode,
and cesium reservoir will cause them to remain essentially constant.
Hence the converter will operate on one volt-ampere curve at DC and
low frequencies but will shift to another at high frequencies. The
analysis presented below illustrates how the source and sink thermal
resistances can cause dynamic effects and the numerical example shows
the order of magnitude of the effects that can be expected for most
systems.

Analysis

1. A lumped parameter linearized analysis was used to determine the dynamic characteristics. The nomenclature for the analysis is listed below:

    C_a - specific heat of anode material

    C_c - specific heat of cathode material

    C_v - specific heat of cesium reservoir

    E_I - intercept voltage of linear volt-ampere curve

    I - electrical current

    Io - steady state value of current

    K_a - thermal conductance, anode to heat sink

    K_c - thermal conductance, cathode to anode

    K_e - cathode to anode effective thermal conductance due to electron cooling

    K_p - thermal conductance, cesium reservoir to heat sink

    K_R - effective thermal conductance for radiant heat transfer, cathode to anode

    K_s - thermal conductance, heat source to cathode

    K_v - thermal conductance, anode to cesium reservoir

    M_a - anode mass

    M_c - cathode mass

    M_v - cesium reservoir mass

    P - converter output power

    R_g - internal resistance of converter

    R_{go} - steady state value of internal resistance

    s - laplace operator

    T_a - anode temperature

- 64 -

T_c - cathode temperature

T_{cs} - cesium reservoir temperature

T_o - heat sink temperature

T_s - fictitious heat source temperature

V - converter terminal voltage

V_o - steady state terminal voltage

$F_i \left(\dfrac{730\ T_s}{T_{ao}} \right)$ - defined by Figure 4.4-12 of Progress Report No. 5

$F_i \left(T_{cs},\ T_c \right)$ - defined by Figure 4.4-13 of Progress Report No. 5

$F_g \left(\dfrac{730T_s}{T_{ao}} \right)$ - defined by Figure 4.4-14 of Progress Report No. 5

$F_g \left(T_{cs},\ T_c \right)$ - defined by Figure 4.4-15 of Progress Report No. 5

σ - proportionality constant for radiant heat transfer

The analytical result desired is an expression for G, the dynamic impedance of the converter where

$$G = \frac{\Delta V}{\Delta I}$$

A linear volt-ampere curve is assumed for the converter and the electrical schematic becomes
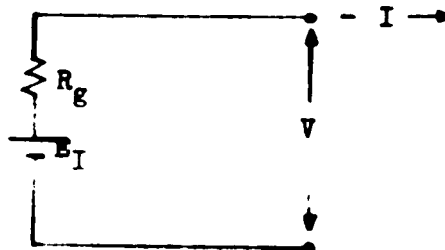
from which the following relation can be written

$$V = E_I - I R_g$$

- 65 -

In this expression E_I and R are not constants but are functions of T_c, T_a and T_{cs} so the linearized form of the above expression becomes:

1.) $\Delta V = \Delta E_I - I_o \Delta R_g - R_{go} \Delta I$.

The relations showing how T_c, T_a, and T_{cs} affect E_I and R_g were presented in Progress Report No. 5.

Before these are used a thermal circuit of the converter is reduced to determine the transfer functions from ΔI, the independent variable and ΔT_c, ΔT_a and ΔT_{cs}. These transfer functions combined with the relations describing ΔE_I and ΔR_g as functions of ΔT_c, ΔT_a and ΔT_{cs} can then be substituted into Equation 1.) to obtain the desired result, ΔV as a function of ΔI.

Figure 4.4-1B shows the assumed thermal circuit for the converter which is shown schematically in Figure 4.4-1A.

The following equations can be written from the thermal schematic:

Basic equations	Linearized Form
$Q_1 = K_s (T_s - T_c)$	$\Delta Q_1 = K_s \Delta T_s - K_s \Delta T_c$
$Q_1 = Q_o + V \cdot I + C_c M_c s T_c$	$\Delta Q_1 = \Delta Q_o + I_o \Delta V + V_o \Delta I + C_c M_c s \Delta T_c$
$Q_o = Q_a + Q_v + C_a M_a s T_a$	$\Delta Q_o = \Delta Q_a + \Delta Q_v + C_a M_a s \Delta T_a$
$Q_a = f\left(T_a^4 - T_o^4\right)$	$\Delta Q_a = K_a (\Delta T_a - \Delta T_o)$
$Q_v = K_v (T_a - T_{cs})$	$\Delta Q_v = K_v \Delta T_a - K_v \Delta T_{cs}$
$Q_v = Q_p + C_v M_v s T_{cs}$	$\Delta Q_v = \Delta Q_p + C_v M_v s \Delta T_{cs}$
$Q_p = f(T_{cs}^4 - T_o^4)$	$\Delta Q_p = K_p (\Delta T_{cs} - \Delta T_o)$

$$Q_0 = Q_c + Q_R + Q_e$$

where

$$\Delta Q_0 = K_c \left(\Delta T_c - \Delta T_a \right) + K_R \Delta T_c + K_e \Delta I$$

$$Q_c = f(T_c, T_a)$$

$$Q_R = f(T_c, T_a)$$

$$Q_e = f(T_c, T_a, I)$$

The last equation for Q_0 was derived in Progress Report No. 5 where plots for Q_e, and Q_R, and Q_c were presented in Figures 4.4-26, 4.4-27, and 4.4-28, respectively. In linearizing this equation assumptions were made that Q_R was independent of T_a and Q_e was independent of both T_c and T_a.

These linearized equations are shown in block diagram form in Figure 4.4-2. From this point on the sink temperature, ΔT_0, was not brought along in the analysis as an independent variable. Changes in T_0 will have little affect on the converter performance since heat rejected varies with the fourth power of temperature and T_0 is generally considerably smaller than T_a or T_{cs}. Reduction of Figure 4.4-2 provides the following expression for the cathode temperature.

2.) $\Delta T_c = G_{10} \Delta T_s - G_{11} \Delta V - G_{12} \Delta I.$

where

$$G_{10} = \frac{1}{\frac{(K_c + K_R)/K_s}{(1 + K_c)/A} + (1 + \mathcal{T}_s s)}$$

$$G_{11} = \frac{I_0}{K_s} G_{10}$$

$$G_{12} = G_{10}\left[\frac{V_o}{K_s} - \left(\frac{K_e}{K_c + K_R}\right)\left(1 + \mathcal{T}_s s\right)\right] + \frac{K_e}{K_c + K_R}$$

where $A = K_a(1 + \mathcal{T}_a s) + \dfrac{K_p K_v (1 + \mathcal{T}_{cs} s)}{K_p + K_v(1 + \mathcal{T}_{cs} s)}$

and the time constants are

$$\mathcal{T}_s = \frac{C_c M_c}{K_s} \quad ; \quad \mathcal{T}_a = \frac{C_a M_a}{K_a} \quad ; \quad \mathcal{T}_{cs} = \frac{C_v M_v}{K_p}$$

The expression for anode temperature is:

3.) $\Delta T_a = G_{20}\Delta T_s - G_{21}\Delta V - G_{22}\Delta I$

where

$$G_{20} = \frac{1}{\dfrac{A}{K_s} \dfrac{(K_c + A)}{(K_c + K_R)} (1 + \mathcal{T}_s s)}$$

$$G_{21} = \frac{I_o}{K_s} G_{20}$$

$$G_{22} = \left[\frac{V_o}{K_s} - \left(\frac{K_e}{K_c + K_R}\right)\left(1 + \mathcal{T}_s s\right)\right] G_{20}$$

and for the cesium reservoir temperature

4.) $\Delta T_{cs} = G_{30}\Delta T_s - G_{31}\Delta V - G_{32}\Delta I$

$$G_{30} = G_{20} \; G_{33}$$

$$G_{31} = G_{21} \; G_{33}$$

$$G_{32} = G_{22} \; G_{33}$$

where

$$G_{33} = \frac{\left(\dfrac{k_v}{k_v + k_p}\right)}{1 + \left(\dfrac{k_p}{k_v + k_p}\right)\mathcal{T}_{cs} s}$$

These are the expressions needed for ΔT_c, ΔT_a, and ΔT_{cs} in terms of the independent variables ΔI and ΔT_s and the dependent variable ΔV. Next expressions for ΔR_g and ΔE_I in terms of ΔT_c, ΔT_a, and ΔT_{cs} must be obtained.

Progress Report No. 5 presented the following expressions for E_I and R_g:

$$E_I = 0.55 \; W \cdot X$$

$$W = F_1\left(\frac{730T_a}{T_{ao}}\right)$$

$$X = F_1\left(T_{cs}, \; T_c\right)$$

$$R_g = 0.0325 \; Y \cdot Z$$

$$Y = F_g\left(\frac{730T_a}{T_{ao}}\right)$$

$$Z = F_g\left(T_{cs}, \; T_c\right)$$

In linearized form these become

5.) $\quad \Delta E_I = K_1 \Delta T_a + K_2 \Delta T_{cs} + K_3 \Delta T_c$

$$K_1 = 0.55 \; X_o \; \frac{dW}{dT_a}$$

$$K_2 = 0.55 \; W_o \; \frac{dX}{dT_{cs}}\bigg|_{T_{co}}$$

$$K_3 = 0.55 \; W_o \; \frac{dX}{dT_c}\bigg|_{T_{cso}}$$

6.) $\Delta R_g = K_4 \Delta T_a + K_5 \Delta T_{cs} + K_6 \Delta T_c$

$$K_4 = 0.0325 \ Z_o \ \frac{dY}{dT_a}$$

$$K_5 = 0.0325 \ Y_o \ \frac{\partial Z}{\partial T_{cs}}\Big|_{T_{co}}$$

$$K_6 = 0.0325 \ Y_o \ \frac{\partial Z}{\partial T_c}\Big|_{T_{cso}}$$

Here the subscript "o" indicates the nominal or D.C. value for the linearization. Equations 1.) through 6.) are now combined to give the transfer functions for ΔI to ΔV and for ΔT_s to ΔV. This combination provides the desired analytical expression for the dynamic impedance and the results are shown in block diagram form in Figure 4.4-3. The diagram easily could be reduced further but the form shown is more convenient for obtaining numerical results. In algebraic form the electrical dynamic impedance is

7.) $$\frac{\Delta V}{\Delta I} = - \frac{G_{12}(K_3 - I_o K_6) + G_{22}(K_1 - I_o K_4) + G_{32}(K_2 - I_o K_5) + R_{go}}{1 + G_{11}(K_3 - I_o K_6) + G_{21}(K_1 - I_o K_4) + G_{31}(K_2 - I_o K_5)}$$

Numerical Example

The numerical values for the constants for a typical vapor converter
are listed below:

$$C_a M_a = 6.17 \text{ w-sec/}^\circ\text{C-cm}^2$$

$$C_c M_c = 1.14 \text{ w-sec/}^\circ\text{C-cm}^2$$

$$C_v M_v = 0.233 \text{ w-sec/}^\circ\text{C-cm}^2$$

$$I_o = 8.47 \text{ amp/cm}^2$$

$$K_a = 0.103 \text{ w/cm}^2\text{-}^\circ\text{C}$$

$$K_c = 4.67 \times 10^{-3} \text{ w/cm}^2\text{-}^\circ\text{C}$$

$$K_e = 1.75 \text{ w/amp}$$

$$K_p = 1.69 \times 10^{-3} \text{ w/cm}^2\text{-}^\circ\text{C}$$

$$K_s = 7.87 \times 10^{-3} \text{ w/cm}^2\text{-}^\circ\text{C}$$

$$K_v = 0.295 \times 10^{-3} \text{ w/cm}^2\text{-}^\circ\text{C}$$

$$K_1 = -0.66 \times 10^{-3} \text{ volts/}^\circ\text{C}$$

$$K_2 = -5.5 \times 10^{-3} \text{ volts/}^\circ\text{C}$$

$$K_3 = 1.87 \times 10^{-3} \text{ volts/}^\circ\text{C}$$

$$K_4 = -0.0650 \times 10^{-3} \Omega\text{-cm}^2/^\circ\text{C}$$

$$K_5 = -0.292 \times 10^{-3} \Omega\text{-cm}^2/^\circ\text{C}$$

$$K_6 = 0.0438 \times 10^{-3} \Omega\text{-cm}^2/^\circ\text{C}$$

$$R_o = 0.0325 \Omega\text{-cm}^2$$

$$V_o = 0.275 \text{ V}$$

$$T_{ao} = 730^\circ\text{C}$$

$$T_{co} = 1330^{\circ}C$$

$$T_{cso} = 300^{\circ}C$$

$$W_o = 1.0$$

$$X_o = 1.0$$

$$Y_o = 1.0$$

$$Z_o = 1.0$$

The methods used in evaluating some of these constants deserve some comment. In evaluating K_s, a first reaction might be that the source (sun) temperature is so high compared to the cathode temperature that a constant heat flux should be considered. However, the characteristics of the mirror system for concentrating the solar energy are such that increasing the cathode temperature reduces the heat flux into the cathode. This characteristic can be represented by a fictitious source temperature and a source to cathode thermal resistance, K_s. A value for K_s was obtained in the following manner:

$$Q_1 = K_s(T_s - T_c)$$

and

$$\Delta Q_1 = - K_s \, \Delta T_c \text{ for constant } T_s$$

Thus

$$K_s = - \frac{\Delta Q_1}{\Delta T_c} = - \frac{\Delta Q_1/Q_{1o}}{\Delta T_c} \cdot Q_{1o}$$

where Q_{1o} is the steady state value of heat into the cathode.

From a typical curve* showing Q_1/Q_s versus T_c (Q_s = solar heat flux), Q_{10} was determined and

$$\frac{\Delta Q_1/Q_{10}}{\Delta T_c}$$

was evaluated from the slope of the curve. These provided the necessary numerical information to evaluate a fictitious K_s describing the characteristics of the collector system.

The value for K_a was obtained in the following manner:

$$Q_a = \sigma (T_a^4 - T_o^4) \simeq \sigma T_a^4$$

$$\Delta Q_a = 4 \sigma T_{ao}^3 \Delta T_a = \frac{4 \sigma T_{ao}^4}{T_{ao}} \Delta T_a = \frac{4 Q_{ao}}{T_{ao}} \Delta T_a$$

From this we define:

$$K_a = \frac{4 Q_{ao}}{T_{ao}}$$

The same approach was used to evaluate K_p.

The constants K_1 through K_6 were evaluated from Figures 4.4-12 through -15 in Progress Report No. 5. Slopes of the appropriate curve at the steady state values provide the values.

*Figure 7, D.L. Purdy, "Solar Thermionic Power System" - Americal Rocket Society Paper No. 60 ARS 1311.

- 73 -

Using these constants the various transfer functions were evaluated and are as follows:

$$\tau_a = 60 \text{ sec.}, \quad \tau_{cs} = 140 \text{ sec.}, \quad \tau_s = 145 \text{ sec.}$$

$$A = \frac{24.3 \times 10^{-3} \, (1 + 149s + 5280 \, s^2)}{(1 + 20.8s)} \quad w/cm^2\text{-}^\circ C$$

$$G_{10} = \frac{0.453 \, (1 + 128s + 4430s^2)}{D}$$

$$G_{11} = 1080 \, G_{10} \qquad {}^\circ C/volt$$

$$G_{12} = \frac{101 \, (1 + 146s + 5150s^2 - 2970s^3)}{D} \quad amp/cm^2\text{-}^\circ C$$

$$G_{20} = \frac{0.177(1 + 20.8s)}{D}$$

$$G_{21} = 1070 \, G_{20} \quad {}^\circ C/volt$$

$$G_{22} = \frac{-21.1(1 + 20.8s) \, (1 + 187s)}{D} \quad amp/cm^2\text{-}^\circ C$$

where:

$$D = (1 + 66s)^3$$

$$G_{33} = \frac{0.148}{(1 + 119s)}$$

These values were used in the transfer function blocks of Figure 4.4-3 yielding the resulting block diagram shown in Figure 4.4-4. Some assumptions were made to minimize the complexity of the block diagram of Figure 4.4-4. The numerator of block G_{51} (Figure 4.4-4) was approximated as $(1 + 66s)^2$. From a bode plot it was found that the following was a reasonable approximation for the combination of G_{51}, G_{52} and G_{53}:

$$G_{51} \cdot G_{52} \cdot G_{53} = \frac{0.626(1 + 25s) \left[1 + 2(.815)(157s) + (157s)^2 \right]}{(1 + 119s)(1 + 66s)^3}$$

$$\simeq \frac{0.626}{(1 + 63s)}$$

In block G_{41} the negative time constant was assumed negligible and was omitted. The combination of G_{41}, G_{42} and G_{43} was found to be very closely approximated by

$$G_{41} + G_{42} + G_{43} = \frac{0.164(1 + 83s)^3}{(1 + 115s)(1 + 66s)^3}$$

From a Bode plot it was determined that this combination was approximately:

$$G_{41} + G_{42} + G_{43} \approx \frac{0.164}{(1 + 58s)}$$

After the reduction of the feed-forward and feed-back loop the block diagram appears as:
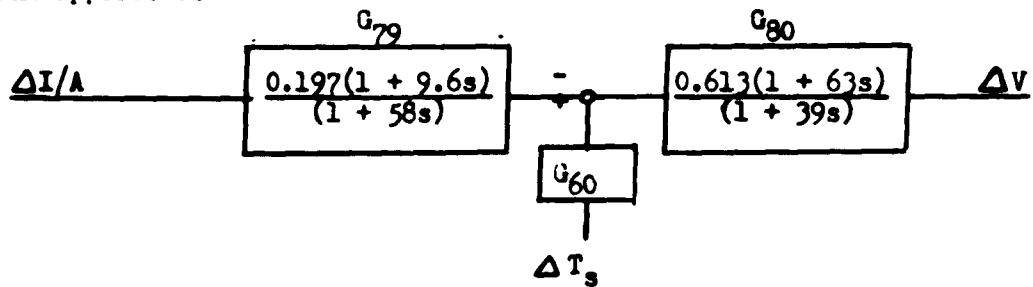
Further reduction yields:
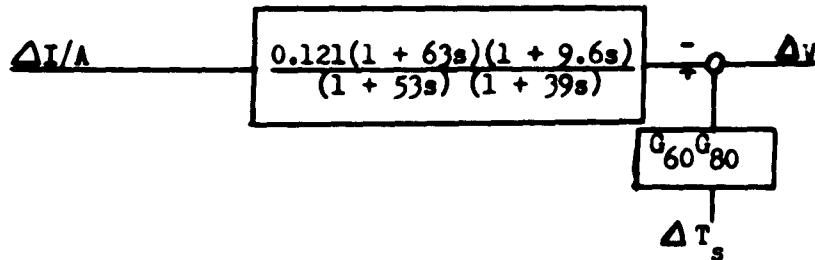
Bode plots were used to obtain reasonable approximations for both blocks and the final result is shown in Figure 4.4-5.

4.4.2   Results and Conclusions

The analytical results for the dynamic impedance of a thermionic converter are shown in block diagram form in Figure 4.4-3 and are expressed by equation 7 which is listed in 4.4-1 under the "Analysis" section. An equivalent electrical circuit is a convenient means of representing the dynamic impedance of a power source; an equivalent circuit for the numerical example is shown in Figure 4.4-6. All these results are for a single thermionic converter. If several converters were placed electrically in series to provide a higher generator output voltage, the dynamic impedance still would be characterized by the time constant shown in these results since the converters would be thermally in parallel. The gain of the transfer function or the DC internal impedance, however, would have a higher value which would be a multiple of the number of converters being used.

The results show approximately a 4 to 1 decrease in gain or internal impedance magnitude for current perturbations from DC to high frequencies. Although the impedance change is significant, the associated time constants are sufficiently large (approximately 10 sec. and 40 sec.) that little interaction should occur with external regulators which have characteristic switching frequencies of hundreds to thousands of cycles per second.

Figure 4.4-1B   Thermal Circuit for Vapor Converter

Figure 4.4-1A   Schematic of Vapor Converter

- 77 -
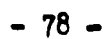
Figure 4.4-2   Block Diagram of Basic Linearized Equations for a Thermionic Converter
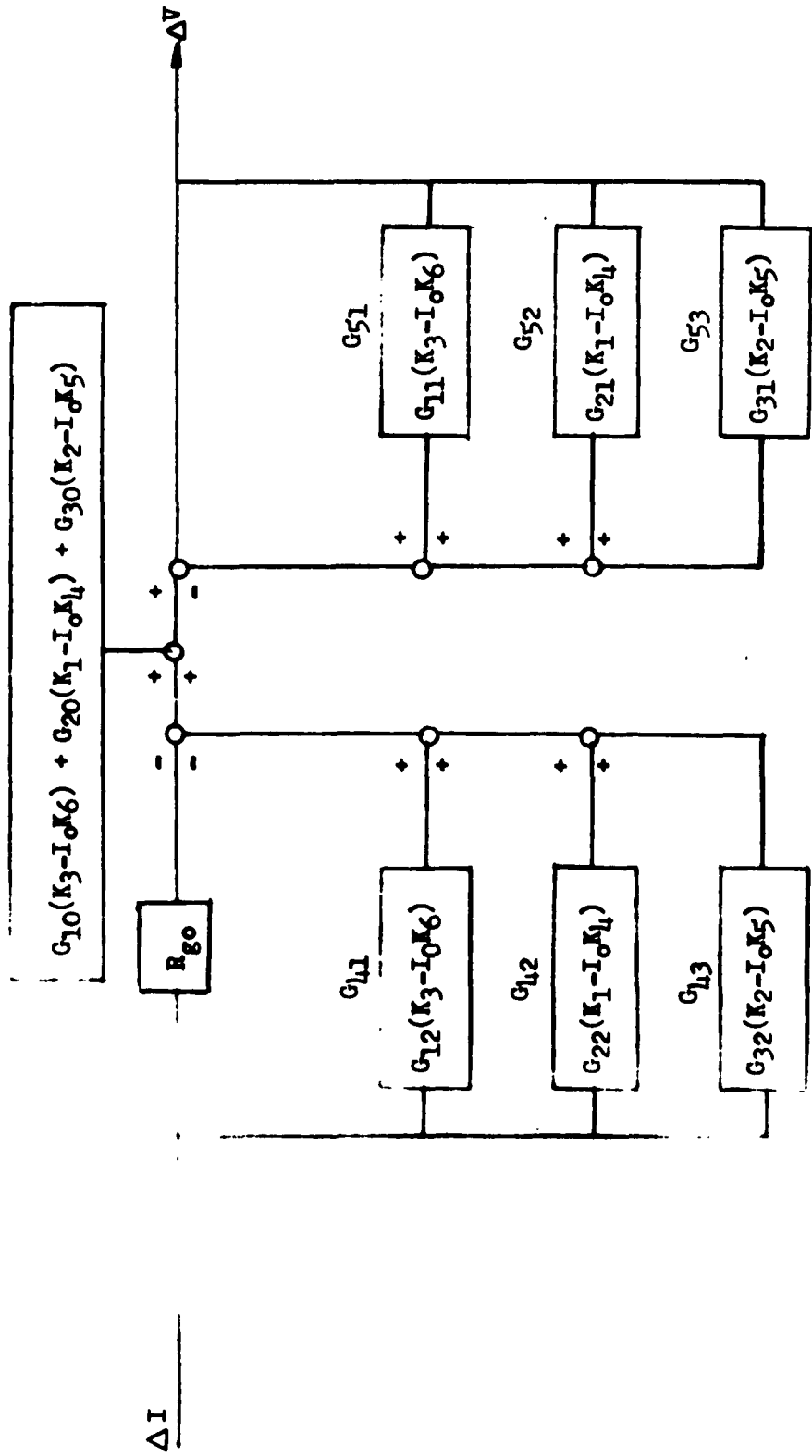
Figure 4.4-3   Block Diagram Representing Dynamic Impedance of a Thermionic Converter
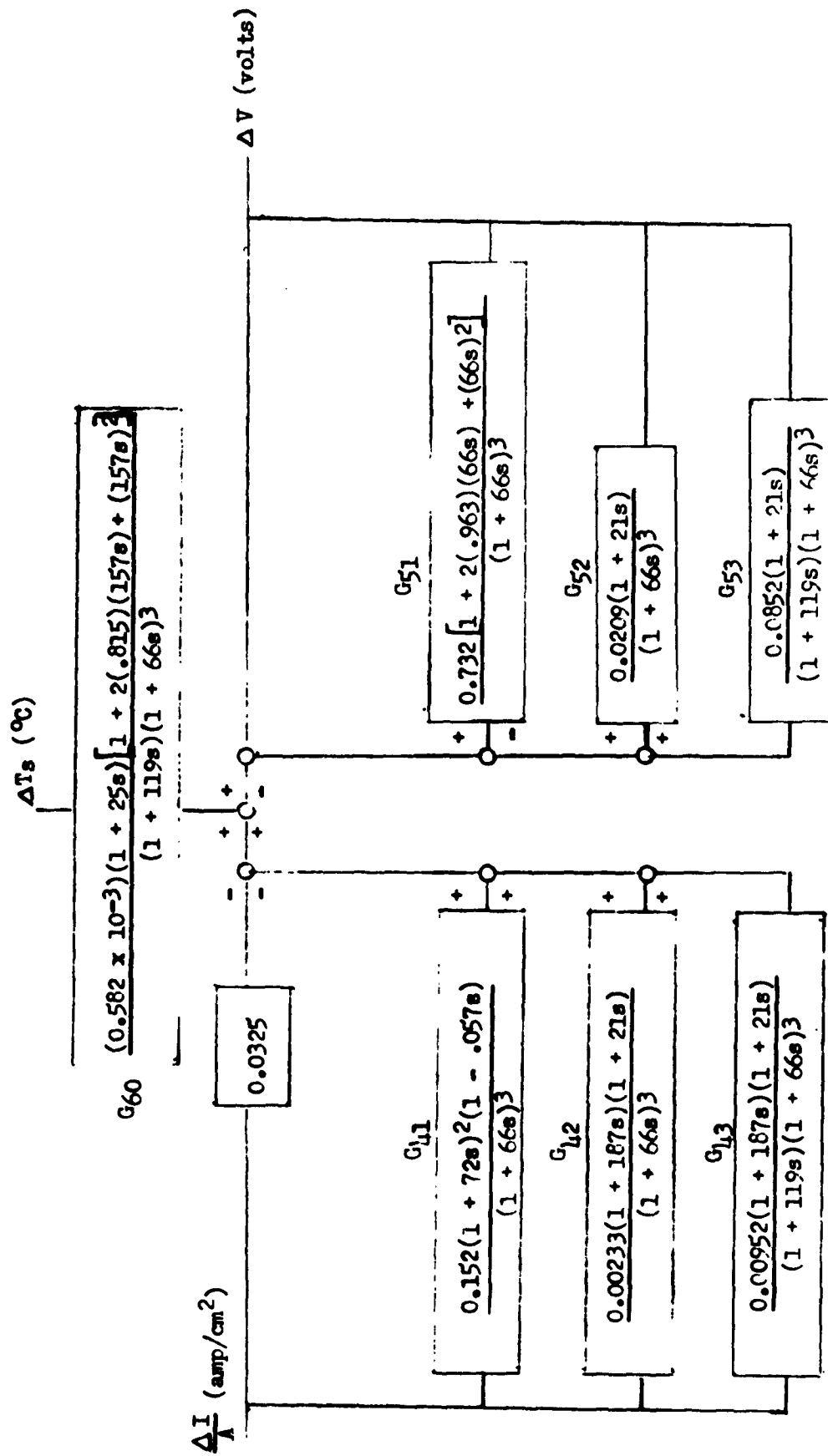
Figure 4.4-4   Block Diagram in Numerical Form of a Vapor Thermionic Converter

$$G_{60} \quad \frac{(0.582 \times 10^{-3})(1 + 25s)\left[1 + 2(.815)(157s) + (157s)^2\right]}{(1 + 119s)(1 + 66s)^3}$$

$$0.0325$$

$$G_{51} \quad \frac{0.732\left[1 + 2(.963)(66s) + (66s)^2\right]}{(1 + 66s)^3}$$

$$G_{52} \quad \frac{0.0209(1 + 21s)}{(1 + 66s)^3}$$

$$G_{53} \quad \frac{0.0852(1 + 21s)}{(1 + 119s)(1 + 66s)^3}$$

$$G_{41} \quad \frac{0.152(1 + 72s)^2(1 - .057s)}{(1 + 66s)^3}$$

$$G_{42} \quad \frac{0.00233(1 + 187s)(1 + 21s)}{(1 + 66s)^3}$$

$$G_{43} \quad \frac{0.00952(1 + 187s)(1 + 21s)}{(1 + 119s)(1 + 66s)^3}$$

ΔV (volts)

ΔT_s (°C)

$\dfrac{\Delta I}{A}$ (amp/cm^2)

$$\frac{\Delta I}{A} \cdot (\text{amp/cm}^2) \quad \boxed{0.121 \; \frac{(1 + 9.6s)}{(1 + 39s)}} \quad \xrightarrow{\;\;} \Delta V \text{ (volts)}$$

A = Cathode Area in cm^2

$$\boxed{\frac{0.324 \times 10^{-3}}{(1 + 39s)}}$$

ΔT_s (°C)
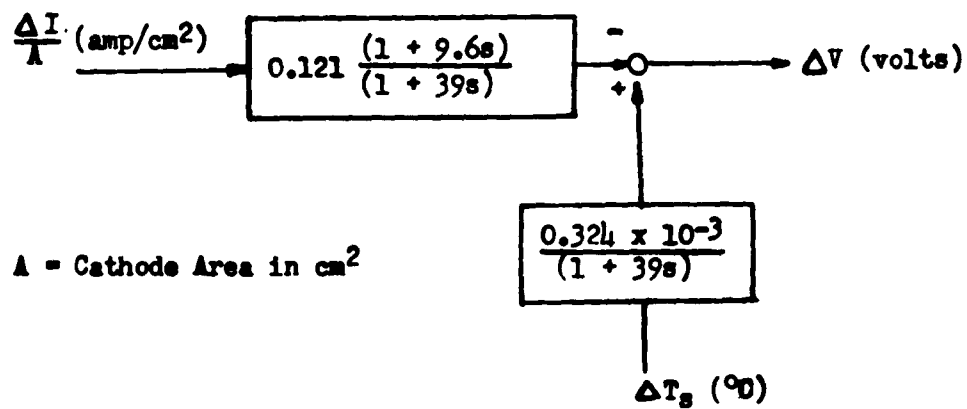
Figure 4.4-5

Block Diagram of Numerical Results for a Vapor Thermionic Converter

- 81 -
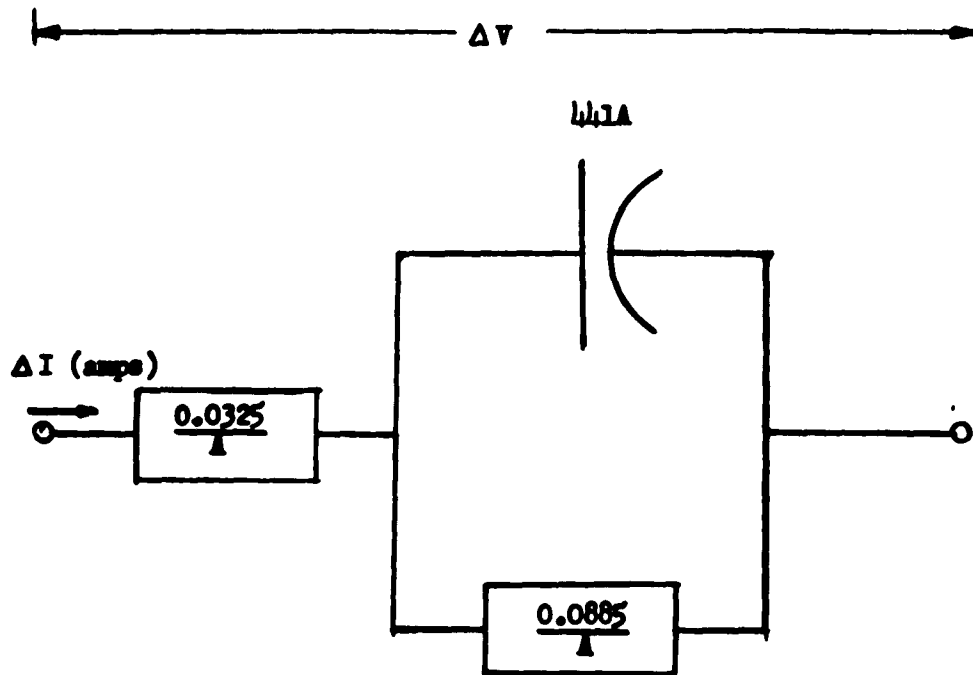
A = Area of Cathode in cm^2

Figure 4.4-6

Equivalent Circuit of a Vapor Thermionic Converter

4.5   **Voltage Control by Combination Switching and Series Regulating Circuits**

4.5.1   **Introduction**

During this reporting period, the analysis of a transistorized switching and series regulation circuit was completed. This included:

1. The development of typical total weight per unit power versus circuit efficiency curves for power levels of 1 KW and 10 KW (the 25 watt and 250 watts were presented in Fig. 4.5-9 through 4.5-12 of progress report #5).

2. The development of the relationship between volume and weight in the form of $\frac{volume}{weight}$ vs efficiency curves.

3. The investigation of the design limitations of the switching and series regulating circuit at various voltage and power levels.

The circuit, assumed transistor characteristics, assumed form factor and nomenclature were presented in section 4.5.1, 4.5.5, and figures 4.5-1, 4.5-5 of progress report #5.

4.5.2   **Weight per Unit Power Curves**

Results

In progress report #5, an analytical procedure for determining the weight per unit output power for a switching and series regulating circuit was discussed. The results are presented in the form of weight per unit power $\left(\frac{W_{TOT}}{P_D}\right)$ vs circuit efficiency (η_H) curves for various values of load voltage (V_L) and inherent source regulation (B). This form is convenient in evaluating regulation systems containing the switching circuit, either alone or in conjunction with external converter and inverter circuits. The various operating points evaluated are shown in Table 4.5-1.

Table 4.5-1

Output Power	Load Voltage	Inherent Source Regulation	
25 watts	6, 12, 28, 40	100%	40%
250 watts	6, 12, 40	100%	40%
1 KW	12, 20, (28), 10, 100	100%	40%
10 KW	20, (28), 10, 100	100%	40%

The 25 and 250 watt curves were presented in figures 4.5-9 through 4.5-12 of progress report #5. The 1 KW and 10 KW cases were completed during this reporting period and are shown in figures 4.5-1 through 4.5-4 of this report. In the 1 KW and 10 KW plots, the 28 volt curves

were obtained by interpolation from the other voltage points. The dotted portions of the curves are approximate since a per transistor saturation resistance less than the assumed value of .01 ohms is required to achieve the values indicated.

Analysis

The analytical method for generating the weight per unit power vs circuit efficiency curves for the 1 and 10 KW cases is the same as presented in section 4.5.2 of progress report #5 with two exceptions:

1. In order to obtain a reasonable fin effectiveness (.3 or greater), larger fin base plate thicknesses, t_B, were assumed for the 1 and 10 KW cases. The assumed values were $t_B = .05"$ for 1 KW and $t_B = .5"$ for 10 KW. This change causes equations 4.5-26, -29, -30 of progress report #5 to become respectively:

$$W_c = A_f \, \rho_c \left[t_B + t_c \, (1 + \tfrac{2}{H}) \right] + 2t_c \, \rho_c \, H$$

$$W_{TOT} = 2N_T W_t + A_f \, \rho_c \left[t_B + t_c \, (1 + \tfrac{2}{H}) \right]$$

$$+ \; 2t_c \, \rho_c \, H + \frac{(.0013 \, H - .0003) \, (P_{req})^{3.45}}{A_f^{\, 2.45}}$$

$$A_f \; (opt.) = P_{req} \left[\frac{2.45 \, (.0013 \, H - .0003)}{\rho_c t_B + \rho_c t_c \, (1 + \tfrac{2}{H})} \right]^{\tfrac{1}{3.45}}$$

2. A sign error was discovered in the derived expression for the maximum allowable value of saturation resistance (Eqn. 4.5-22 of progress report #5) which decreases the severity of the restriction. The correct expression is:

$$R_{s\;max} = \frac{E_L^{\;2} \, B - \frac{(B + 1)}{M} - \frac{V_{ces}}{E_L}}{P_D \, Z}$$

where: $Z = C + \sqrt{C^2 + D}$

$$C = \frac{E_L}{4M \, V_{ces}} \left[M \, (B - 1) - (B + 1) \right] - 1$$

and:

$$D = \frac{E_L}{2 \, V_{ces}} \left[B(M - 1) + 2 \right] - M$$

In view of this correction, the 250 watt, B = 100%, 6 volt $\frac{W_{TOT}}{P_D}$ vs η_M curve, shown dashed in figure 4.5-11 of progress report #5 is not restricted and should be considered as firm data.

In all other respects, the generation of the 1 and 10 KW curves is the same as previously used for 25 and 250 watts.

4.5-3 <u>Volume Characteristics</u>:

<u>Results</u>

The total volume (or volume per unit power) can be obtained from the total weight (or weight per unit power) by application of a volume to weight ratio (V_{TOT}/W_{TOT}). Figure 4.5-5 shows the (V_{TOT}/W_{TOT}) ratio as a function of minimum circuit efficiency for the various power levels of interest. Note that the volume so obtained applies to a circuit partially optimized with respect to weight and does not represent any optimization with respect to volume.

<u>Analysis</u>

For the assumed package configuration (see figure 4.5-5 of progress report #5), the volume can be expressed as:

(4.5-1) $\qquad V_{TOT} = A_f (1 + t_B + l)$

<div style="margin-left:2em">

where A_f is the fin base plate area in in^2;
1 inch is the assumed enclosure thickness;
t_B is the assumed base plate thickness in inches,
and l is the fin length, in inches, obtained from the minimum weight fin design computer program (see para. 4.5.2.6 of progress report #5).

</div>

Using equation 4.5-29 of progress report #5 the ratio of package volume to package weight can be expressed as:

(4.5-2) $\qquad \dfrac{V_{TOT}}{W_{TOT}} = \dfrac{1 + t_B + l}{\dfrac{2N_T w_t}{A_f} + \rho_c\left[t_B + t_c\left(1 + \dfrac{2l}{H}\right)\right] + \dfrac{2\rho_c T_c H}{A_f} + (.0013\,H - .0003)\left(\dfrac{P_{req}}{A_f}\right)^{3.45}}$

The variation of equation 4.5-2 with voltage level and/or source regulation is small; thus allowing a single curve for each power level.

As a result of the partial optimization of total weight (see sect. 4.5.2.7 of progress report #5) an optimum value of A_f is obtained. Physically, however, A_f must be equal to or greater than $A_T N_T$, the total base area of the power transistors; Therefore:

(4.5-3) $\qquad A_f = A_{f(opt)}$ when $A_{f(opt)} \geq A_T N_T$

$\qquad\qquad\quad A_f = A_T N_T$ when $A_{f(opt)} < A_T N_T$

The points when $A_f = A_{f(opt)} = A_T N_T$ are indicated by vertical

dashed lines on fig. 4.5-5. To the left of these points, A_f = $A_{f(opt)} > A_T N_T$; to the right, A_f = $A_T N_T > A_{f(opt)}$.

4.5.4 Design Considerations

Generally when designing a power supply the load voltage will be specified. Furthermore, the inherent source regulation will usually be determined by efficiency or life considerations. Under these conditions, only certain discrete open circuit voltages are possible for each power source unit. As a result only discrete values of switching circuit efficiency are achievable in any given application.

The relationship between power source unit open circuit voltage E_O, and efficiency η_M is given by:

$$(4.5-4) \qquad E_o^2 + E_o E_L \left[\frac{1}{\eta_M \left(\frac{1}{\beta} + \frac{1}{\beta 2}\right)} - (1 + B) + \frac{\left(1 + V_{cem}\right)\left(\frac{2}{\beta} + \frac{1}{\beta 2}\right)}{\left(\frac{1}{\beta} + \frac{1}{\beta 2}\right)} \right]$$

$$+ \frac{(B + 1) E_L^2}{\left(\frac{1}{\beta} + \frac{1}{\beta 2}\right)} \left[1 + \frac{V_{cem}}{E_L} - \frac{1}{\eta_M} \right] = 0$$

Fig. 4.5-6 and 4.5-7 show equation 4.5-4 evaluated for various values of V_L, for B = 100% and B = 40% respectively. In these figures a V_{cem} of .2 and a β of 15 were assumed.

For a series arrangement, the open circuit voltage of a power source unit is restricted to multiples of the open circuit voltage of a single cell. The open circuit voltage of a single cell is, in turn, generally restricted in some manner dependent upon the type of source involved. For the hydrogen-oxygen and hydrogen-air fuel cells, the equivalent open circuit (intercept) voltage is .95V and .9 volts respectively. These values are determined by the chemical processes involved. For a single thermionic converter, the open circuit voltage is a function of cathode temperature but the cathode temperature is largely dictated by efficiency considerations and heat source capabilities. The open circuit voltage of a single thermoelectric couple is similarly determined by the temperature difference between the hot and cold junction and, in practice, this would be largely determined by source, sink, and material considerations.

By way of illustration, the single cell open circuit voltage of a hydrogen-air fuel cell is shown on figs. 4.5-6 and 4.5-7. For a 6 volt source consisting these cells, the max. switching circuit of efficiency is approximately 89.2% for a source regulation of 100% and 85.8% for a source regulation of 40%. The typical open circuit voltage of a lead telluride thermocouple with a temperature differential of 800°F is .2 volts, giving higher max. switching circuit

efficiencies, particularly at low output voltages. The intercept voltage of a vapor thermionic converter at a cathode temperature of 1330°F and optimum anode and cesium reservoir temperatures is .55V, midway between the H_2-air fuel cell and the P_bT_e thermoelectric couple.

The internal resistance of each power source unit is related to the open circuit voltage E_o, the output voltage V_L, andthe power output P_o, and the defined source regulation B.

(4.5-5)

$$R_g = \frac{E_o E_L}{P_D}\left[1 - \frac{1}{(B+1)\eta_M}\right]$$

Figures 4.5-6 and 4.5-7 and equation 4.5-5 can be used in conjunction with the weight per unit power vs efficiency curves for either estimating the efficiency and weight of a switching circuit for use with a specific power supply or, conversely, estimating the generator requirements in order for the circuit to exhibit a particular efficiency and/or power per unit weight.

Example: Let it be assumed that a regulated hydrogen-air fuel cell power supply is required which has a rated output of 1 KW at 28 VDC. Because of fuel cell life and efficiency considerations, it is desirable to operate the cell stack at an inherent regulation of approximately 40%. Then from the 28 volt line of fig. 4.5-7, the switching circuit efficiency for source units consisting of 1, 2, or 3 cells can be determined.

No. of Cells per Unit	Open Circuits Voltage, E_o	Switching Circuit Efficiency
1	.9 volts	96.8%
2	1.8 "	94.4%
3	2.7 "	91.9%

Using the efficiency in fig. 4.5-2, the weight per unit power (and weight) of the switching circuit can be determined.

Open Circuit Voltage, E_o	Weight/Power	Weight
.9 volts	2.5 lbs/KW	2.5 lbs
1.8 "	2.8 lbs/KW	2.8 "
2.7 "	3.5 lbs/KW	3.5 "

Using the E_o and η_M values, the R_g can be determined from equation 4.5-5.

E_o	R_g
.9 volts	.0066 ohms
1.8 "	.0122 "
2.7 "	.0168 "

The designer could then use the switching circuit efficiency and weight data in conjunction with fuel cell weight curves to determine the best combination for this particular application. In this particular

example, the lowest circuit weight occurs at the highest efficiency. Thus, the minimum weight power supply would be achieved by using one cell (E_0 = .9 volts) per power source unit.
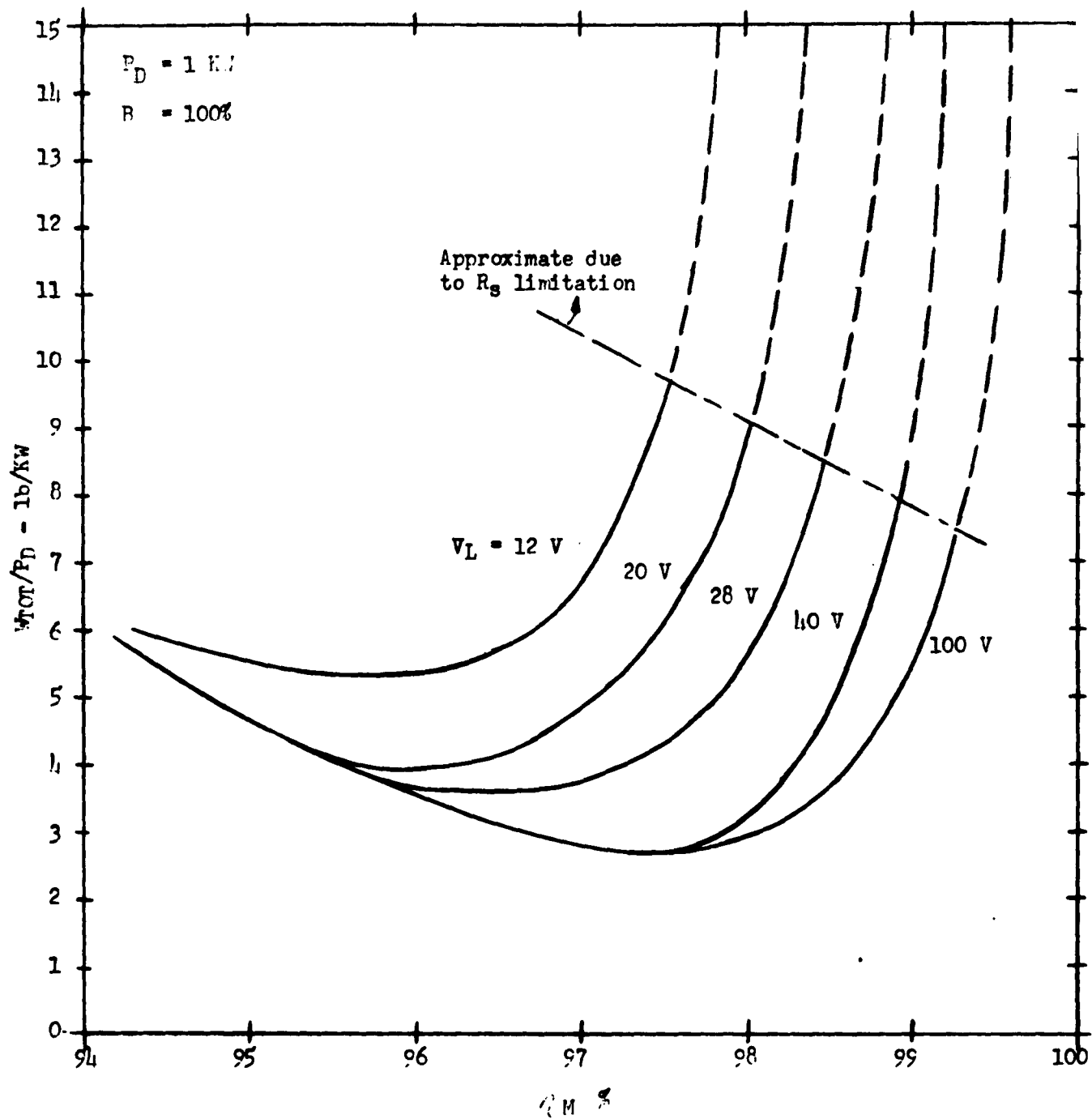
Figure 4.5-1

Weight Per Unit Power Versus Minimum Circuit Efficiency
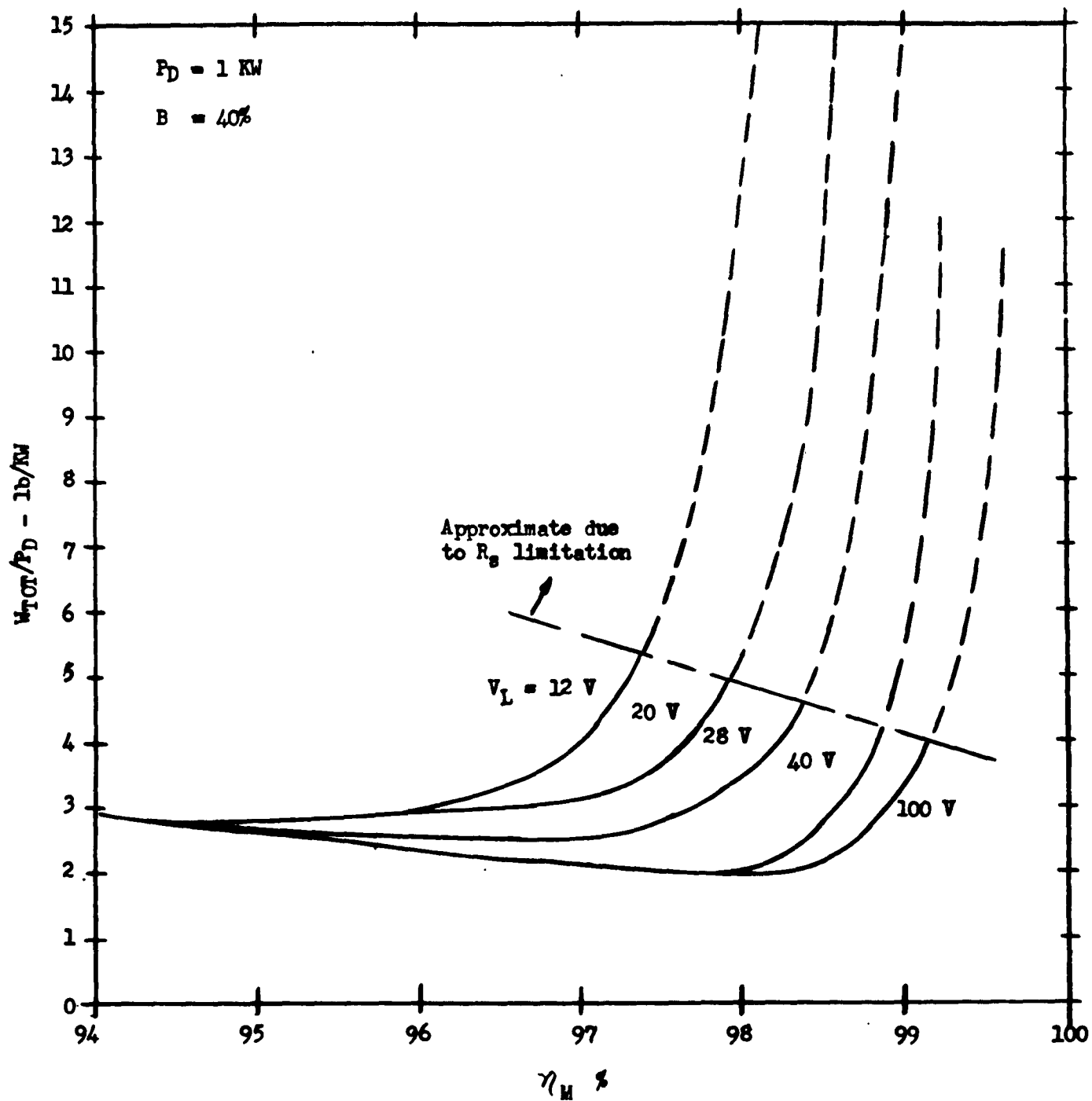
Figure 4.5-2

Weight Per Unit Power Versus Minimum Circuit Efficiency
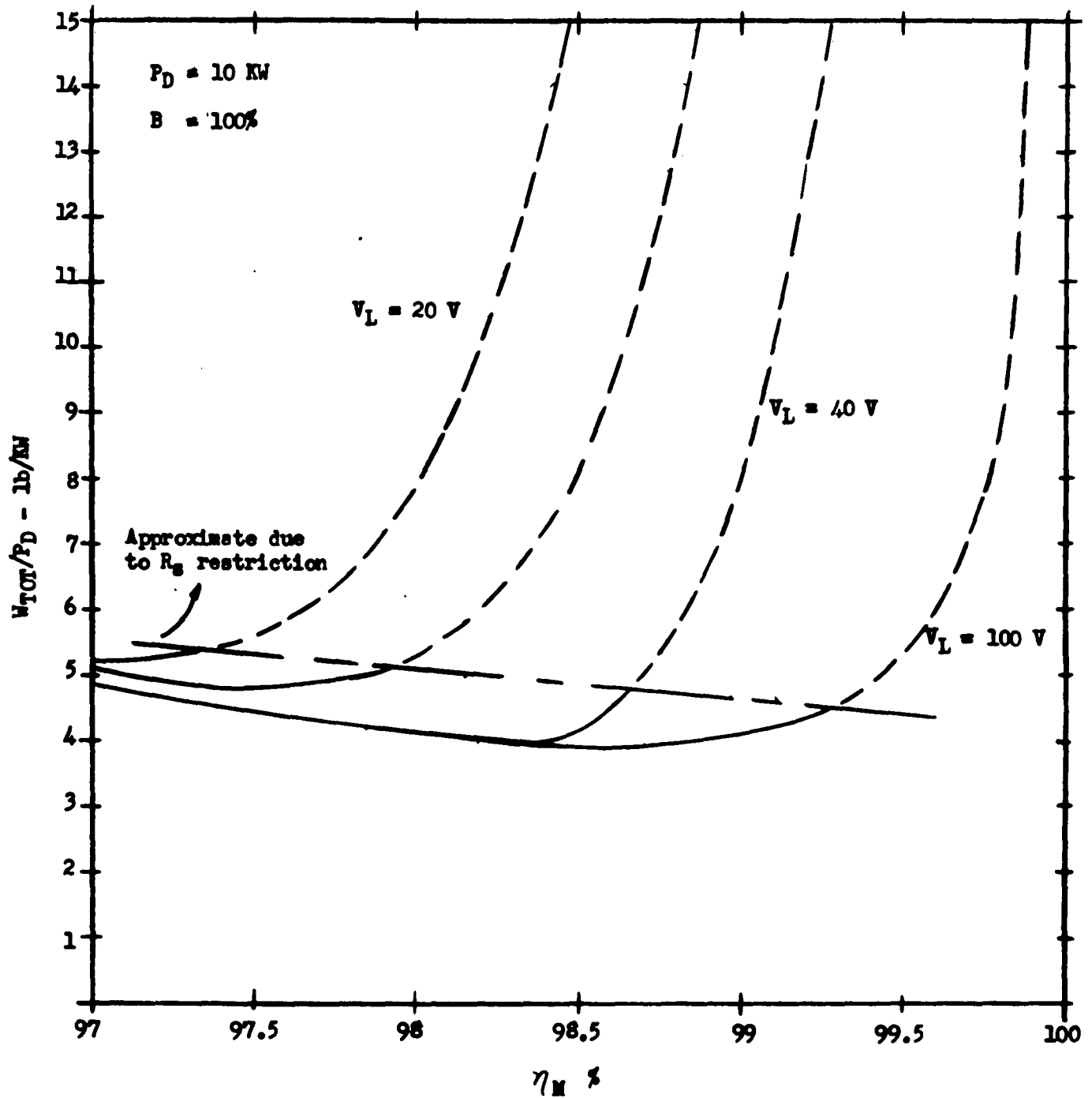
Figure 4.5-3

Weight Per Unit Power Versus Minimum Circuit Efficiency
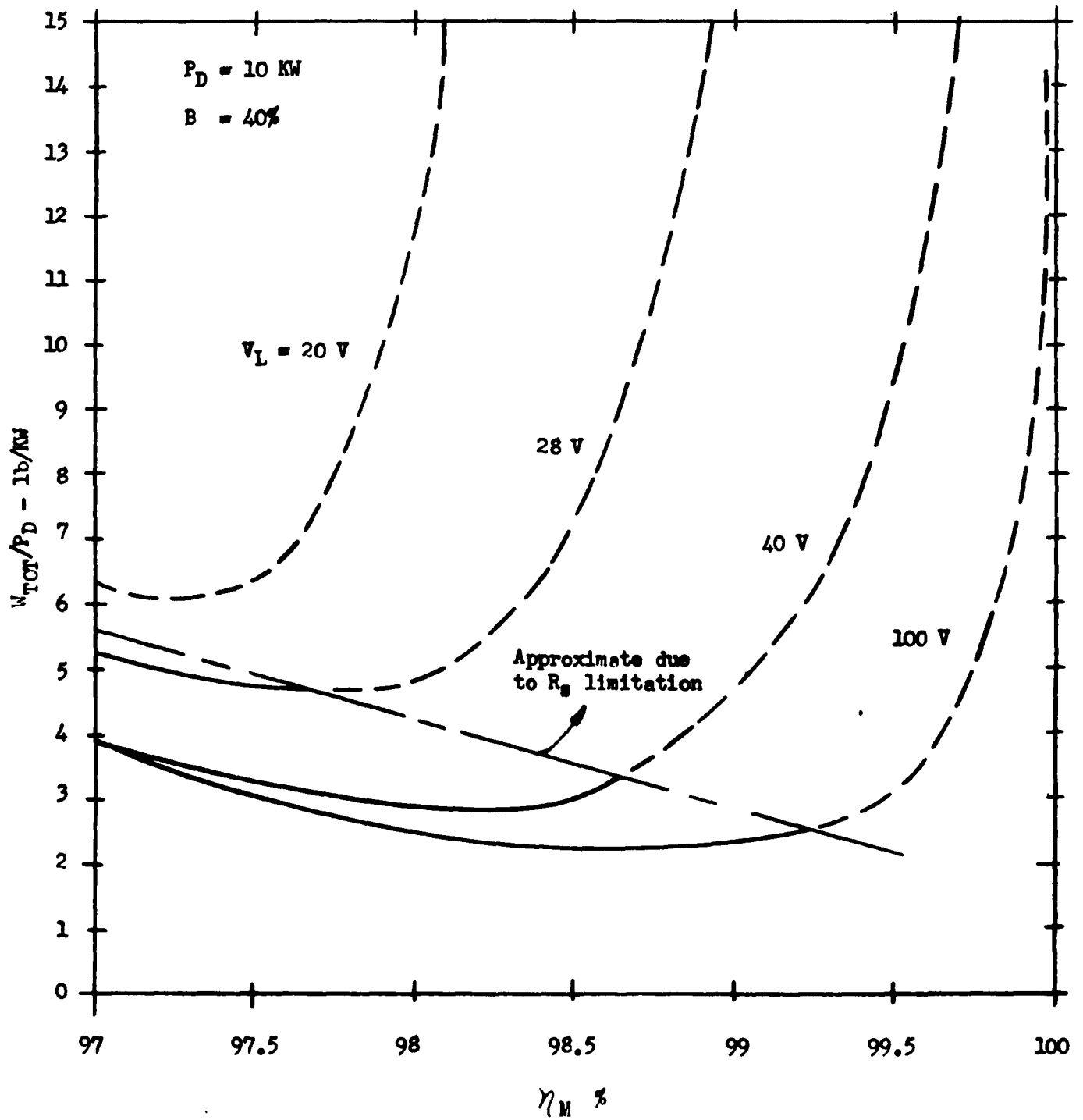
Figure 4.5-4

Weight Per Unit Power Versus Minimum Circuit Efficiency
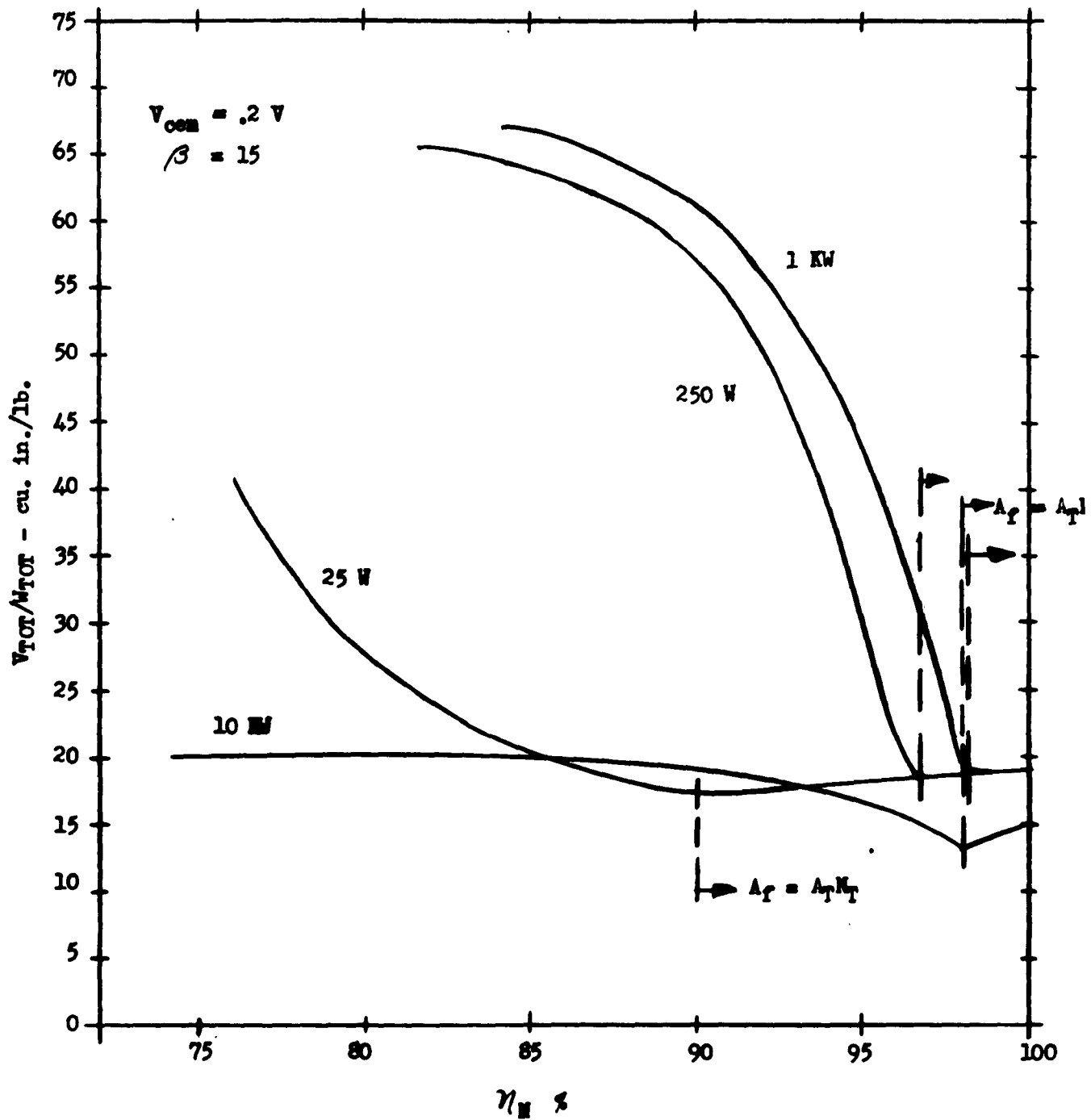
Figure 4.5-5

Volume to Weight Ratio Vs. Minimum Efficiency
for Power Levels of Interest
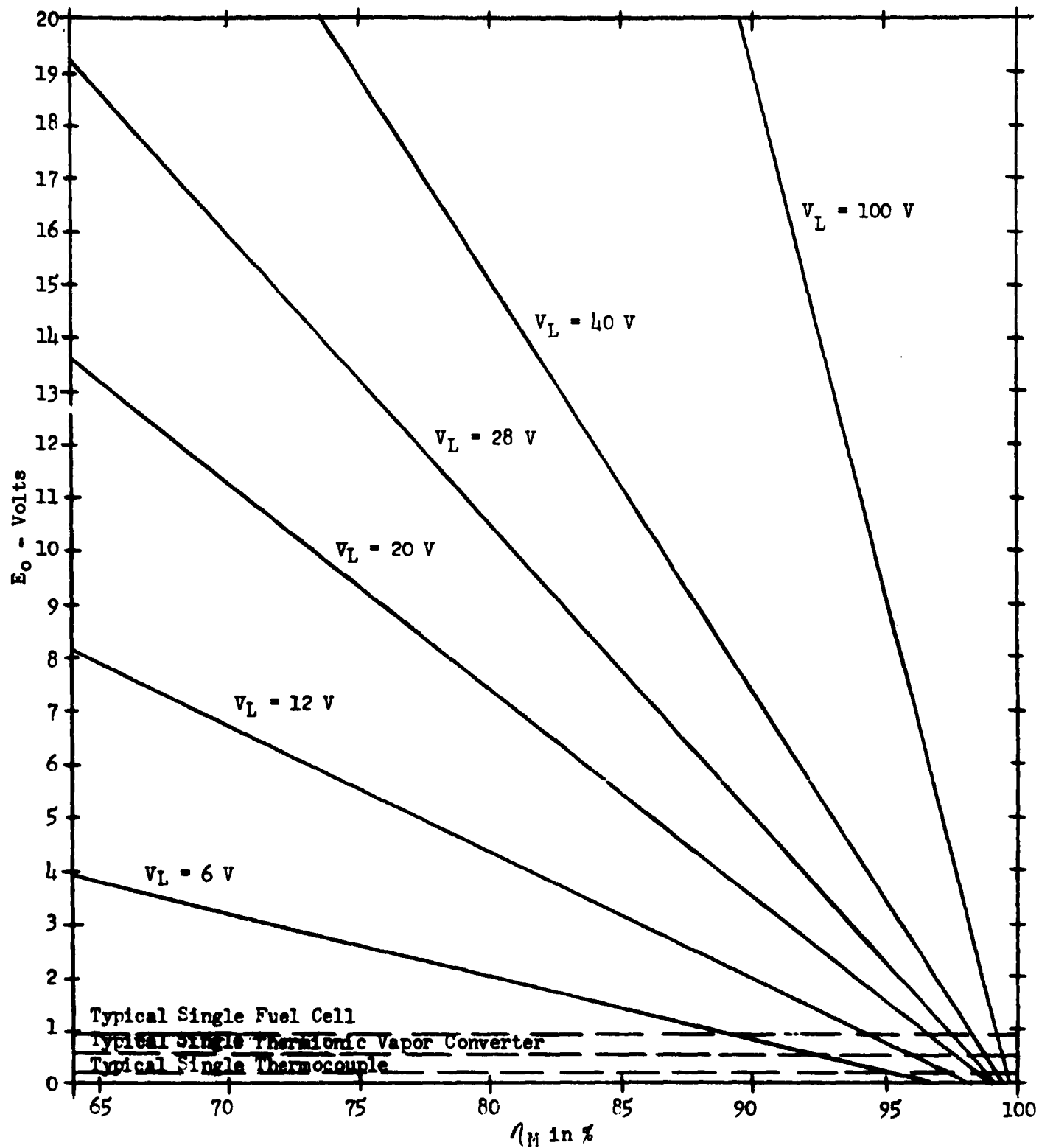
Figure 4.5-6

Open Circuit Voltage (E_0) of a Power Source Unit
Versus Circuit Efficiency for 100% Source Regulation
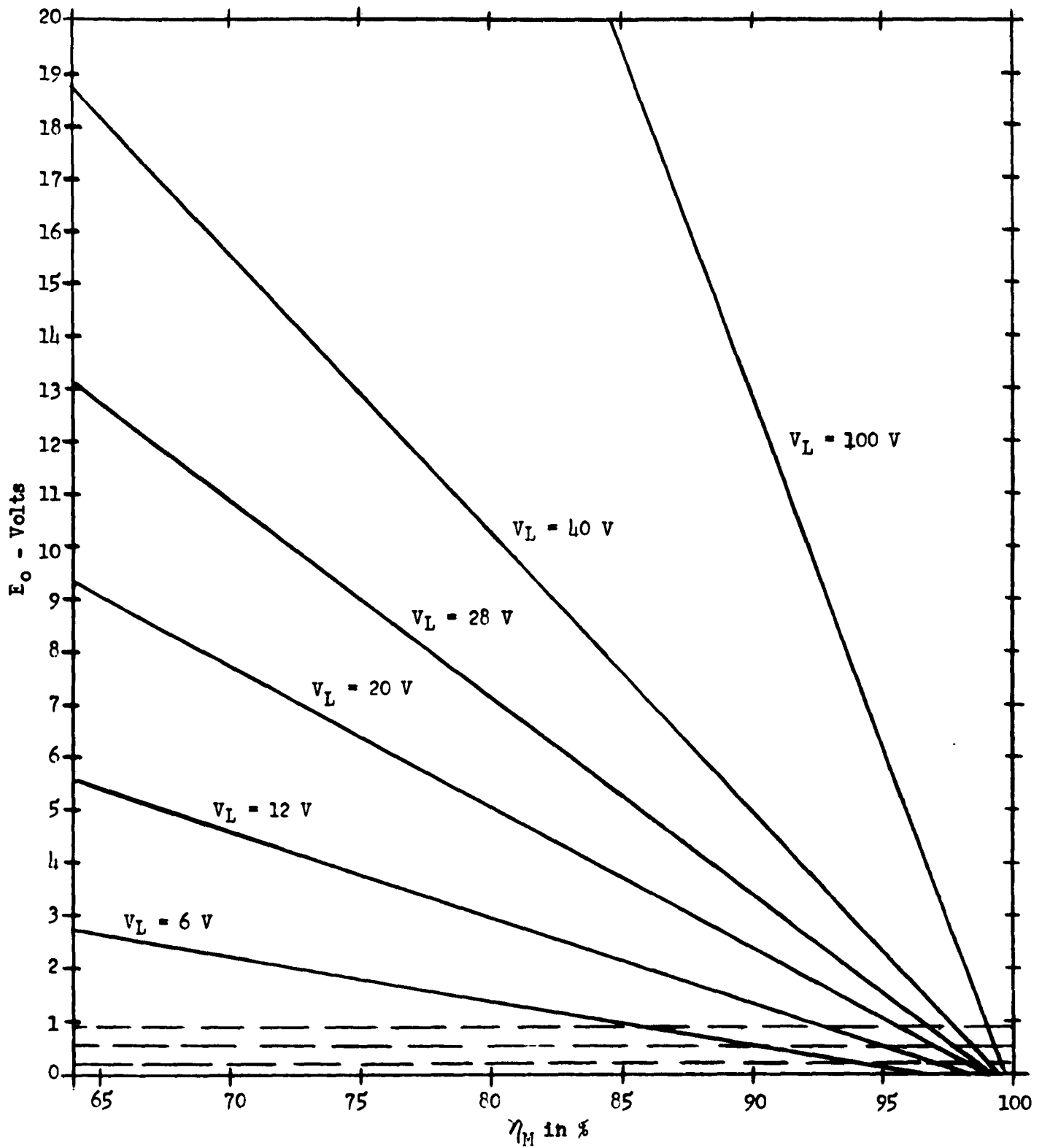
Figure 4.5-7

Open Circuit Voltage (E_o) of a Power Source Unit
Versus Circuit Efficiency for 40% Source Regulation

- 95 -

5.0 TECHNICAL PROGRESS - EXTERNAL VOLTAGE CONVERSION AND REGULATION

5.1 Resume'

Durirg the past reporting period, effort has been applied to four major areas of investigation. A summary of the progress is included in this status report. This portion of the report is divided into four major areas of investigation as follows:

1. Study of the "Flyback" circuit using power transistors.
2. Summary of SCR Voltage conversion circuits.
3. Quantitative evaluation of DC-AC power transistor conversion circuits.
4. Evaluation of low input voltage conversion circuits.

Item 1 includes a presentation of weight vs efficiency for the "Flyback" step up circuit (DC-DC) using power transistors as the switching element. Curves are presented for the following Design Points:

Power Output - P_c	25 W			250 W			1 KW		
Input Voltage Regulation -R (Per cent)	0	40	100	0	40	100	0	40	100
ESFL - Full Load Input Voltage				6	6	6			
	12	12	12	12	12	12	12	12	12
	20	20	20	20	20	20	20	20	20

Table "A"

Item 2 includes a general summary discussion of SCR voltage converter circuits. Item 3 includes a presentation of circuits selected and evaluated for DC-AC inverters utilizing power transistors. Curves of weight vs efficiency have been plotted from the following Design Points:

Power Output - P_c	25 W			250 W			1 KW		
Input Voltage Regulation -R (Per cent)	0	40	100	0	40	100	0	40	100
							12	12	12
E_{SFL} = Full Load Input Voltage	20	20	20	20	20	20	20	20	20
	40			40			40	40	40

Table "B"

Item 4 is a presentation of circuits selected and evaluated for low input voltages. Curves of weight vs. efficiency for both DC-DC, and DC-AC transistor circuits have been plotted for the following Design Points:

Power Output - P_o	25 W			250 W		
Input Voltage Regulation -R_s (Per cent)	0	40	100	0	40	100
E_{SFL} = Full Load Input Voltage	1 6	1 6	1 6	1 6	1 6	1 6

Table "C"

In all cases the weight information presented in section 5.0 of these reports includes the major electrical component weight only. In order to obtain the packaged weight, the weight of structural and mounting hardware must be added. In this case a curve giving the ratio of packaged weight to major electrical component weight has been established based on previous hardware experience. This curve is shown in figure 5.1-1. Thus, in order to obtain package weight in any case, it is only necessary to multiply the major component weight by the appropriate factor as obtained from figure 5.1-1.

Another item of interest is the volume of the overall electrical circuit package. Figure 5.5-2 shows a curve giving a packaged volume factor which can be used to calculate volume from the major component weight data.

Figure 5.1-1

Curve Showing the Relationship Between Packaged Converter
Weight and Calculated Circuit Weight as a Function of
Converter Output Power Rating

$$\text{Packaged Weight}\left(\frac{\text{lbs.}}{\text{KW}}\right) = K_1 \left[\frac{W_c}{P_c}\right]$$

K_1 = packaged weight factor

$\dfrac{W_c}{P_c}$ = major electrical component weight
in lbs/KW

Converter Output Power Rating - Kilowatts (P_c)

K_1 - Packaged Weight Factor

Figure 5.1-22

Curve Showing the Relationship Between Packaged Converter
Volume and Calculated Circuit Weight as a Function of
Converter Output Power Rating

Packaged Volume $\left(\dfrac{in^3}{KW}\right) = K_2 \left[\dfrac{W_c}{P_c}\right]$

K_2 = packaged volume factor

$\dfrac{W_c}{P_c}$ = major electrical component weight in lbs/KW.

K_2 - Packaged Volume Factor

Converter Output Power Rating - Kilowatts (P_c)

5.2   DC-DC Flyback Step-Up Circuit Investigation

5.2.1   Introduction

The results of the study of the flyback circuit (figure 5.2-1) using silicon controlled rectifiers was presented in progress report no. 5 for the 20 volt input 10 KW condition. This circuit was considerably lighter and more efficient than the other DC-DC circuits considered for this operating condition. Consequently, it was decided to explore the use of a flyback circuit employing power transistors at lower loads and other voltages. The particular conditions considered are indicated in Table "A" of section 5.1.

5.2.2   Results

The results of the power transistor flyback circuit investigation are shown in figures 5.2-7 through 5.2-9. In each case the weight per unit power is shown for various source voltages and source voltage regulations.

5.2.3   Discussion of Results

Effect of Source Voltage and Source Regulation

The unique characteristics of the flyback circuit may best be determined by examination of figure 5.2-8. First, the zero percent source regulation curve is not always the lightest for a given source voltage condition. For example, at a source voltage of 20 volts, the 40% input regulation circuit is lighter than the zero per cent case. Also, it should be noted that at a source voltage of 12 volts, the condition of 40% source regulation results in a heavier circuit than do either the zero or 100% regulation condition. These results are best understood in the light of the following considerations.

One criterion for optimum employment of this circuit is that the difference between the source voltage and load voltage under no load conditions should be as small as possible. This helps minimize inductor size. This is the reason for the low weight conditions at 40% regulation for 20 volts and 100% regulation at 12 volts.

A second characteristic of the circuit is that the inductance of the reactor is proportional to the square of the no load source voltage. Thus, at each source voltage the inductance would be smallest for zero per cent regulation. This characteristic tends to favor minimum weight at zero per cent regulation.

A third criterion for optimum employment of this circuit generally is that the full load current should be small to result in a minimum $\frac{1}{2}I^2L$. As the voltage is reduced from 20 to 12 to 6 volts the full load current increases. Hence, the weight tends to be greatest for the higher current and lower voltage conditions.

The 6 volt family of curves shows the 100% regulation curve to be heavier than the 40% regulation curve, which is the opposite of what occurs with the 12 volt source. The reason for this is that the difference between no-load source voltage and load voltage is not as severely affected by source regulation at 6 volts as it is at 12 volts.

The best performance is obtained with sources having no-load voltages of about 28 volts. For example, a 20 volt source should have about 40% regulation for best performance while a 14 volt source should have about 100% regulation for best performance.

Effect of Power

The inherent nature of conventional electrical apparatus such as transformers and reactors is that the per unit weight decreases and the efficiency increases for increasing power levels. The results presented in figures 5.2-7, 5.2-8, and 5.2-9 substantiate this fact. For example, the reactor power handling capability is related to the product of total flux and window current. The iron cross-section as well as the core window area varies as the square of a linear dimension. Therefore, the product of flux and window current varies as the 4th power of a linear dimension. However, weight and losses go up as the 3rd power of a linear dimension.

Efficiency

The slope of the curves in figures 5.2-7 through 5.2-9 is relatively shallow. This indicates the maximum efficiency limit has not been reached. A large portion of the total losses occur in the reactor. Hence, a further trade-off of reactor weight for capacitor weight appears to be possible from the standpoint of reducing total losses. Also, the use of more iron and copper in the reactor could improve efficiency at a still profitable rate.
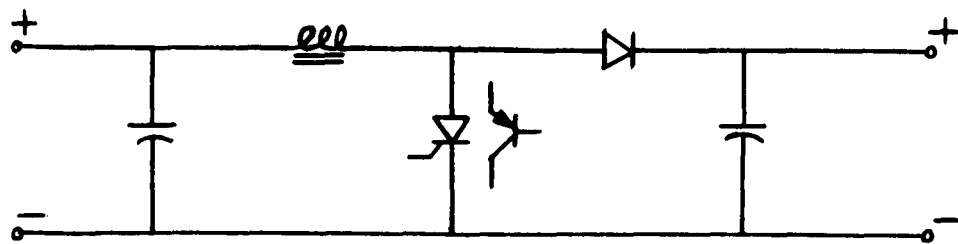
Figure 5.2-1   BEDFORD STEP-UP CIRCUIT (Flyback)
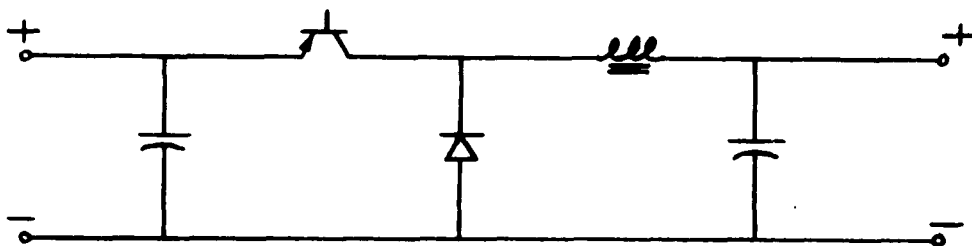
Figure 5.2-2   MORGAN STEP-DOWN CIRCUIT
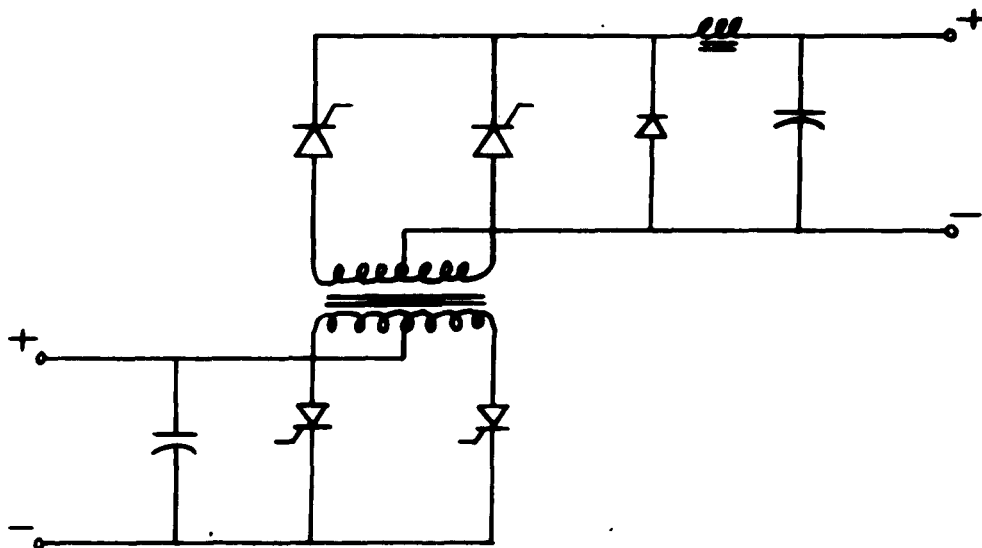
Figure 5.2-3   CENTER TAP TRANSFORMER
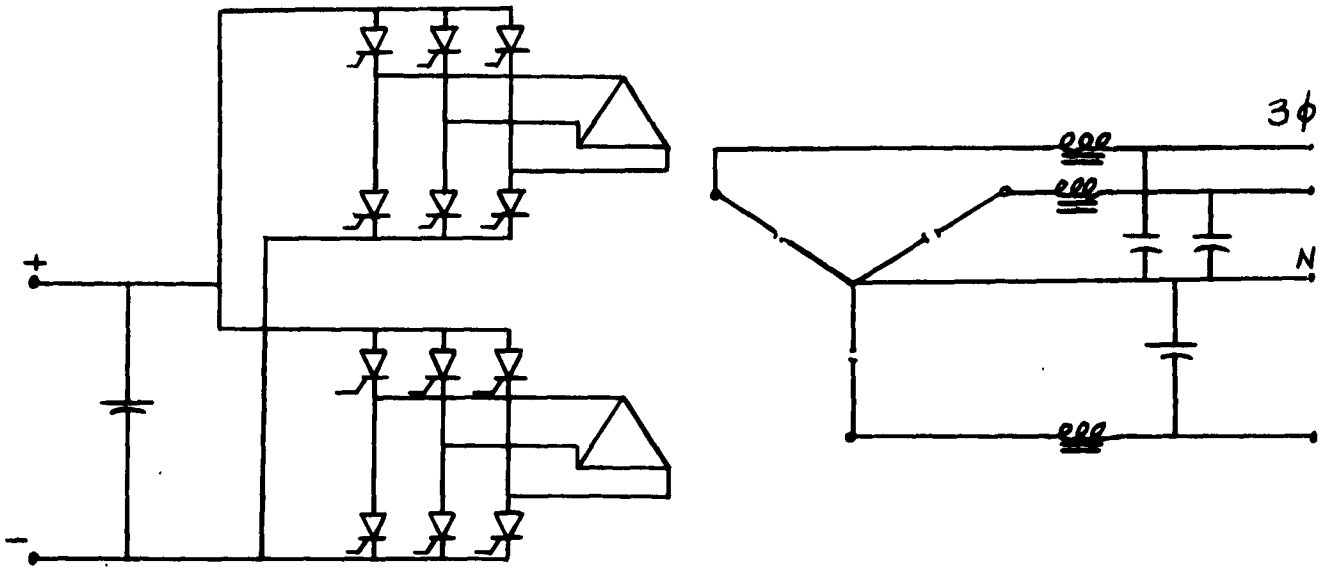
Figure 5.2-4   VOLTAGE REGULATION BY PHASE SHIFT
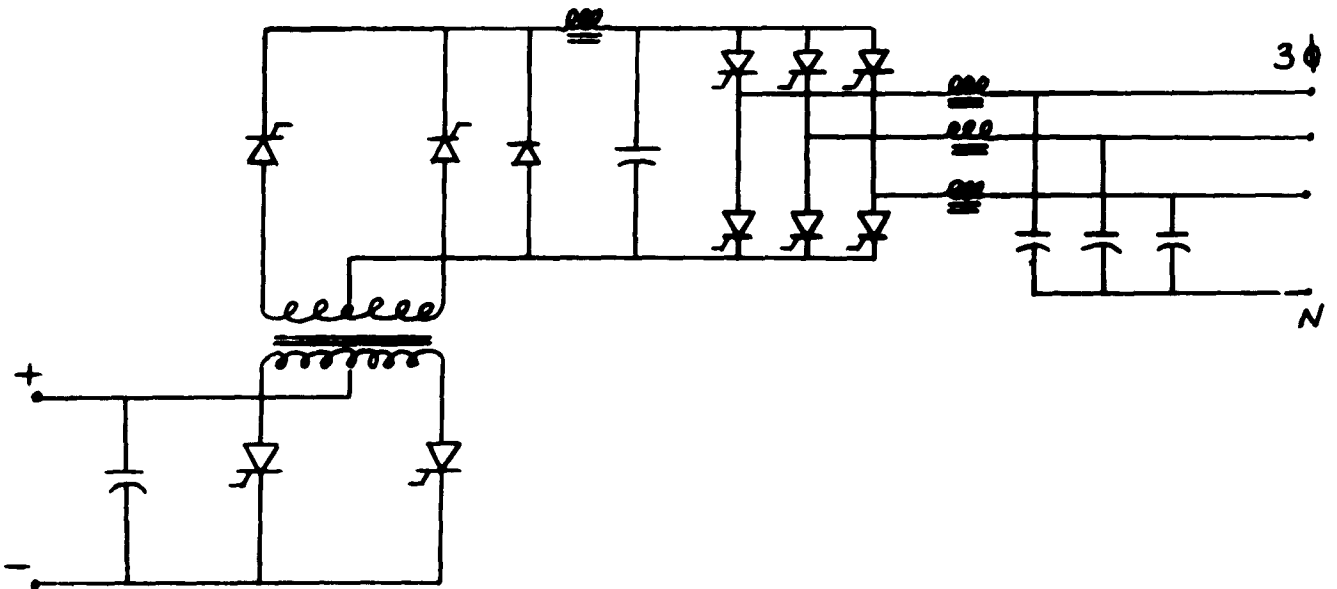
Figure 5.2-5   TRC REGULATION WITH CENTER TAP TRANSFORMER
IN DC SECTION
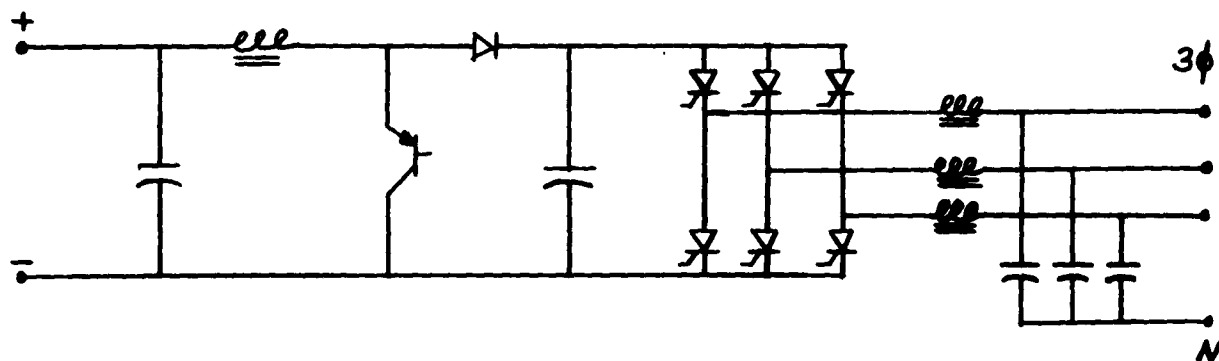
Figure 5.2-6   TRC REGULATION WITH BEDFORD
                 STEP-UP CIRCUIT IN DC SECTION

Converter Weight Curves

Nomenclature:

E_{SFL} = Full Load Input Voltage

W_c = Converter Weight (Major Components Only)

P_c = Converter Rated Output Power

R_s = Input Voltage Regulation

η_c = Full Load Converter Efficiency

Circuit of Figure)

DC to 28v DC

Output Power 1000 watts

E_{SFL}

12 v

20 v

Radiation R_s

40%

80%

20%

40%

η_c (%) $\rightarrow$

80   85   90   95   100

$\frac{W_c}{P_c}\left(\frac{\#}{Kw}\right)$

80

60

40

20

0

Figure 5.2-7

Circuit of Figure 11
DC to 28v DC
5:1 p.u. power 250 watts

Converter Weight Curves
(Kilograms/Cm) (D_0/V_0)

Figure 3:2.8

Figure 5...

5.3   **Silicon Controlled Rectifier Conversion Circuits**

5.3.1   **Summary of the DC-DC Voltage Converter Circuit Study**

The Bedford Step-up Circuit shown in figure 5.2-1 was studied for
10 KW rating, and the results were reported in figure 8 of
Progress Report No. 5. These results are not in line with the
1000, 250, and 25 watt results in figures 5.2-7 through 5.2-9 of
this report. The 10 KW circuit employed SCR switching elements while
the 1000, 250 and 25 watt circuits used power transistors. More
power is lost in the forward drop of the SCR's which in turn
necessitates heavier heat sinks. Also, alumalytic capacitors were
assumed for the SCR circuit while light weight tantalytic capacitors
were considered with the power transistor circuits.

The center tap transformer converter circuit of figure 5.2-3 was
previously studied and the results reported in figure 5-9 of
Progress Report No. 5. This circuit handles commutating energy in
an efficient operation, and it appears to be best employed to step
down power with SCR's. Although the Morgan Step-Down circuit
of figure 5.2-2 does not lend itself to efficient SCR switching,
it is possible that a power transistor switching element might make
this circuit lighter and more efficient than the center tap
transformer circuit for the case of voltage step down applications.
Unfortunately, the allowable effort did not permit evaluation of
the transistorized Morgan Step-Down circuit.

5.3.2   **Summary of the DC-AC (3ϕ) Voltage Converter Study**

Table 5.3-1 shows typical performance characteristics of the phase-
shift regulated inverter circuit of figure 5.2-4 for a source having
40% regulation. Table 5.3-2 shows similar data for the TRC regulated
inverter circuit of figure 5.2-5. Regulation by phase-shift
(figure 5.2-4) appears best at higher voltages because the current
is least and the forward watts in the SCR's is minimized. The TRC
regulated inverter of figure 5.2-5 appears best at low voltage
because the high source current passes through only one SCR which
results in a minimum of forward watts loss. The single transformer
used in the circuit of figure 5.2-5 is lighter and more efficient
than the two 3-phase transformers of figure 5.2-4 despite the fact
both primary and secondary windings are one way. Normally, a
square wave transformer is heavier than a sine wave transformer.
However, this effect is more than offset by splitting power six ways
in the two 3-phase transformers. Essentially, one circuit requires
six transformers and the other only one.

Figure 5.2-6 is a new circuit not yet evaluated quantitatively. On
the basis of our previous work, it appears to hold great promise for
medium and high voltage sources. It incorporates the Bedford Step-Up
circuit in the regulating stage, and it has no need for a heavy
transformer.

The circuits in figures 5.2-5 and 5.2-6 have a neutral which is
created by virtue of the wye point of the output filter capacitors.

Figure 5.2-4 displays a conventional neutral from the output transformer. The circuits of figures 5.2-3 through 5.2-5 provide electrical isolation between load and source while those of figures 5.2-1, 5.2-2, and 5.2-6 do not.

Table 5.3-3 summarizes the SCR circuits which our calculations have shown generally to yield least weight and highest efficiency. The circuit shown in Figure 5.2-6 is included on the basis of a qualitative evaluation only.

TABLE 5.3-1 PERFORMANCE CHARACTERISTICS OF SCR PHASE SHIFT REGULATOR OF FIGURE 5.2-4 (FOR 40% SOURCE REGULATION TAKEN FROM FIGURES 5-12, 5-13 and 5-14 IN P.R. NO. 5)

SOURCE VOLTAGE =	20 V		40 V		100 V	
Load	#/kw	% eff.	#/kw	% eff.	#/kw	% eff.
10 kw	50	77	30	85.4	25	92.2
1 kw	-	-	45	82.5	40	89.5
250 watts	-	-	55	79	-	-

TABLE 5.3-2 PERFORMANCE CHARACTERISTICS OF SCR TRC REGULATOR OF FIGURE 5.2-5 (FOR 40% SOURCE REGULATION TAKEN FROM FIGURES 5-15, 5-16, and 5-17 IN P.R. NO.5)

SOURCE VOLTAGE =	20 V		40 V		100 V	
Load	#/kw	% eff.	#/kw	% eff.	#/kw	% eff.
10 kw	50	81	30	85.4	25	90
1 kw	-	-	45	82	40	86.3
250 watts	-	-	55	78.7	-	-

TABLE 5.3-3 SCR CIRCUITS YIELDING LEAST WEIGHT AND HIGHEST EFFICIENCY

DC to 28 Volts DC	Circuit
Step-Up	Figure 5.2-1
Step-Down	Figure 5.2-3
DC to 3∮ 115 Volts AC	
20 V Source	Figure 5.2-5
40 V Source	Figure 5.2-4, 5.2-5, 5.2-6
100 V Source	Figure 5.2-4, 5.2-6

5.4 Power Transistor DC-AC Inverter Circuits

5.4.1 Introduction

A selection and evaluation of DC-DC transistor circuits was presented in Progress Report No. 5. The results of a continuation of that effort as applied to DC-AC transistor circuits is presented herein. The requirements for the AC power system have been specified in Progress Report No. 4, June 30, 1961, Section 5.1. The basic output power requirements are listed below:

Frequency — 400 cps ± 1% steady state
Output Voltage — 115 volts, 1∅ for power outputs ≩ 1 KW
Voltage tolerance — ± 1% of steady state value
Power factor — .5 P.F.
Harmonic Content — Total harmonic content:
Not greater than 5% of the fundamental (rms) with no individual harmonic exceeding 4% of the fundamental over rated load with .5 p.f. (Lagging)

Circuits have been selected for discrete design parameters as listed in Table B, section 5.1, of this report. The most promising circuit techniques have been selected and evaluated on the basis of the following assumptions and limitations:

1. Output power requirements will at least meet the minimum requirements as stated above.

2. Inverter will be capable of delivering a 25% overload current - however, all specifications of frequency stability, voltage tolerance and harmonic content do not apply at the overload conditions.

3. All calculations are based on room temperature (20-25°C) operation with no forced air, liquid or other means of cooling considered.

4. Standard commercially available components have been assumed throughout.

5. Source input voltage refers to input voltage at rated full load.

6. Transistor and other semiconductor weights include the weights of appropriate heat sinks.

7. The maximum allowable ripple at the source shall not exceed ± 5% of average state input voltage.

8. Calculations of efficiency are based on circuit losses at rated load only.

Figure 5.4-1 represents a well known circuit configuration which has been used with considerable success. The circuit is sometimes referred to as a half-wave push-pull converter. For relatively low power outputs and low input voltages the simplicity of the circuit warrants its selection as the approach to be used for DC-AC inversion. At any given instant of time, the only circuit components in series with the power current is one-half of the primary of transformer T_1 and a switching transistor. To minimize size of the filter required at full load, transistor Q_1 and Q_2 conduct for intervals of 120°. At this conduction angle, there is no third harmonic voltage present in the output of transformer T_1. Voltage regulation is achieved by varying the conduction angle. Since the harmonic content of the output voltage is a function of the conduction angle, the output waveshape distortion increases somewhat at light loads.

The sine wave filtering employed in figure 5.4-1 consists of a resonant inductance and capacitance tuned for the fundamental frequency of 400 cps. The tuned LC is in turn shunted by capacitor C_2. This technique of filtering has the advantage of minimizing current drawn at light loads. Another advantage is the flexibility available to the circuit designer. The relationship between L_1, C_1, C_2, can be varied over a wide range in order to achieve the optimum weight of the overall filter.

For inverters rated at 25 watts at an input voltage of 20 volts, input voltage regulation of 0%, 40% and 100%, the approach shown in figure 5.4-1 is justified. The feedback diodes shown will enable the circuit to operate with inductive loading. The use of multistage filtering and more rigorous techniques of maintaining voltage control are not justified at the low power level because the added circuit complexity will result in increased circuit weight. The circuit was also evaluated at a 40 volt input, 0% regulation. The definition of 0% regulation (as stated in P.R.#5, September 1961) does not imply a zero impedance source, but rather implies a source capable of delivering a constant voltage over its rated load.

Circuit B - Figure 5.4-2

A power system with a power output rating of 250 watts with a DC input voltage that varies 2 to 1 is sufficiently complex to justify utilizing circuit techniques that heretofore would not have decreased the system weight per unit efficiency. The proposed circuit configuration utilizes two independent push-pull inverters with the secondaries of the output transformers connected in series. Voltage control is achieved by phase shifting section B (figure 5.4-2) with respect to Section A. To minimize or eliminate the third harmonic present in the out voltage, both unit A and unit B operate with a conduction angle of 120°. Since the output voltages of T_1 and T_2 are

added simultaneously and the individual voltages do not contain any third harmonic, the resultant output voltage will also be free from any third harmonic component. The basic difference between circuit D and circuit E is in the method of controlling the output voltage.

One of the factors considered in the selection of circuit E is that two transformers are required whereas only one is used in circuit D. Although the sum of the power ratings for the two transformers of circuit E is the same as required for the single transformer of circuit D, the total weight per unit power is greater and the efficiency less due to the lower performance capabilities of smaller transformers. In low power ratings, the weight predominance of the transformer favors circuit D whereas in larger power ratings, other factors such as component ratings and filter size become significant and thus tend to favor circuit E.

Circuit G - Figure 5.4-4

The task of simultaneously controlling output voltage and maintaining the harmonic content to less than 5% while the DC input voltage is varying 40% to 100% is somewhat difficult. One idea which has been advanced by the General Engineering Laboratory utilizes a circuit arrangement which is similar to the phase controlled configuration shown in Circuit E. Again, the basic circuit consists of two groups of a push-pull type configuration with the secondaries of the output transformers connected in series. The method of voltage control however, is somewhat different. As shown in figure 5.4-4, complimentary transistors 1 and 3 and 2 and 4 each have multiple conduction periods during any one-half cycle of a 400 cps time base. The control circuit must be so arranged that complimentary pairs of transistors have equal conduction times during the positive and negative half-cycle time interval. Voltage control is achieved by varying the length of the conduction pulses. In order to minimize the harmonic content the conduction time of the pulses must maintain symmetry about an axis at 90° and 270° of a 400 cps sine wave.

The primary advantage of this circuit is a reduction of harmonics over the rated load range of the inverter. The primary disadvantage is the added complexity of the control circuit. The added control complexity however, can be justified at higher power levels as well as with the severe input voltage regulation.

Circuit H - Figure 5.4-5

Circuit H in figure 5.4-5 represents a configuration which was selected for unconventional sources having a higher output voltage. The operation of the circuit is identical to circuit G. The only major difference is the bridge configuration allows the output transformers to be utilized most effectively from the standpoint of weight and efficiency.

- 113 -

5.4-3 Circuit Evaluation

Results

The results of the DC-AC circuit evaluation are shown in figures 5.4-6 through 5.4-9. It must be emphasized that the weights as shown represent the major component weight only. Curves have been plotted and presented elsewhere in the report to determine total packaged equipment weight.

The curves in general, follow the same patterns that developed previously in the evaluation of DC-AC circuits using Silicon Controlled Rectifiers. The change in weight for the same efficiency is greatest between 0% and 40% regulation. The curves also show decreased weight as the input voltage increases.

In figure 5.4-7 there is a slight ambiguity in the results for 100% regulation and 40% regulation. The circuit selected for 100% regulation consists of phase controlled inverter sections to achieve voltage regulation. The results generally indicate this circuit is lighter in weight than for the circuit selected for 40% input regulation. Since circuit E can be used for 40% regulation also, it would be the better of the two circuits from a weight standpoint.
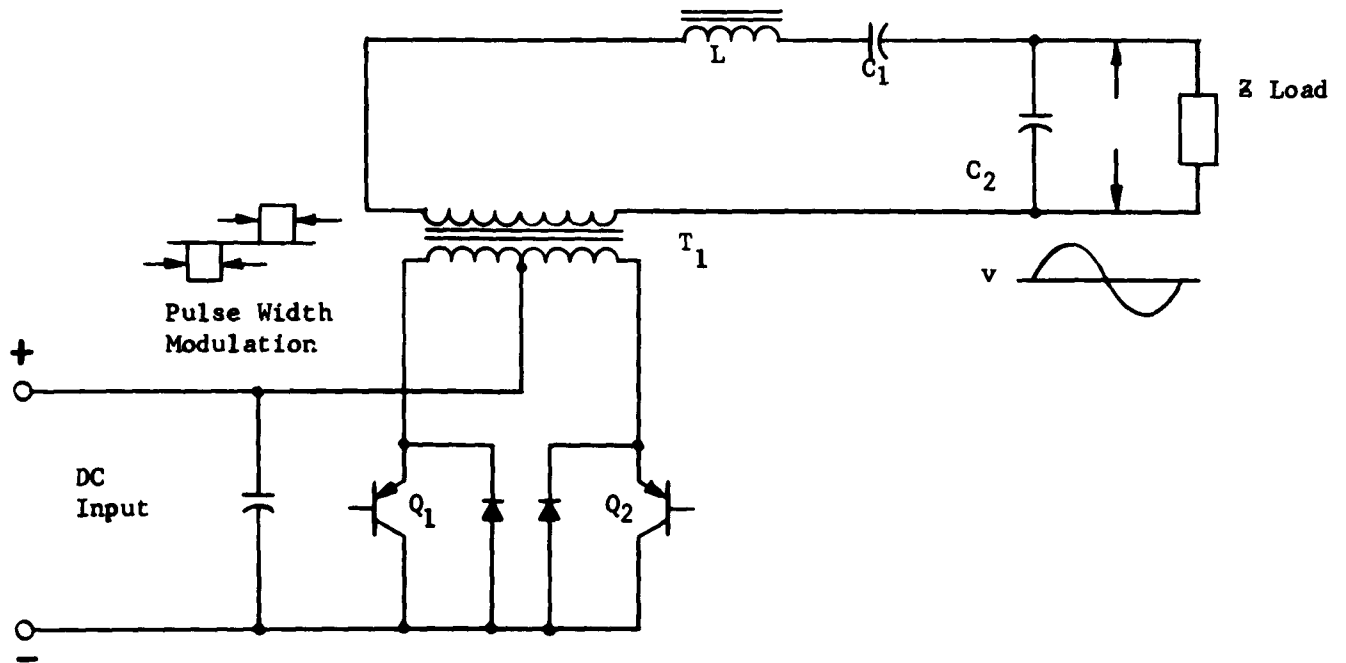
EVALUATED FOR:

Full Load Output Power	25 W			250 W	
Source Voltage Regulation	0%	40%	100%	0%	40%
Full Load Input	20	20	20	20	20
Voltage	40			40	

NOTE: Output Power at .5 P.F. (lag)
                400 cps, 115 v
                single phase
                    than 5% total harmonics

FIGURE 5.4-1

SINGLE PHASE TRANSISTOR INVERTER DC-AC

PHASE CONTROLLED

CIRCUIT E
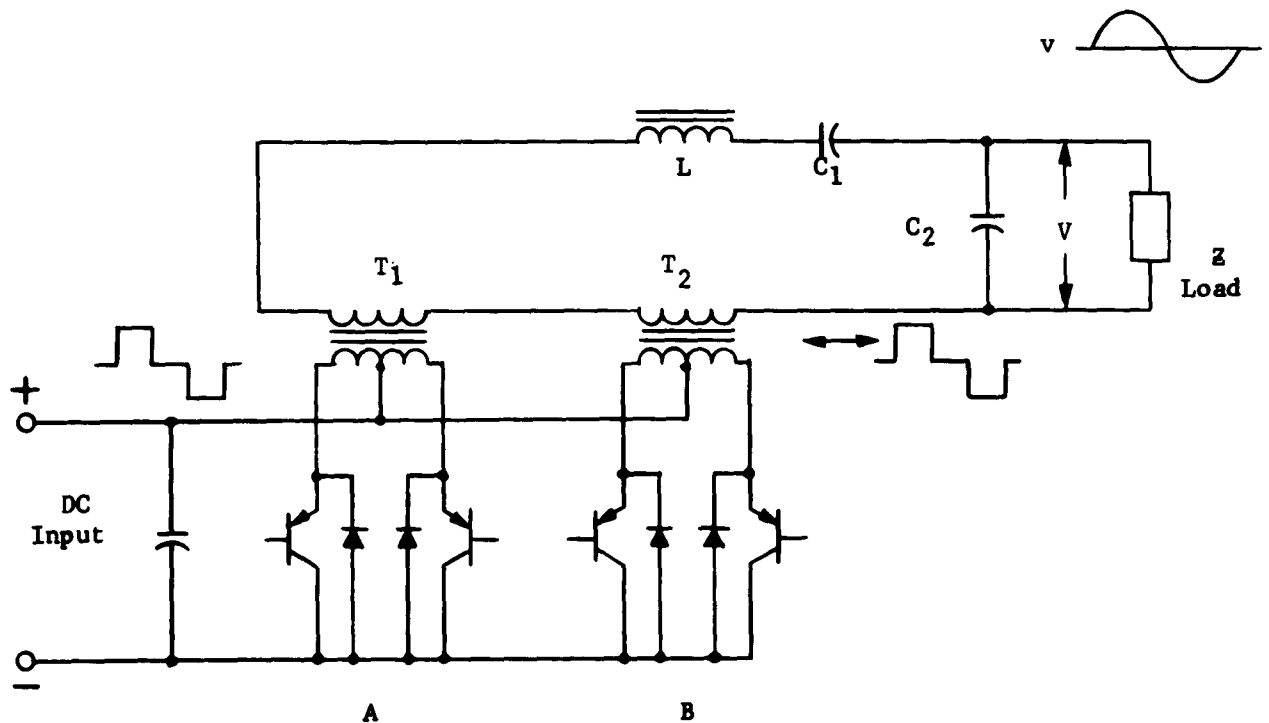
EVALUATED FOR:

Full Load Output Power	250 W	Output Power at .5 P.F. Lag 400 cps, 115 v Single Phase than 5% total harmonics
Source Voltage Regulation	100%	
Full Load Input Voltage	20 v	

FIGURE 5.4-2

SINGLE PHASE TRANSISTOR INVERTER DC-AC

CIRCUIT F
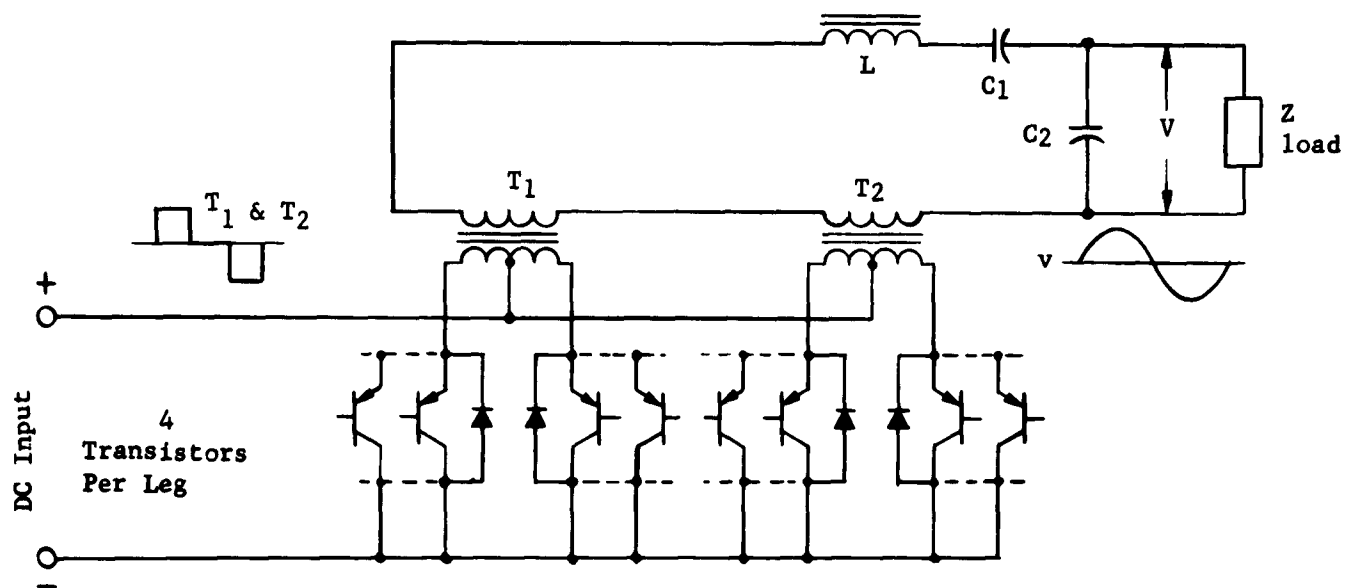
EVALUATED FOR:

Full Load Output	1 KW	Output Power at .5 P.F. Lag
		400 cps, 115 v
Source Voltage	0 %	single phase
Regulation		than 5% total
		harmonics
Full Load Input	12 v, 40 v	
Voltage		

FIGURE 5.4-3

EVALUATED FOR: 1

Full Load Output Power: 1 KW

Source Voltage Regulation: 40%, & 100%

Full Load Input Voltage 12 v

FIGURE 5.4-4

SINGLE PHASE TRANSISTOR INVERTER DC-AC

CIRCUIT H
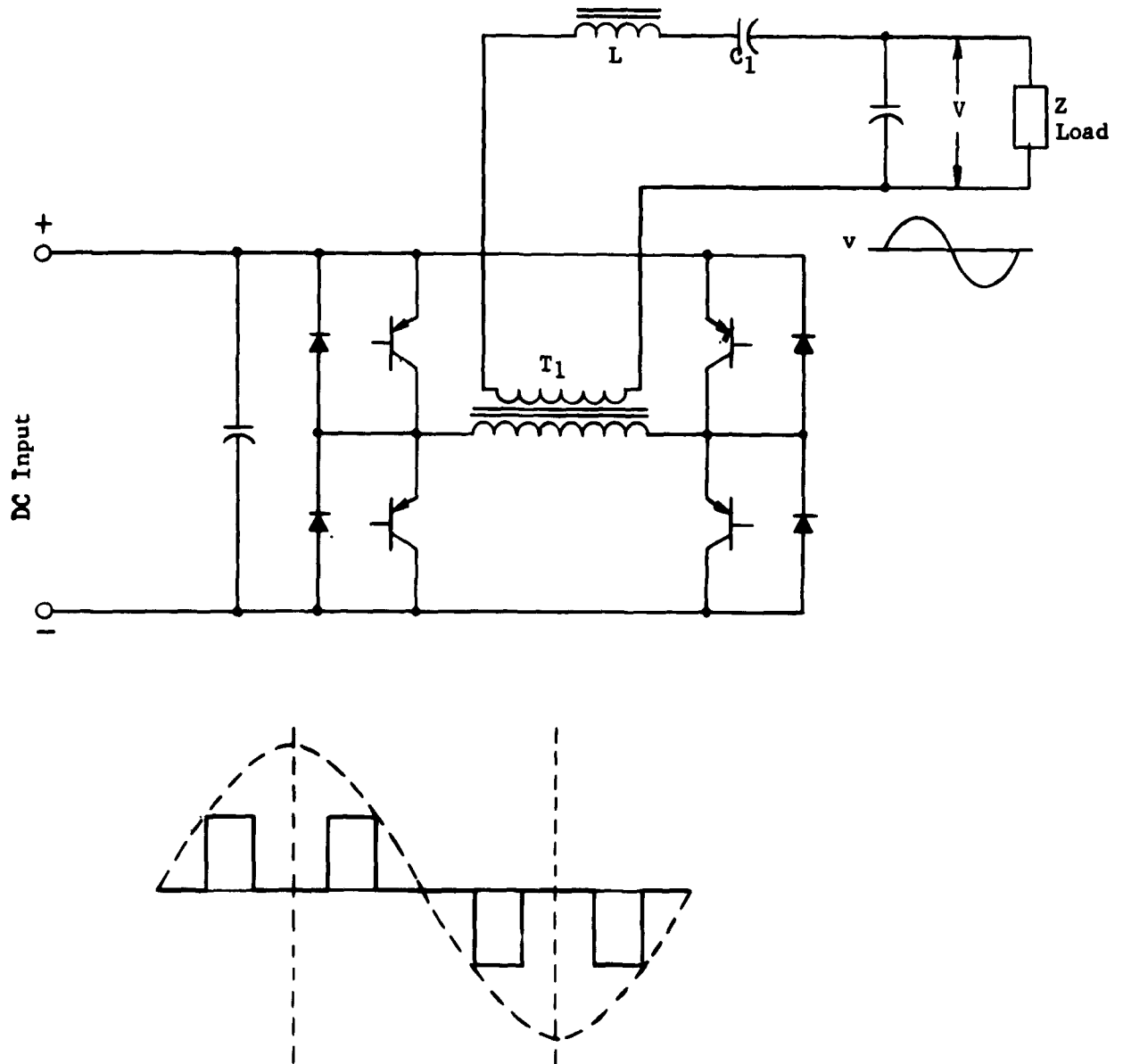
EVALUATED FOR:

Full Load Output Power: 1 KW
Source Voltage Regulation: 40% & 100%
Full Load Input Voltage: 40 v

FIGURE 5.4-5
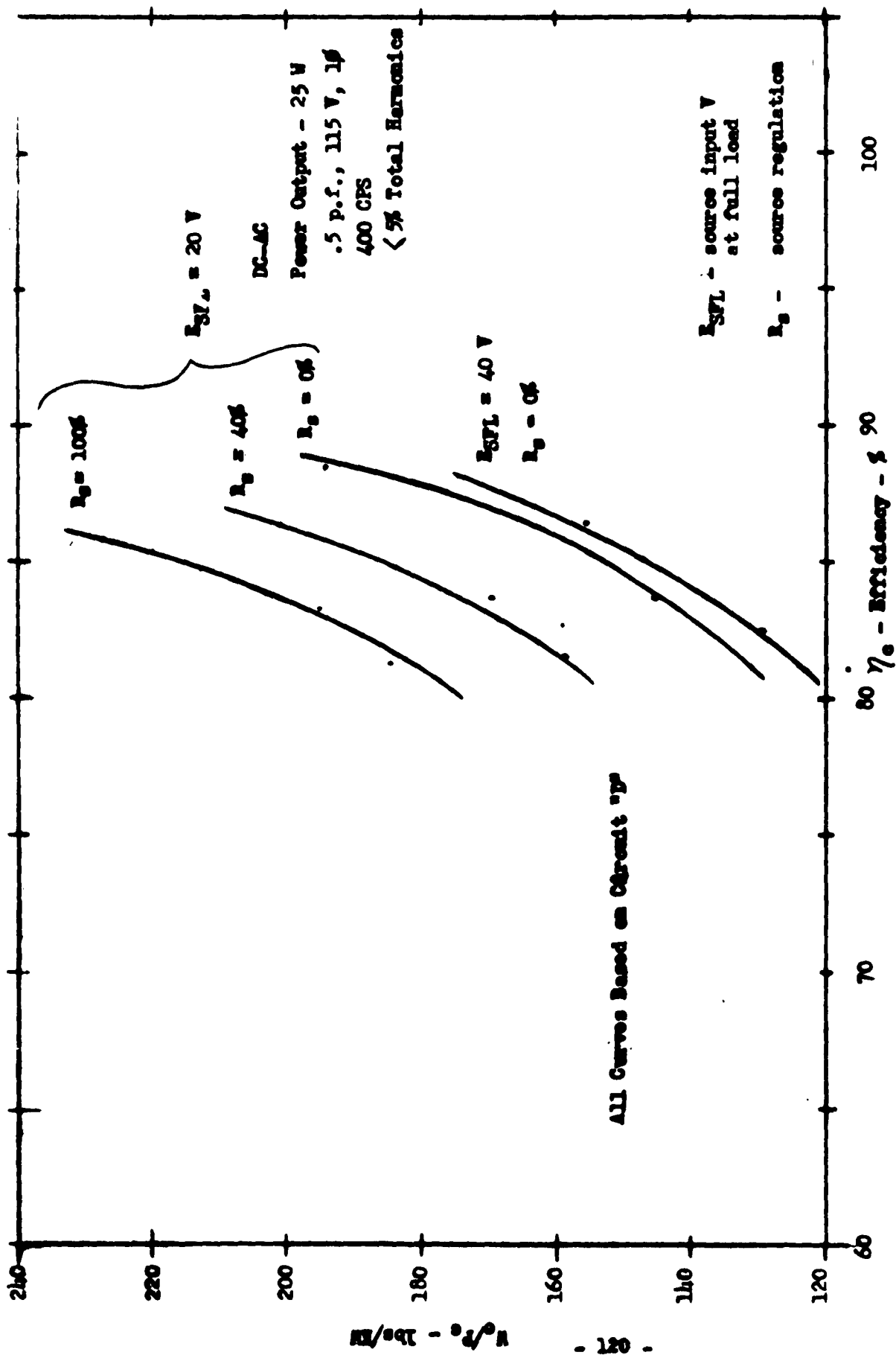
Figure 5.4-6

Converter Weight
(Major Components Only)

All Curves Based on Circuit "D"

E_{SIL} = 20 V

DC-AC

Power Output - 25 W

.5 p.f., 115 V, 1ϕ

400 CPS

< 5% Total Harmonics

R_g = 100%

R_g = 40%

R_g = 0%

E_{SIL} = 40 V

R_g = 0%

E_{SIL} - source input V at full load

R_g - source regulation

V_o/P_o - lbs/KW

η_c - Efficiency - %

- 120 -
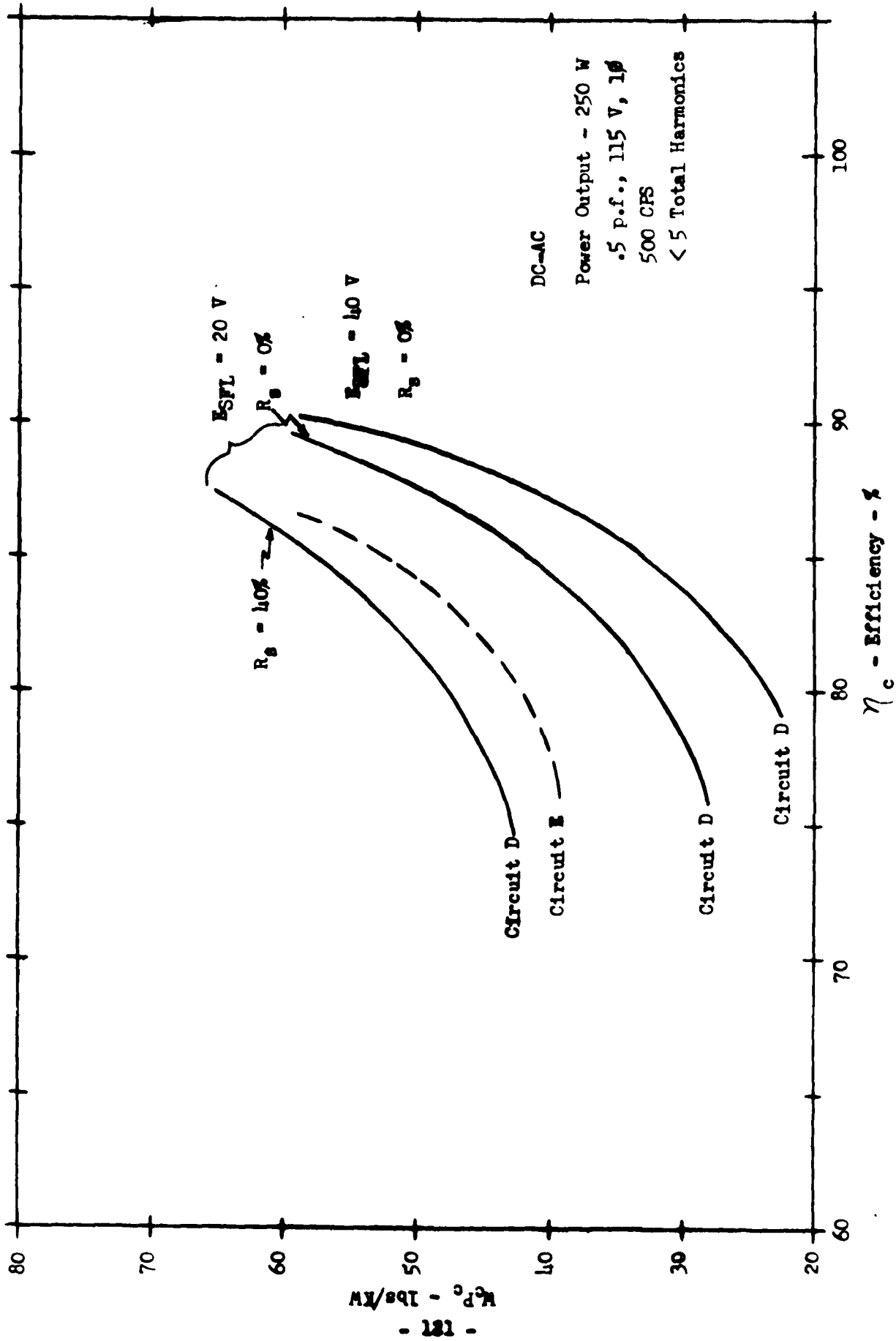
Figure 5.4-7

Converter Weight
(Major Components Only)
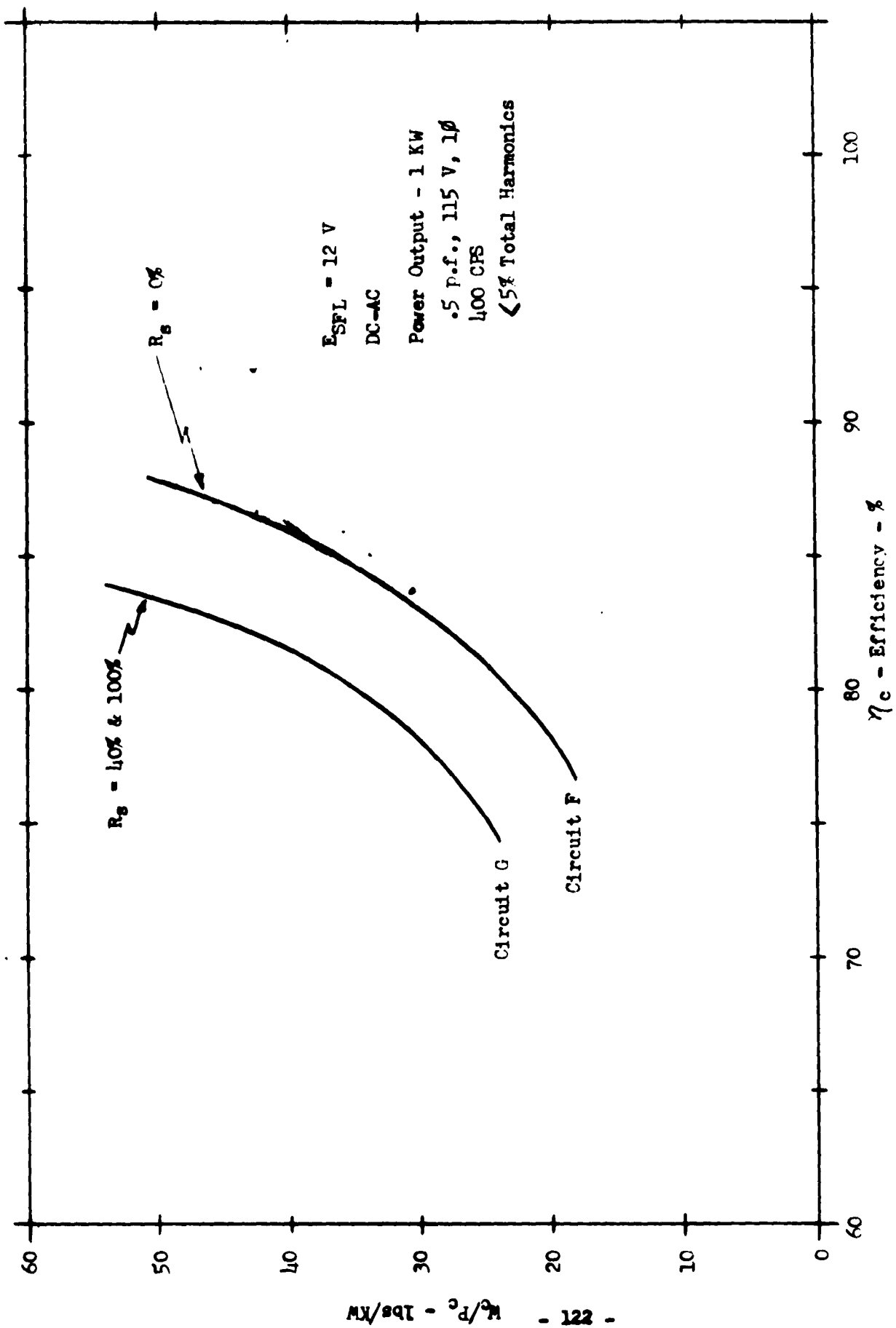
Figure 5.4-8

Converter Weight
(Major Components Only)

E_{SFL} = 12 V

DC-AC

Power Output - 1 KW
.5 p.f., 115 V, 1ø
400 CPS
< 5% Total Harmonics

R_s = 0%

R_s = 40% & 100%

Circuit G

Circuit F

η_c - Efficiency - %

W_c/P_c - lbs/KW

- 126 -
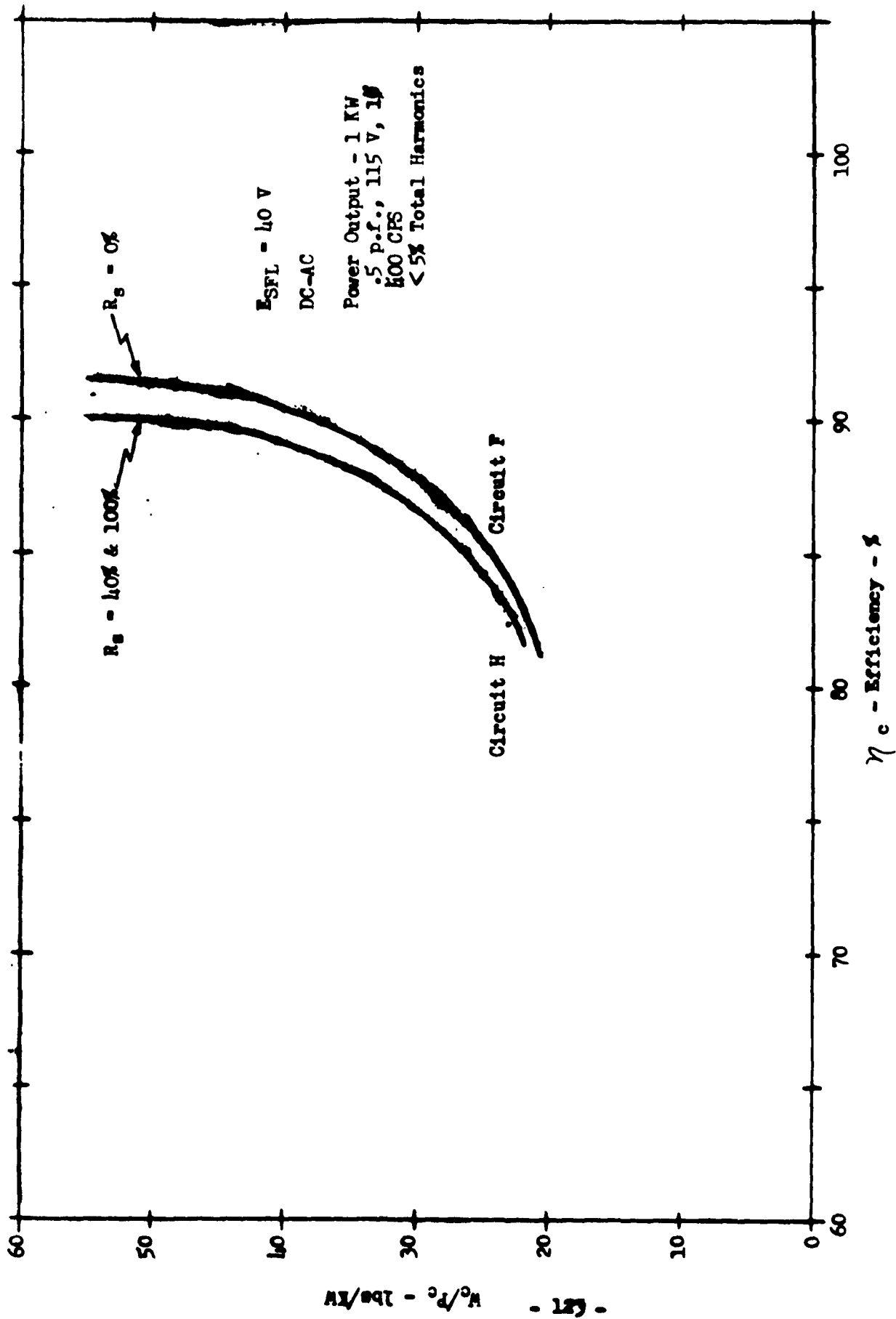
Figure 5.4-9

Converter Weight
(Major Components Only)

- 127 -

<u>Evaluation of Low Input Voltage Conversion Circuits</u>

This portion of the power transistor circuitry is a continuation
of the investigation concerned with input voltages of 1 and 6 volts
as reported in Progress Report No. 5. The basic circuits and con-
cepts have been discussed in previous reports. The circuit con-
figurations used in evaluating the circuits are presented here
along with the curves of calculated weight and efficiency.
Figures 5.5-1 and 5.5-2 show the DC-DC converter circuits.
Figures 5.5-3 and 5.5-4 show the DC-AC converter circuits.

<u>Results</u>

The weight per unit power curves for the DC-DC voltage converters
are shown in Figures 5.5-5 thru 5.5-8 for full load source voltages
of 1.0 and 6.0 volts and full load powers of 25 and 250 watts. Of
course, as anticipated, these low voltage circuits are heavy and
relatively inefficient. Also, it should be noted that the circuit
is considerably simpler and lighter if it does have to provide a
regulation function.

The weight per unit power curves for the DC-AC inverters are shown
in Figures 5.5-9 thru 5.5-12. In Figure 5.5-9 the characteristics
of both the step-wave inverter and the pulse inverter are shown for
the 25 watt, 6 volt input case. It is evident that the step-wave
inverter is considerably more efficient; thus only its weight
characteristics were calculated at the other load and voltage
conditions.

As in the case of the DC-DC voltage converters, these low input
voltage DC-AC inverters are heavy and relatively inefficient.
Thus, it is evident that these very low input voltages should
be avoided where possible.
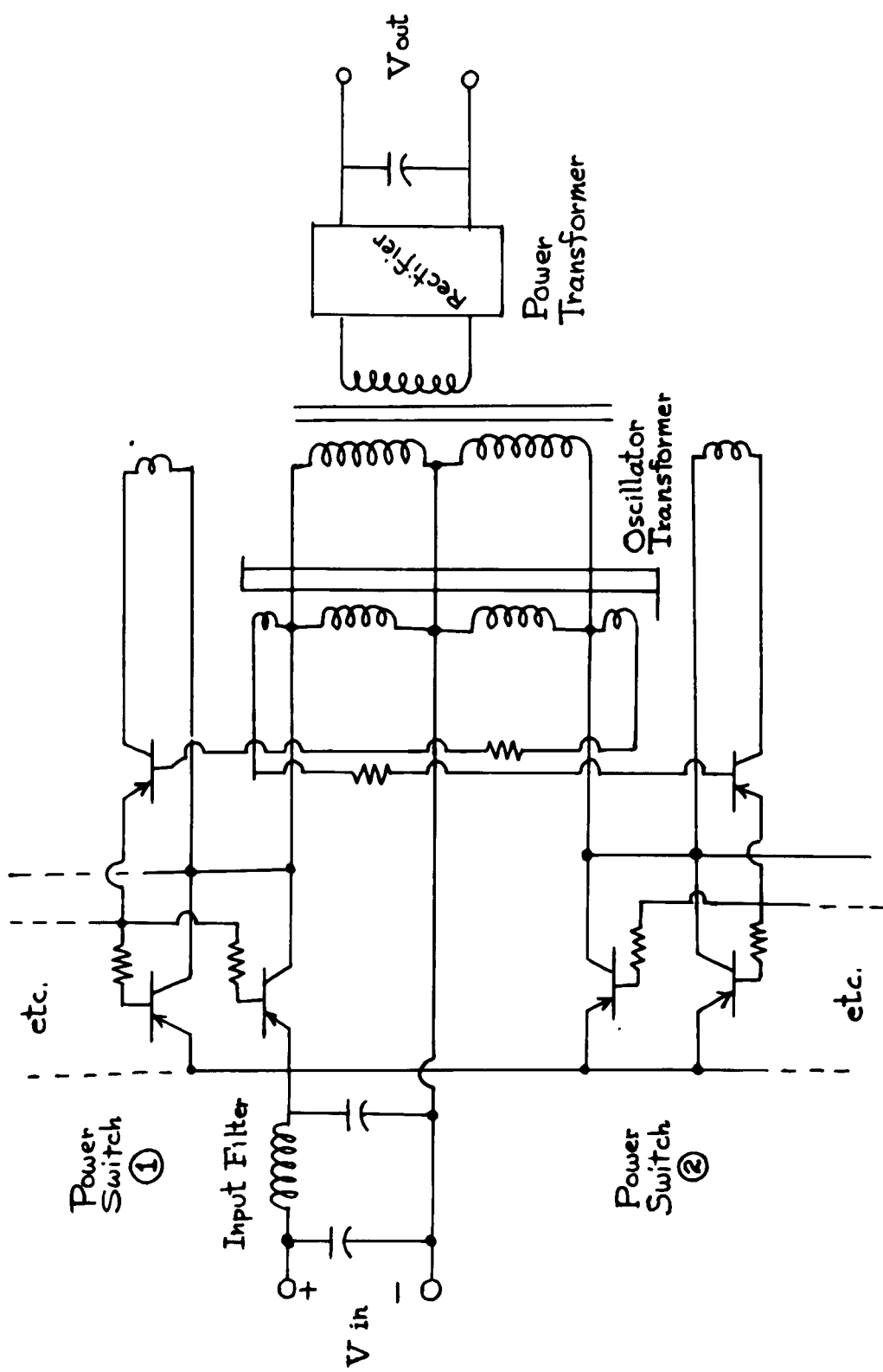
Figure 5.5-1 Low Source Voltage DC – DC Converter For Zero Percent
Source Regulation
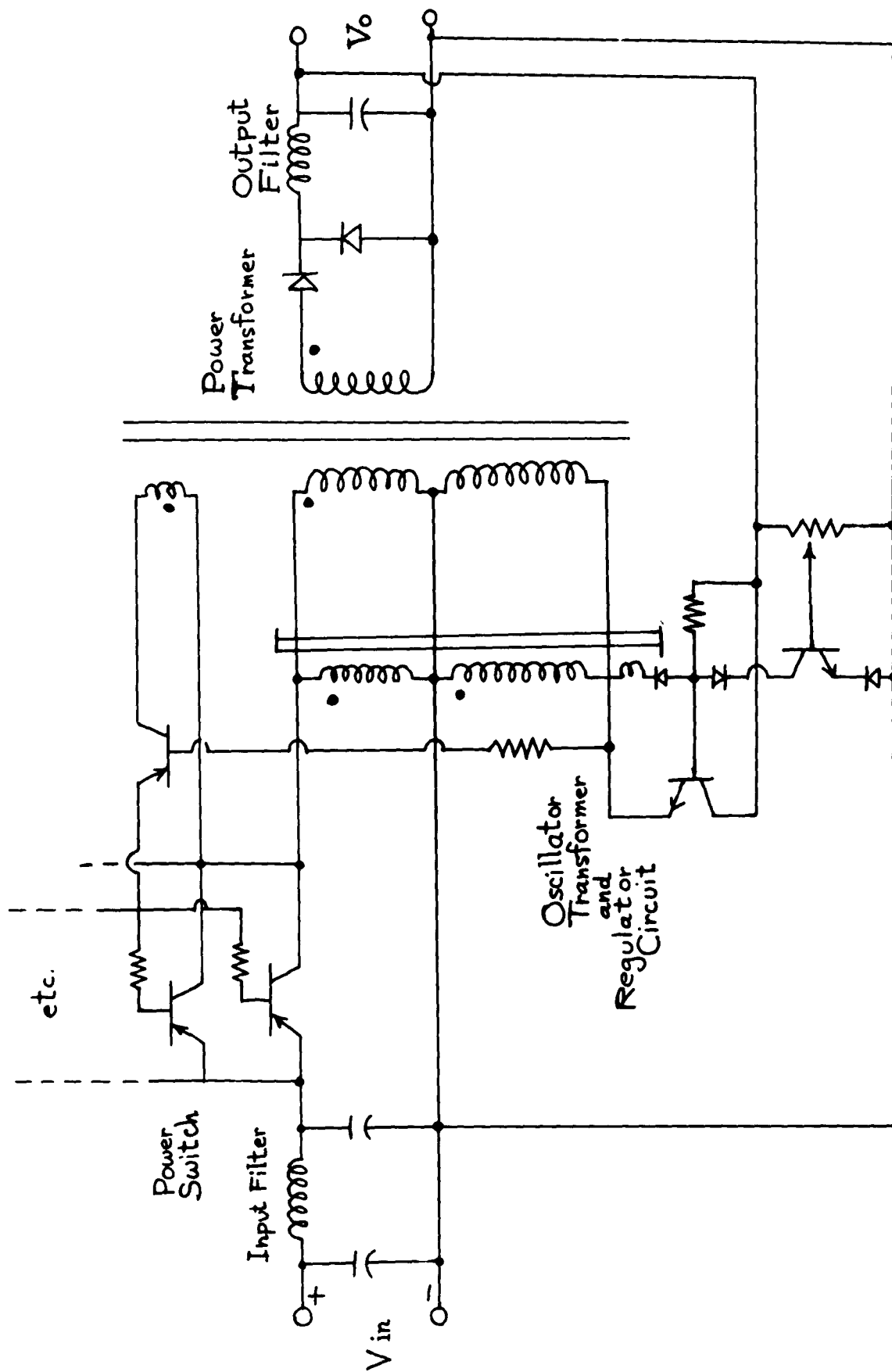
Figure 5.5-2 Low Source Voltage DC - DC Converter For 40 and 100 Percent Source Regulation
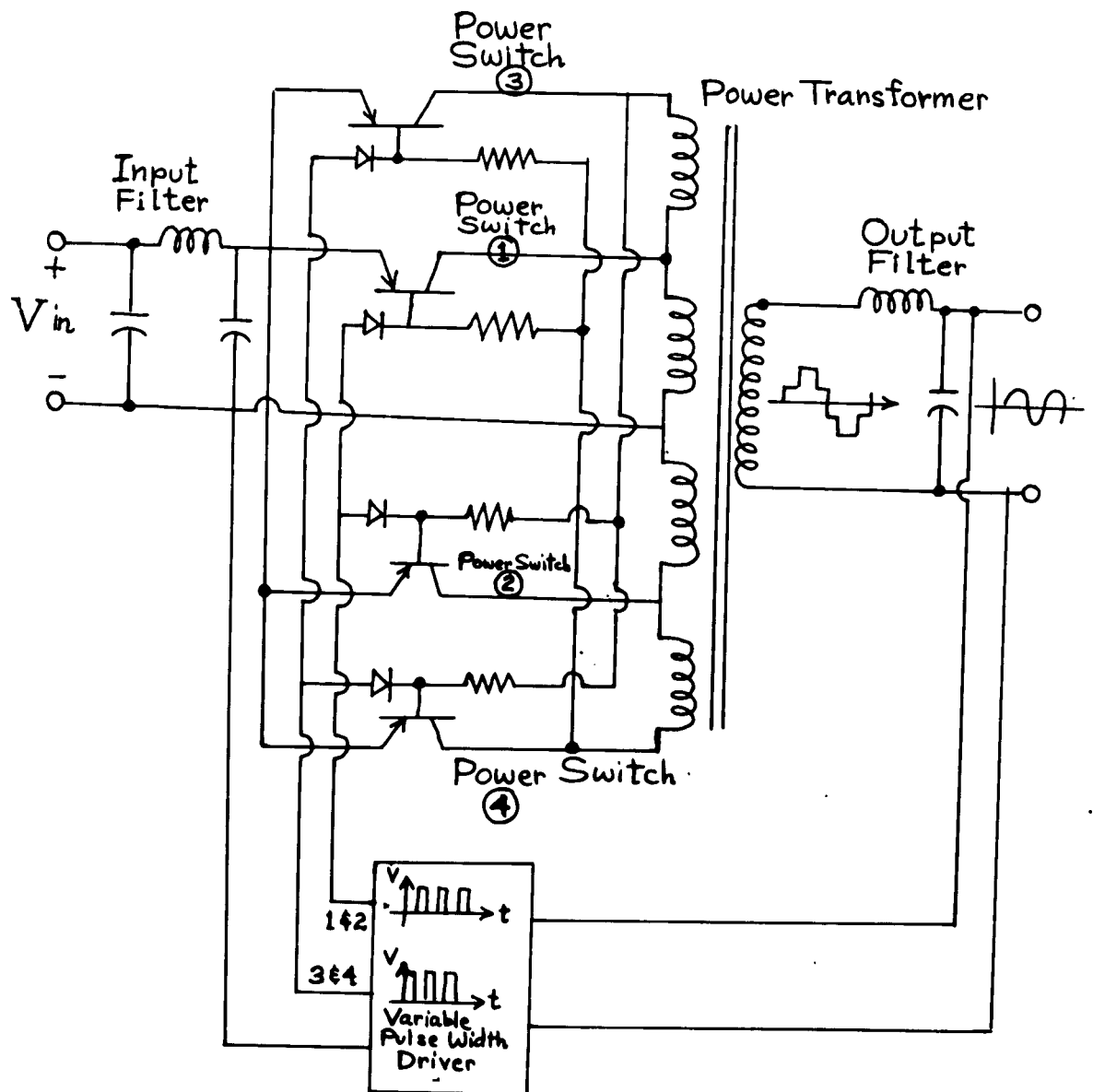
Figure 5.5-3 Low Source Voltage Step Wave Inverter
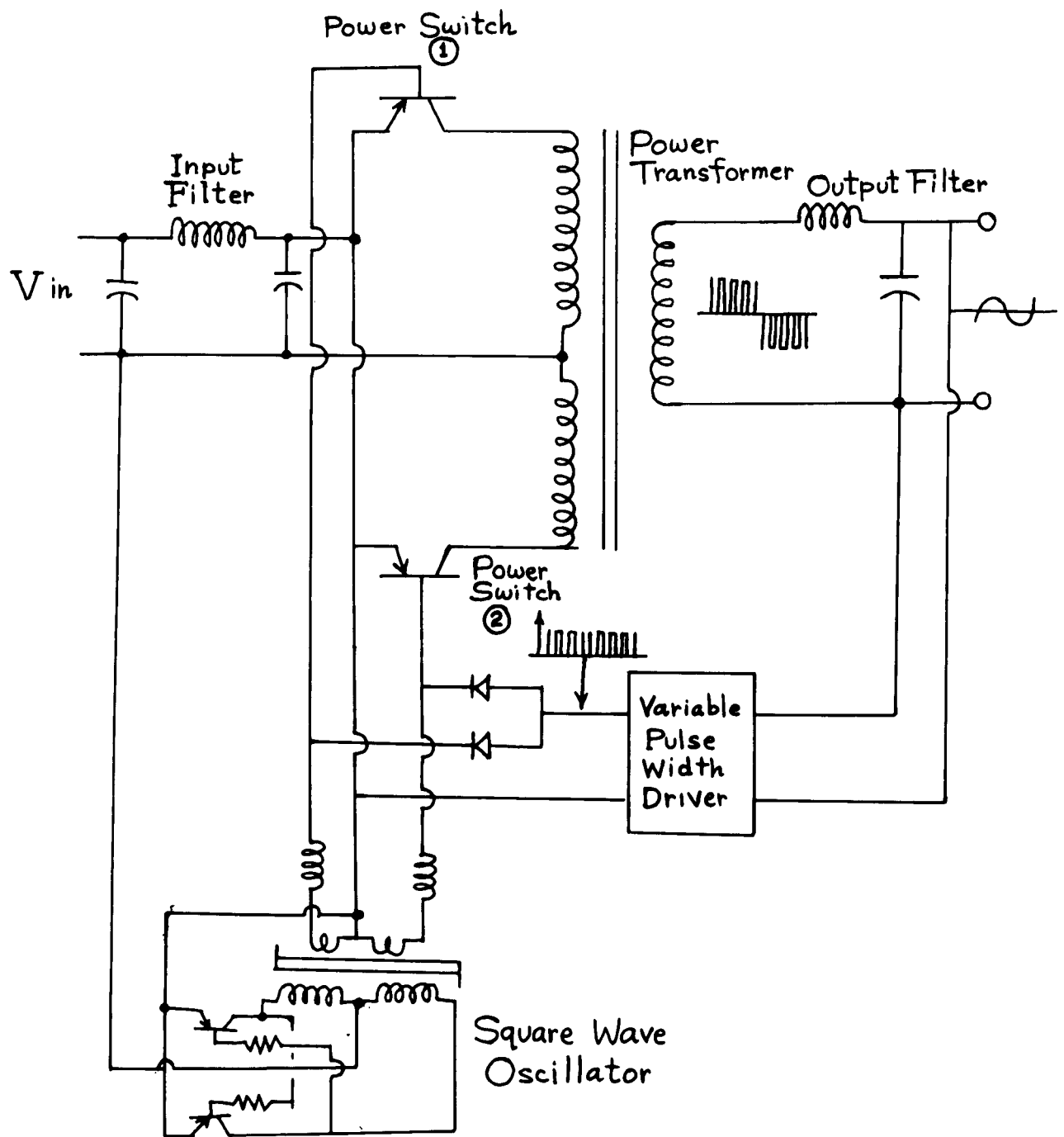
Figure 5.5-4 Low Source Voltage Pulsed Wave Inverter
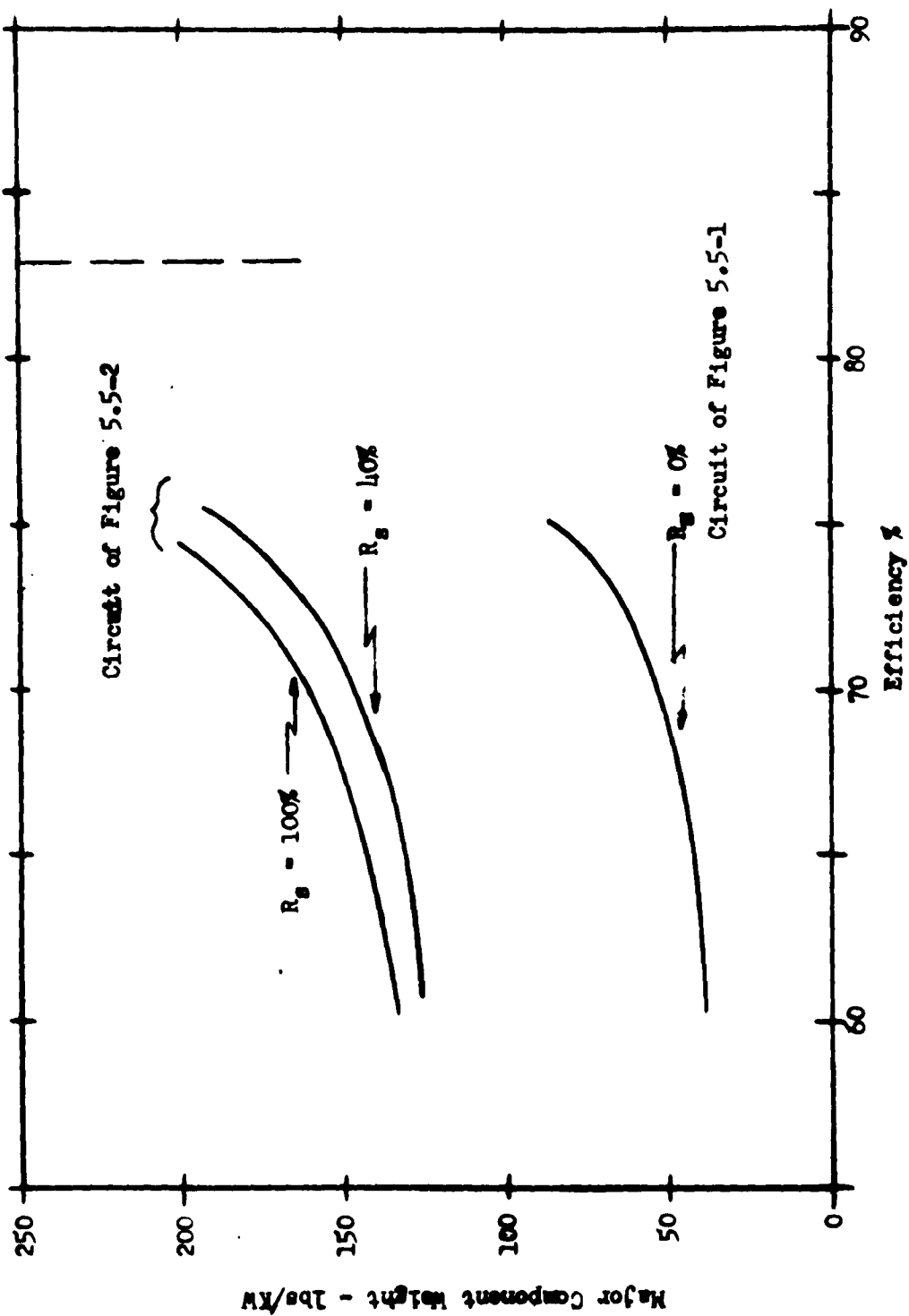
Figure 5.5-5

DC-DC Voltage Converter

Full Load Input Voltage = 1.0 Volt   Full Load Power = 25 watts
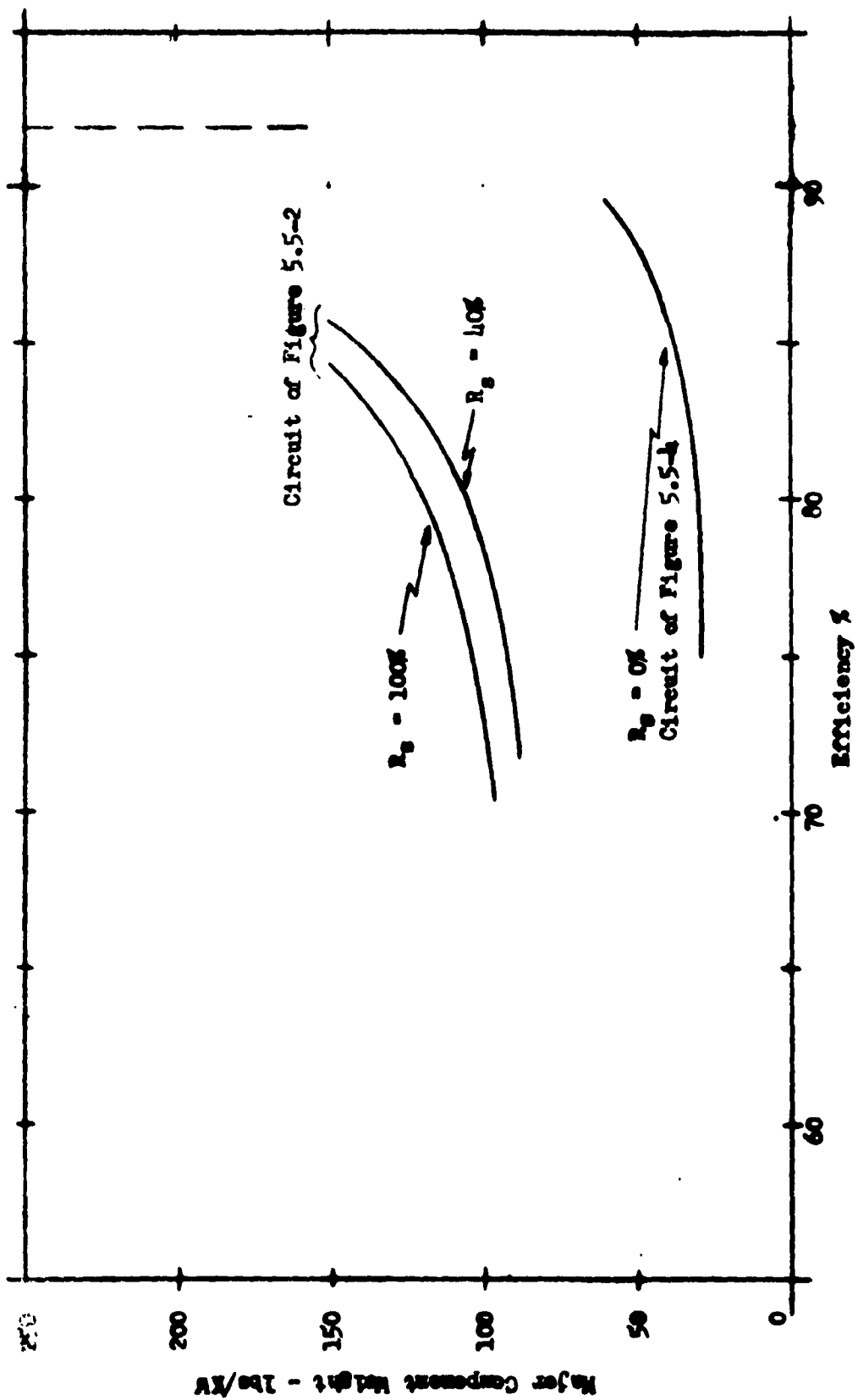
Figure 5.5-6

DC-DC Voltage Converter

Full Load Input Voltage = 6.0 Volts   Full Load Power = 25 Watts

Major Component Weight - lbs/kw

250 200 150 100 50 0

Circuit of Figure 5.5-2

R_s = 100%

R_s = 10%

R_s = 0%

Circuit of Figure 5.5-1

60 70 80 90

Efficiency %
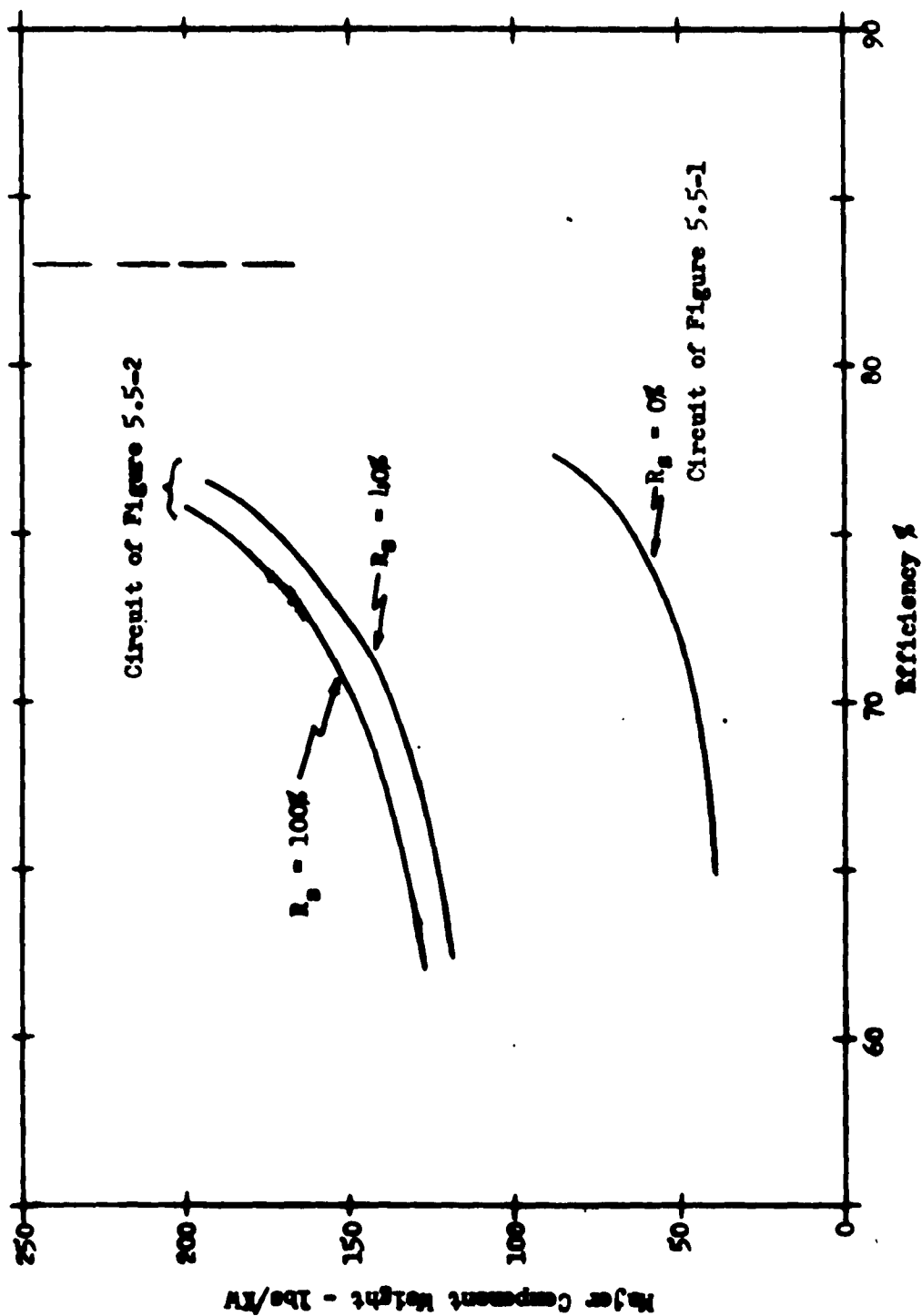
Figure 5.5-7

DC-DC Voltage Converter

Full Load Input Voltage = 1.0 Volt   Full Load Power = 250 Watts

Efficiency %
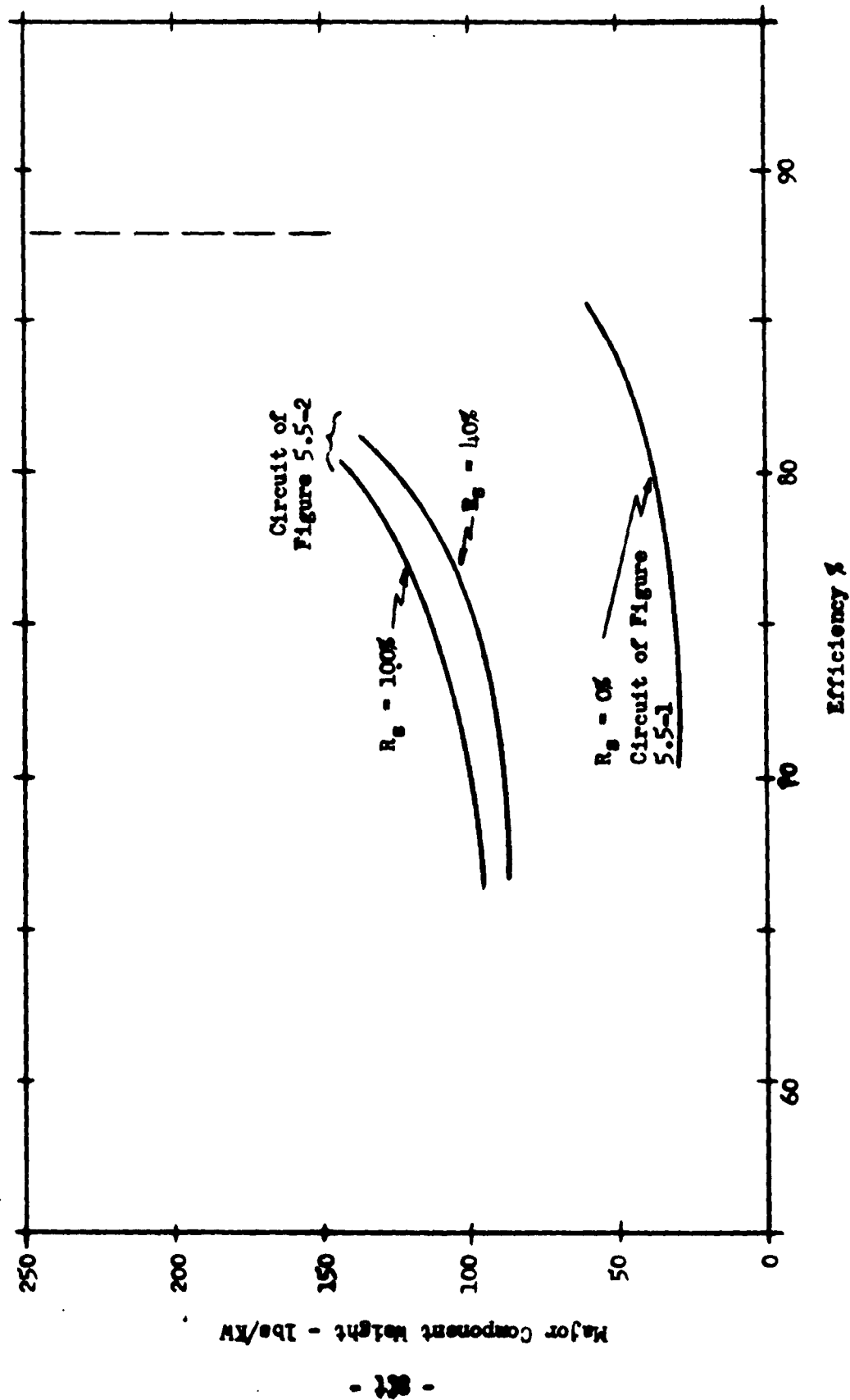
Figure 5.5-8

DC-DC Voltage Converter

Full Load Input Voltage = 6.0 Volts   Full Load Power = 250 Watts
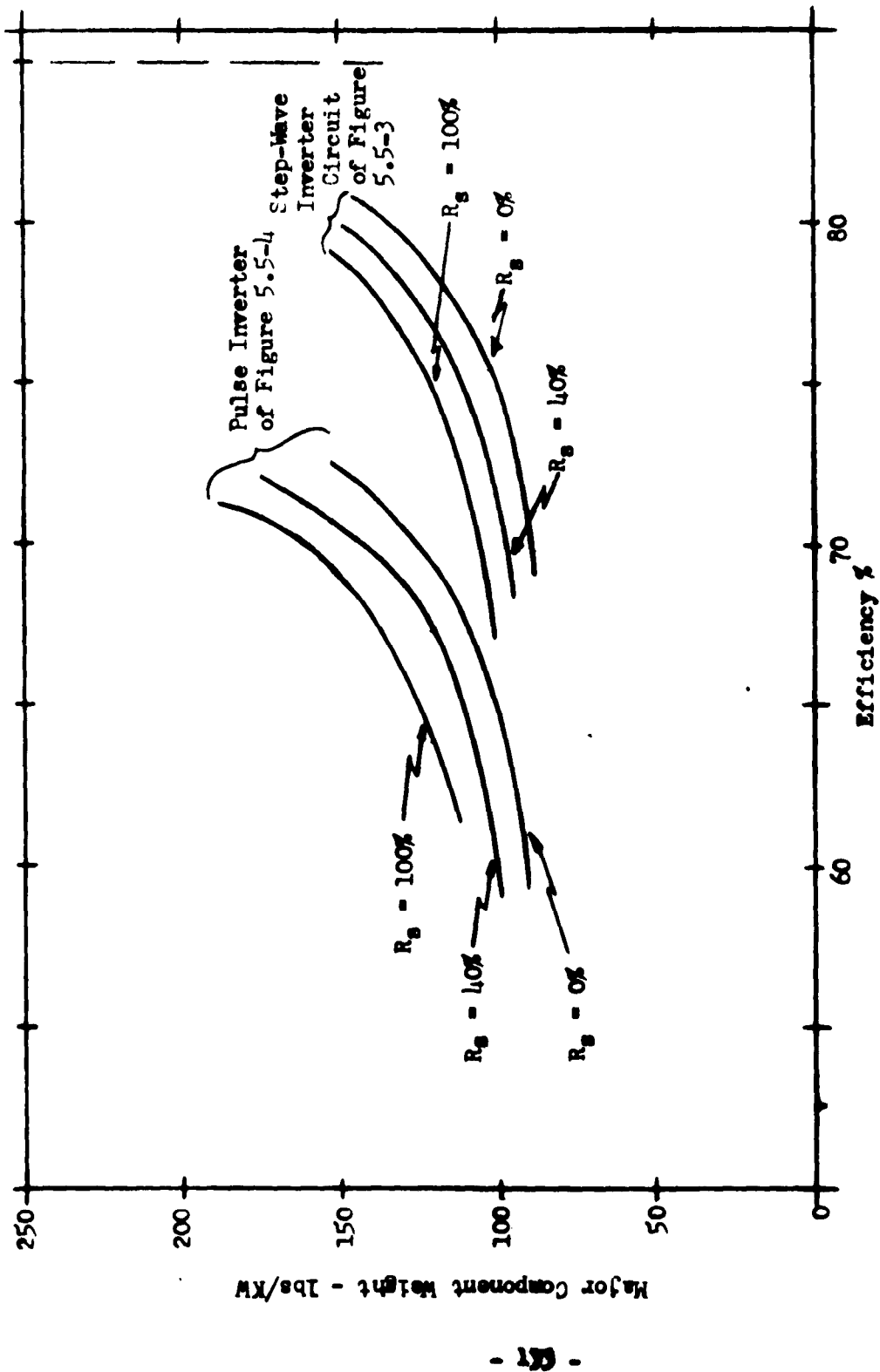
Figure 5.5-9

DC-AC Voltage Inverter (1∅)

Full Load Input Voltage = 6.0 Volts   Full Load Power = 25 Watts
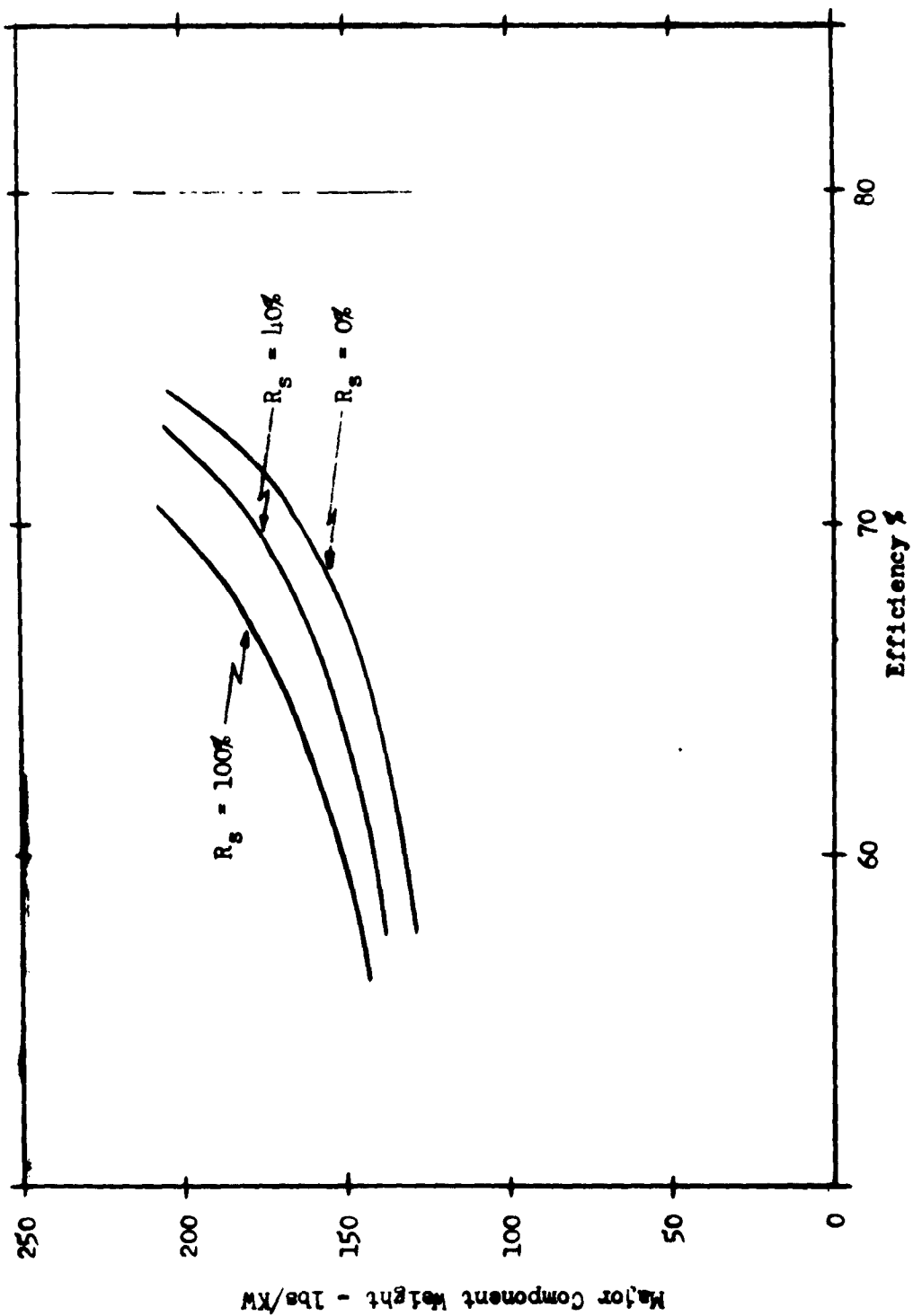
DC-AC Step-Wave Inverter (1∅) Circuit of Figure 5.5-3

Figure 5.5-10

Full Load Input Voltage = 1.0 Volt   Full Load Power = 25 Watts
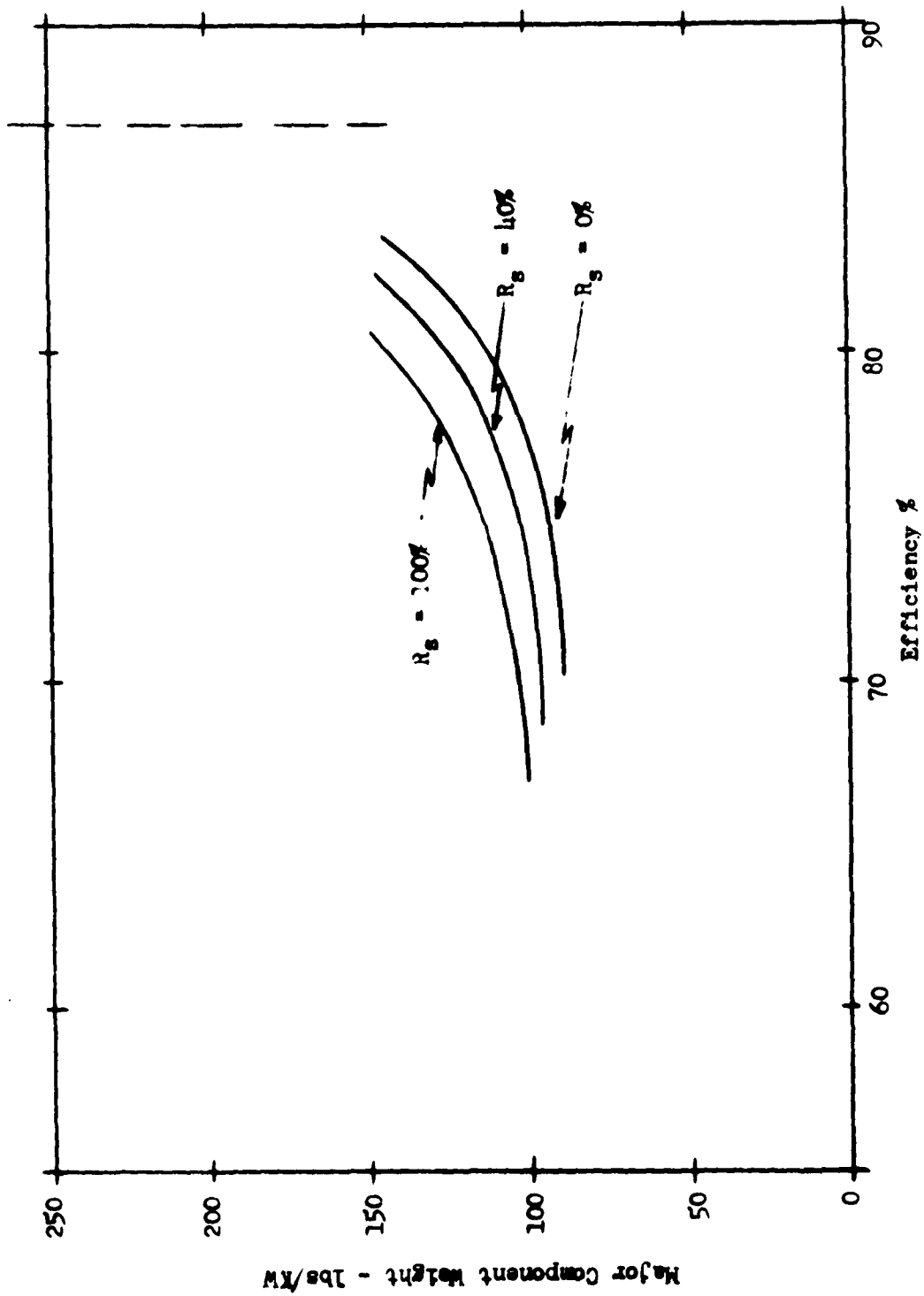
Figure 5.5-11

DC-AC Step-Wave Inverter (1∅) Circuit of Figure 5.5-3

Full Load Input Voltage = 6.0 Volts   Full Load Power = 250 Watts
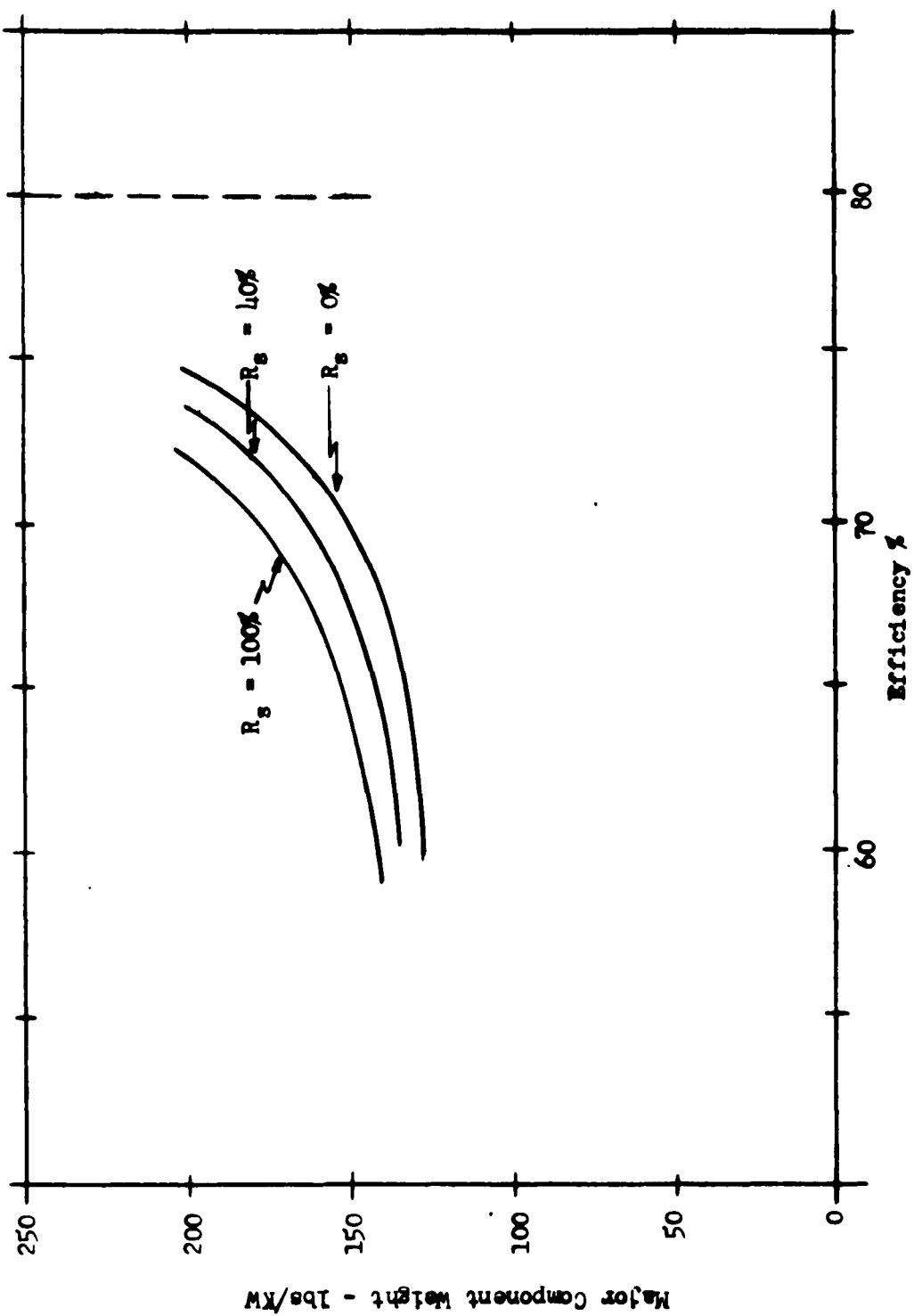
Figure 5.5-12

DC-AC Step-Wave Inverter Circuit of Figure 5.5-3

Full Load Input Voltage = 1.0 Volts   Full Load Power = 250 Watts

6.0   Technical Progress - Systems Task

6.1   Resume'

During the past report period the planned system effort was completed. Optimum combinations of source voltage control and external voltage regulation were determined for selected circuits and state of the art components. Overall system weight characteristics for systems incorporating voltage conversion and regulation were also established. In addition a laboratory model system was built and tested.

Section 6.2 presents the results of the effort in determining the optimum combinations of source voltage control and external voltage regulation. It was determined that the optimum combination involves incorporating all of the voltage regulation either in the source or else in the external voltage converter. The particular optimum approach varies with power level and source voltage level.

Section 6.3 shows overall system weight characteristics for both 28 V. DC and 115 V., 400 cps AC outputs. The results indicate that for the case of a DC output, the minimum weight system is one incorporating a switching circuit to control load voltage by varying the number of power source units in series as load is varied. This, however, necessitates a minimum source voltage of 28 volts. The next lowest weight approach is the use of a flyback circuit in which case the maximum source voltage under any load condition must not exceed 28 volts. Except for these items, the source voltage should be maintained as large as possible in order to minimize system weight.

The results of the laboratory model system testing are presented in Section 6.4. The laboratory system consisted of a fuel cell power source and DC-DC voltage converter of a 50 watt capacity. The performance of the system closely agreed to that predicted for it.

6.2 Optimum Source Voltage Control and External Voltage Converter Combinations

6.2.1 Introduction

Foregoing sections of this and previous reports have presented the characteristics of both source voltage control methods and external voltage converter-regulators. Since the optimum system may incorporate a combination of source voltage control and external voltage regulation, the individual characteristics must be combined in order to establish the optimum system. In this section, the optimum weight versus efficiency characteristics of various combinations are determined. In addition, the characteristics of these combinations are compared with those where all voltage regulation is achieved in the external converter circuitry.

In Section 4.0 of this and previous progress reports, various methods of source voltage control were presented and discussed. Of all of these methods, the only one which appears to be universally applicable is that of varying the number of power source units in series or parallel in order to achieve the desired output voltage as load is varied. This approach has been presented in detail in Section 4.5 of the various progress reports. In addition it became evident early in the study that the optimum combination of source voltage regulation and external voltage regulation would involve providing all of the voltage regulation function either at the source or else in the external voltage converter. This results from the fact that incorporating any significant amount of the voltage regulation function in the external voltage converter increases circuit complexity and weight considerably. However, there is only a small additional weight and efficiency penalty to the external voltage converter for a 100% input voltage regulation versus, for example, a 20% input voltage regulation. This is particularly true in the lower power applications.

The only type of source voltage control considered in this section is the technique of varying the number of power source units in series as presented in Section 4.5 of this and previous progress reports. As described in that section, this switching approach also incorporates a series regulating feature which allows zero output voltage regulation at the expense of a small loss in efficiency. This type of source voltage control was only one considered in this section since it is the only technique which is universally applicable and has the capability of zero output voltage regulation. Weight versus efficiency data used for this series switching method of source voltage control is that presented in Section 4.5 of this and Progress Report No. 5.

The technique for combining the source series switching circuit data with the external voltage converter data was explained in Section 6.2 of Progress Report No. 5. As indicated there, the approach is one of achieving maximum efficiency and minimum weight by using the optimum combination of series switching circuit efficiency and external voltage converter efficiency.

6.2.2   Results

The weight per unit power versus efficiency characteristics for various combinations of series switching and external voltage converter circuits is shown by Figures 6.2-1 through 6.2-26. Figures 6.2-1 through 6.2-14 show these data for the cases where a DC output of 28 volts is required. Figures 6.2-15 through 6.2-26 presents the information for the cases where a 400 cps AC output is required. Each figure shows the weight per unit power for a particular output power and full load source voltage condition. The solid line curves are for the case of a 100% inherent source regulation while the dashed line curves are for 40% inherent source regulation. In those cases where the curves apply to a combination of a series switching circuit and an external voltage converter, points of various external voltage converter efficiencies are indicated. Of course, the corresponding series switching circuit efficiency can be obtained by dividing the net efficiency by the external voltage converter efficiency at the particular point of interest. Knowing the individual efficiencies at any point permits determination of the individual weight and volume characteristics from the original data given in Sections 4.5 and 5.0 if this should be desired. In particular, this is a necessary procedure if total volume information is needed since system volume data is not presented.

Each curve is labeled as to the circuit of combination used by means of appropriate abbreviations. The definition of these abbreviations along with figure number of the circuit is given by Table 6.2-1. The location of primary weight data is also given in Table 6.2-1.

The weight information given by Figures 6.2-1 through 6.2-26 is in terms of total weight per unit power and thus includes the package weight factor indicated in Figure 5.1-1 for the external voltage converters.

In the case of each figure, the optimum approach is that which gives the lowest weight for any given efficiency. In some cases this optimum approach is a combination of series switching at the source with an external voltage converter. In other cases the optimum is the incorporation of all of the voltage regulation in the external voltage converter.

The optimum combinations for various load, input voltage, and power conditions are indicated in Table 6.2-2.

The results of this section are used in the Section 6.3 to follow. The limitations and significance of these results are also discussed in detail in that section.

TABLE 6.2-1, LIST OF CIRCUITS

Circuit Abbreviation	Circuit Description	Circuit Diagram In		Weight Vs. Efficiency Data Given In	
		Progress Report	Fig.	Progress Report	Fig.
LV-1	DC-DC, Low Voltage Transistor Circuit, 0% Reg.	6	5.5-1	6	5.5-5 5.5-6 5.5-7 5.5-8
LV-2	DC-DC, Low Voltage Transistor Circuit, 40% & 100% Reg.	6	5.5-2	6	5.5-5 5.5-6 5.5-7 5.5-8
BFB(T)	DC-DC, Transistorized Flyback Circuit	6	5.2-1	6	5.2-7 5.2-8 5.2-9
BFB(S)	DC-DC, SCR Flyback Circuit	6	5.2-1	5	5-8
CKT A	DC-DC, Modified Push Pull DC Transformer Circuit (Transistor)	5	5-18	5	5-21 5-22 5-23 5-24 5-25 5-26 5-27
CKT B	DC-DC, Morgan Step-Up Circuit (Transistor)	5.	5-19	5	5-21 5-22 5-24 5-26
CKT C	DC-DC, Modified Morgan Step-Down Circuit (Transistor)	5	5-20	5	5-23 5-25 5-27
TRC(DC)	DC-DC, Time Ratio Control SCR Circuit	6	5.2-3	5	5-9 5-10 5-11
PC	DC-AC, 3∅, Phase Control SCR Circuit	6	5.2-5	5	5-12 5-13 5-14

TABLE 6.2-1, (Cont'd)

Circuit Abbreviation	Circuit Description	Circuit Diagram In		Weight Vs. Efficiency Data Given In	
		Progress Report	Fig.	Progress Report	Fig.
TRC(AC)	DC-AC, 3∅, SCR Inverter With TRC Regulator	6	5.2-4	5	5-15 5-16 5-17
SWI	DC-AC, 1∅, Low Voltage Transistor Step Wave Inverter	6	5.4-3	6	5.5-9 5.5-10 5.5-11 5.5-12
PWI	DC-AC, 1∅, Low Voltage Transistor Pulse Wave Inverter	6	5.4-4	6	5.5-9
CKT D	DC-AC, 1∅, Pulse Width Modulated Transistor Inverter	6	5.4-1	6	5.4-6 5.4-7
CKT E	DC-AC, 1∅, Phase Controlled Transistor Inverter	6	5.4-2	6	5.4-7
CKT F	DC-AC, 1∅, Transistorized Inverter for 0% Regulation	6	5.4-3	6	5.4-8 5.4-9
CKT G	DC-AC, 1∅, Two Section Pulse Width Modulated Transistor Inverter	6	5.4-4	6	5.4-8
CKT H	DC-AC, 1∅, Transistor Bridge Type Inverter	6	5.4-5	6	5.4-9
SC	Series Switching Circuit (Transistor) for Source Voltage Control	5	4.5-1	5 6	4.5-8 thru 4.5-12 4.5-1 thru 4.5-4

TABLE 6.2-2

OPTIMUM SOURCE VOLTAGE CONTROL AND

EXTERNAL VOLTAGE CONVERTER COMBINATIONS

Output	Rated Load (Watts)	Full Load Source Voltage	Inherent Source Regulation	Minimum Weight System
28 V. DC	25	6	40,100	SC + LV 1
"	25	12	40	SC + CKTA, ($\eta_n < 82\%$)
"	25	12	40	BFB(T), ($\eta_n \geq 82\%$)
"	25	12	100	SC + CKT A, ($\eta_n < 74\%$)
"	25	12	100	BFB(T), ($\eta_n > 74\%$)
"	25	20	40,100	SC + BFB(T)
"	25	40	40,100	SC + CKTA, ($\eta_n < 79\%$)
"	25	40	40,100	CKT C, ($\eta_n > 79\%$)
"	250	6	40,100	SC + BFB(T)
"	250	12	40,100	BFB(T)
"	250	40	40	CKT B
"	250	40	100	CKT C
"	1000	12	40,100	BFB(T)
"	1000	20	40	BFB(T)
"	1000	20	100	SC + BFB(T)
"	1000	40	40,100	SC + CKTA
"	1C00	100	40,100	SC + TRC(DC)
"	10,000	20	40	BFB(S)
"	10,000	20	100	TRC(DC)
"	10,000	40	40,00	TRC(DC)
"	10,000	100	40,100	TRC(DC)
AC, 1∅	25	6	40,100	SWI
"	25	20	40,100	CKT D
"	25	40	40,100	CKT D
"	250	6	40,100	SWI
"	250	20	40	SC + CKTD, ($\eta_n < 82\%$)
"	250	20	40	CKT E, ($\eta_n > 82\%$)
"	250	20	100	SC + CKT D, ($\eta_n < 85\%$)
"	250	20	100	CKT D, ($\eta_n > 85\%$)
"	250	40	40,100	SC + CKT D
"	1000	12	40,100	SC + CKT F
"	1000	40	40,100	CKT H
AC, (3∅)	1000	100	40,100	PC
"	10,000	20	40,100	TRC(AC)
"	10,000	40	40,100	PC ($\eta_n < 86\%$)
"	10,000	40	40,100	TRC (3∅), ($\eta_n > 86\%$)
"	10,000	100	40,100	PC
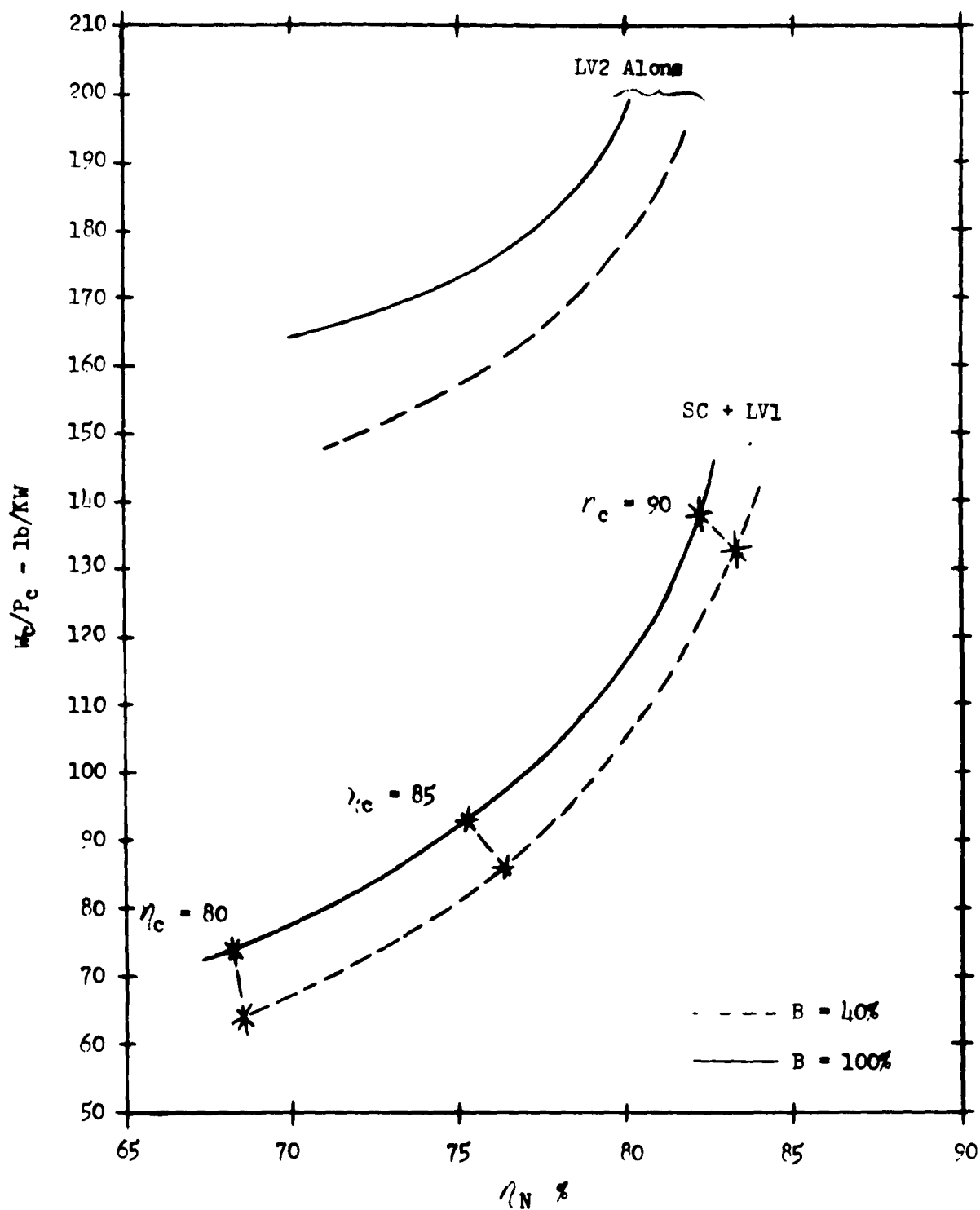
Figure 6.2-1

Total Weight Per Unit of Output Power Versus Net Efficiency for
Various External Voltage Converter-Regulators and Source Voltage Control
Combinations

Output = 25 Watts, 28 VDC

E_{SFL} = 6 Volts
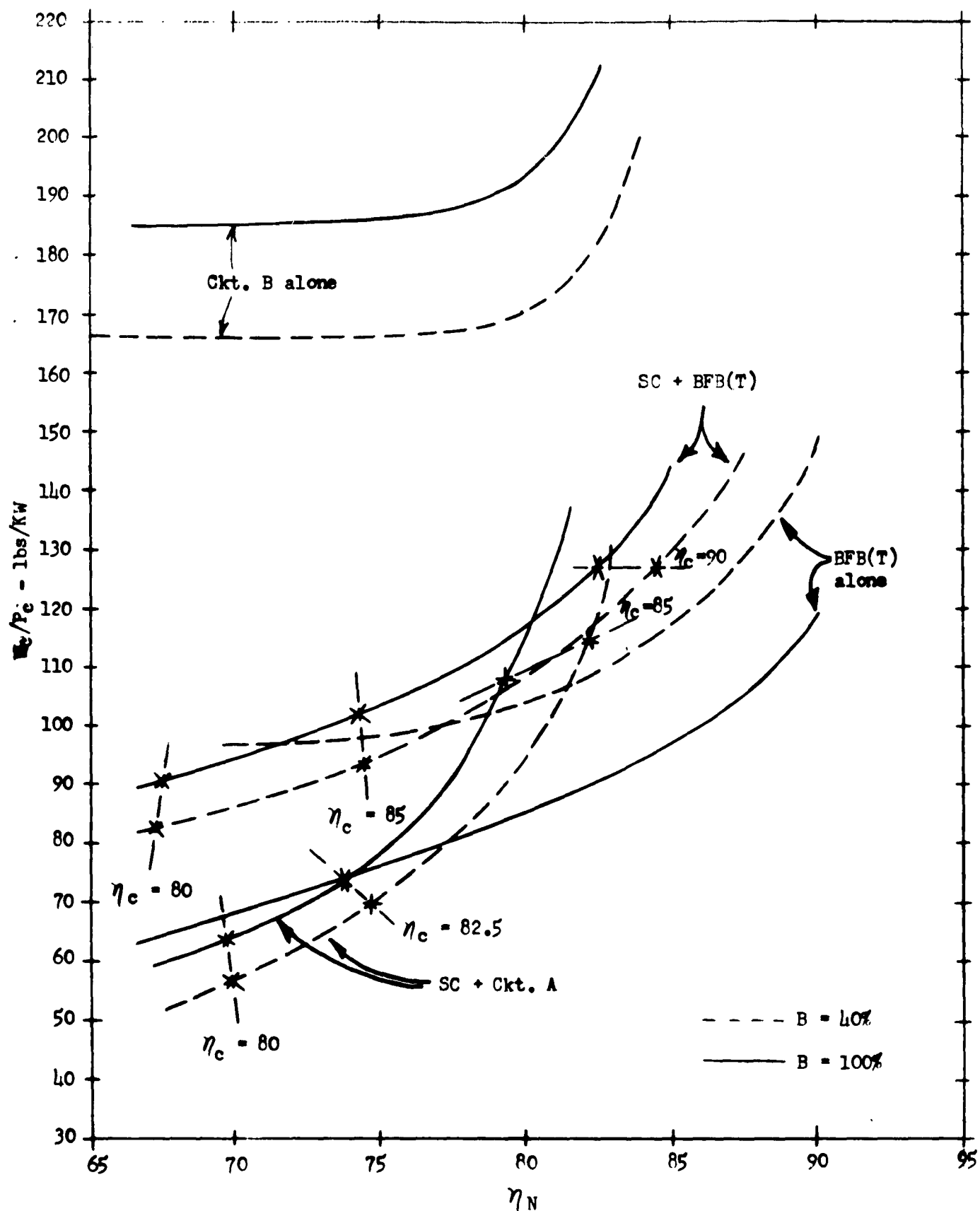
Figure 6.2-2

Total Weight Per Unit of Output Power Versus Net Efficiency for Various External
Voltage Converter-Regulators and Source Voltage Control Combinations

Output = 25 watts, 28 VDC

E_{SFL} = 12 Volts

Figure 6.2-3

Total Weight Per Unit of Output Power
Versus Net Efficiency for Various External
Voltage Converter-Regulators and Source
Voltage Control Combinations
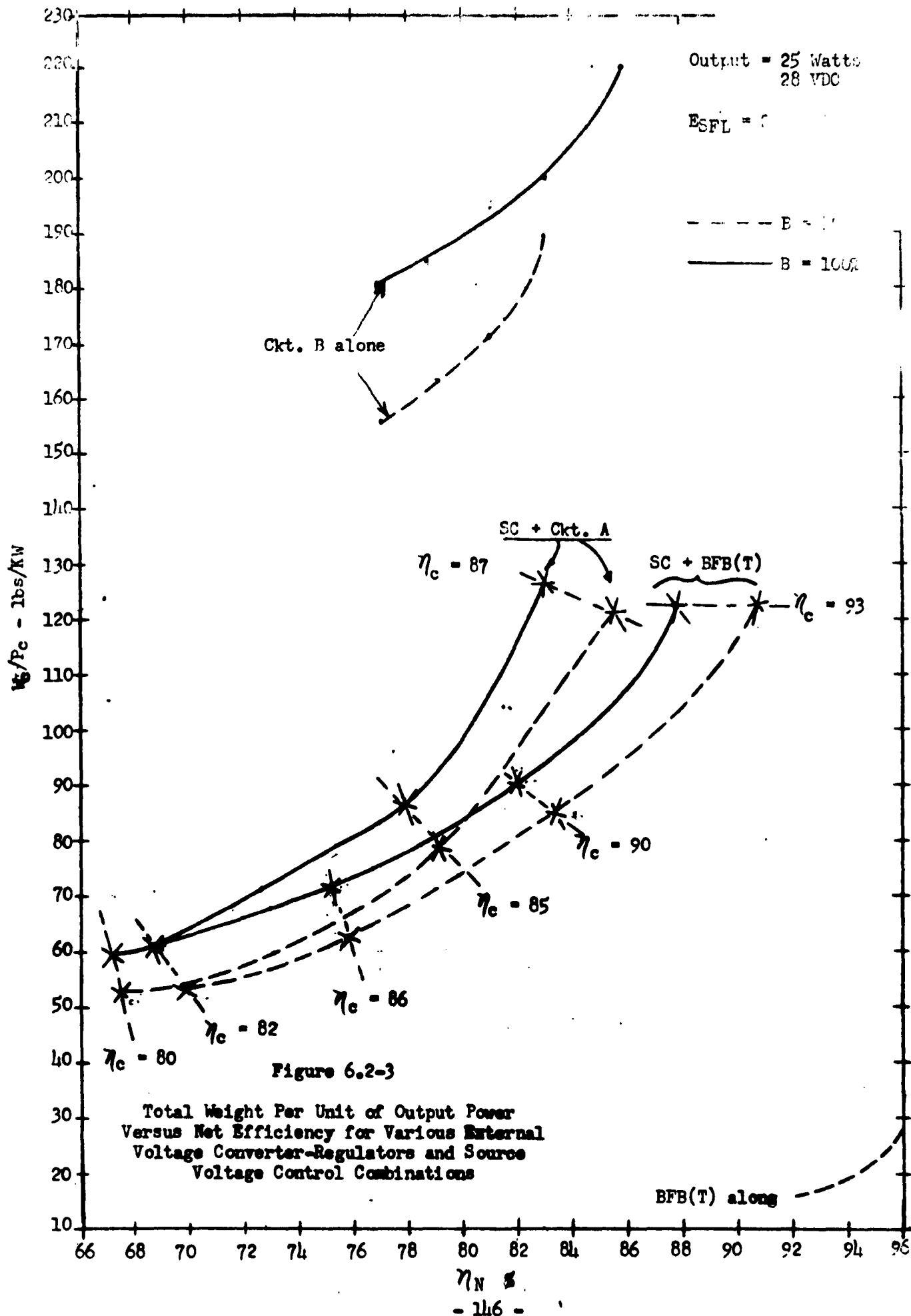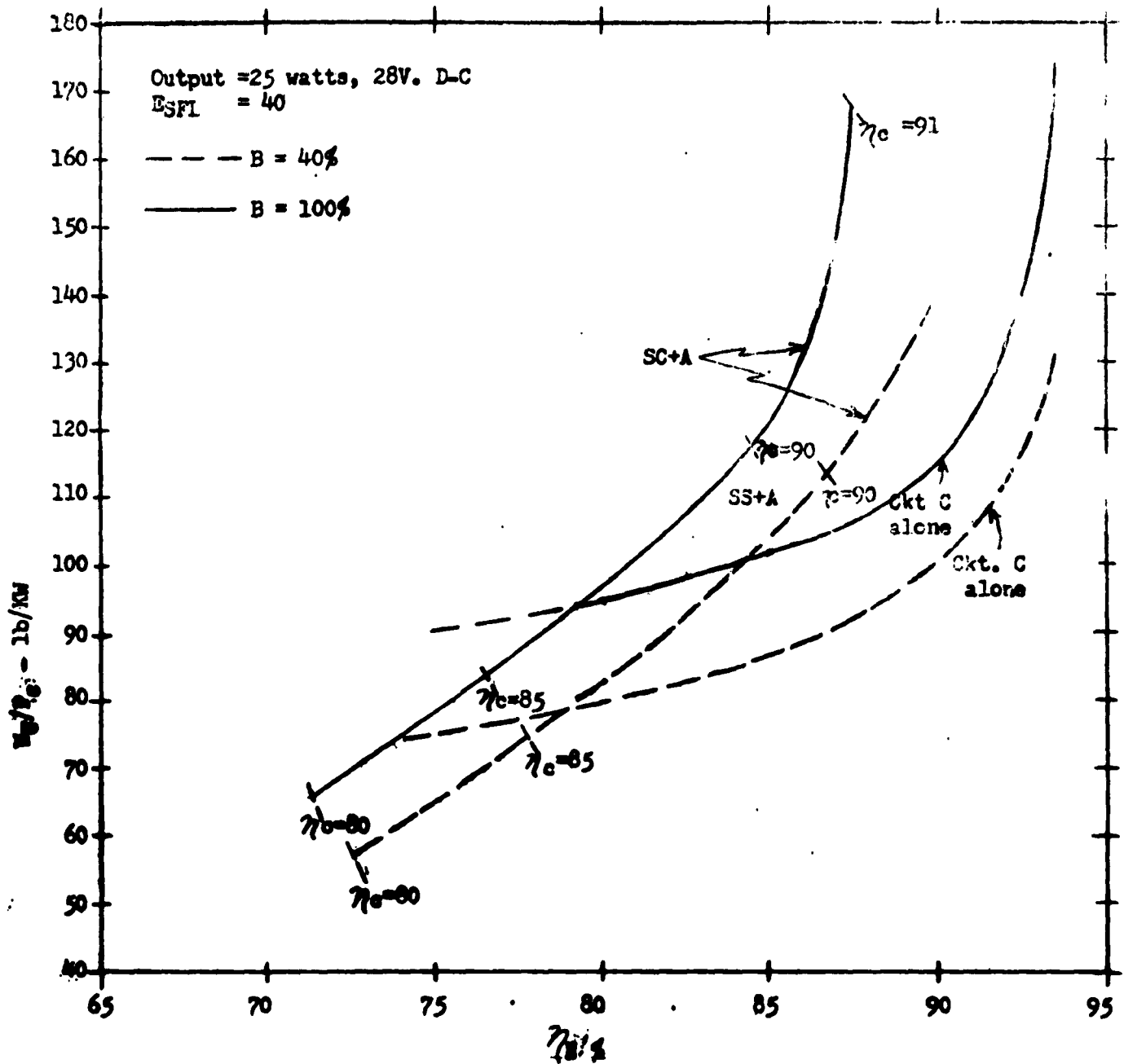
Figure 6.2-4: Total weight per unit of output power versus net efficiency for various external voltage converter-regulators and source voltage control combinations.
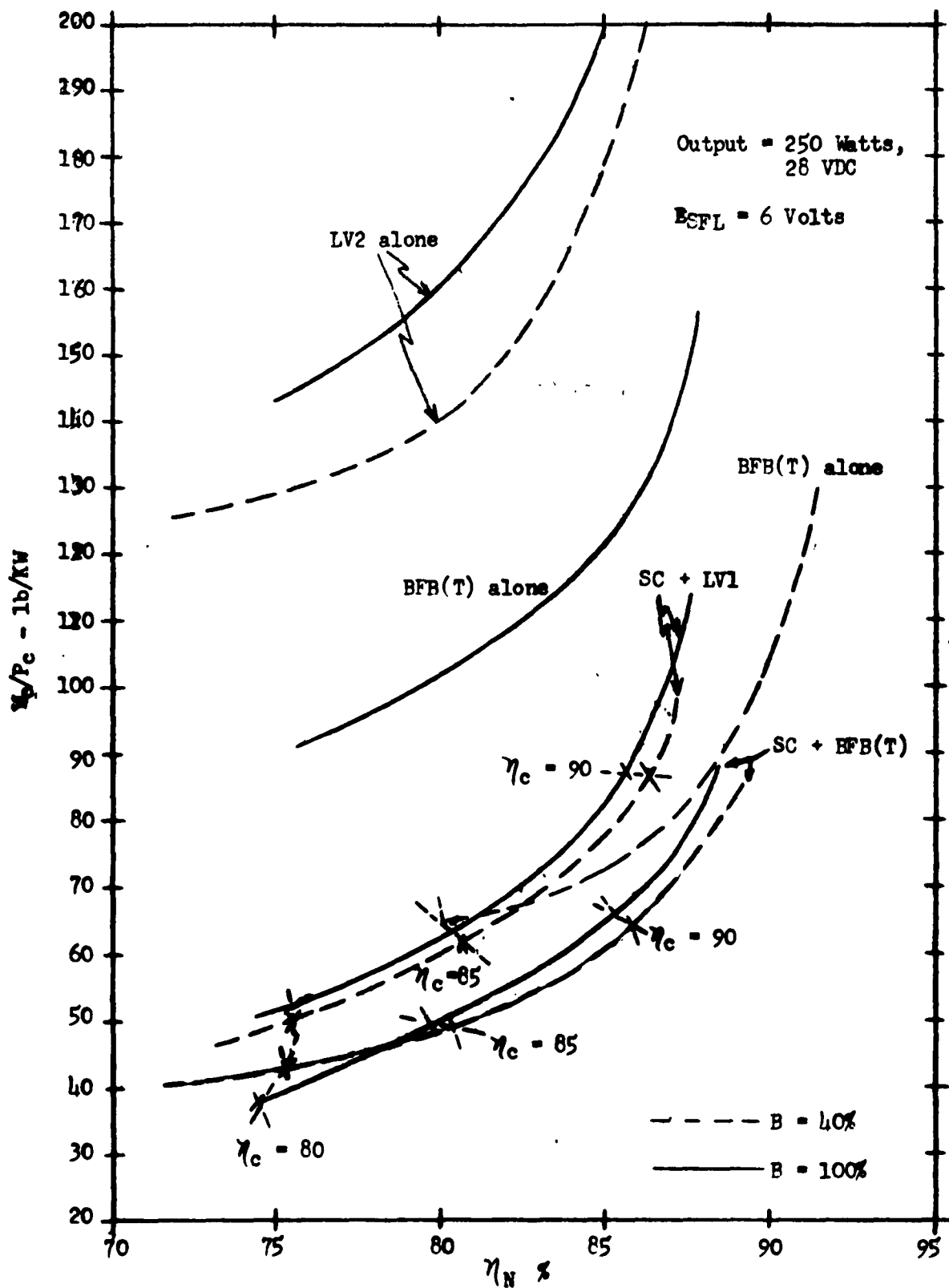
Figure 6.2-5

Total Weight Per Unit of Output Power Versus Net Efficiency for Various External Voltage Converter-Regulators and Source Voltage Control Combinations
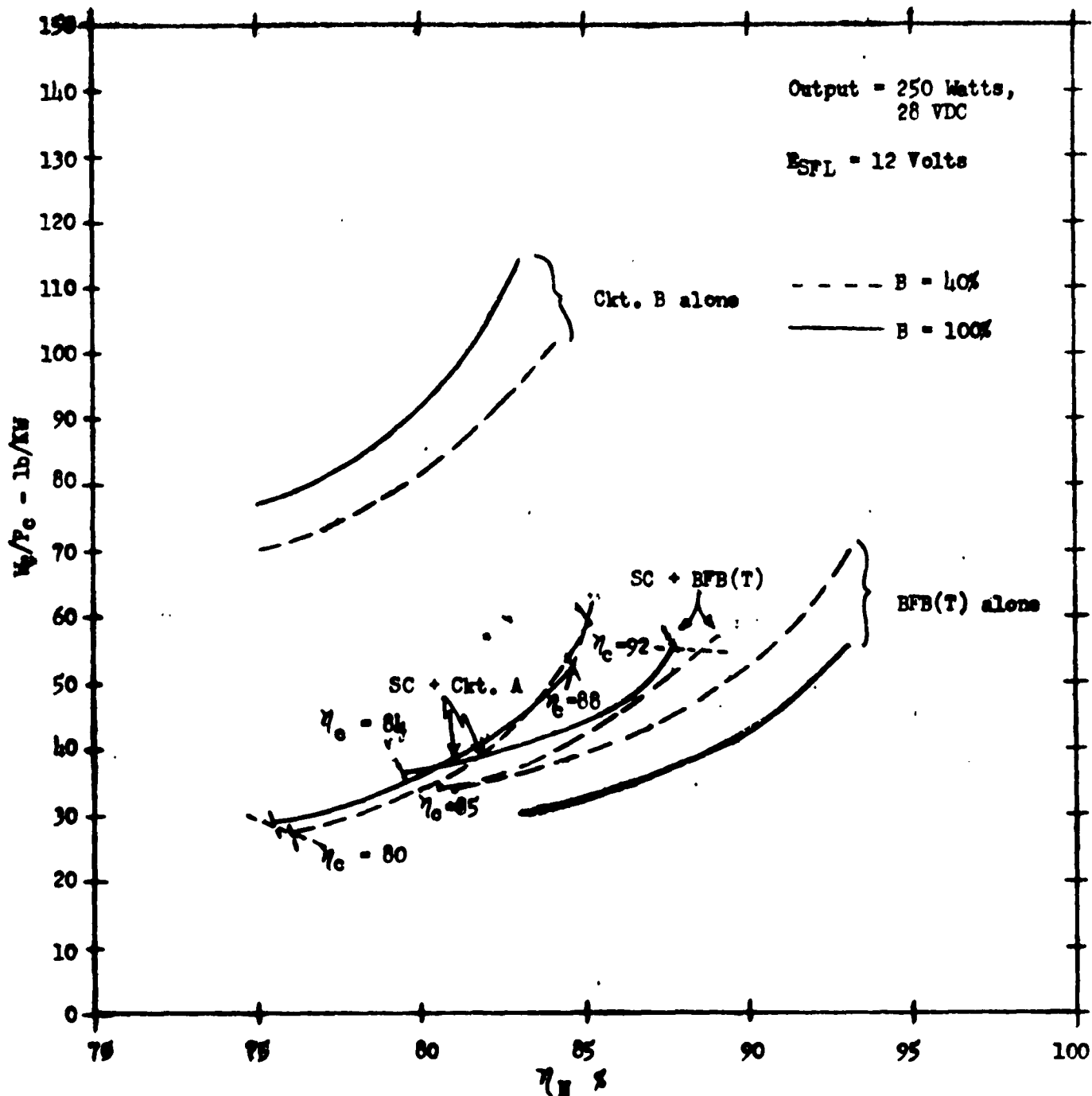
Figure 6.2-4

Total Weight Per Unit of Output Power Versus Net Efficiency for Various
External Voltage Converter-Regulators and Source Voltage Control Combinations
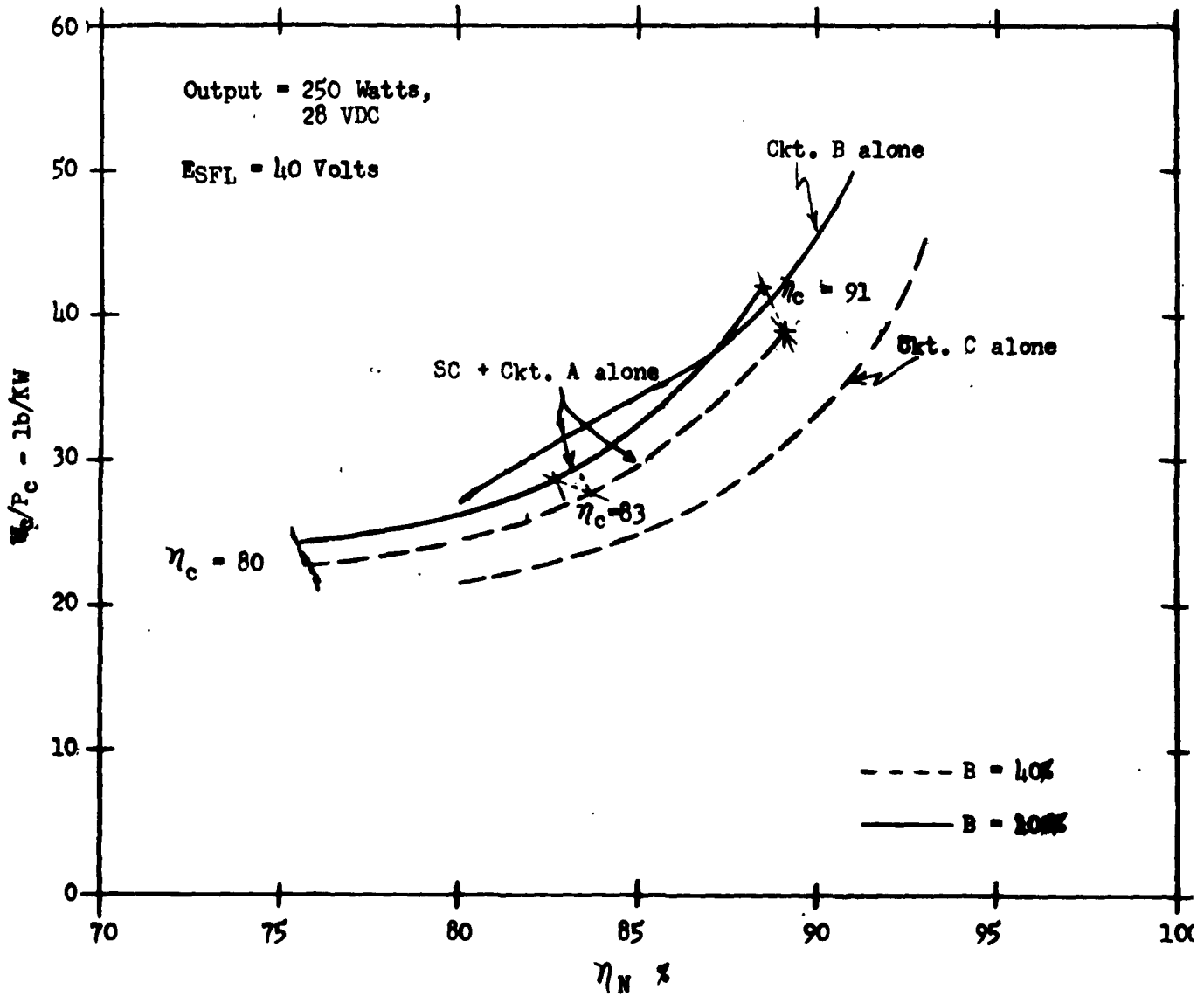
Figure 6.2-7

Total Weight Per Unit of Output Power Versus Net Efficiency for Various
External Voltage Converter-Regulators and Source Voltage Control Combinations
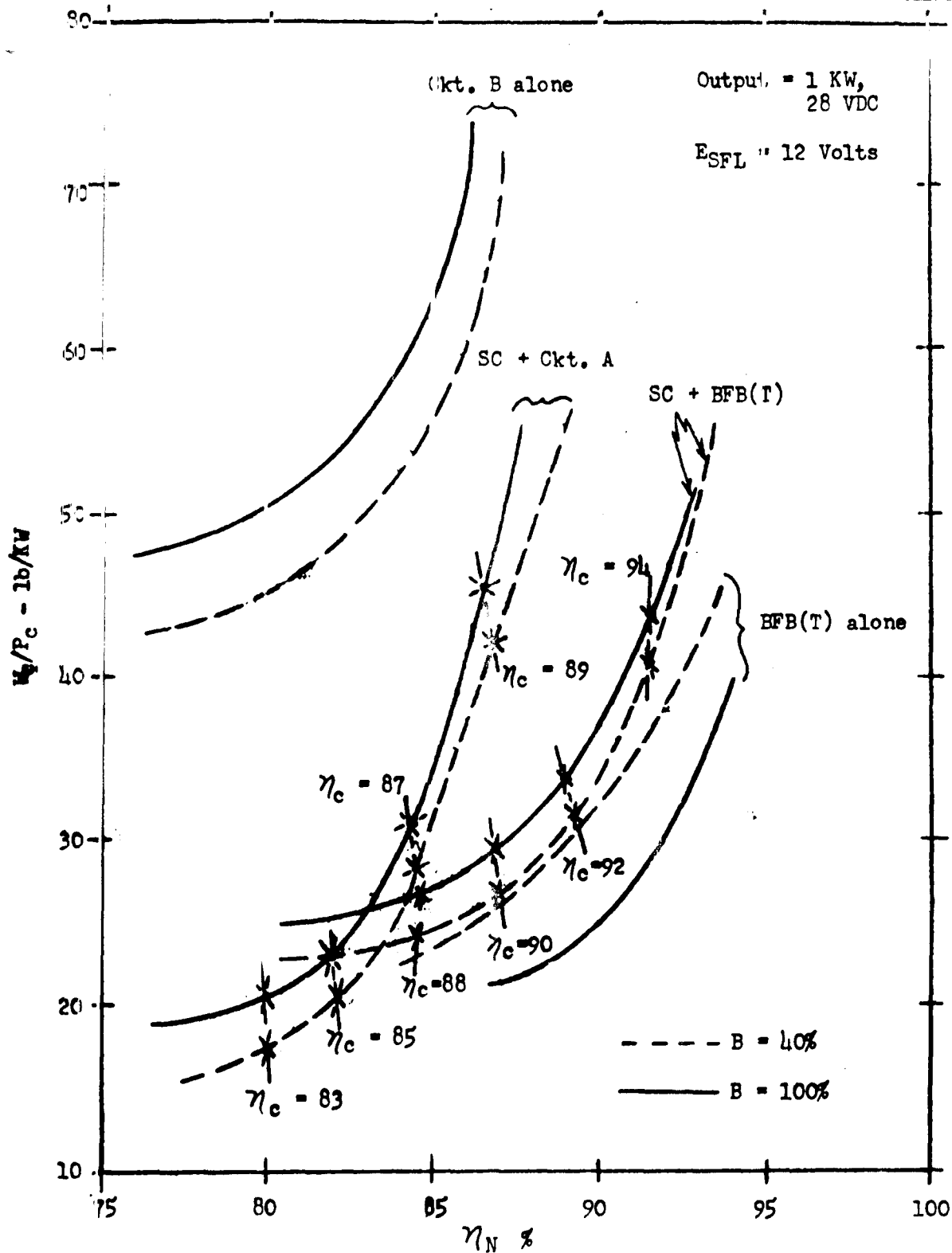
Figure 6.2-8

Total Weight Per Unit of Output Power Versus Net Efficiency for Various
External Voltage Converter-Regulators and Source Voltage Control Combinations
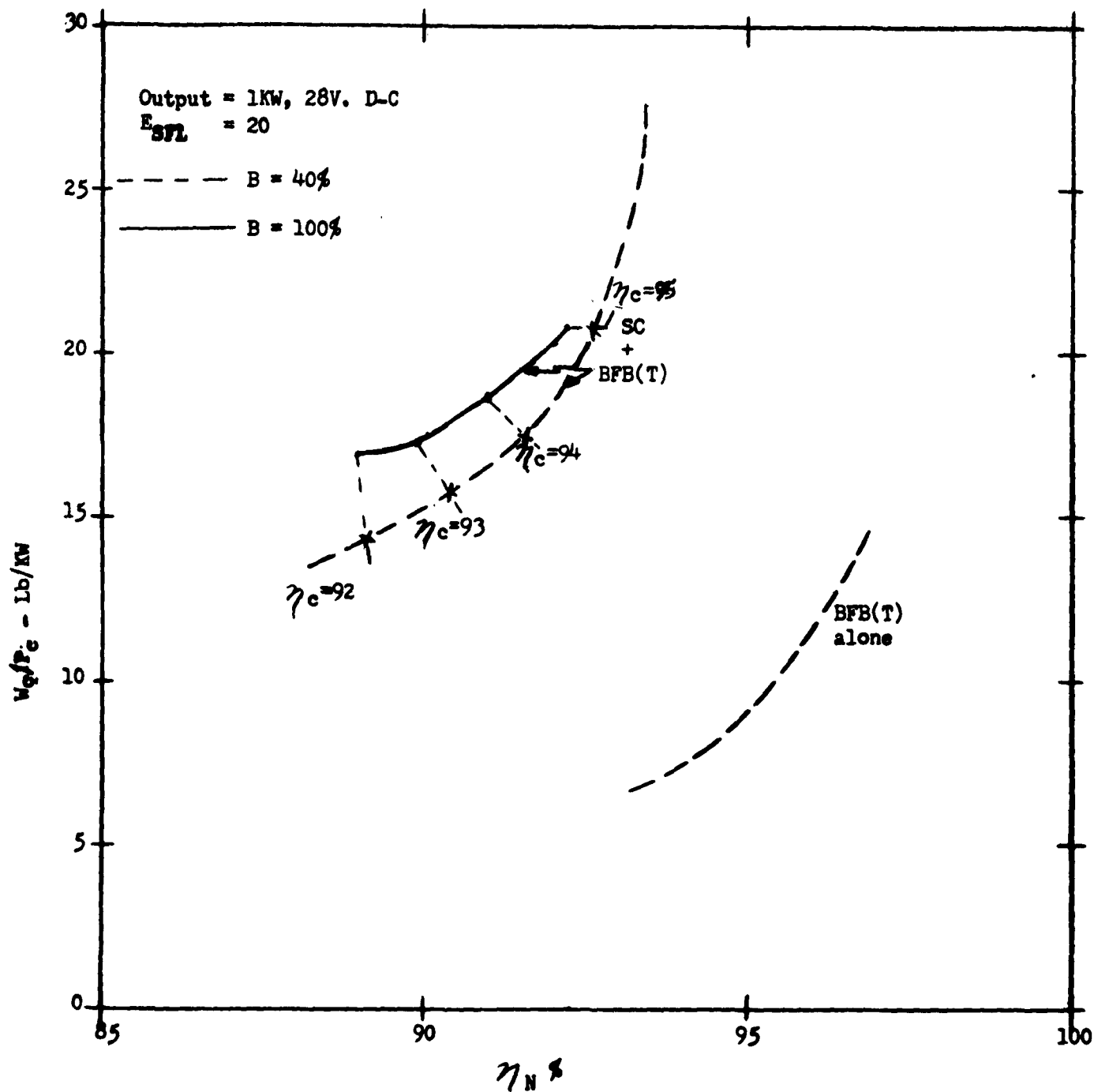
Figure 6.2-9

Total weight per unit of output power versus net efficiency for various external voltage converter-regulators and source voltage control combinations.

- 152 -
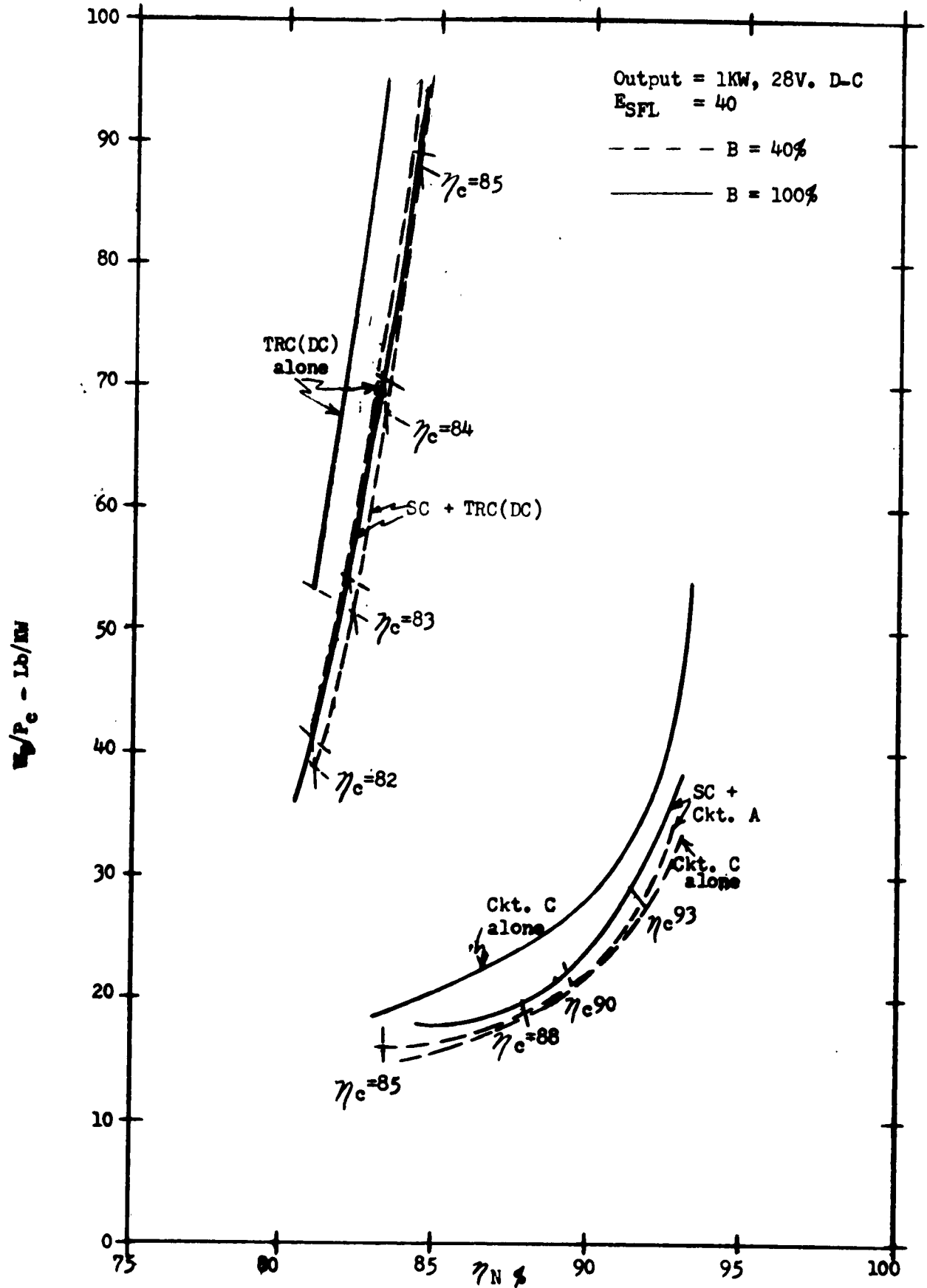
Figure 6.2-10

Total weight per unit of output power versus net efficiency for various external voltage converter-regulators and source voltage control combinations.
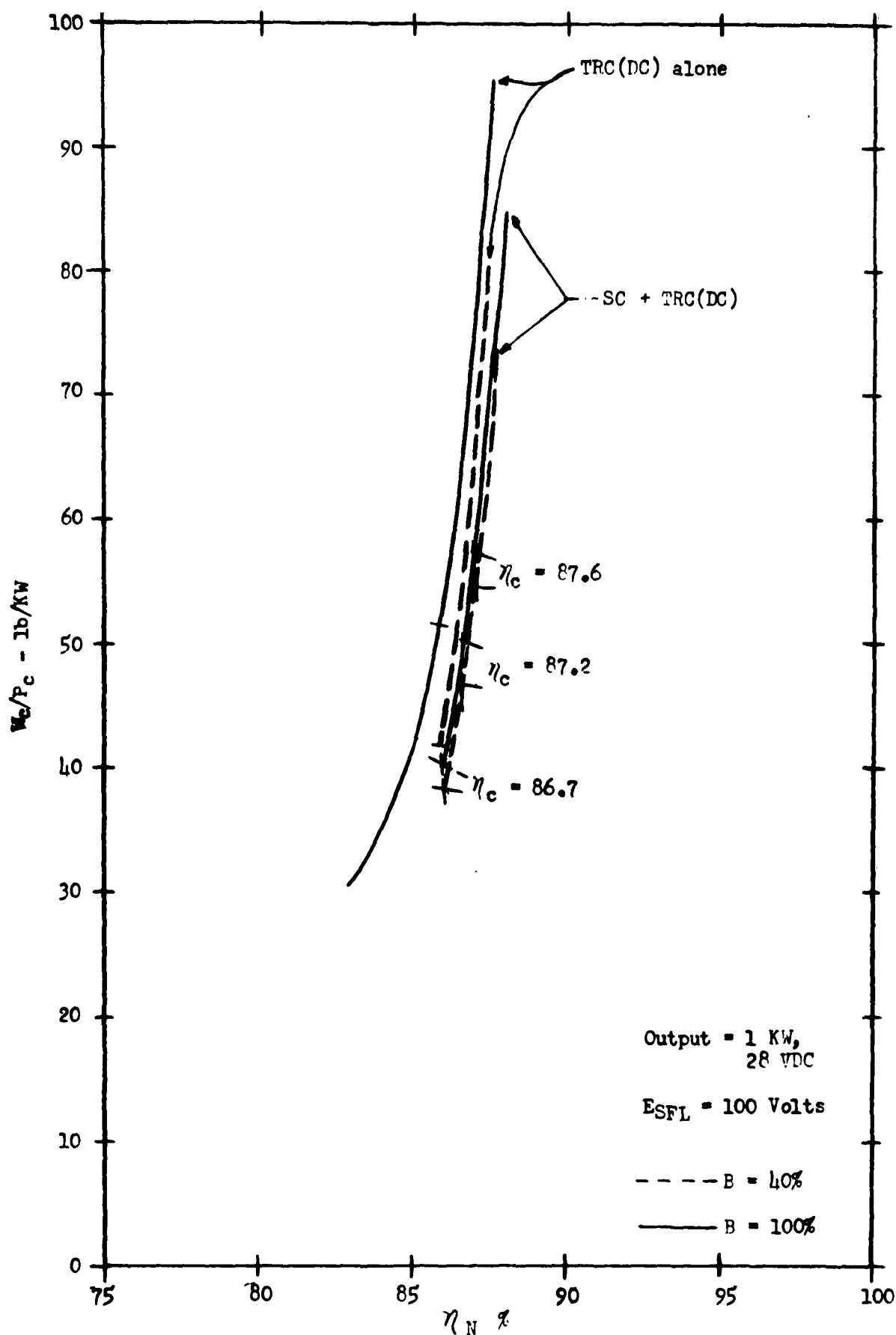
Figure 6.2-11

Total Weight Per Unit of Output Power Versus Net Efficiency for Various
External Voltage Converter-Regulators and Source Voltage Control Combinations
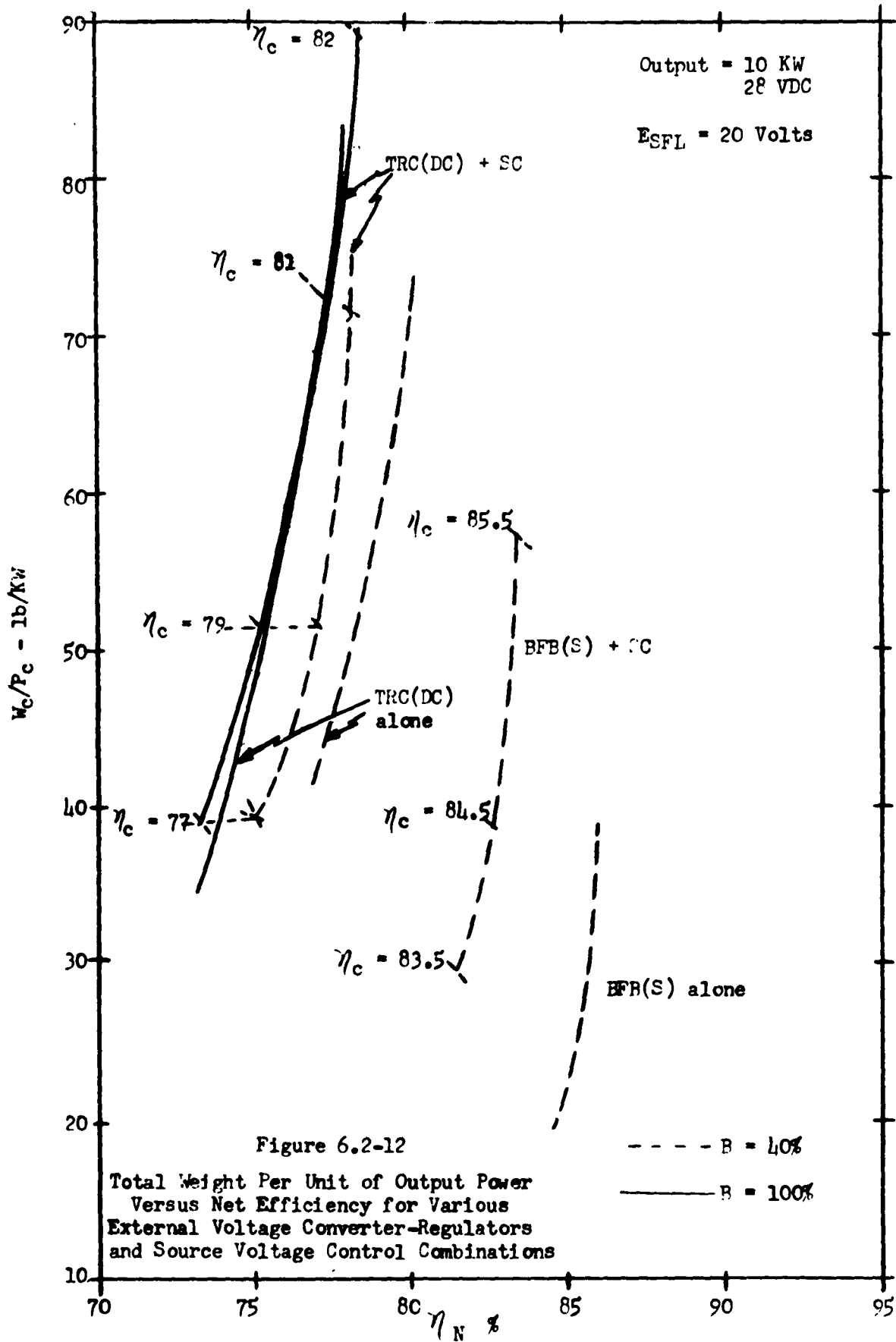
Figure 6.2-12

Total Weight Per Unit of Output Power
Versus Net Efficiency for Various
External Voltage Converter-Regulators
and Source Voltage Control Combinations
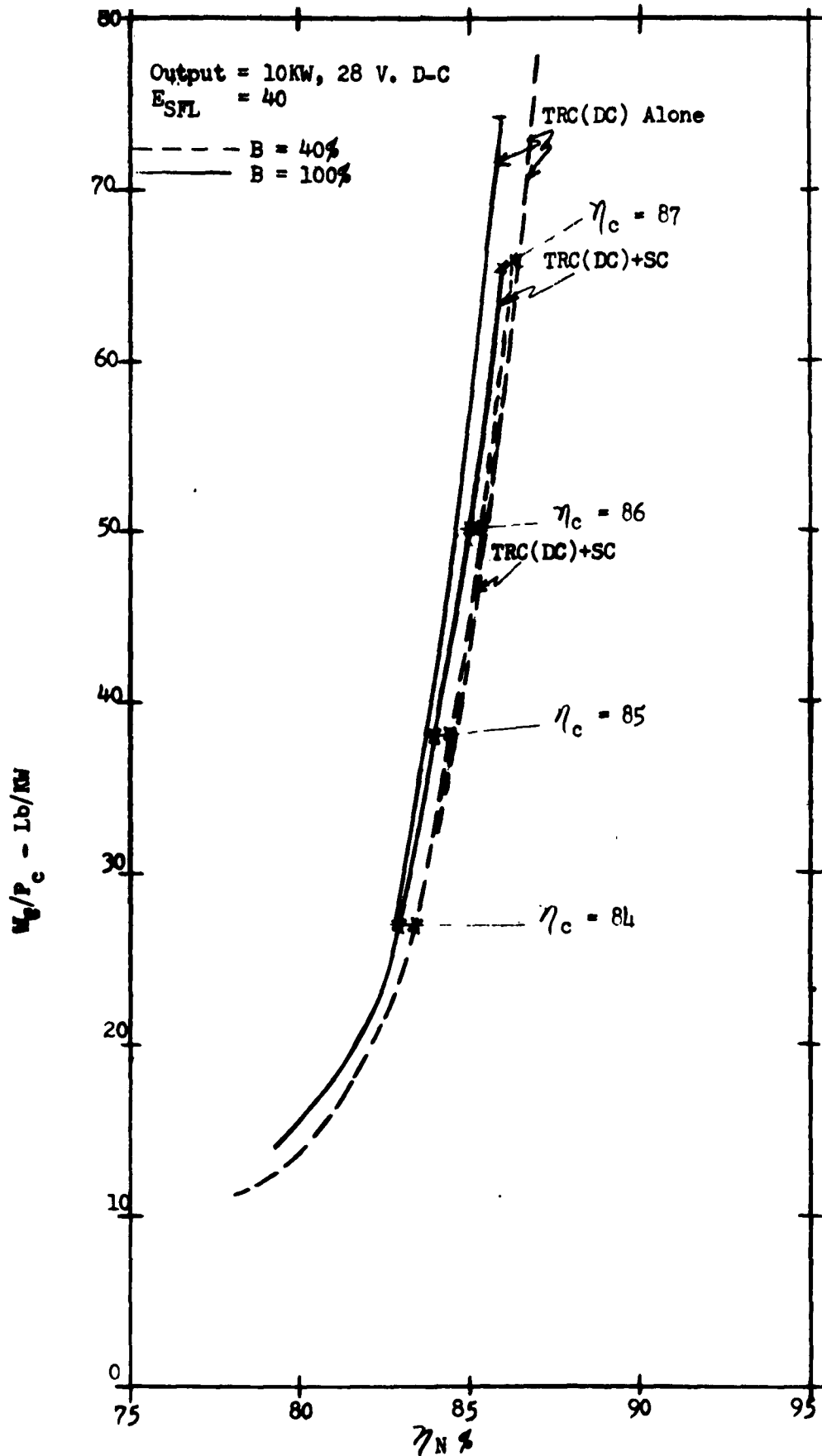
Figure 6.2-13

Total weight per unit of output power versus net efficiency
for various external voltage converter-regulators and
source voltage control combinations.
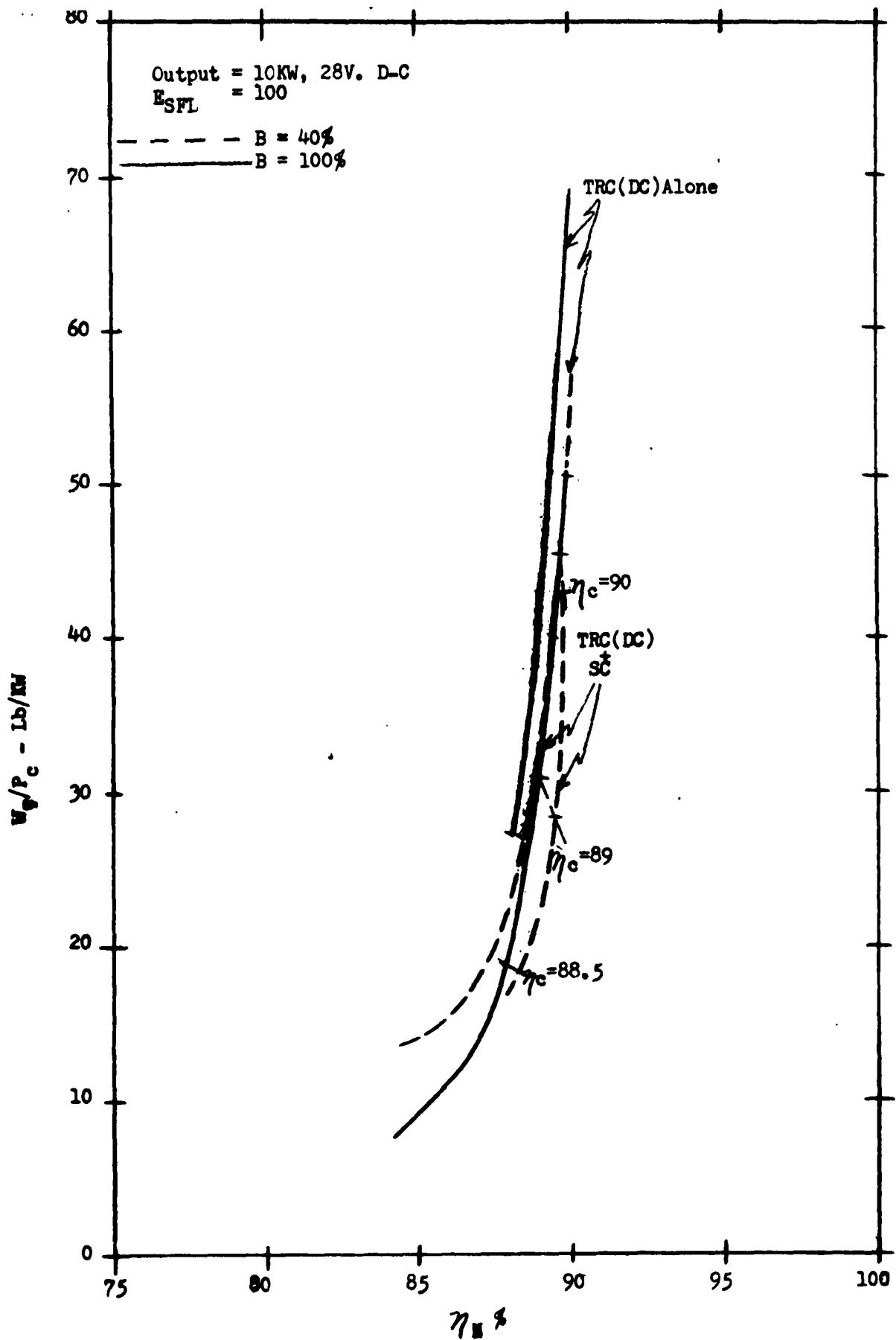
Figure 6.2-14

Total weight per unit of output power versus net efficiency for various external voltage converter-regulators and source voltage control combinations.
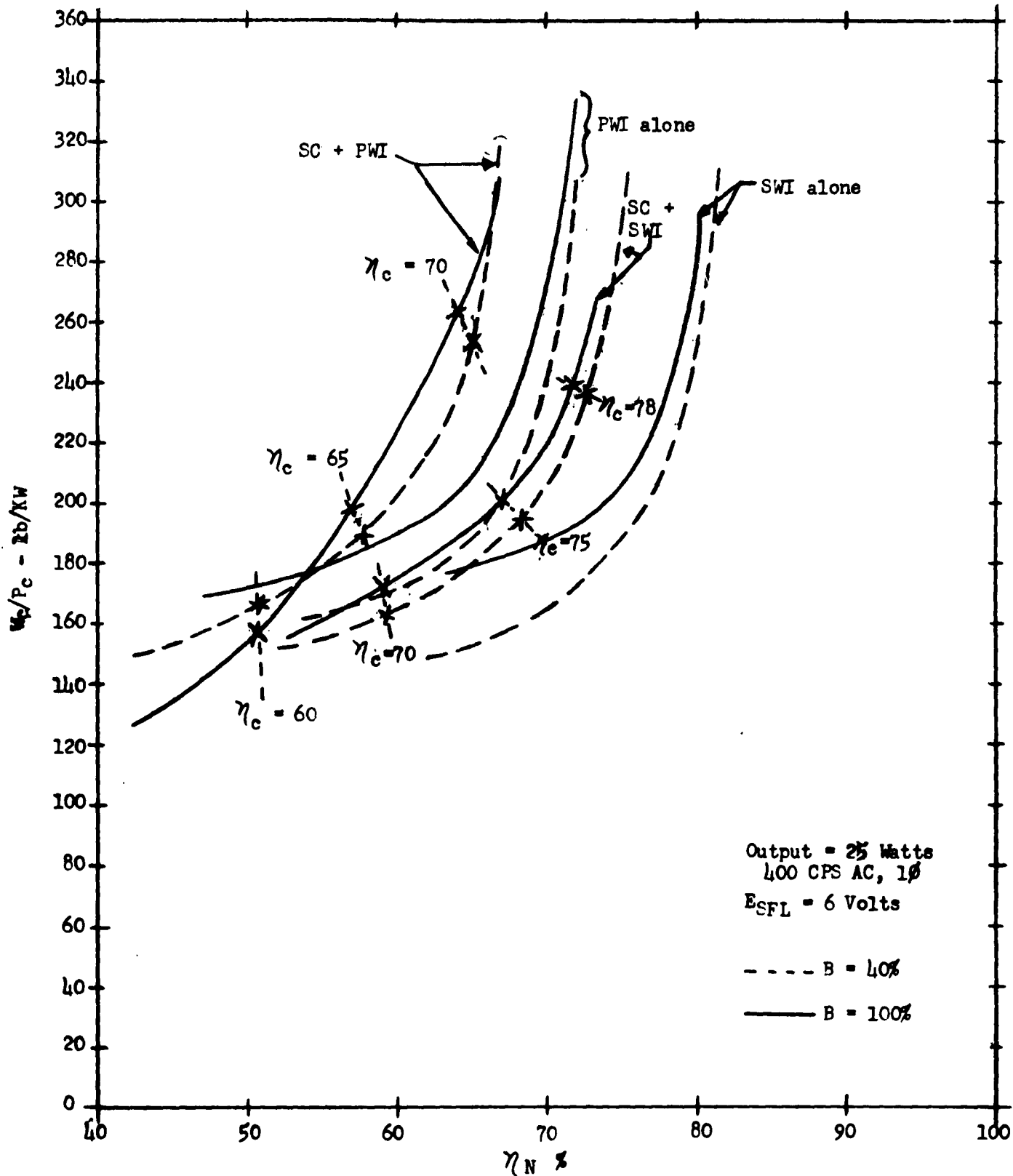
Figure 6.2-15

Total Weight Per Unit of Output Power Versus Net Efficiency for Various
External Voltage Converter-Regulators and Source Voltage Control Combinations
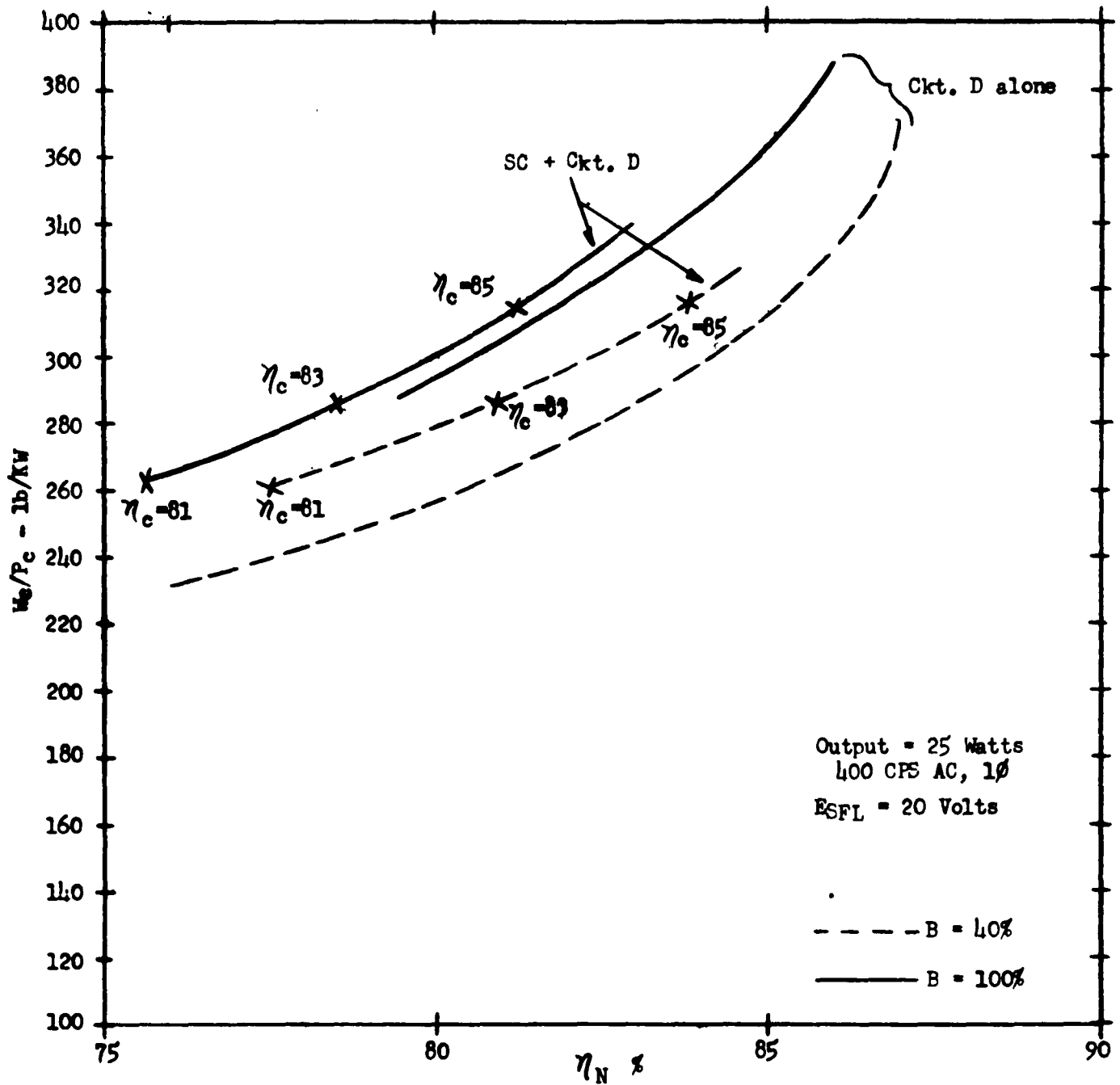
Figure 6.2-16

**Total Weight Per Unit of Output Power Versus Net Efficiency for Various
External Voltage Converter-Regulators and Source Voltage Control Combinations**
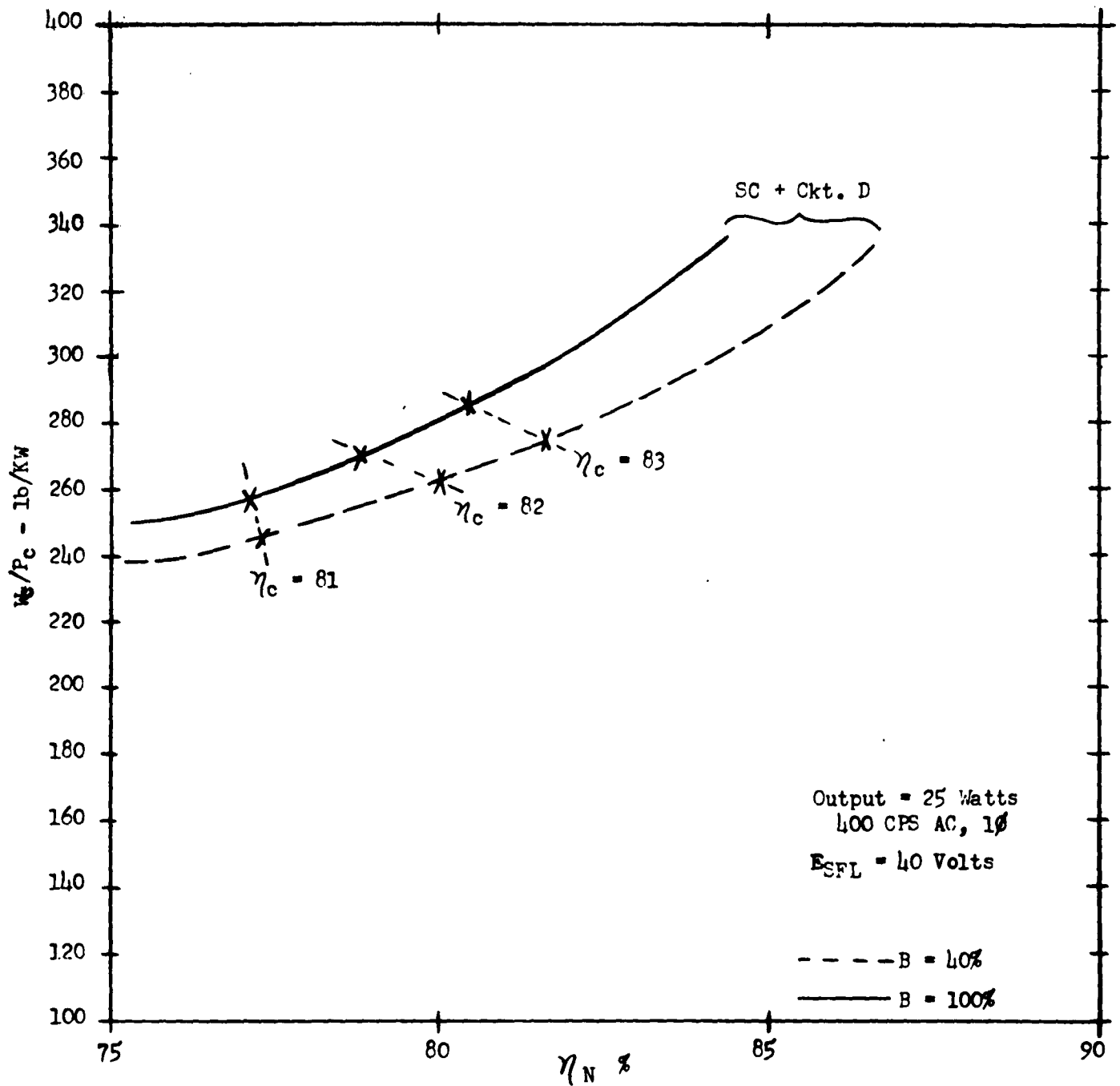
Figure 6.2-17

Total Weight Per Unit of Output Power Versus Net Efficiency for Various
External Voltage Converter-Regulators and Source Voltage Control Combinations
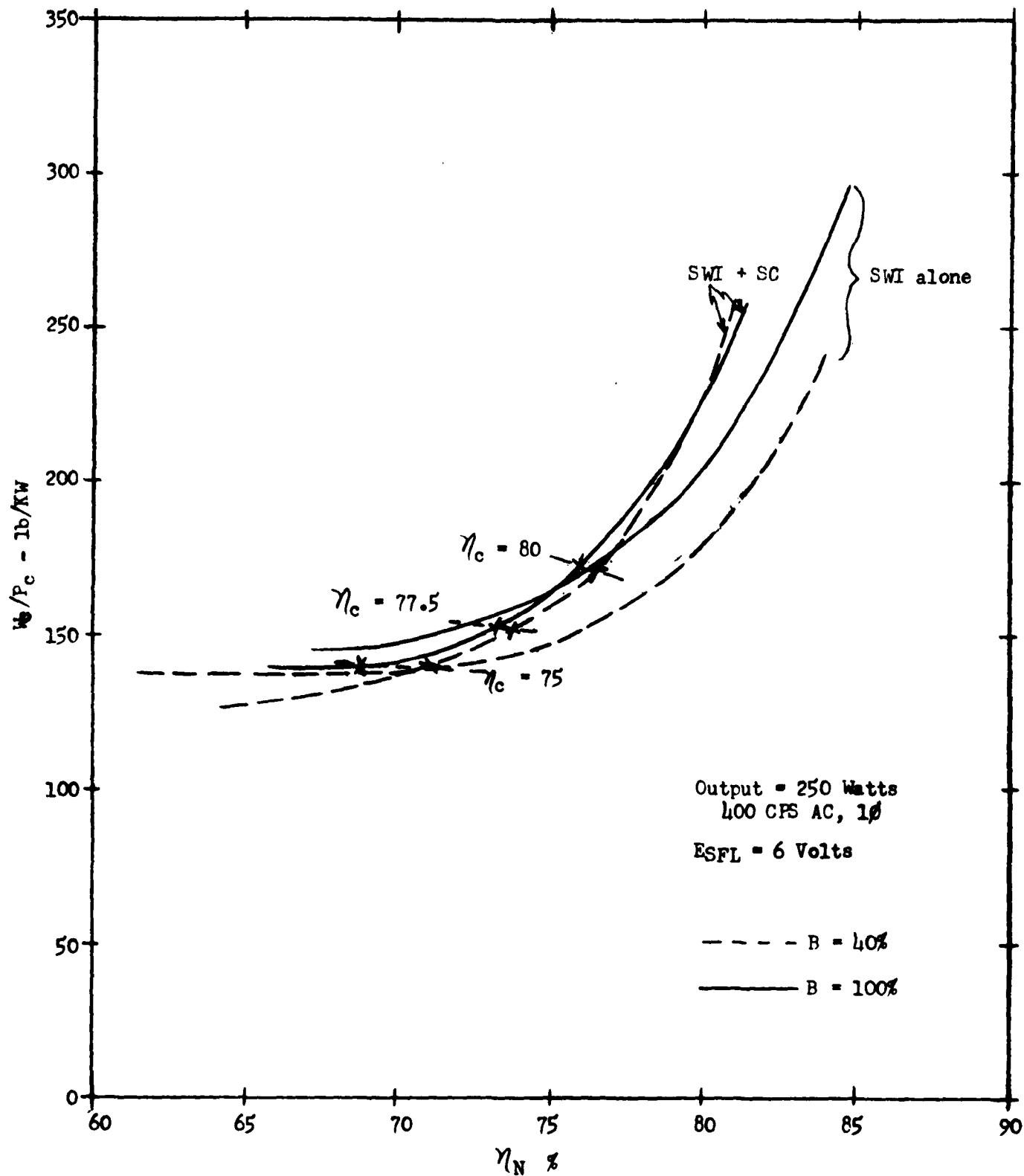
Figure 6.2-18

Total Weight Per Unit of Output Power Versus Net Efficiency for Various
External Voltage Converter-Regulators and Source Voltage Control Combinations
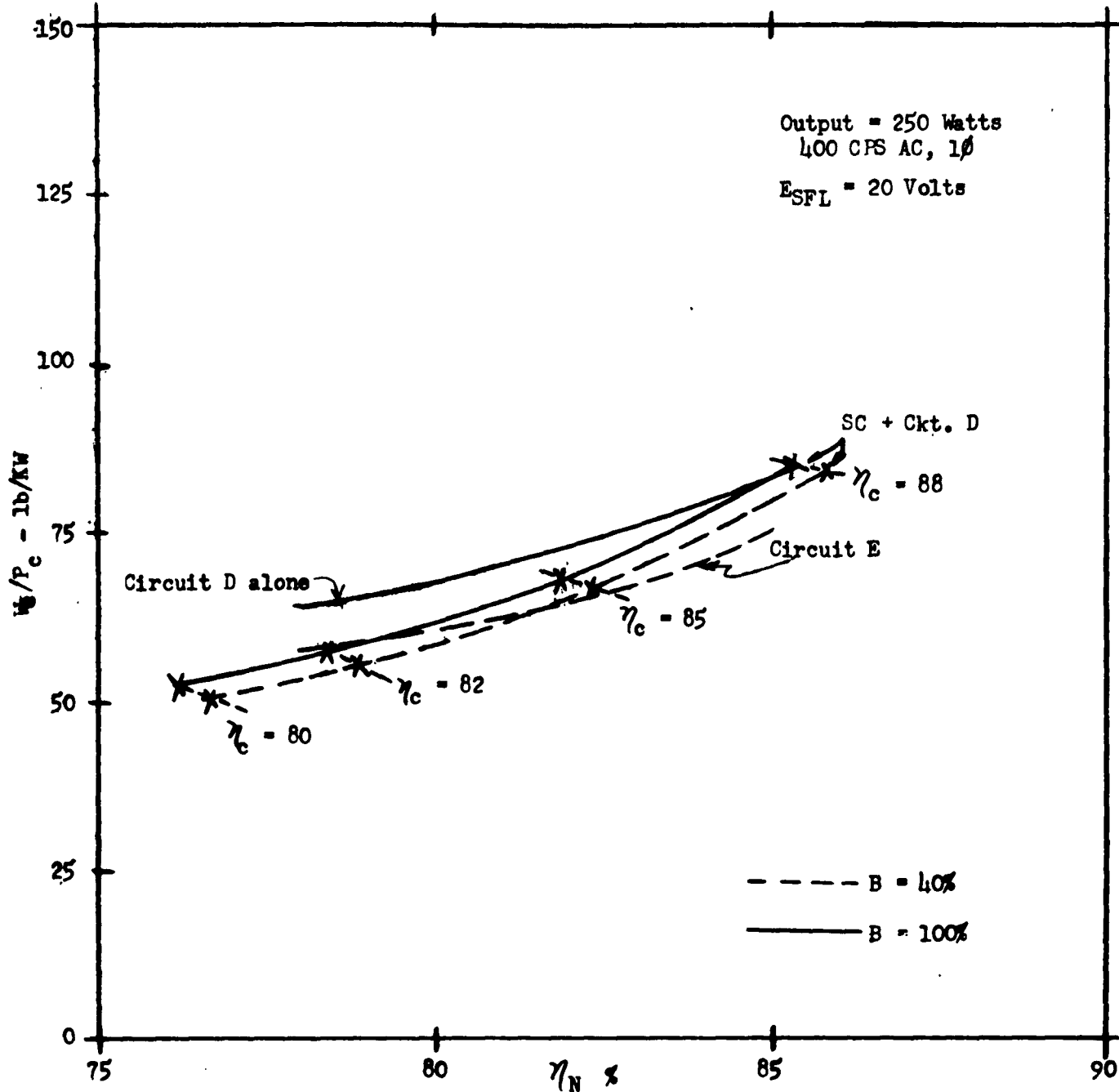
Figure 6.2-19

Total Weight Per Unit of Output Power Versus Net Efficiency for Various
External Voltage Converter-Regulators and Source Voltage Control Combinations

Figure 6.2-20

Total Weight Per Unit of Output Power Versus Net Efficiency for Various
External Voltage Converter-Regulators and Source Voltage Control Combinations
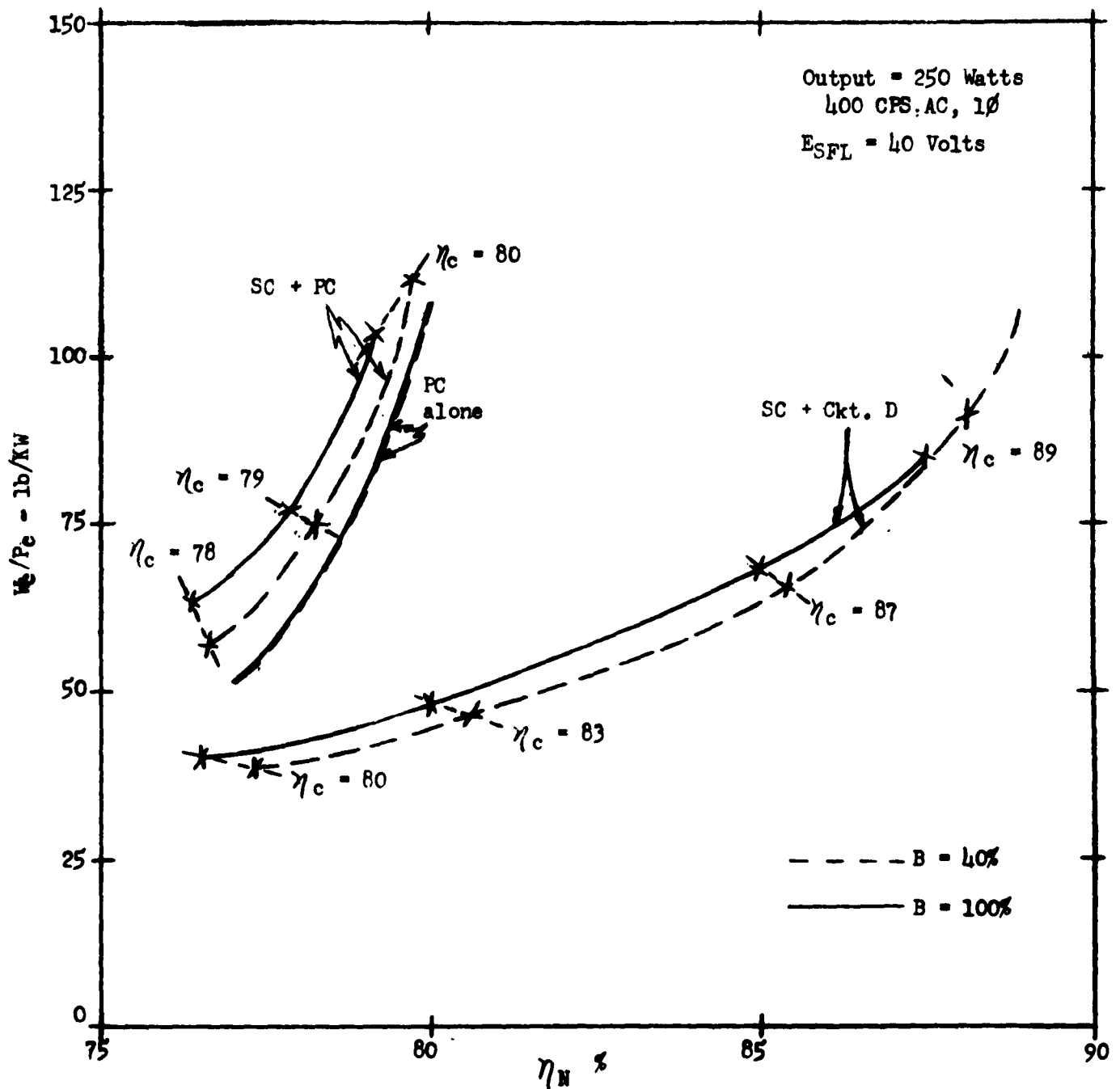
Figure 6.2-20

Total Weight Per Unit of Output Power Versus Net Efficiency for Various
External Voltage Converter-Regulators and Source Voltage Control Combinations
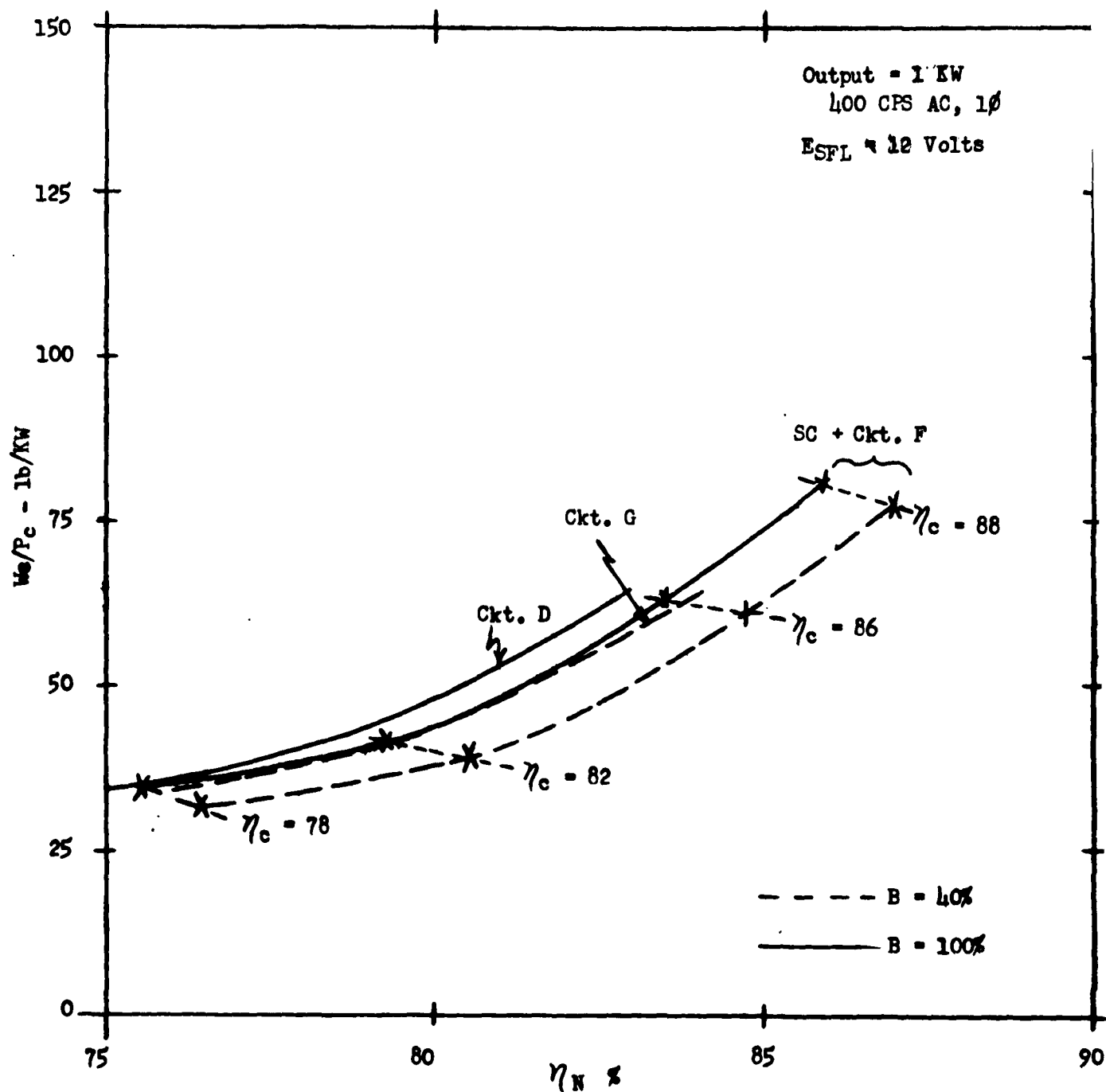
Figure 6.2-22

Total Weight Per Unit of Output Power Versus Net Efficiency for Various
External Voltage Converter-Regulators and Source Voltage Control Combinations
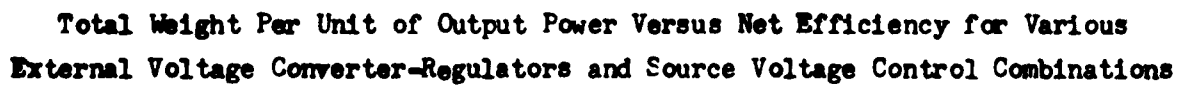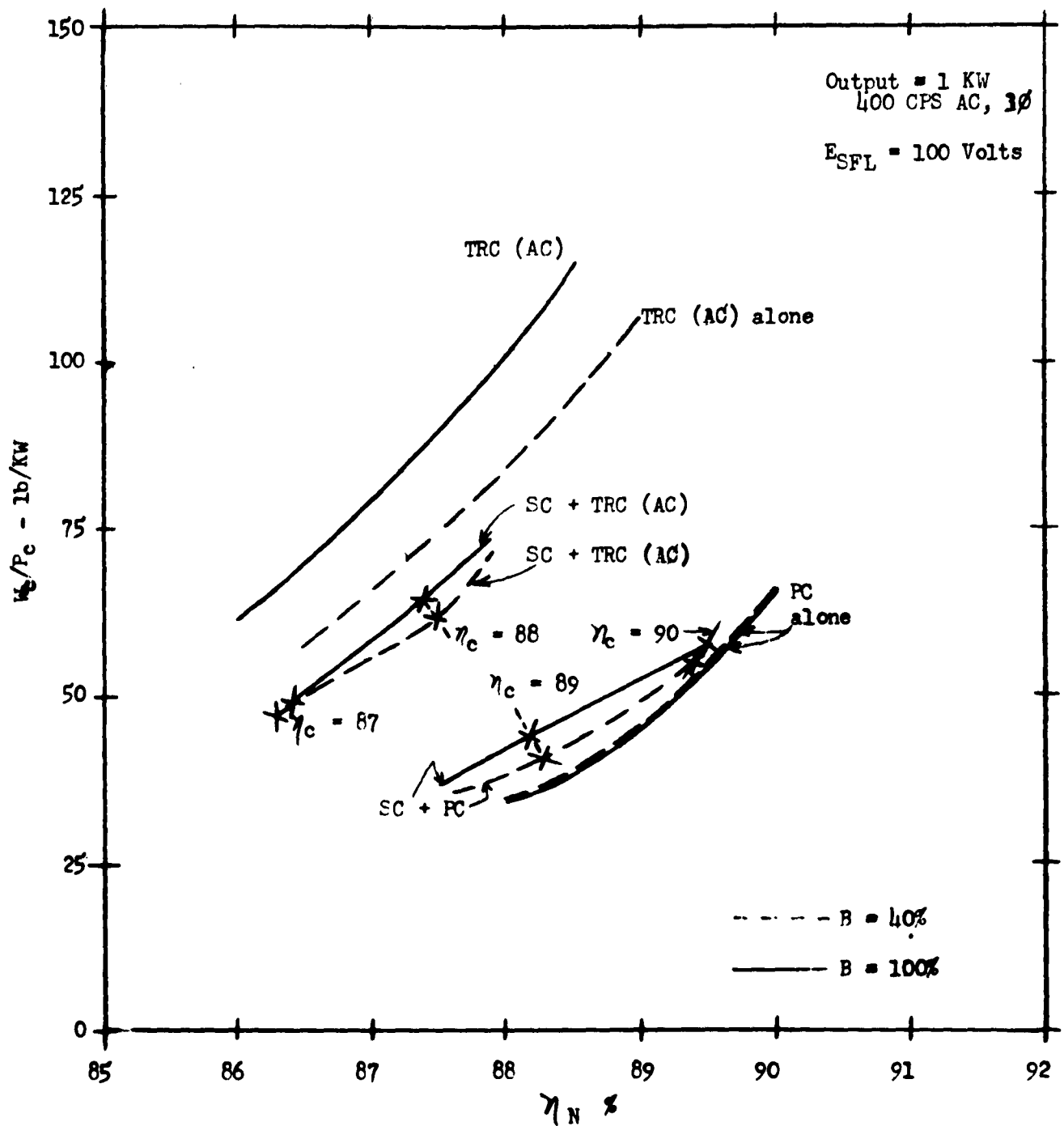
Figure 6.2-23

Total Weight Per Unit of Output Power Versus Net Efficiency for Various
External Voltage Converter-Regulators and Source Voltage Control Combinations
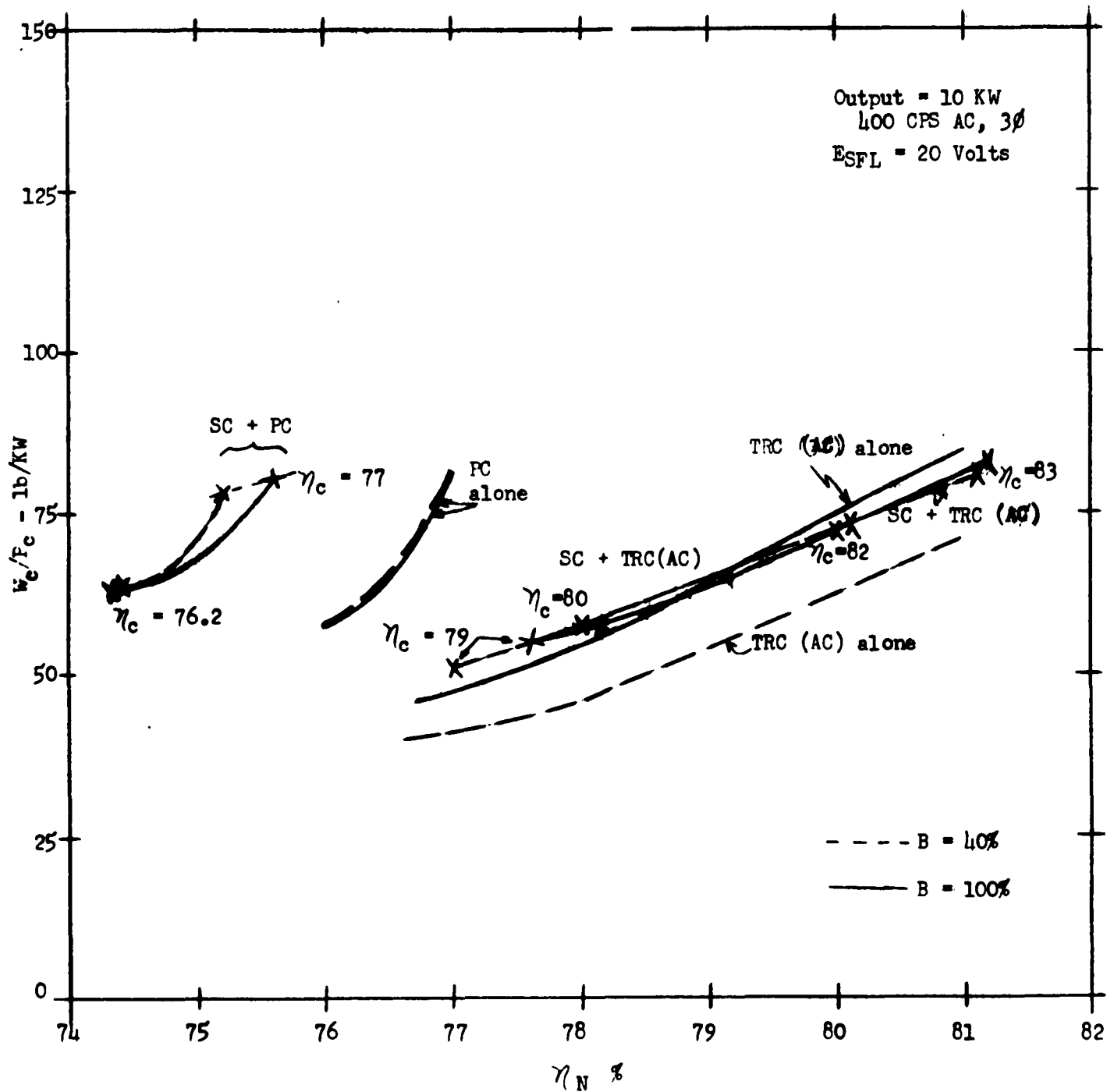
Figure 6.2-24

Total Weight Per Unit of Output Power Versus Net Efficiency for Various
External Voltage Converter-Regulators and Source Voltage Control Combinations
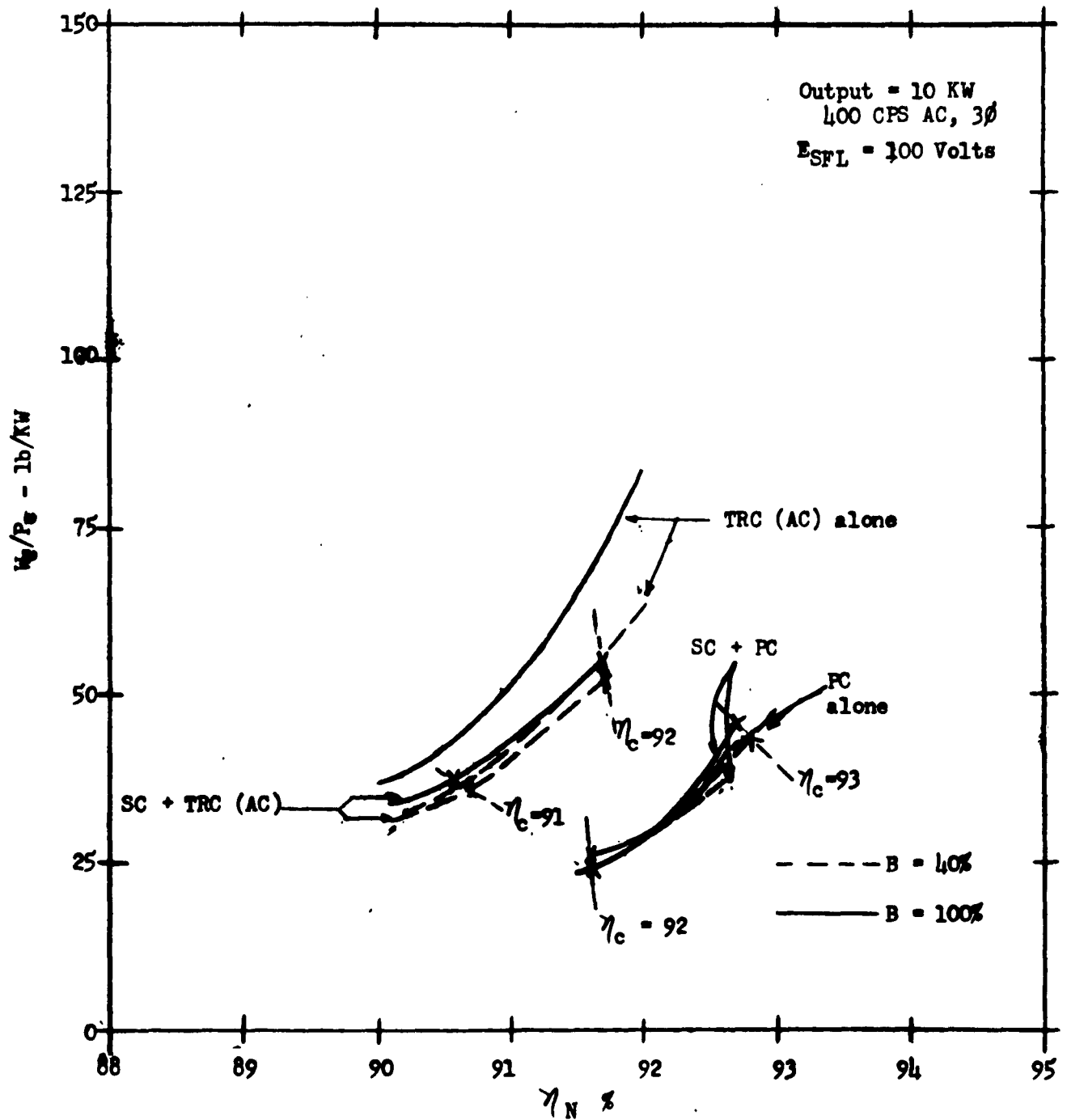
Figure 6.2-25

Total Weight Per Unit of Output Power Versus Net Efficiency for Various
External Voltage Converter-Regulators and Source Voltage Control Combinations
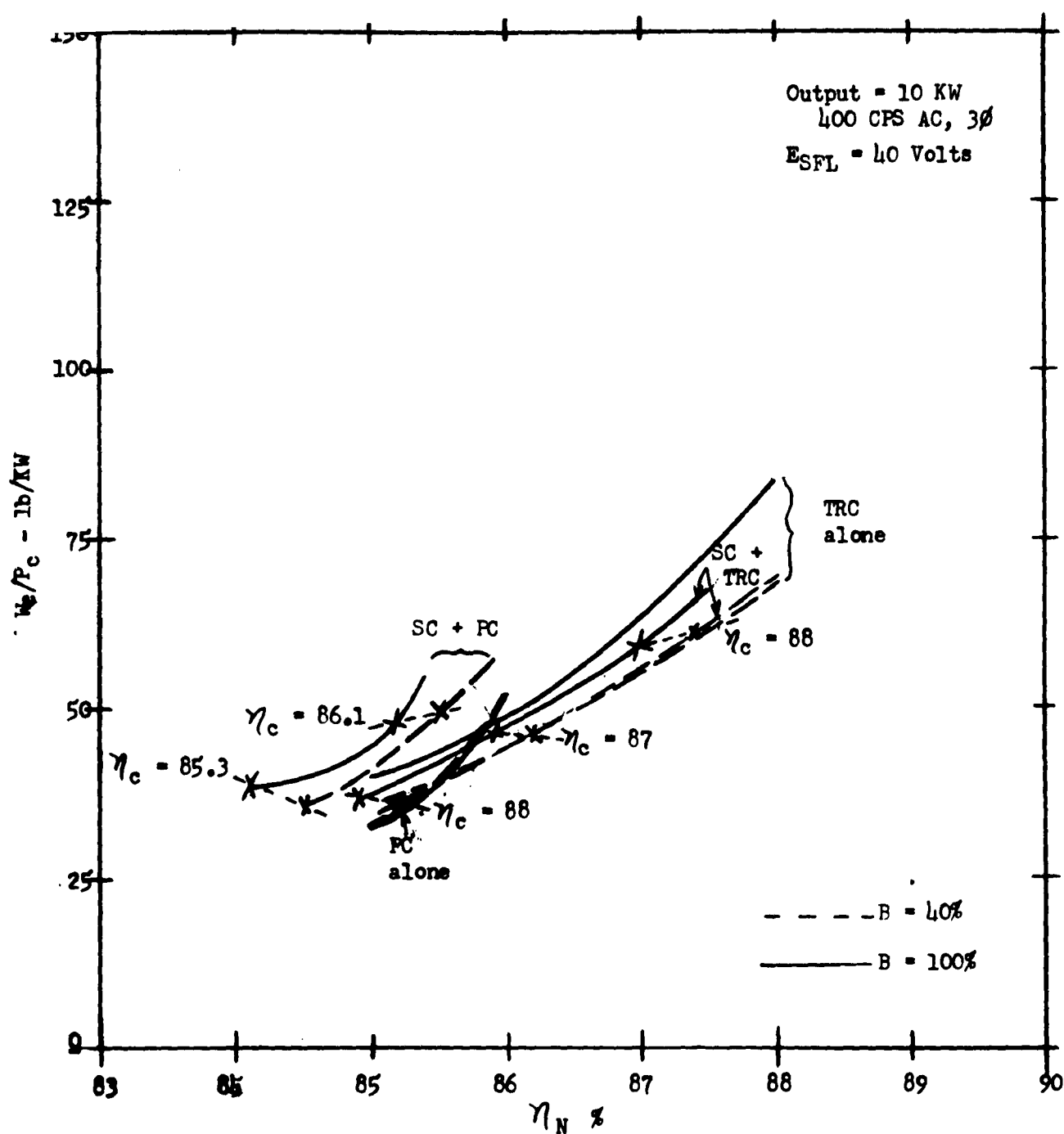
Figure 6.2-26

Total Weight Per Unit of Output Power Versus Net Efficiency for Various
External Voltage Converter-Regulators and Source Voltage Control Combinations

6.3　　Optimum Overall Systems

6.3.1　Introduction

　　　In Section 6.2 the optimum combinations of source voltage
control and external voltage regulation were determined for
selected power, source voltage and source voltage regulation condi-
tions. Curves giving total weight per unit power versus overall
efficiency for each of the combinations were also presented. In
this section these characteristics are combined with power source
characteristics in order to determine the weight per unit power
characteristics of overall systems (fuel, power source, voltage
converter and regulator) which utilize the optimum voltage regu-
lation combinations arrived at in Section 6.2. In this case the
criteria for optimization was that of achieving the minimum over-
all system weight consistent with other performance requirements
such as output voltage regulation, load range, ripple content,
etc. Although minimum weight is not always an important criteria,
it is the more usual requirement in military applications, thus
it was selected. Of course, minimum weight will also tend to
yield minimum volume.

　　　The following analysis shows how the minimum weight system
was obtained. The results are presented in such a manner as to
show the weight penalty to the power source of incorporating
voltage regulation and conversion in the system. In addition,
the effects of source voltage level, output power level, and
inherent source voltage regulation are demonstrated. The results
given apply to all types of power sources. It is only necessary
to know the weight per unit of output power of the source and fuel
supply. This value, of course, is dependent upon the type of
source and amount of fuel required for the particular mission.
For long missions fuel weight is predominant; whereas, for short
missions, the energy converter and voltage converter weight are
significant.

6.3.2　Analysis

　　　This analysis will derive the equations for total system
weight and the criteria for minimum weight. The total system
weight is:

(6.3-1)　　　$W_T = W_s + W_c$

where:

W_T = Total system weight

W_s = Source weight including accessories and fuel required for a given mission.

W_c = Weight of the voltage regulation and conversion function.

By means of some manipulation equation 6.3-1 can be written as:

(6.3-2)

$$\frac{W_T}{P_c} = \frac{P_s}{P_c} \left[\frac{W_s}{P_s} \right] + \frac{W_c}{P_c}$$

where:

P_c = Rated output power

P_s = Power out of the source to the voltage converter and regulator at rated output conditions.

However,

$$\frac{P_c}{P_s} = \frac{\eta}{100}$$

where:

η = Net efficiency of the voltage converter-regulation function in percent.

Thus, equation 6.3-2 can be written in terms of weight per unit power and efficiency as follows:

(6.3-3)

$$\frac{W_T}{P_c} = \frac{100}{\eta} \left[\frac{W_s}{P_s} \right] + \frac{W_c}{P_c}$$

Of course,

(6.3-4)

$$\frac{W_c}{P_c} = F(\eta)$$

as given by the figures of Section 6.2. Choosing a high value of net voltage converter efficiency (η) will result in large voltage converter weight per unit power (W_c/P_c) and also produce a large total system weight per unit power (W_T/P_c). Low values of net voltage converter efficiency also result in a large total system weight per unit of output power since the power source must be large to supply the large power loss of the voltage converter-regulator.

Thus, it is evident that there must be some optimum value of converter efficiency η_m which produces minimum total system weight. This value can be found by letting:

$$\frac{\partial \left(\frac{W_T}{P_c}\right)}{\partial \eta_m} = 0$$

Differentiating equation 6.3-3 in this manner yields:

$$\frac{\partial \left(\frac{W_T}{P_c}\right)}{\partial \eta_m} = -\frac{100}{\eta_m^2}\left[\frac{W_s}{P_s}\right] + \frac{\partial \left(\frac{W_c}{P_c}\right)}{\partial \eta_m} = 0$$

or

$$(6.3-5) \quad \frac{\eta_m^2}{100}\left[\frac{\partial \frac{W_c}{P_c}}{\partial \eta_m}\right] = \frac{W_s}{P_s}$$

Equation 6.3-5 gives the condition which must be satisfied if minimum total system weight is to be achieved. In performing the differentiation indicated previously, it was assumed that the source weight per unit power is not a function of the voltage converter efficiency

Equation 6.3-3 may also be written as follows:

$$(6.3-6) \quad \frac{\left(\frac{W_T}{P_c}\right)}{\left(\frac{W_s}{P_s}\right)} = \frac{100}{\eta_m} + \frac{\left(\frac{W_c}{P_c}\right)}{\left(\frac{W_s}{P_s}\right)}$$

In this case the quantity on the left side of the equation is the ratio of total system weight per unit of output power to source weight per unit power. For an ideal voltage converter and regulator which had 100% efficiency and zero weight, this ratio would be one. Thus, this ratio will always be greater than one and indicates the penalty in system weight produced by the addition of a voltage conversion and regulation function.

It is this ratio that is calculated and shown in the result curves.

In order to make the resultant overall system data generally useful, several values of source weight per unit power (W_s/P_s) between the values of 50 and 1,000 pounds per kilowatt were selected and the corresponding values of total system weight determined. The voltage converter and regulator data was obtained from the curves given in Section 6.2. In the case of each point only the minimum weight voltage conversion and regulation system was chosen. The minimum system weight was established by applying the criteria of Equation 6.3-5. Thus, for example, for a source weight per unit power (W_s/P_s) of 100, the voltage converter and regulator efficiency was chosen such that

$$\frac{\eta_m^2}{100} \quad \frac{d\left(\frac{W_c}{P_c}\right)}{d\eta_m} = 100$$

The corresponding efficiency (η_m), voltage regulator and converter weight per unit power (W_c/P_c), and source weight per unit power (W_s/P_s) were then used in Equation 6.3-6 to obtain the system characteristics.

6.3.3 Results

The ratio of total system weight per unit of output power to the source weight per unit of power $\frac{W_T}{P_c} / \frac{W_s}{P_s}$ is shown in Figures 6.3-1 through 6.3-20 as function of full load source voltage (E_{SFL}), full load power (P_c), inherent source voltage regulation (B) and source weight per unit power, (W_s/P_s). Figures 6.3-1 through 6.3-10 display the information for the 28 volt DC output; whereas, Figures 6.3-11 through 6.3-20 present it for the 400 cps AC output.

In most applications the inherent source voltage regulation (B) and the source weight per unit of source power (W_s/P_s) are determined by application considerations. Once these characteristics are determined, the additional system weight penalty produced by the voltage conversion and regulation function can be readily determined from one of Figures 6.3-1 through 6.3-20.

Example

The possible use of the data presented in this section is best illustrated by a simple example. Let it be assumed that following are the requirements of a given application.

$$\text{Output Power } (P_c) = 250 \text{ watts}$$

$$\text{Output Voltage} = 28 \text{ VDC}$$

Additional requirements in terms of mission length, duty cycle, etc. would be specified. The power source including fuel supply could be initially sized and optimized to yield minimum weight. Let it be assumed that this optimization led to the following values.

$$\text{Inherent Source Regulation } (B) = 40\%$$

$$\text{Source Weight Per Unit of Source Power } (W_s/P_s) = 250 \text{ lbs/KW}$$

$$\text{Selected full load source voltage } (E_{SFL}) = 12 \text{ volts}$$

Then from Figure 6.3-5, the ratio of total system weight per unit of output power to the source weight per unit of output power is:

$$\frac{W_T/P_c}{W_s/P_s}$$

thus

$$W_T/P_c = 1.33 \times 250 = 332 \text{ lbs/KW}$$

Figure 6.3-5 indicates that the optimum system is one which uses the flyback circuit. The weight per unit power versus efficiency for a flyback circuit with this power and voltage level is given by Figure 6.2-6. Also, substituting the previously obtained numbers into Equation 6.3-6 gives the additional relationship between efficiency and weight per unit power for the flyback circuit as:

$$(6.3\text{-}7) \qquad 1.33 = \frac{100}{\eta_N} + \frac{W_c/P_c}{250}$$

The only combination of efficiency and W_c/P_c which satisfies both Equation 6.3-7 and Figure 6.2-6 is:

$$\eta_N = 91.5\%$$

$$W_c/P_c = 60. \text{ lbs/KW}$$

These numbers define the operating point of flyback circuit for minimum overall system weight. In addition, of course, the actual output power of the power source is:

$$P_s = \frac{100 P_c}{\eta_N}$$

$$= \frac{250}{.915}$$

$$P_s = 273. \text{ watts}$$

Thus, the power source and fuel supply would have to be sized to deliver 273 watts.

If the actual value of output power significantly changed the optimum source design point from a value of $B = 40\%$ and $W_s/P_s = 250$ lbs/KW, initially determined, it would be necessary to repeat the above steps using the newly determined values. However, it is unlikely that such a recalculation would normally be required. It will be noted that the effect of adding a voltage converter and regulator is one of increasing the total system weight 33% over the system weight which would be required if the voltage converter were not needed. This increase in system weight is the result of two factors. First, the voltage converter weight increases the system weight. Secondly, a larger source and more fuel is required to supply the power lost in the voltage converter due to the fact that it is not 100% efficient.

6.3.4   Discussion of Results and Conclusions

DC Output

Examination of the system curves for a 28 volt D-C output (Figures 6.3-1 through 6.3-10) leads to some significant conclusions. First, it should be noted that if possible the full load source voltage (E_{SFL}) should be selected at 28 volts. This permits output voltage control by use of the switching circuit alone and results in an overall system which is considerably lighter than any other choice. The second best choice of full load source voltage is 20 volts for an inherent source voltage regulation of 40% and 14 volts for an inherent voltage regulation of 100%. These conditions permit use of a minimum weight flyback circuit. In either case the source voltage indicated is the upper limit which can be used with the straight flyback circuit. This is due to the fact that the flyback circuit can only step up voltage, thus the open circuit voltage of source must never exceed 28 volts at any load condition when using the flyback circuit.

Except for the above mentioned items, the weight penalty tends to decrease rapidly as the source voltage increases. This, of course, demonstrates quantitatively the advantage of keeping the source voltage as high as practical. In particular, every attempt should be made to stay above a full load source voltage of 10 volts.

It will also be noted that the curves for a particular power level extend over only a finite source voltage range. Thus, in the case of 25 watts the voltage range is 1 to 40 volts while for 10 KW the range is 20 to 100 volts. As discussed in previous progress reports these voltage ranges were selected as being reasonable for fuel cell, thermoelectric, and thermionic power sources for the particular power conditions.

With the exception of the 10 KW case, the curves indicate that the weight penalty of the voltage conversion and regulation function decreases as the power output increases. Except for the switching circuit point at 28 volts, the 10 KW curve is based on voltage converter circuits employing silicon controlled rectifiers (SCR) while all other power conditions employ circuits containing power transistors. If power transistor circuits had been employed for the 10 KW condition it is highly probable that the 10 KW curve would be below 1.0 KW curve. Preliminary judgement indicated that SCR circuits might be optimum for power levels above 1.0 KW, thus power transistor circuits were not evaluated at the 10 KW level. The results of this study, however, indicate that power transistor circuits may still be the better choice at the 10 KW level. This fact is illustrated by the curves of figures 6.3-21 and 6.3-22. These curves compare the efficiency and weight characteristics of similar type SCR and power transistor circuits. The efficiency and weight points plotted on these curves are those which yield a minimum weight system when the source weight per unit of source power is 1000 lbs/KW. Figure 6.3-22 shows the efficiency and weight as function of output power level for a full load source voltage of 40 volts. Figure 6.3-21 shows efficiency and weight as a function of full load source voltage for an output power level of 1.0 KW. It will be noted that in both cases the transistor circuits are approximately 10% more efficient and considerably lighter than the SCR circuits. This then leads to the conclusion that transistor circuits are the better ones for the load range of 10 watts to 10 KW and the source voltage range of 1.0 to 100 volts being considered by this study. Unfortunately, the practical consideration of voltage rating may limit the use of transistors to a maximum reasonable voltage of 50 to 80 volts whereas the voltage capability of SCR's is now several hundred volts. In addition, the maximum current capability of present transistors is considerably less than that of SCR's. This fact tends to favor SCR's for use in large power applications.

Nevertheless, it still can be concluded that power transistor circuits are the best approach for the general load and voltage range of this study. Thus, it is evident that the SCR data presented in the system curves of 6.3-1 through 6.3-20 do not yield the minimum weight system.

It is believed that the transistor circuitry data does represent the best available within the state of the art and the performance requirements specified. More efficient, lighter weight systems are possible providing the performance requirements are relaxed. In particular, for example, limiting the load variation to something considerably less than full load to no load could result in a considerable system weight reduction.

AC Output

The AC output systems do not exhibit any particular preferred source voltages as did the DC systems. This is due to the fact that an inversion function is always required to obtain a AC output whereas in the case of DC output only a voltage regulation is required under certain conditions. In all other aspects, however, the comments pertaining to the DC output systems also apply to the AC output systems.

It will be noted that in the case of the 25 watt power level, the system weight is higher at a source voltage of 20 volts than at a voltage of 6 volts. This is the result of a choice of two different types of circuits in evaluating these conditions. The six volt condition assumes a stepped wave inverter; whereas, a square wave type of inverter was considered at the 20 volt point. It is highly probable that if a stepped wave inverter had been considered at the 20 volt point, the resultant system would have been lighter than that shown and would have fallen on a continuation of the curve through the 6 volt point.

Figure 6.3-1: Overall System Weight Characteristics

Output = 28 VDC $\quad \dfrac{W_0}{P_s} = 50$ lbs/KW $\quad$ B = 40%

Figure 6.3-2: Overall System Weight Characteristics
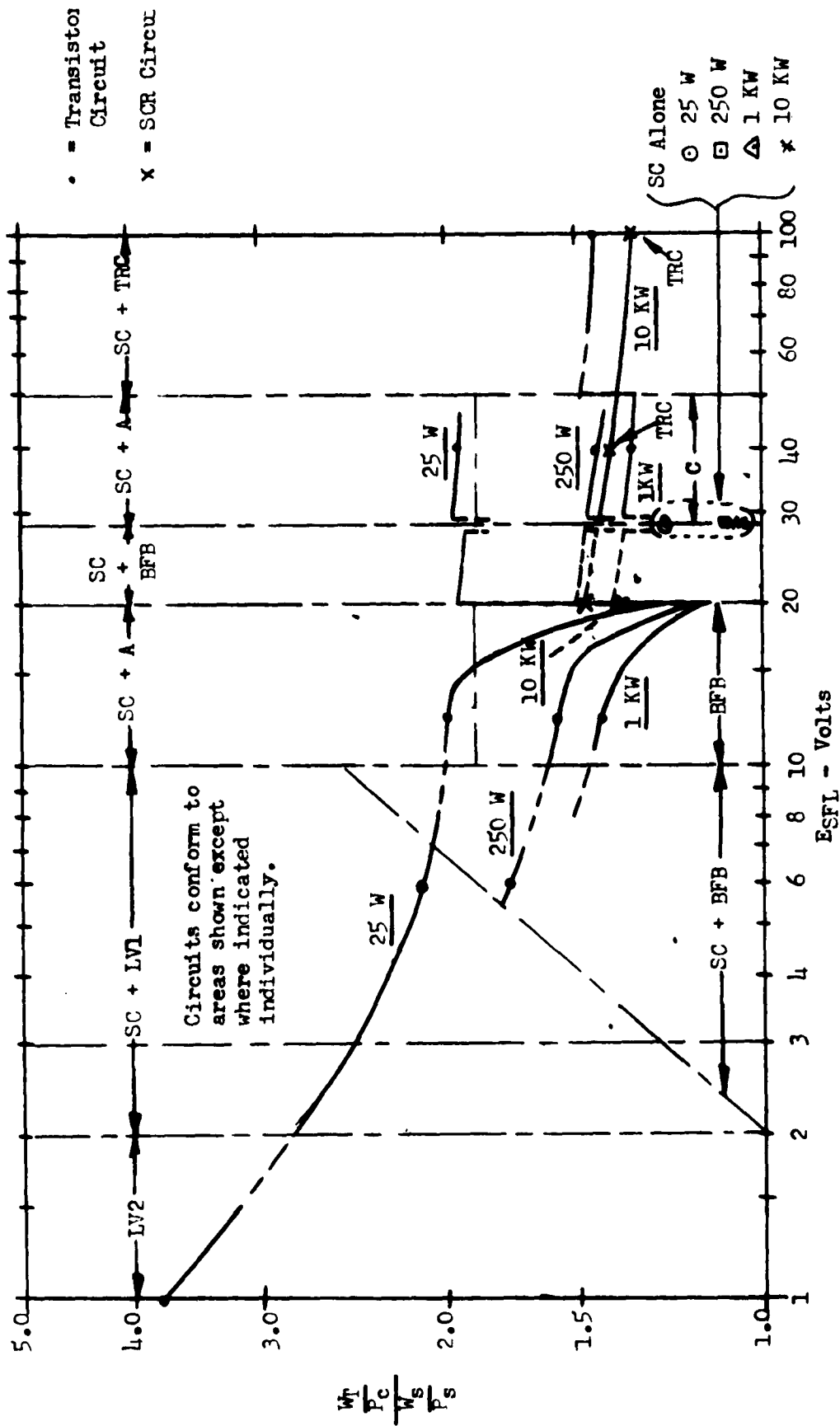
Figure 6.3-3: Overall System Weight Characteristics

Output = 28 VDC $\frac{W_s}{P_s}$ = 100 lbs/KW   B = 40%
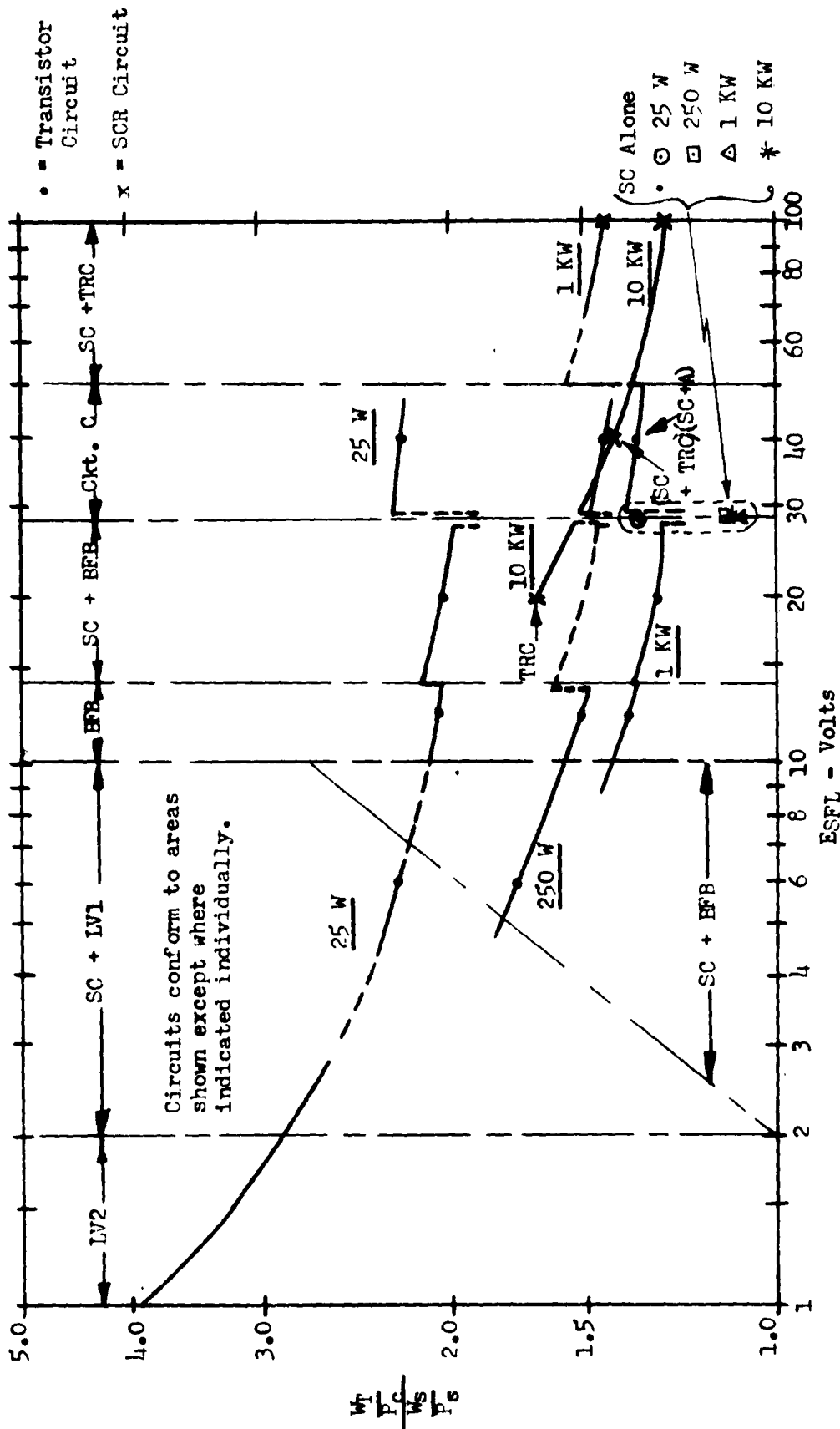
Figure 6.3-4: Overall System Weight Characteristics

Output = 28 VDC $\frac{W_s}{P_s} = 100$ lbs/KW B = 100%
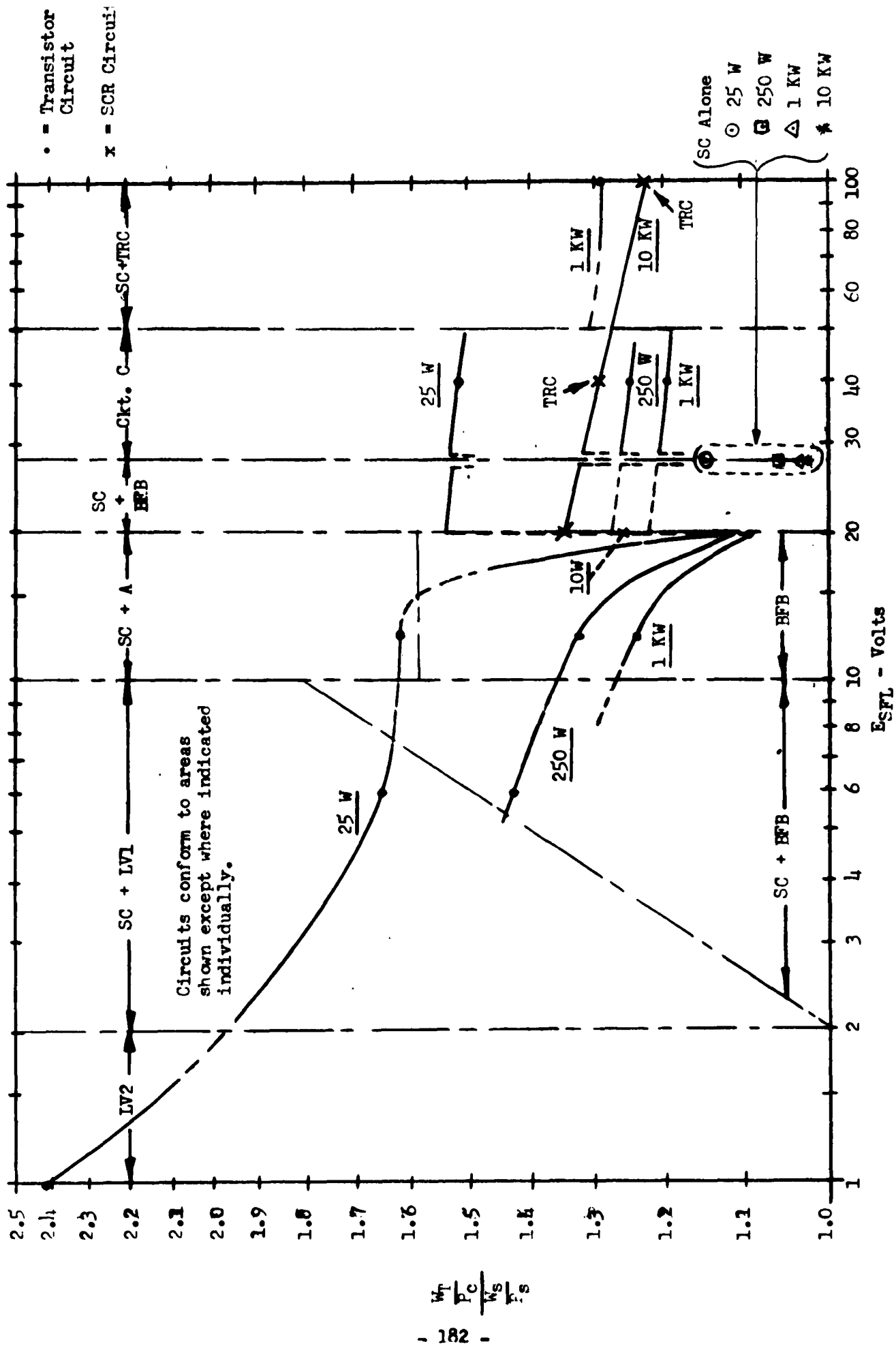
Figure 6.3-5: Overall System Weight Characteristics

Output = 28 VDC $\frac{W_s}{P_s}$ = 250 lbs/KW   B = 40%
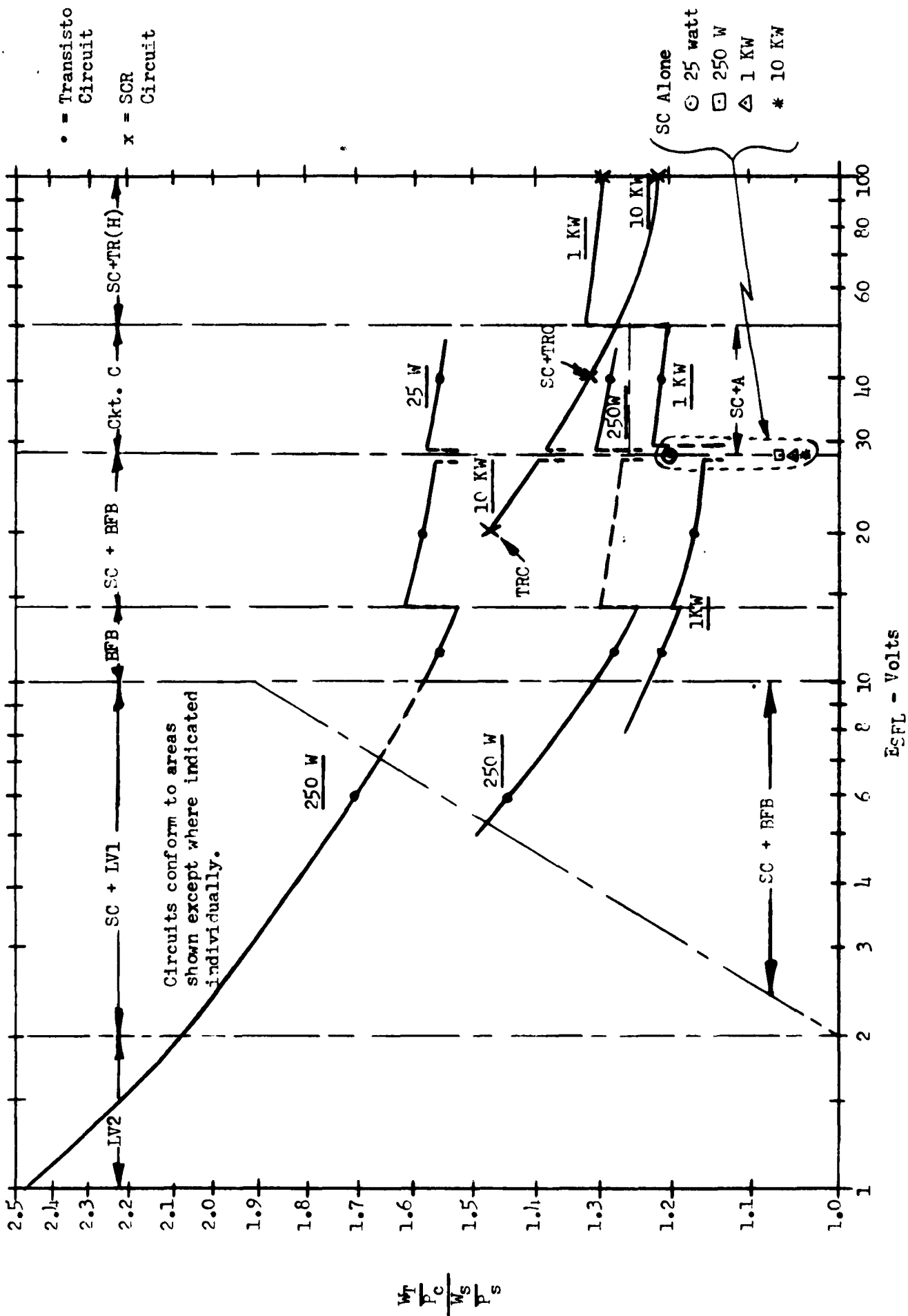
Figure 6.3-6: Overall System Weight Characteristics

Output = 28 VDC $\frac{W_S}{P_S}$ = 250 lbs/KW   R = 100%

Figure 6.3-7: Overall System Weight Characteristics

Output = 28 VDC $\frac{W_s}{P_s}$ = 500 lbs/KW   B = 40%
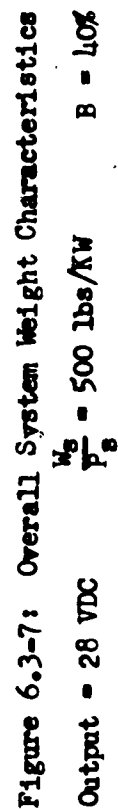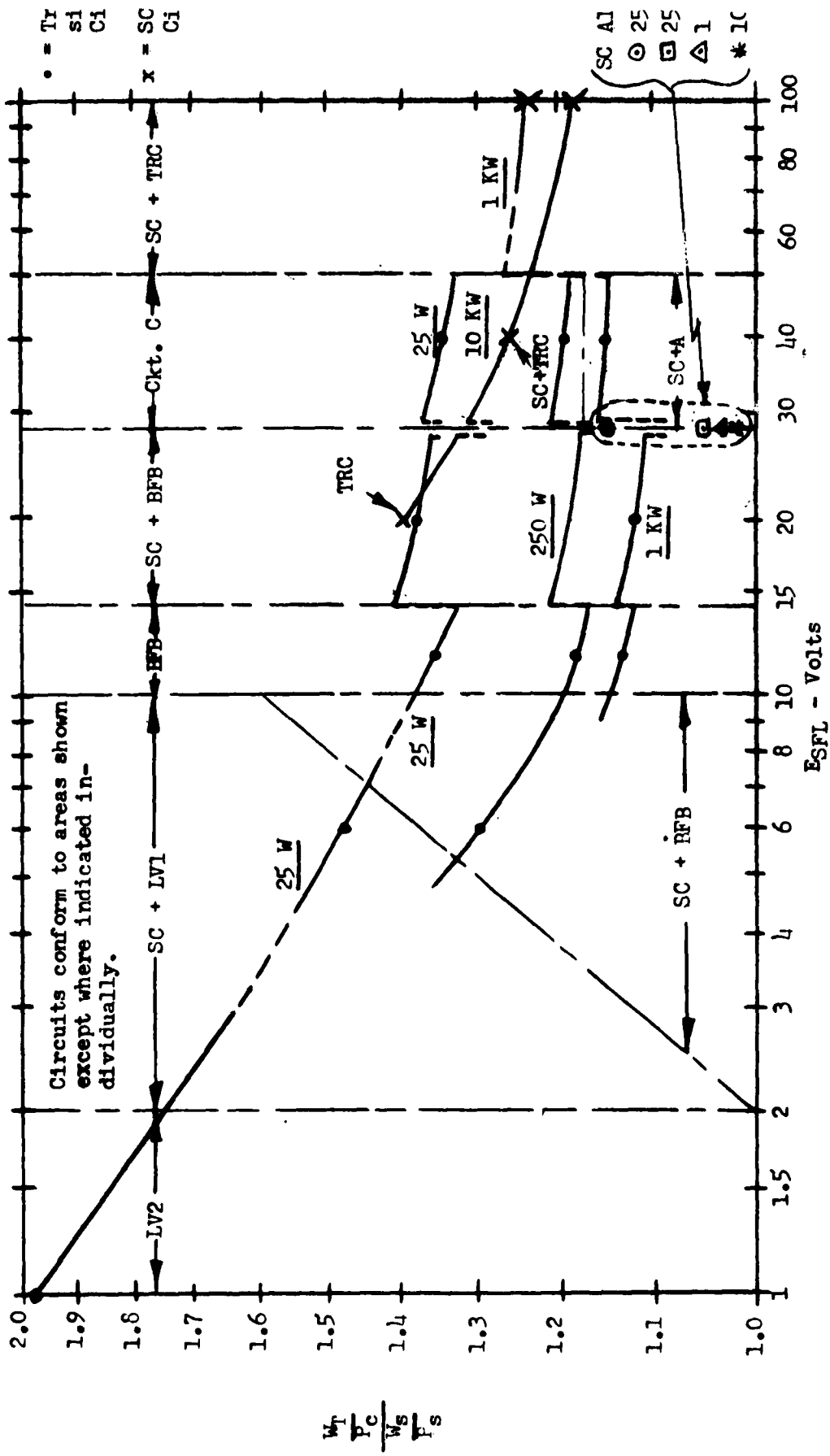
Figure 6.3-8: Overall System Weight Characteristics

Output = 28 VDC $\frac{W_s}{P_s}$ = 500 lbs/KW   B = 100%

Figure 6.3-9: Overall System Weight Characteristics

Output = 28 VDC $\frac{W_s}{P_s}$ = 1,000 lbs/KW B = 40%

Figure 6.3-10: Overall System Weight Characteristics

Output = 28 VDC $\quad \dfrac{W_s}{P_s} = 1,000$ lbs/KW $\quad B = 100\%$

Figure 6.3-11: Overall System Weight Characteristics

Output = 400 CPS, AC $\dfrac{W_S}{P_R}$ = 50 lbs/KW   B = 40%

Figure 6.3-12: Overall System Weight Characteristics

Output = 400 CPS, AC $\frac{W_s}{P_s} = 50$ lbs/KW   B = 100%
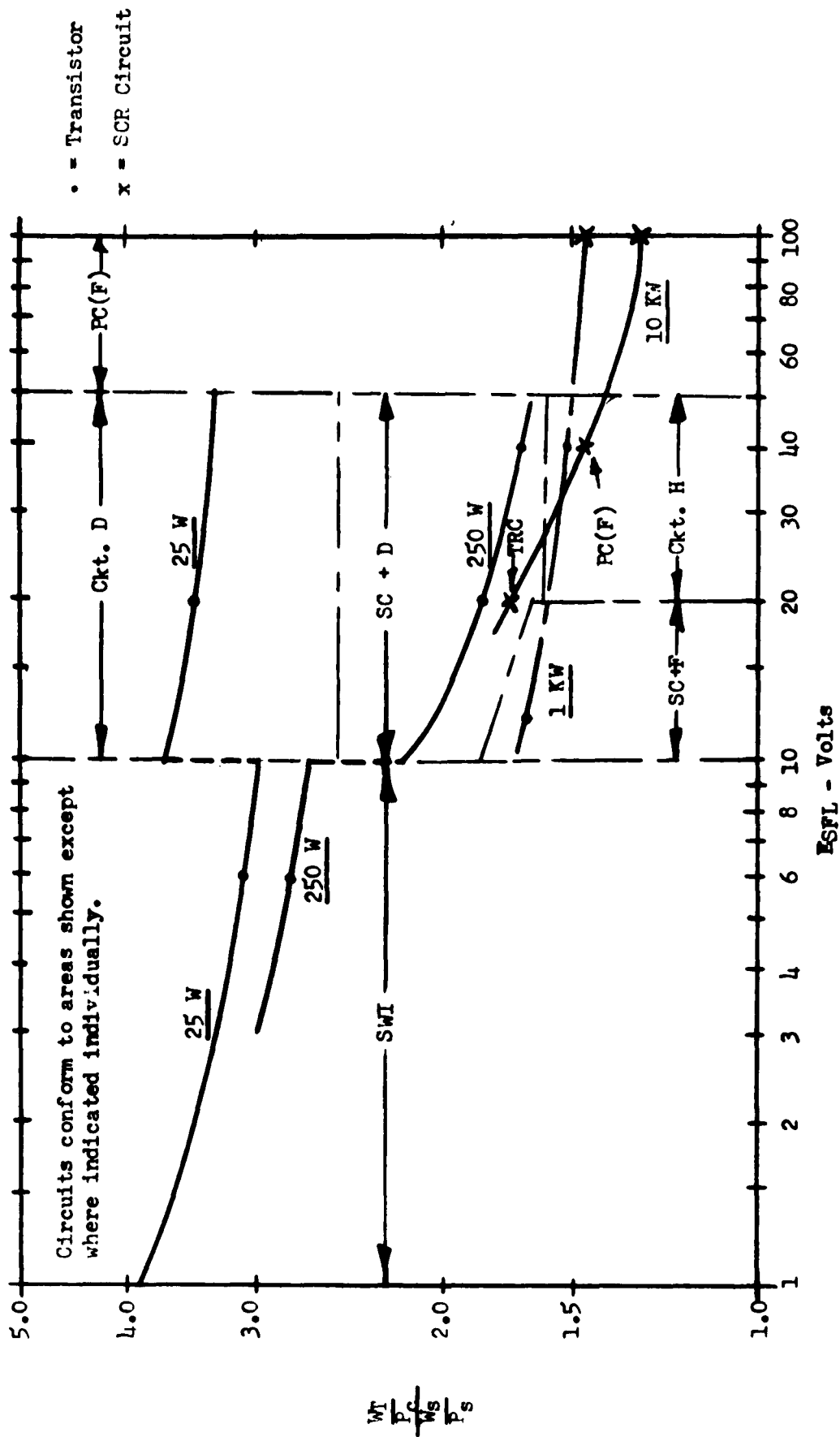
Figure 6.3-13: Overall System Weight Characteristics

Output = 400 CPS, AC $\qquad \dfrac{W_s}{P_s}$ = 100 lbs/Kw $\qquad$ B = 40%
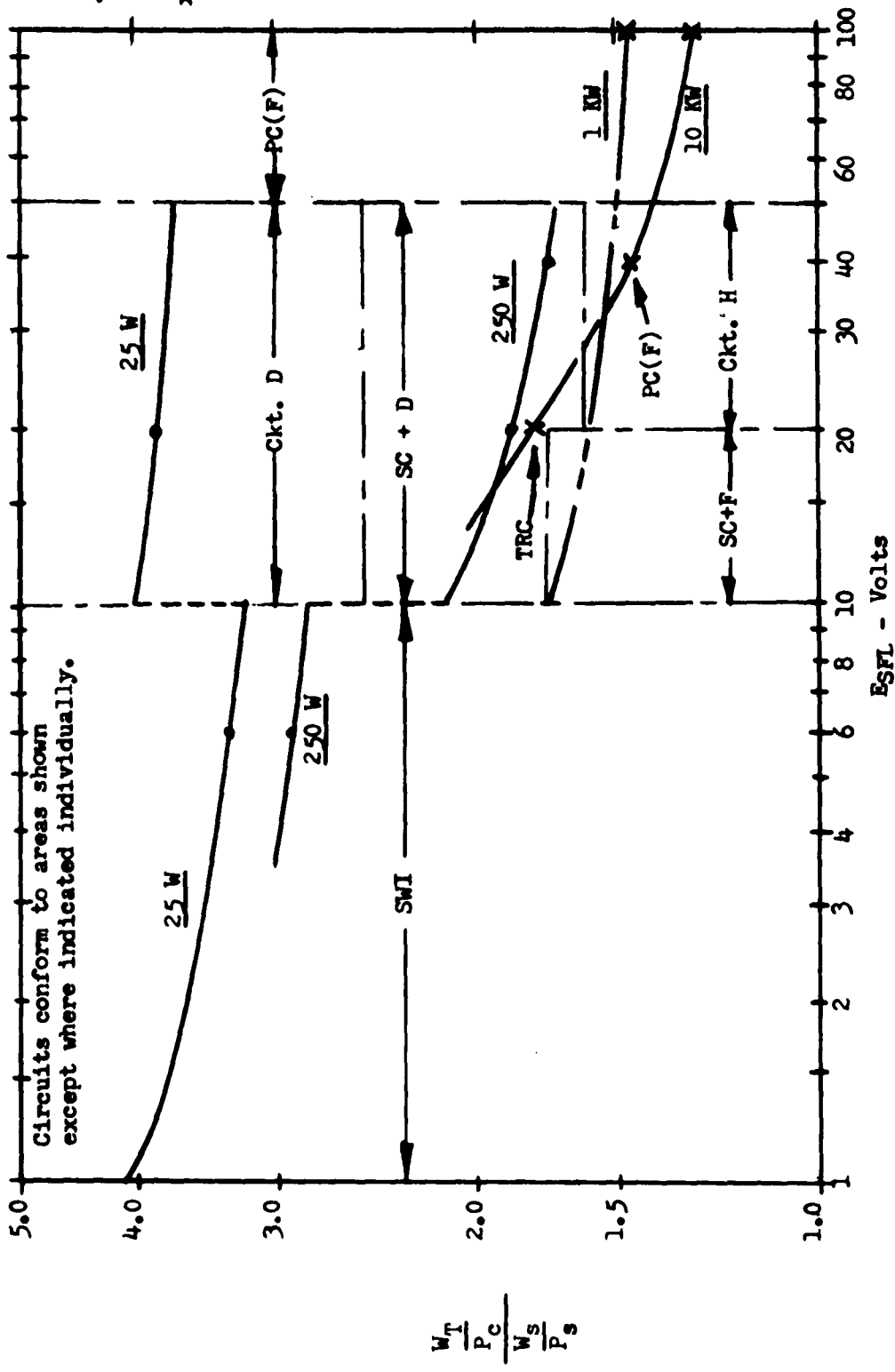
Figure 6.3-14: Overall System Weight Characteristics

Output = 400 CPS, AC $\frac{W_s}{P_s}$ = 100 lbs/KW   B = 100%
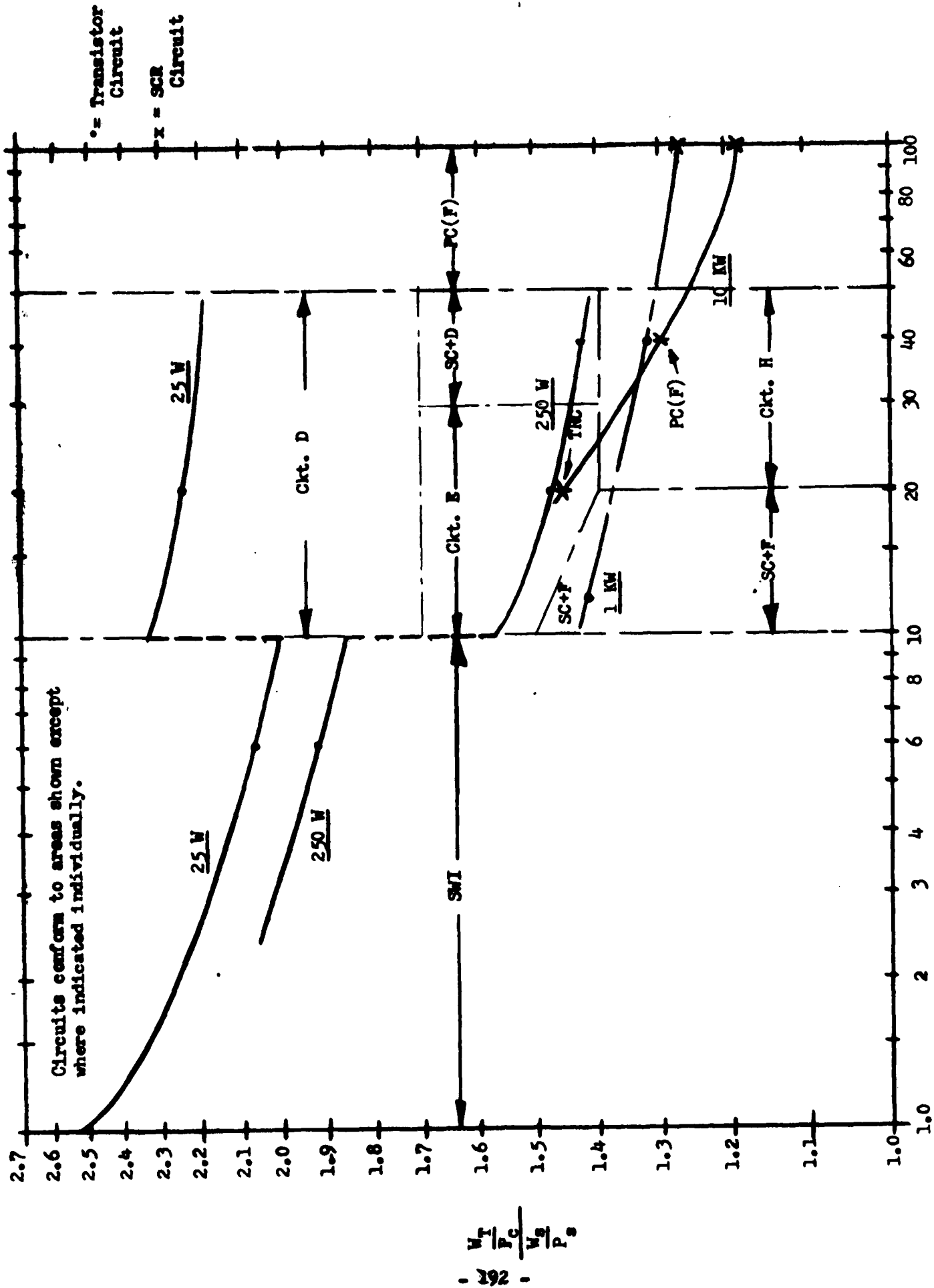
Figure 6.3-15: Overall System Weight Characteristics
Output = 400 CPS, AC W_S = 250 lbs/KW   B = 40%
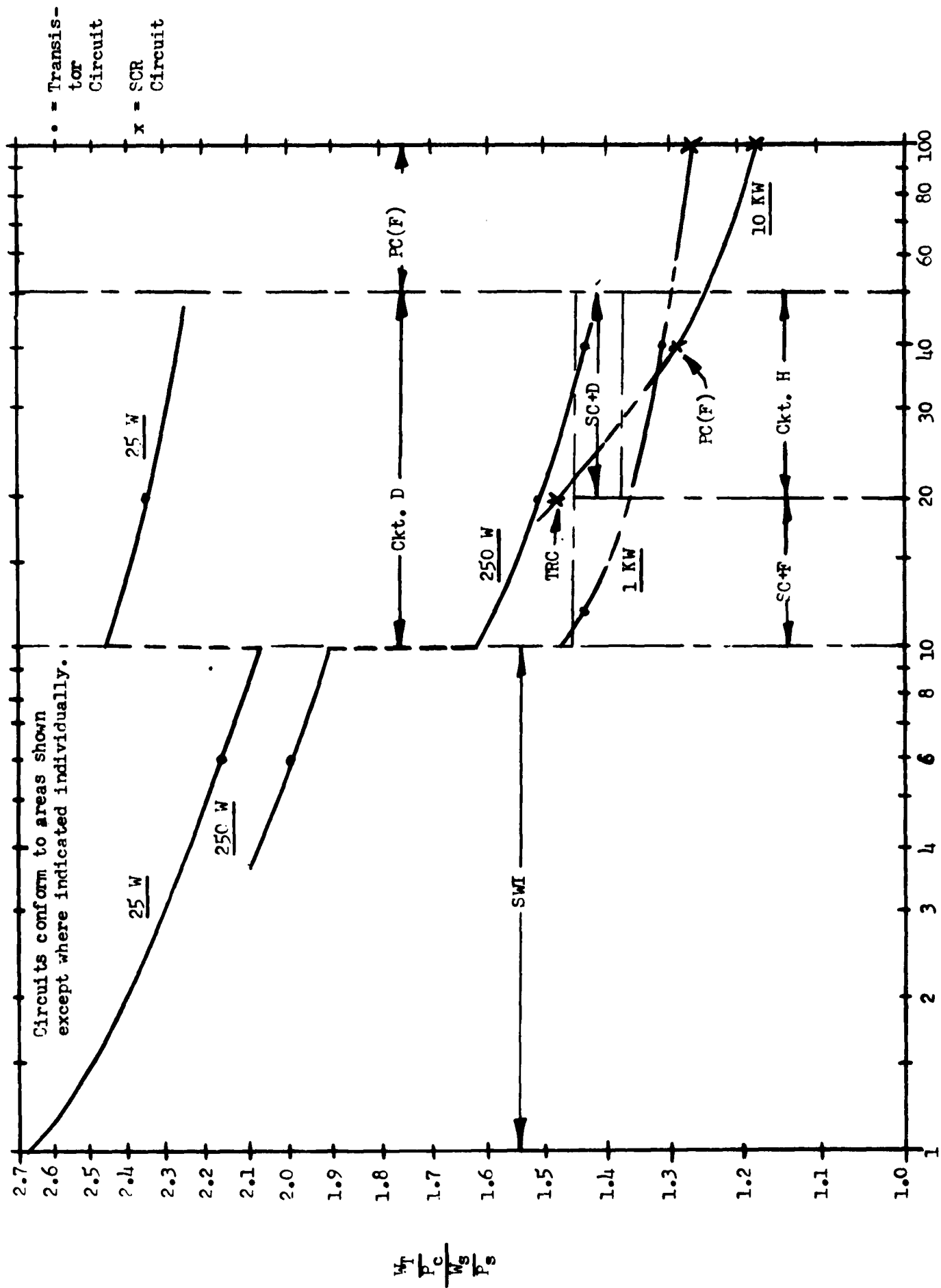
Figure 6.3-16: Overall System Weight Characteristics   Output = 400 CFS, AC $\frac{W_S}{P_S}$ = 250 lbs/KW   B = 100%
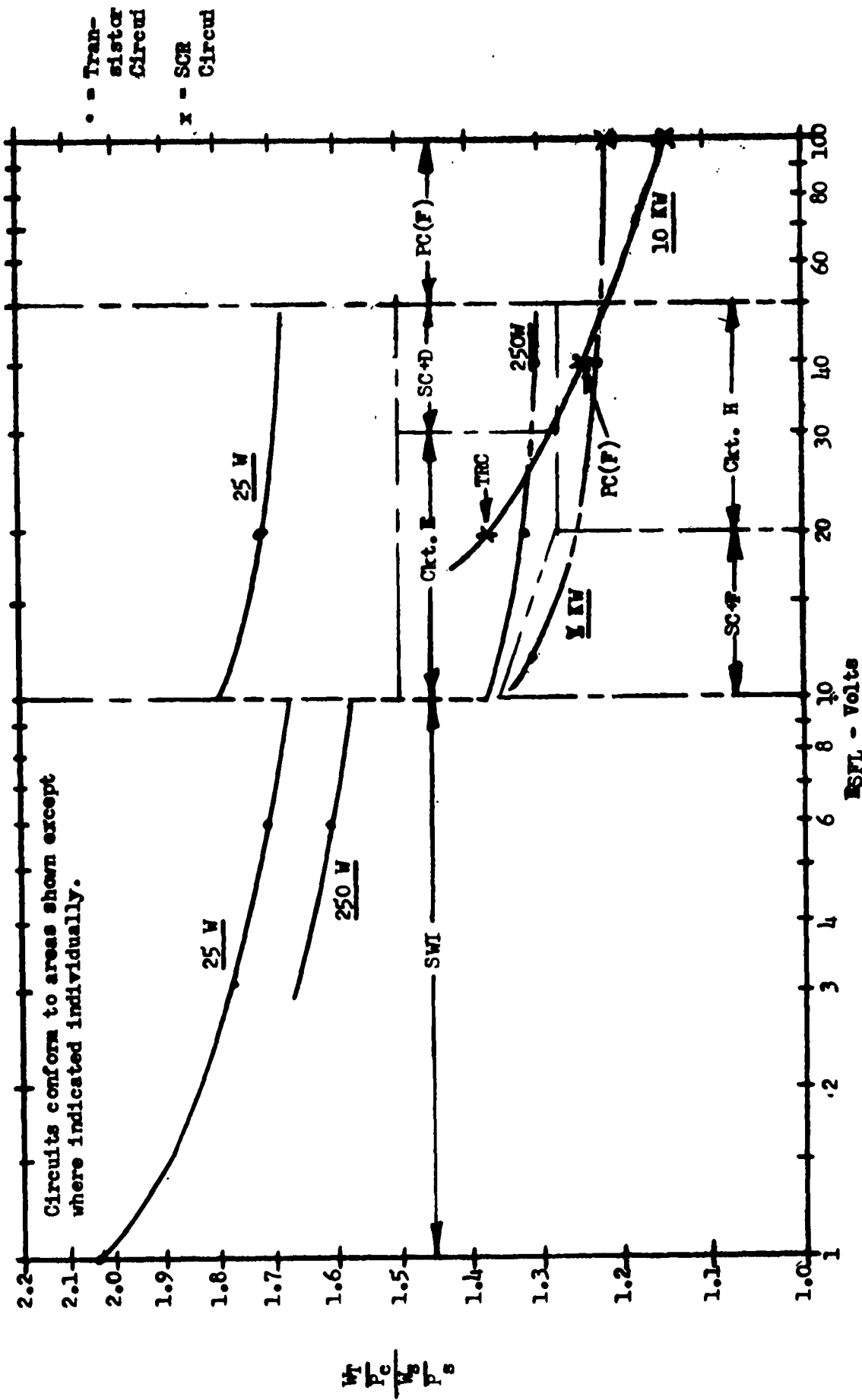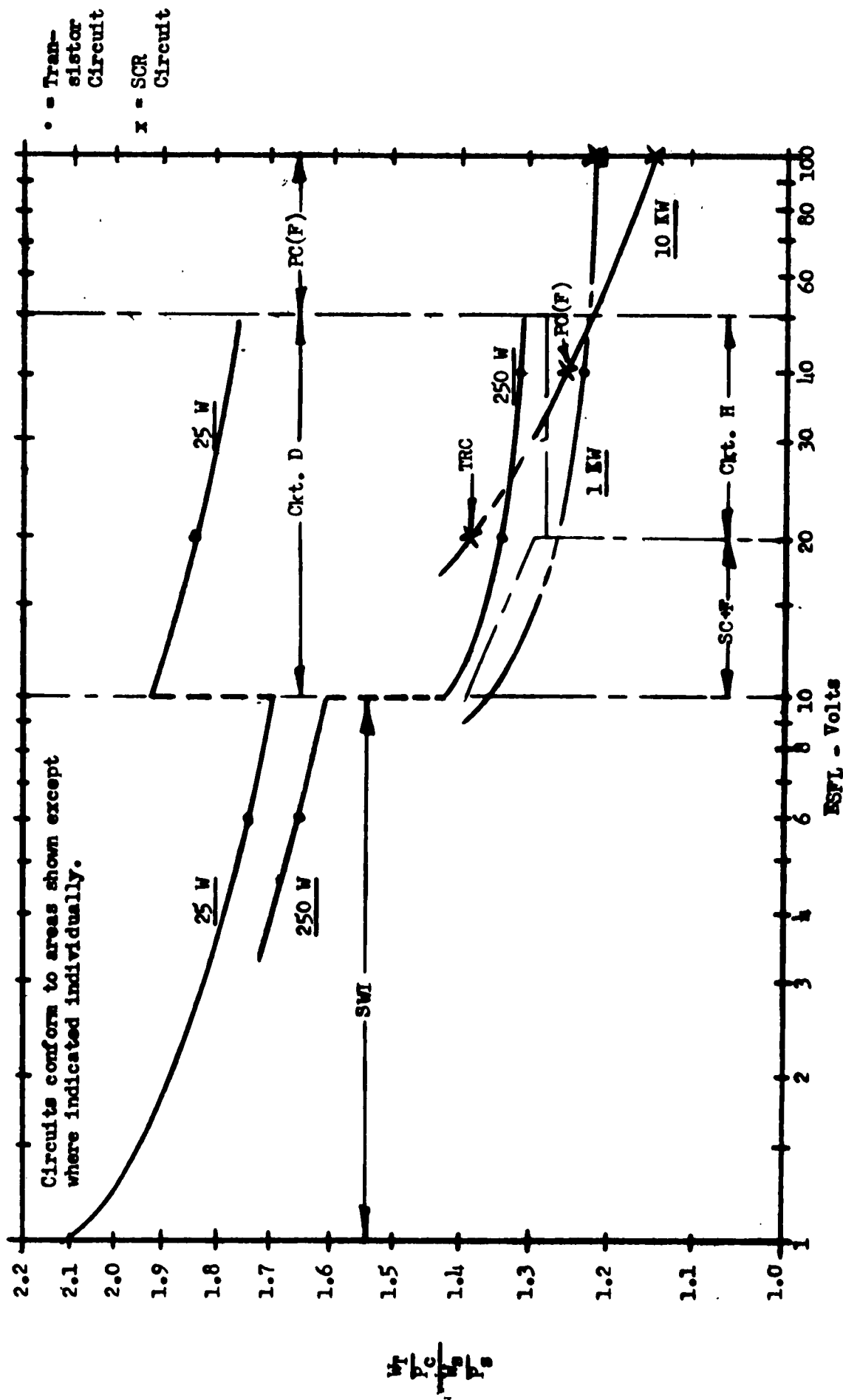
Figure 6.3-17: Overall System Weight Characteristics

Output = 400 CPS, AC $\frac{W_t}{P_c}$ = 500 lbs/Kw   B = 40%

Circuits conform to areas shown except where indicated individually.

• = Transistor Circuit

x = SCR Circuit

25 W

250 W

25 W

250 W

1 KW

10 KW

Ckt. D

Ckt. H

PC(F)

PC(F)

TRC

SWI

SC-F

$\frac{W_S}{P_C} + \frac{W_C}{P_C} + \frac{W_t}{P_t}$

ESPL - Volts

2.2 2.1 2.0 1.9 1.8 1.7 1.6 1.5 1.4 1.3 1.2 1.1 1.0

1 2 3 4 6 8 10 20 30 40 60 80 100

Figure 6.3-18: Overall System Weight Characteristics

Output = 400 CPS, AC $\frac{W_S}{P_S}$ = 500 lbs/KW   B = 100%

Figure 6.3-19: Overall System Weight Characteristics

Output = 400 CPS, AC $\frac{W_s}{P_s}$ = 1,000 lbs/KW   B = 40%
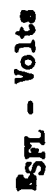
Figure 6.3-20: Overall System Weight Characteristics

Output = 400 CPS, AC $\frac{W_s}{P_s}$ = 1,000 lbs/KW   B = 100%
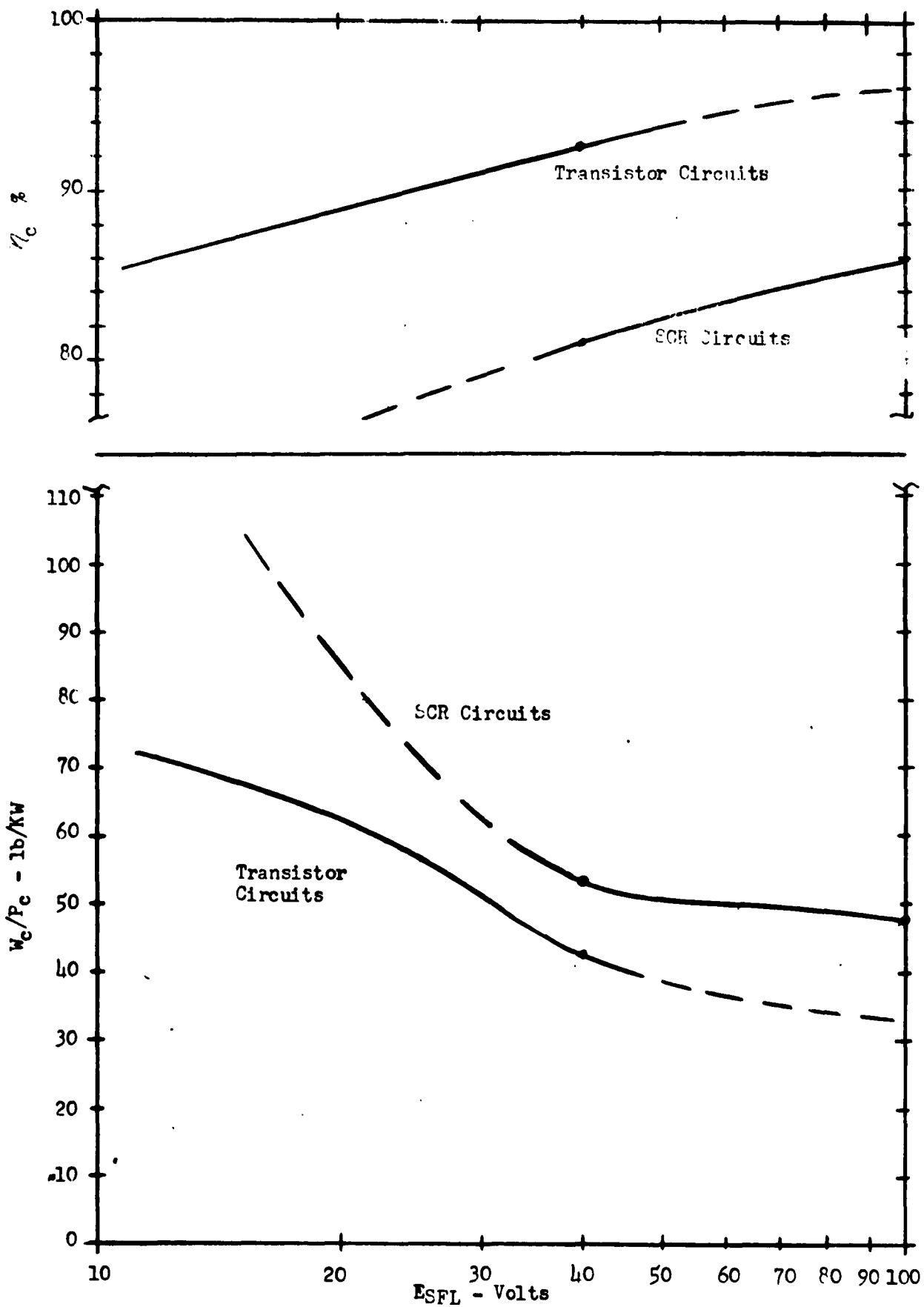
Figure 6.3-21: Comparison of Efficiency and Weight of Similar Transistor and Silicon Controlled Rectifier Circuits as a Function of Source Voltage for a Power Level of 1 KW Based on a Minimum Weight System Where $W_s/P_s = 1000$ lbs/KW
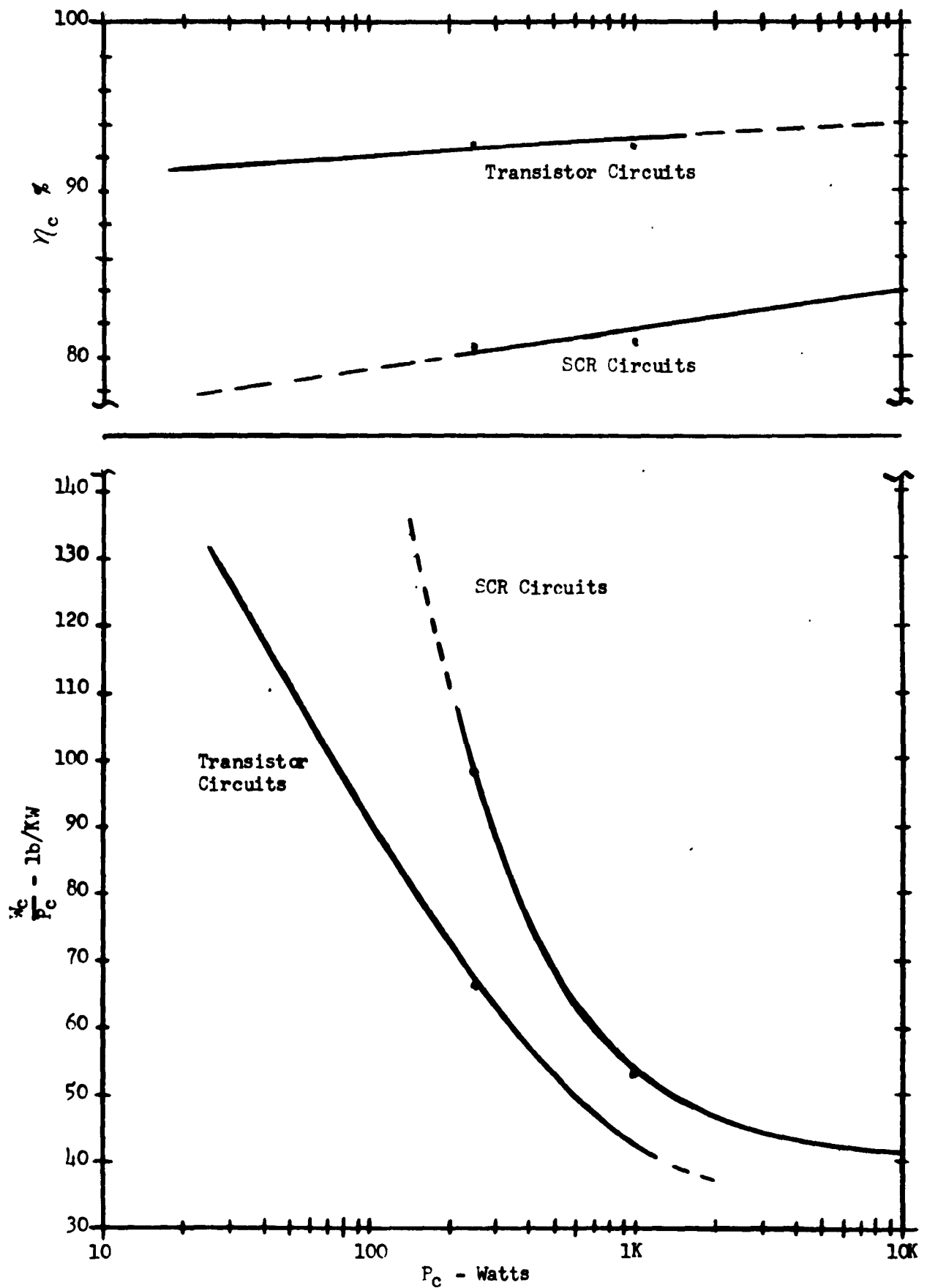
Figure 6.3-22: Comparison of Efficiency and Weight of Similar Transistor and Silicon Controlled Rectifier Circuits as a Function of Power Level for a Source Voltage of 40 Volts, B = 100%, Based on a Minimum Weight System Where W_s/P_s = 1000 lbs/KW

6.4   Laboratory System

6.4.1   Introduction

During the past report period a laboratory model system consisting of fuel cell power source and a DC-DC voltage converter was completed and tested. The purpose of this laboratory model system was to demonstrate the optimum principles of voltage conversion and regulation as arrived at in this study.

The laboratory model system is described in detail in the following paragraphs and its performance characteristics as determined by test are presented.

6.4.2   System Description

A photograph of the laboratory model system is shown in Figure 6.4-1. The power source is a 16 cell hydrogen-air ion exchange membrane fuel cell. It has a rated output power of 60 watts at an output voltage of 12 volts. Its no load voltage is approximately 16 volts giving it an inherent voltage regulation of about 33%.

The DC-DC voltage converter and regulator uses a modified Morgan circuit. The complete circuit diagram is shown in Figure 6.4-2. In this case the power portion of the circuit is shown by the heavy lines. The voltage converter has a rated output of 50 watts at 28 volts DC and is designed to operate with an input voltage of 10 to 20 volts. The circuit operates at a fixed frequency of 800 cps and achieves output voltage control by varying the "on" time during any given cycle.

The results of the study as indicated in previous sections indicate that the modified Morgan circuit is not the optimum circuit, but rather the flyback circuit is lighter and more efficient. Unfortunately, selection of the laboratory model circuit had to be made before the study was complete. At the time of the selection, the modified Morgan circuit appeared to be the best. It was not until later in the study that the flyback circuit was uncovered. However, even though the modified Morgan circuit is not optimum, it still demonstrates the capability of achieving the performance results predicted during the analytical study. Thus, it helps to establish the validity of the assumptions made during the study.

6.4.3   System Performance Results

Power Source Characteristics

The fuel cell characteristics are shown in Figure 6.4-3. Both the volt-ampere and source output power curves are presented.

Voltage Regulation Characteristics

Figure 6.4-4 shows the fuel cell output voltage and the voltage converter output voltage as a function of system output power. It will be noted that the voltage converter output voltage is well within the voltage limits of 28 + 1 volts for an output power range of 2 watts to 56 watts. In the same range the fuel cell output voltage varied between 15.5 and 11.0 volts. These curves demonstrate the very adequate job of voltage regulation and conversion achieved by the laboratory model system.

Efficiency

Figure 6.4-5 shows the voltage converter efficiency as a function of output power. The efficiency hits a peak of approximately 82.5% at 35 watts and has an efficiency above 80% for the output power range of 17 to 52 watts. The efficiency achieved is close to the predicted value of 83% for this circuit. These results help substantiate the validity of design assumptions used throughout the study.

Figure 6.4-6 shows the overall thermal efficiency of the fuel cell plus voltage converter as a function of the output power of the system. This shows that the overall thermal effic. cy is well above 40% throughout most of the power range.

Transient Response

Figure 6.4-7 and 6.4-8 show the transient response characteristics of a fuel cell voltage and current, and converter output voltage for a step application and removal of load between 6 watts and 50 watts. It will be noted that the voltage converter output voltage remains essentially constant on the basis of the time scale of these traces. However, the transient response of the fuel cell voltage and current is slow taking approximately 50 seconds to settle out at a new condition.

Figure 6.4-9 shows the actual output voltage transient response on expanded time scale for step load application and removal. It will be noted that the output voltage transient settles out in approximately .06 seconds.

Voltage Ripple

Figure 6.4-10 shows the converter output voltage ripple for a 50 watt output load. The magnitude of this ripple is approximately 0.2 volt. It is nearly sinusoidal with a fundamental frequency of approximately 800 cps.

Figure 6.4-11 shows the voltage and current ripple at the fuel cell output for a 50 watt output system load. This ripple is a distorted square wave with a voltage ripple being of a magnitude of approximately 0.12 volt and the current ripple being of a magnitude of approximately 0.8 amps. Again, the frequency is approximately 800 cps. The ratio of the voltage ripple magnitude to the current ripple magnitude is an indication of the A-C output impedance of the fuel cell at 800 cps. This checks closely to what is predicted for the AC impedance of this fuel cell stack based on the fuel cell dynamic impedance information presented in Progress Report No. 4

Figure 6.4-1

203
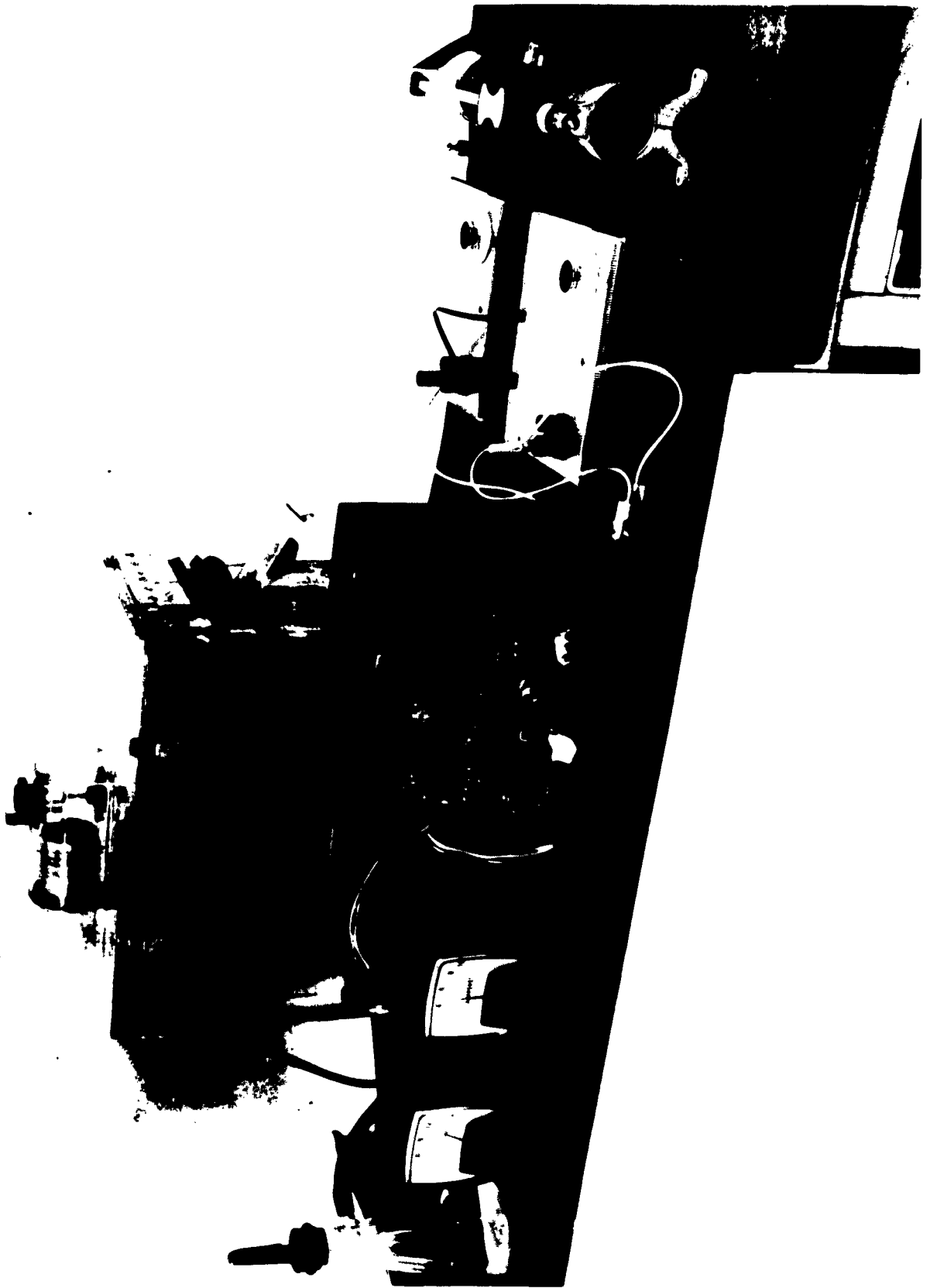
PARTS LIST

50 WATT CONVERTER

Q1	2N1522		D1	1N92	
Q2	2N491		D2	4JA3011BH1AC1 (GE)	
Q3	2N525		D3	" "	
Q4	2N1304		D4	1N93	
Q5	2N244		D5	1N540	

DZ1	1N957		L	110mH	
DZ2	1N430				

SR1	Core No. 51002-10		T1	Core No. 51001-10
	N1 14 turns			N6 36 turns
	N2 100 turns			N7 12 turns
	N3 100 turns			N8 4 turns
	N4 100 turns			N9 240 turns
	N5 500 turns			

R1	510	1/2W	R9	500	2 1/2W	C1	0.25 mfd	200 WVDC
R2	856	1/2W	R10	270	2 W	C2	750 mfd	30 WVDC
R3	18	2 W	R11	10K	1 W	C3	37,000 mfd	25 WVDC
R4	120	1/2W	R12	100	1 W	C4	50 mfd	50 WVDC
R5	560	1/2W	R13	1.3K	1/2 W	C5	.068 mfd	600 WVDC
R6	360	1/2W	R14	10	2 W	C6	.22 mfd	200 WVDC
R7	5K	1/2W	R15	100K	1 W			
R8	1.2K	2 W	R16	47	1/2 W			
			R17	220	1/2 W			

Figure 6.4-1a
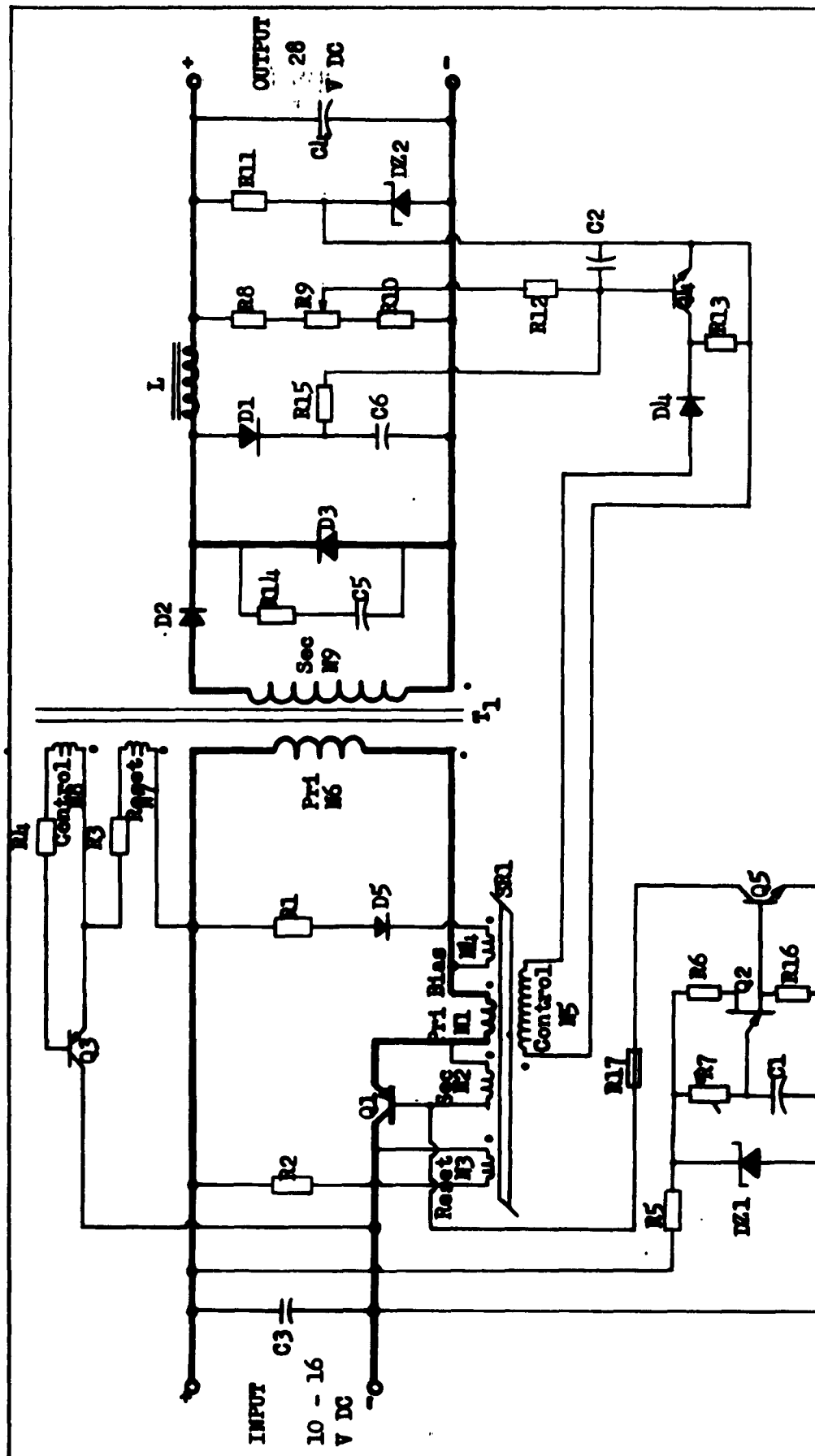
Figure 6.4.2: Fifty Watt DC-DC
Voltage Converter Circuit Diagram

Figure ... Laboratory Model Fuel Cell
Voltage, Power, and Current Characteristics
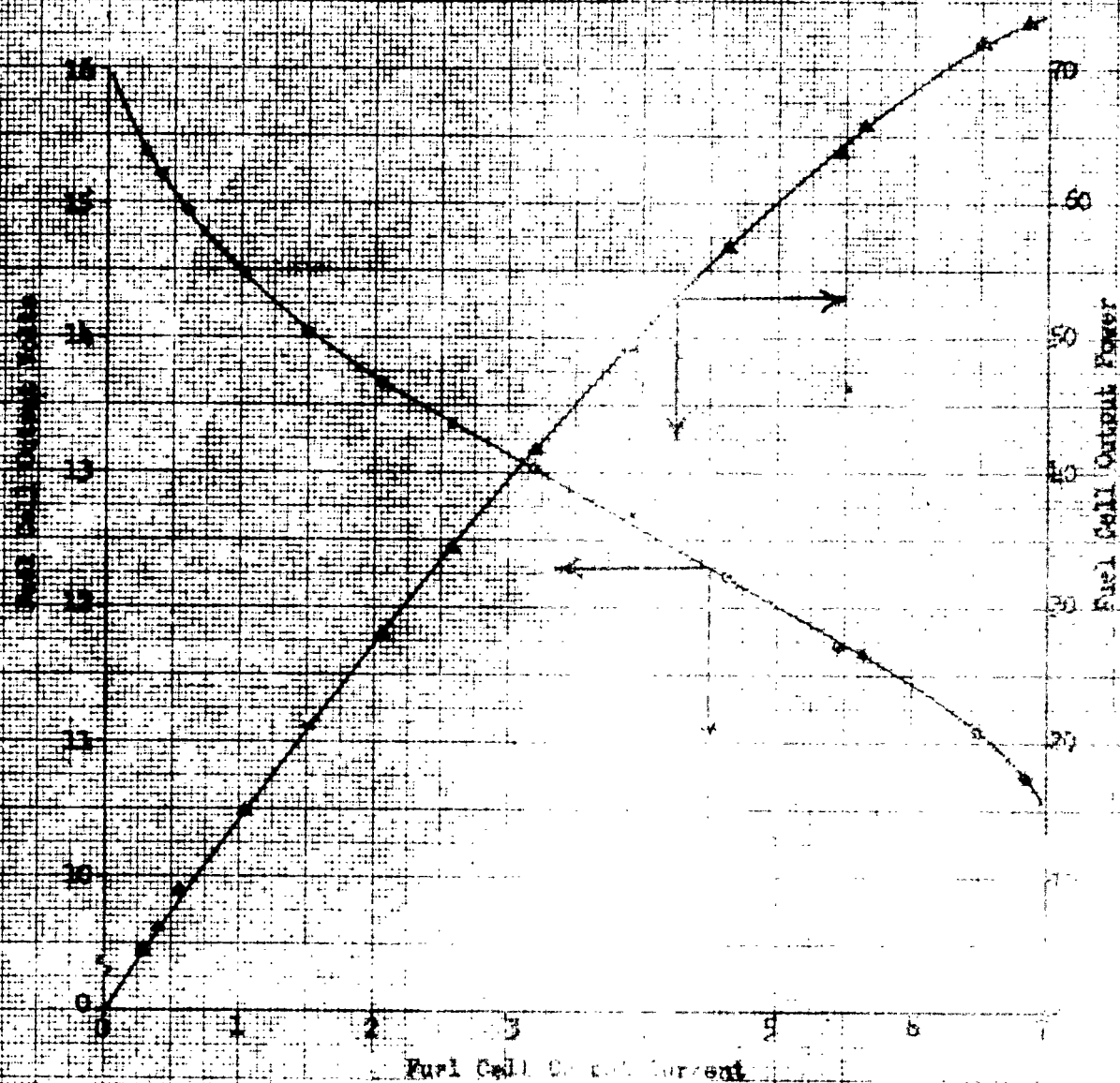
Figure 6.5-4: Fuel Cell and Converter Output Voltage as a Function of Converter Output Power
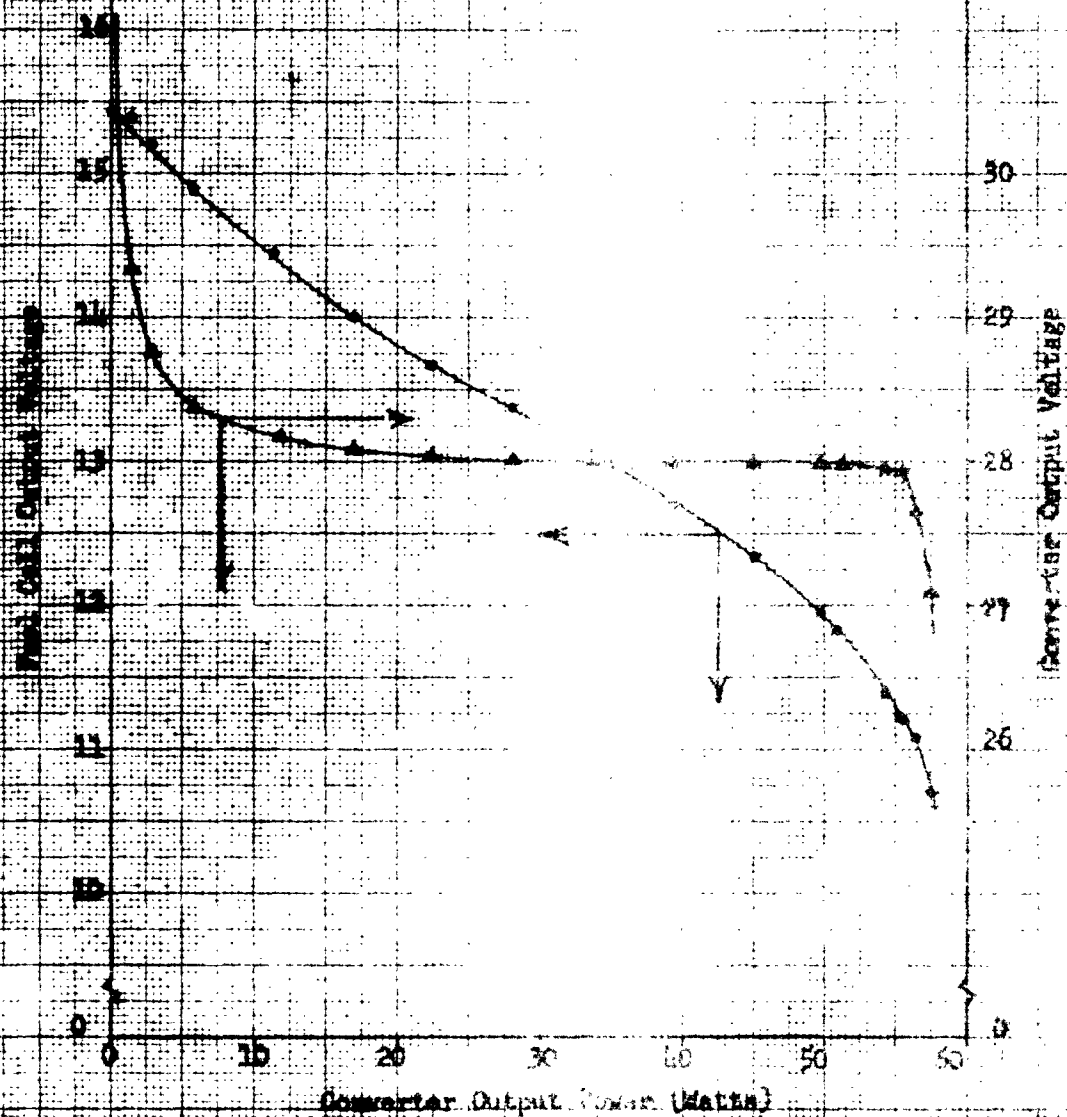
Figure 6.5-5: Voltage Converter Efficiency
as a Function of Output Power
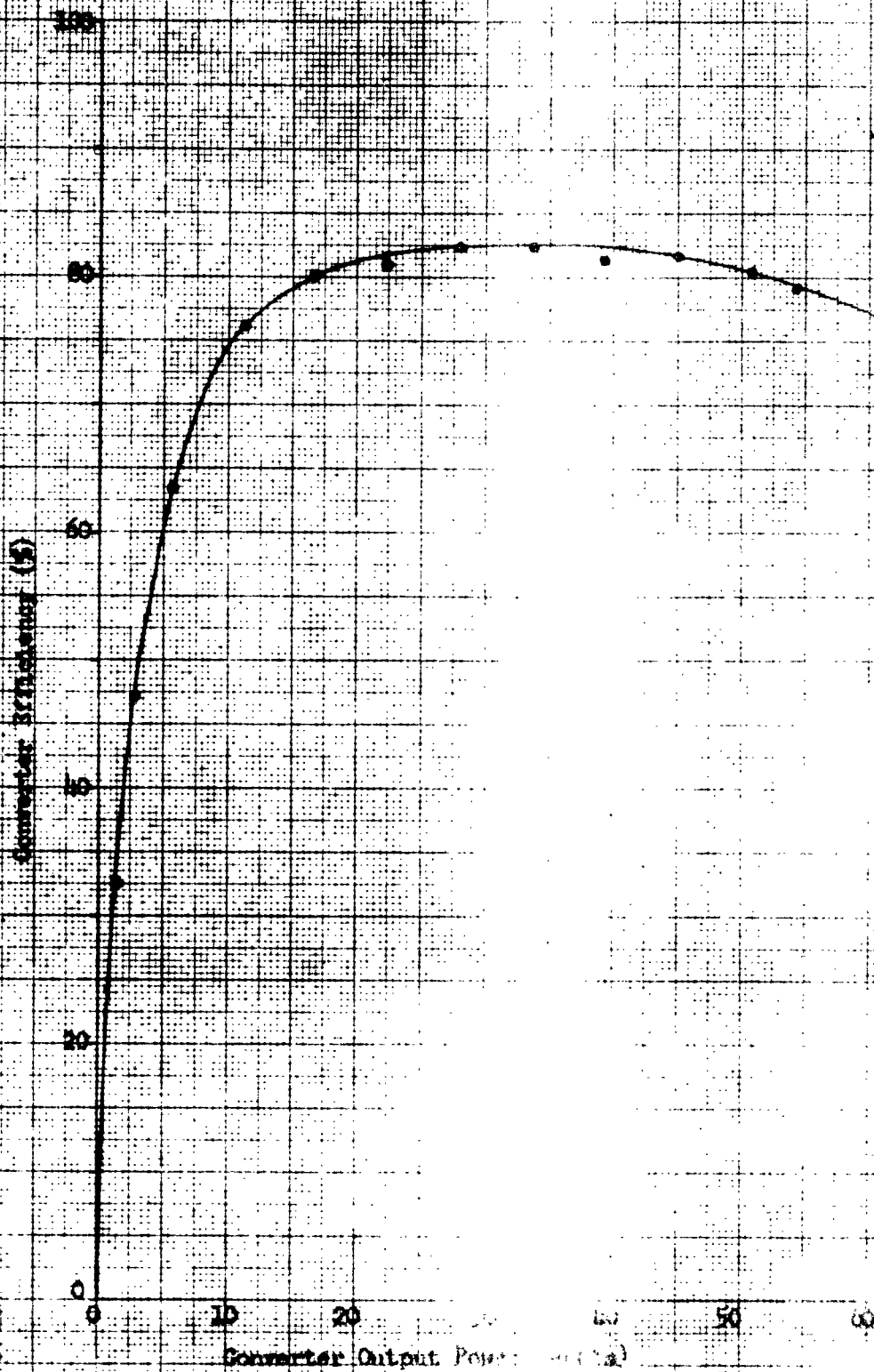
Figure 6.4-6: Overall Laboratory System Thermal Efficiency as a Function of System Output Power
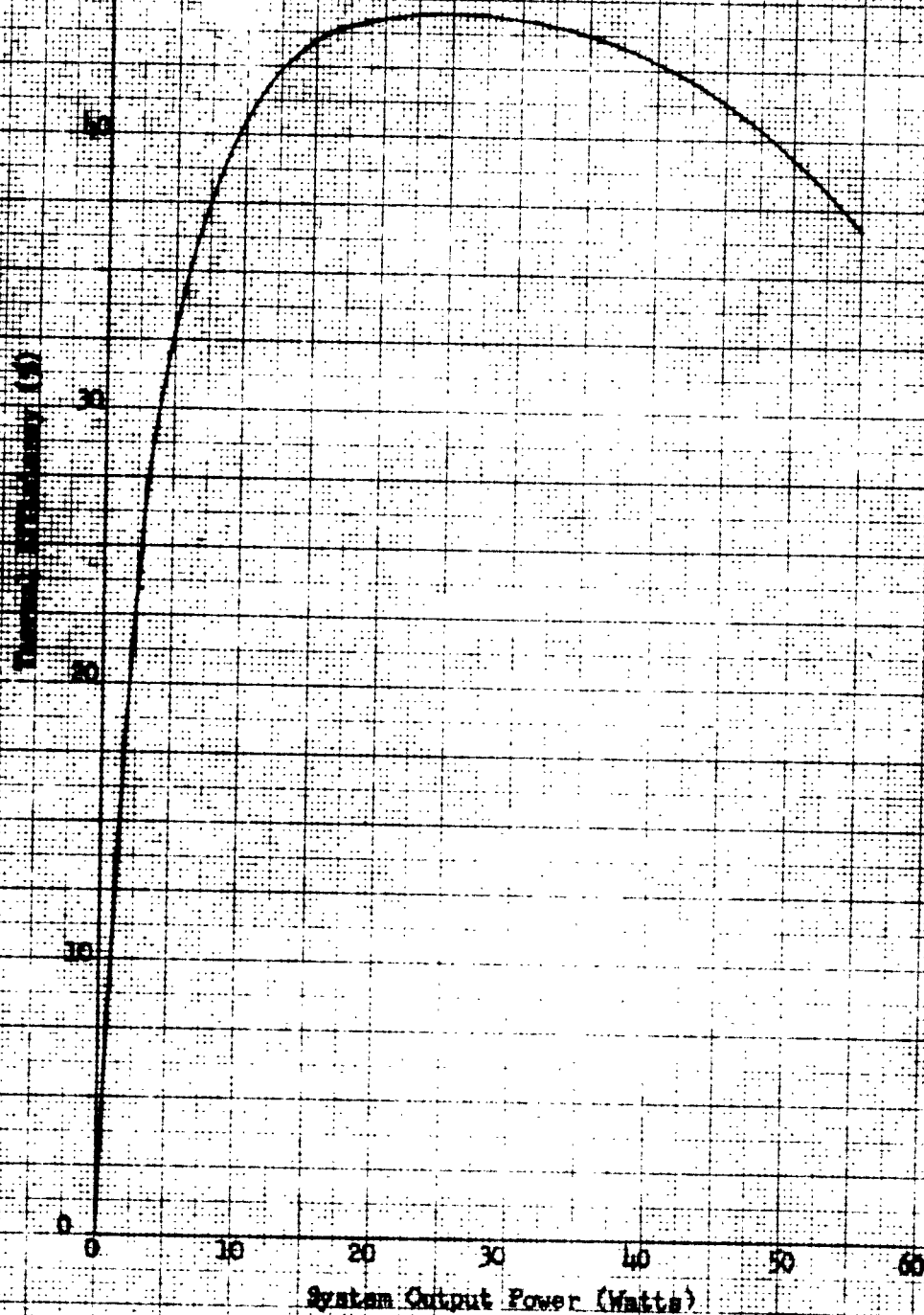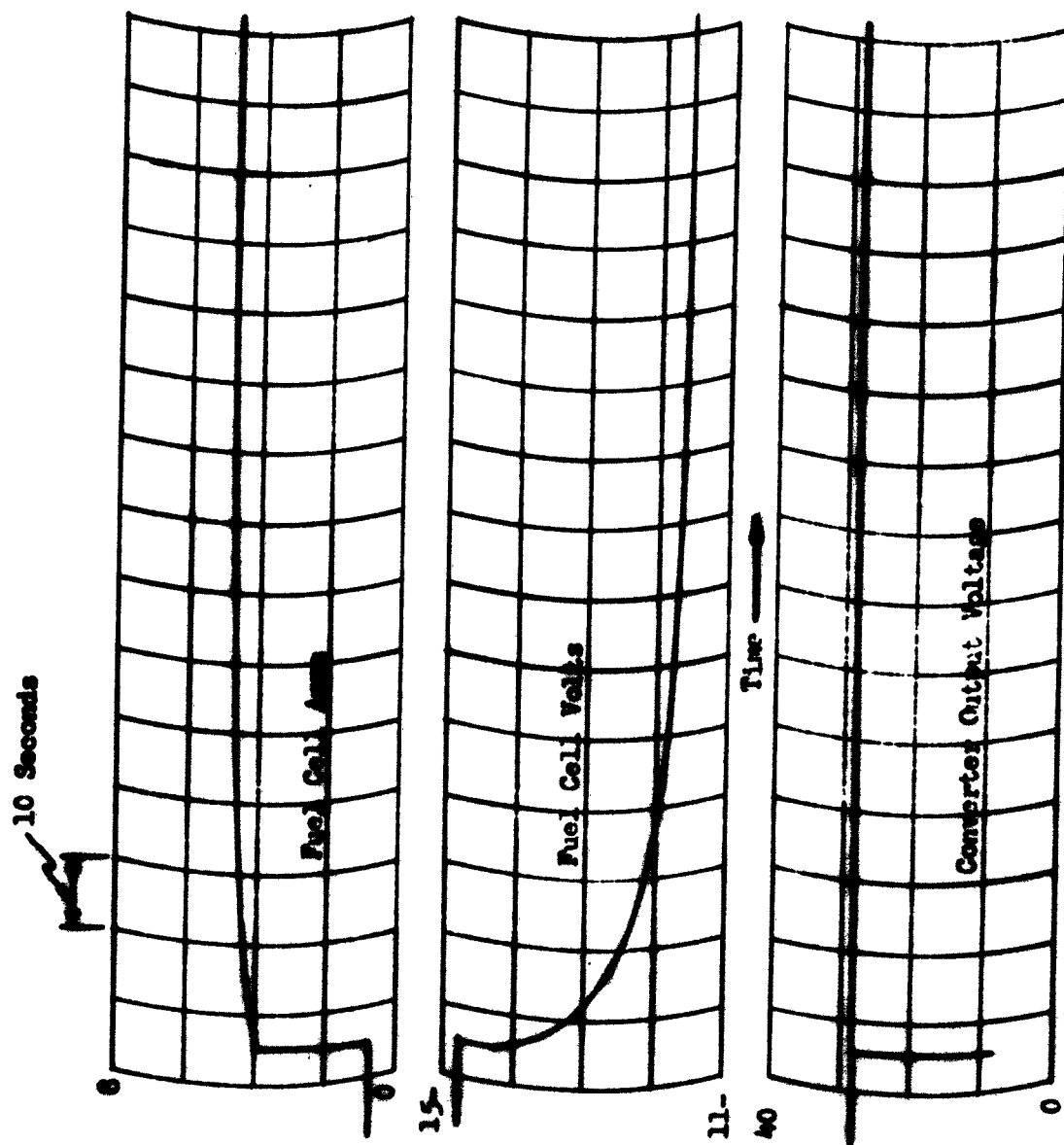
Figure 6.4-7: Laboratory System Transient Response
for a Step Application of Load of 7 to 15 Watts
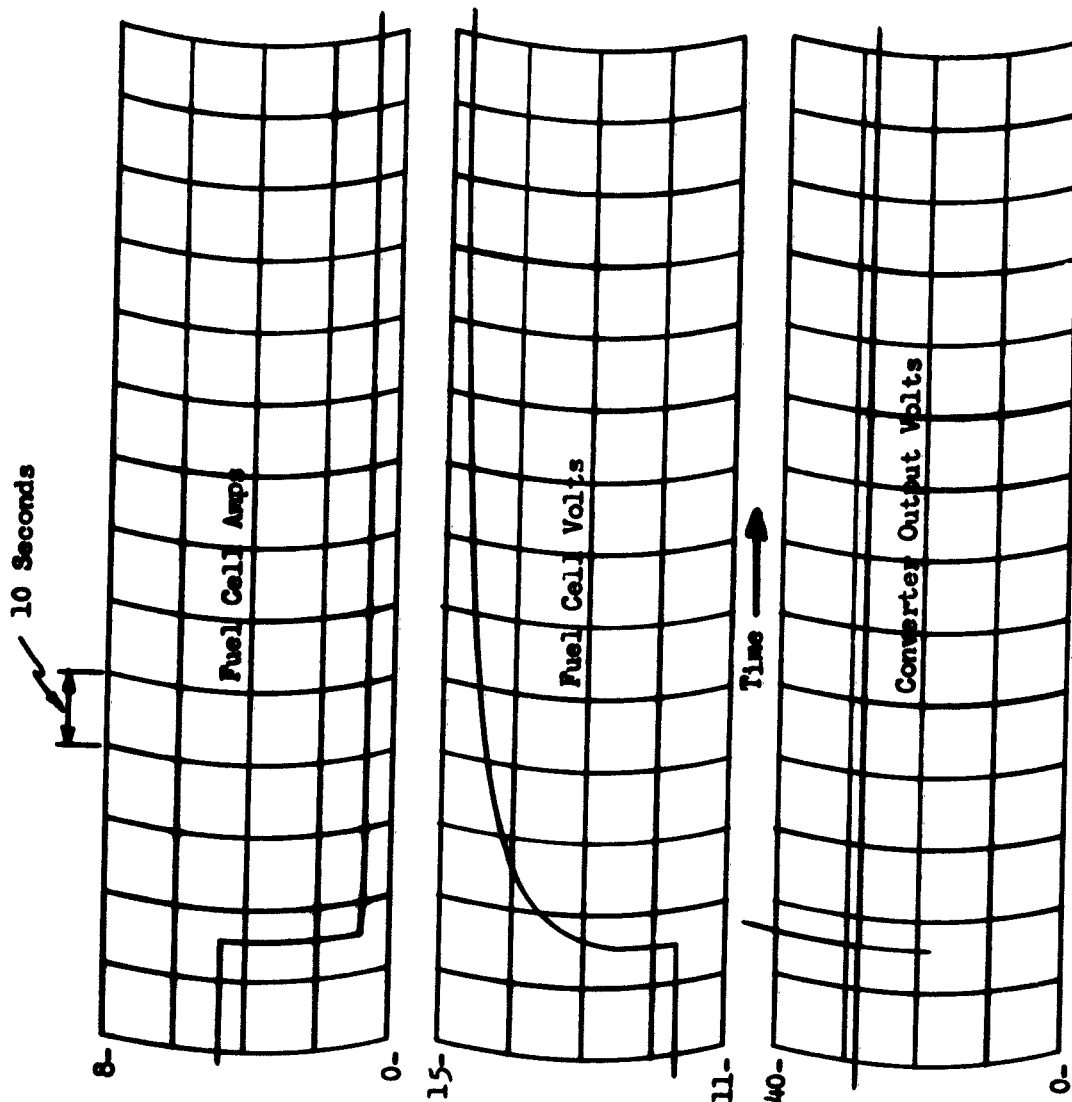
Figure 6.4-8 Laboratory System Transient Response for
a Step Removal of Load of 45 to 7 Watts

- 211 -

Figure 6.4-9

Voltage Converter Output Voltage Transient
Response for Step Application and
Removal of Load between 6.0 and 50 Watts

(a) Load Application

.01 seconds

(b) Load Removal

.01 seconds
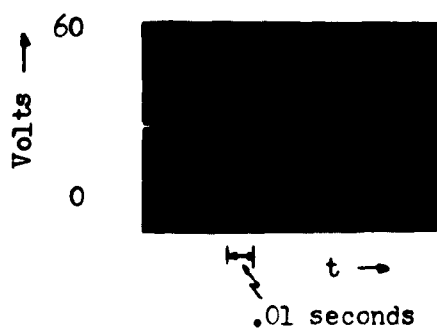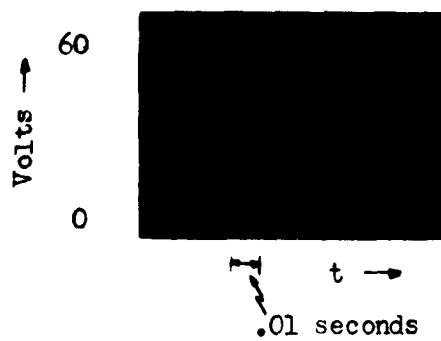
Figure 6.4-10

Voltage Converter Output Voltage
Ripple at a 50 Watt Output Load

0.1 volt ‡   - 28 VDC

.2 millisecond
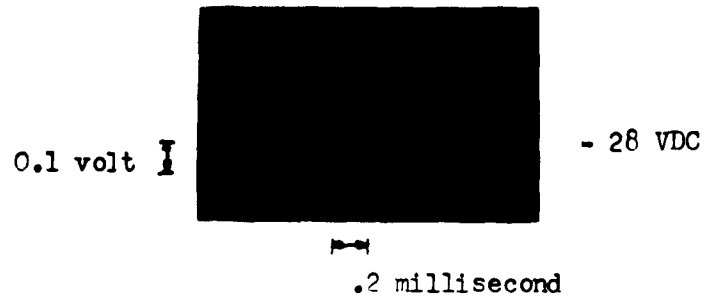
Figure 6.4-11

Voltage Converter Input Voltage
and Input Current at a 50 Watt Output Load

Voltage Ripple
(.24 volts/division)

Current Ripple
(1.2 amps/division)

.2 millisecond
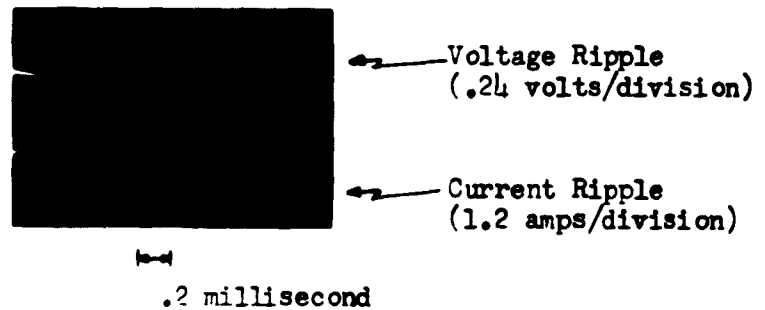
7.0 Topic Index to Progress Reports Nos. 1 Through 6